REPUBLIQUE DU CAMEROUN
Paix-Travail-Patrie
****
UNIVERSITE DE YAOUNDE I
****
CENTRE DE RECHERCHE ET DE FORMATION DOCTORALE EN SCIENCES, TECHNOLOGIES ET GEOSCIENCES
****
UNITE DE RECHERCHE ET DE FORMATION DOCTORALE PHYSIQUES ET APPLICATIONS
****
P.O Box : 812, Yaoundé
Email : crfd_stg@uy1.uninet.cm

REPUBLIC OF CAMEROON
Peace-Work-Fatherland
****
UNIVERSITY OF YAOUNDE I
****
POSTGRADUATE SCHOOL FOR SCIENCE, TECHNOLOGY AND GEOSCIENCE
****
RESEARCH AND POSTGRADUATE TRAINING UNIT FOR PHYSICS AND APPLICATIONS
****
P.O Box : 812, Yaoundé
Email : crfd_stg@uy1.uninet.cm

Generation, Propagation And Stability Of Dissipative Soliton In Nonlinear Systems

Thesis

Submitted and defended publicly in fulfillment of the requirements for the degree of
Doctor of Philosophy in Physics
Speciality: **Mechanics, Materials and Structures**
Option: **Mechanics and complex systems**

BIBLIOTHEQUE UNIVERSITAIRE UYI

Written and Presented by:
DJAZET Alain
Registration number: **12W1936**
M. Sc. in Physics

Under the supervision of

FEWO Serge Ibraïd
Associate Professor,
University of Yaoundé I

KOFANE Timoléon Crépin
Professor,
University of Yaoundé I

Jury:

President: **WOAFO Paul, Professor, University of Yaoundé I;**

Supervisor: - **KOFANE Timoléon Crépin, Professor, University of Yaoundé I;**
- **FEWO Serge Ibraïd, Associate Professor, University of Yaoundé I;**

Members: - **DJUIDJE KENMOE Germaine wife ALOYEM KAZE, Professor, University of Yaoundé I;**
- **KENFACK DJIOTSA Aurelien, Professor, University of Yaoundé I;**
- **BODO Bertrand, Associate Professor, University of Yaoundé I;**
- **MKAM TCOUOBIAP Serges Eric, Associate Professor, University of Buea.**

Year 2021

UNIVERSITE DE YAOUNDE I
UNIVERSITY OF YAOUNDE I

FACULTE DES SCIENCES
FACULTY OF SCIENCE

DEPARTEMENT DE PHYSIQUE

DEPARTMENT OF PHYSICS

ATTESTATION DE CORRECTION DE LA THESE DE DOCTORAT/Ph.D

Nous, Professeur **BODO Bertrand** et Professeur **WOAFO Paul**, respectivement Examinateur et Président du jury de la Thèse de Doctorat/Ph.D de Monsieur **DJAZET Alain** Matricule **12W1936**, préparée sous la direction du Professeur **FEWO Serge Ibraïd** et sous la supervision du Professeur **KOFANE Timoléon Crépin,** intitulée : « **GENERATION, PROPAGATION AND STABILITY OF DISSIPATIVE SOLITON IN NONLINEAR SYSTEMS**», soutenue le **Lundi, 03 Mai 2021**, en vue de l'obtention du grade de Docteur/Ph.D en Physique, Spécialité **Mécanique, Matériaux et Structures**, attestons que toutes les corrections demandées par le Jury de soutenance ont été effectuées.

En foi de quoi, la présente attestation lui est délivrée pour servir et valoir ce que de droit.

Fait à Yaoundé le 12 MAY 2021

Examinateur

Pr. BODO Bertrand

Le Président du Jury

Pr. WOAFO Paul

Le Chef de Département de Physique

UNIVERSITE DE YAOUNDE I
FACULTE DES SCIENCES
Le Chef de Département
DEPARTEMENT DE PHYSIQUE

Nanka Jean-Marie
Bienvenu
Professeur

Contents

Dedications **ix**

Acknowledgments **x**

Abstract **xiii**

Résumé **xiv**

List of abbreviations **xv**

General Introduction **1**

1 Literature review on solitons, laser phenomena and wave propagation **10**

1.1 Introduction 10

1.2 A brief history of soliton concept 11

1.3 Temporal soliton, spatial soliton and dissipative solitons 13

1.3.1 Temporal optical solitons 14

1.3.2 Spatial optical soliton 16

1.3.3 Dissipative optical soliton 19

1.4 Overview on lasers 23

1.4.1 What is a laser 24

1.4.2 Laser model and Maxwell-Bloch equations in a ring resonator 30

1.5 Dissipative solitons in physical systems 33

1.5.1 Scalar CGL model 34

1.5.2 The vector CGL model for laser emission from wide-aperture resonators . 36
1.5.3 Dissipative solitons of (D+1)-dimensional CQ-CGL equation 37
1.6 Conclusion 38

2 Model and methodology of investigations 40

2.1 Introduction 40
2.2 Derivation of the vector (3+1)-dimensional cubic-quintic complex Ginzburg-Landau equation 41
2.2.1 Modeling of the laser vector (3+1)D cubic complex Ginzburg-Landau equation 42
2.2.2 Modeling of the laser vector (3+1)D cubic-quintic complex Ginzburg-Landau equation 48
2.3 Analytical methods 52
2.3.1 Variational method 53
2.3.2 Routh-Hurwitz stability analysis method 55
2.4 Numerical methods 57
2.4.1 Split-step method 57
2.4.2 Fourth-order Runge-Kutta method 59
2.5 Conclusion 60

3 Results and Discussions 61

3.1 Introduction 61
3.2 Stable soliton of the (2+1)D cubic-quintic complex Ginzburg-Landau equation . 62
3.2.1 Variational equations 62
3.2.2 Stability analysis and numerical results 67
3.3 Analysis of the coupled (2+1)D cubic-quintic complex Ginzburg-Landau equation 72
3.3.1 Variational approach for coupled (2+1)D cubic-quintic complex Ginzburg-Landau model for nonsymmetric structures 73
3.3.2 Variational approach for coupled (2+1)D cubic-quintic complex Ginzburg-Landau model for a moving symmetric lattices 84
3.4 Conclusion 95

General Conclusion **96**

Appendices **101**

Bibliography **103**

List of Publications **118**

List of Figures

1.1 Recreation of a solitary wave on the Scott Russell Aqueduct on the Union Canal. Photograph courtesy of Heriot-Watt University **[93]**. 12

1.2 Behavior of the $N = 2$ and $N = 3$ solitons, compared with that of the fundamental ($N = 1$) soliton. Note that the vertical scale for the fundamental soliton has been magnified with respect to that of the other two, with $z_0 = \pi/2$. **[106, 107]**. 16

1.3 Schematic illustration of the lens analogy for spatial solitons. Diffraction acts as a concave lens while the nonlinear medium acts as a convex lens. A soliton forms when the two lenses balance each other such that the phase front remains plane. **[106]**. 17

1.4 Evolution of (a): pulse shapes and (b): optical spectra over a distance of 5LD for an initially unchirped the Gaussian pulse propagates in the anomalous-dispersion regime ($\beta_2 < 0$ of the fiber. **[106]**. 18

1.5 Three sources and three component parts of the concept of dissipative solitons. . 20

1.6 Regions of existence of the two types of solitons (gray) in (a) (ε, μ) and (b) (ε, ν) plane. In each case, the two separate regions are quite distinct. Parameters are shown in the plot. The hatched region corresponds to exploding solitons **[130]**. 22

1.7 Exact soliton profiles (solid lines) of two examples in the (a) upper and (b) lower regions in Fig. 1.6 (b). They are marked by thick black dots in Fig. 1.6 (b). Dashed lines show their corresponding phase profiles **[130]**. 23

1.8 (a)-(d) are important configurations of CO_2 lasers, and (e) is the transitions relevant for the CO_2 laser **[141, 142]**. 26

1.9 Energy levels of He and Ne atoms with the most prominent optical transition at 632.2nm. For nomenclature, the spectroscopic terms are used. For the energy levels, the lifetimes are given as well **[141]**. 27

1.10 examples of optical resonators **[138]**. 29

2.1 Diagrams (a) and (b) represent the resonant contributions to the nonlinear coefficients a and b, respectively. Diagram (c) represent the resonant nonlinear optical response describing third-harmonic generation **[178]**. 45

3.1 Double steady state solution $A-$(red) and $A+$ (blue). (a): $\nu = 0.72$, $\beta = 0.5$, $\delta = -0.1$; (b): $\nu = 0.72$, $\beta = 0.05$, $\delta = -1$. 64

3.2 Domain of stable solutions with $X_3 = Y_2$. (a) $\nu = 0.72$, $\beta = 0.5$, $\delta = -0.1$, (b) $\nu = 0.2$,$\beta = 0.5$, $\delta = -0.01$ and (c) $\nu = 0.72$, $\beta = 0.5$, $\delta = -1$. We can observe the great influence of the parameters system on the stability domain. 66

3.3 Domain of stable solutions with $\delta = -1$ and $\nu = 0.72$, for (a) $\beta = 0.5$, $X_3 = Y_2/2$, (b) $\beta = 0.5$, $X_3 = Y_2/5$; (c) $\beta = 1.5$, $X_3 = Y_2/5$. 68

3.4 Bifurcation diagrams of stable A_- and unstable A_+ solutions with $\nu = 0.2$ in (a): $\beta = 0.05$, $\delta = 0.01$, $\mu = -1.324$; (b): $\beta = 0.05$, $\delta = 0.001$, $\mu = -0.18$; (c): $\beta = 1.5$, $\delta = 0.01$, $\mu = -1.324$; (d): $\beta = 0.05$, $\delta = 0.01$, $\mu = -2.24$. 70

3.5 Profiles of the steady state solution at different positions along the propagation distance with parameters $\nu = 0.72$, $\beta = 0.5$, $\delta = -1$, $\varepsilon = 1.349$, $\mu = -0.3$. (a) z=0, (b) z=10, (c) z=100 and (d) z=4000. 71

3.6 Effective potential U versus (ε, δ_i) in panel (a), and versus (ε, μ) in panels (b) and (c) for the parameters $\delta = -0.01059$, $\beta = 0.49$, $\gamma_i = 0.25118$, $\nu = -1$, and: (a) $\gamma_r = 1.1087$, $\delta_r = -0.5074$, $\mu = -.9$, $X_m = 1.3$, (b) $\gamma_r = 0.9$, $\delta_r = -0.5074$, $\delta_i = 0.04289$, $X_m = 1.3$, (c) $\gamma_r = 0.9$, $\delta_r = -0.35074$, $\delta_i = 0.04289$, $X_m = 0.05$. . 77

3.7 Spatial profile of $\psi_+(x, y)$ (panels (a) to (c)) and $\psi_-(x, y)$ (panels (d) to (f)). (a) and (d) correspond to $t = 0$, (b) and (e) correspond to $t = 100$, while (c) and (f) have been recorded at time $t = 50000$, with the parameters: $\delta = -0.01059$, $\beta = 0.45$, $\varepsilon = 0.456$, $\gamma_r = 0.9$, $\gamma_i = 0.25118$, $\delta_i = 0.04289$, $\delta_r = -0.35074$, $\nu = -1$, $\mu = -0.98047$, and $X_m = 10$. 79

3.8 The density profiles of the space-time behavior of ψ_+ (panels (a) and (c)) and ψ_- (panels (b) and (d)). (a) and (b) correspond to $X_m = 0.5$ and $\gamma_r = 0.9$, while (c) and (d) give the results related to $X_m = 5$ and $\gamma_r = 1.109$. The rest of parameters remains the same as in Fig. 3.7. 80

3.9 Wave space-time dynamics, which corroborates the stability of the dissipative light bullets (a) $\psi_+(x, 0, t)$ and (b) $\psi_-(x, 0, t)$ obtained for the $\gamma_r = 1.109$ and $\delta_r = -0.15074$, with the other parameters keeping the similar values as in Fig. 3.7. 81

3.10 (2+1)D spatial profiles of the light bullet intensities $|\psi_+(x, y)|^2$ (left column) and $|\psi_-(x, y)|^2$ (right column) obtained from direct simulation of Eq. (3.18) at times $t = 0$ [(a) and (b)], $t = 10$ [(c) and (d)], $t = 25$ [(e) and (f)], and $t = 50000$ [(g) and (h)], with the set of parameters: $\delta = -0.01059$, $\beta = 0.45$, $\varepsilon = 0.49$, $\gamma_r = 0.9$, $\gamma_i = 0.25118$, $\delta_i = 0.04289$, $\delta_r = -0.25074$, $\nu = -1$, $\mu = -0.9$, and $X_m = 10$. . . 83

3.11 Potential $U(\varepsilon, \mu)$ for the following set of parameters: $\nu = -1$, $X_0 = 12.5$; (a) $\delta = -0.159$, $\gamma_r = 1.1087$, $\gamma_i = 0.2118$, $\beta = 0.0159$, $\delta_i = 0.1289$, $\delta_r = -0.5074$, (b) $\delta = -0.13761$, $\gamma_r = 1.0535$, $\gamma_i = 0.1001$, $\beta = 0.1761$, $\delta_i = 0.43$, $\delta_r = -0.5016$. 86

3.12 Panels (a) and (b) display the evolution of the amplitude, the pulse widths, the chirp, the unequal wavefront curvatures, the velocity, the central position and the phase with respect to t. Panels (c) and (d) depict the input/output profiles of the solutions ψ_+ and ψ_- for the following set of parameters: $\delta = -0.159$, $\gamma_r = 1.1087$, $\gamma_i = 0.2118$, $\nu = -1$, $\beta = 0.0159$, $\delta_i = 0.1289$, $\delta_r = -0.5074$, and the initial central position $X_0 = 2.5$. 88

3.13 Panels (a) and (b) show the three dimensional spatial evolution as predicted by the stability of the dissipative soliton trapped in the potential well. Panels (c) and (d) display their corresponding spectral evolution V_- and V_+, respectively for the values of parameters $\varepsilon = 0.72$, $\mu = -0.728$ and $X_0 = 15.5$. 89

3.14 Panels (a) and (b) are the periodic evolution of $max(\psi_+(t))$ and $max(\psi_-(t))$ of the dissipative soliton obtained by direct numerical simulation of Eq. (13). The corresponding spectral evolution $max(V_+(t))$ and $max(V_-(t))$ are presented in panels (c) and (d), with $\delta_r = -0.25016$, $\varepsilon = 0.72$, and $\mu = -0.73$, while the rest of parameters remains the same in Figs. 3.11(b). 90

3.15 Potential $U(\varepsilon, \mu)$, as a function ε and μ, for $\delta_r = -0.25016$. The other parameters remain unchanged as in Fig. 3.11(b). 90

3.16 Panels (a) and (b) show the quasi-periodic evolution of $max(\psi_+(t))$ and $max(\psi_-(t))$ of the dissipative soliton by direct numerical simulation of Eq. (13). The corresponding spectrals evolution $max(V_+(t))$ and $max(V_-(t))$ are presented in panels (c) and (d), with $\delta_r = -0.25016$, $\varepsilon = 0.63051$ and $\mu = -0.728$. The rest of parameters are taken from Fig. 3.11(b). 92

3.17 Spatial profiles of the solution $\psi_+(x, y)$ (upper line) and $\psi_-(x, y)$ (bottom line) at different steps of the evolution: (a) and (b) $T = 0$, (c) and (d) $T = 4$, (e) and (f) $T = 10000$, using the following parameters: $\delta = -0.13761$, $\beta = 0.1761$, $\varepsilon = 0.7$, $\gamma_r = 1.0535$, $\gamma_i = 0.1001$, $\delta_i = 0.043$, $\delta_r = -0.25016$, $\nu = -1$, $\mu = -0.73$, and $X_0 = 2.5$. 92

3.18 Spatial profile of the solution $\psi_+(x, y)$ (upper line) and $\psi_-(x, y)$ (bottom line) at different steps of the evolution: (a) and (b) $T = 0$, (c) and (d) $T = 15000$, (e) and (f) $T = 30000$, using the following parameters values: $\delta = -0.13761$, $\beta = 0.1761$, $\varepsilon = 0.7$, $\gamma_r = 1.0535$, $\gamma_i = 0.1001$, $\delta_i = 0.043$, $\delta_r = -0.3$, $\nu = -1$, $\mu = -0.73$, and $X_0 = 12.5$. 93

3.19 Spectral profile $|V_+|^2$ (upper line) and $|V_-|^2$ (bottom line) of the results of Fig. 8, at different steps of the evolution: (a) and (b) $T = 0$, (c) and (d) $T = 15000$, (e) and (f) $T = 30000$. 94

Dedications

My first and foremost dedication is devoted to our almighty **God** who takes care of us every day and guides us on the straight way.

To my deceased father **Mr. NGUITEWO DJEUTSOPMEZA Fidele**, and his wife Mrs. NGUITEWO born **MBADOUET Odette**.

To my deceased uncle **Mr. SOBTEDJOU Antoine**, and his wife Mrs. SOBTEDJOU born **FEUDJO Madeleine**.

Acknowledgments

At the end of the PhD study, I am deeply grateful for the opportunity to have learned from and worked with so many brilliant teachers, collaborators and students. I am happy to express my sincere gratitude to all those from who near or far have accompanied me during these doctoral years. Nevertheless, I will do my best to condense my thoughts about this.

Firstly, I would like to express my sincere gratitude to **God** almighty who gave me the life, the opportunity and the knowledge to reach and to end with the PhD study level.

I have furthermore to thank the persons responsible of the Faculty of Sciences, and the Research and postgraduate training unit for physics and applications who gave and confirmed the permission to go ahead with my thesis.

Professor Serge Ibraïd FEWO has taken me under his supervision since my enrollment in Master II. It is with great satisfaction that I extend my sincere thanks to him. From the research initiation phase to the thesis, he instilled in me the spirit of precision. We have faced several challenges together, and he has always been able to give me reason to continue. His generosity and his advice gave me the strength not to sink.

Professor Crépin Timoléon KOFANE, laureate of the Kwame Nkrumah award. He taught me the course of lasers in Master I, but more importantly, he has taught me how to conduct the research at the highest level. I would like to express to him my most sincere gratitude and also for the topic that they have proposed to me.

For this thesis, I would like to thank the different members of the jury.

I would like to thank **Pr. NDJAKA Jean Marie Bienvenu**, Head of the Department of Physics. I am very grateful for his administrative contribution and encouragement.

I am grateful to **Pr. WOAFO Paul**, Chairman of the Cameroon Physical Society for his teaching, particularly in numerical methods.

It would be very pleasing to recognize trade and constructive discussions combined with

great moments of sharing with my teachers. I have named: **Pr. TCHAWOUA Clement**, **Pr. YEMELE David**, **Pr. PELAP François Berçeau**, **Pr. TALLA Kisito**, **Pr. Germain Hubert BEN-BOLIE**, **Pr. SIEWE SIEWE Martin**, **Pr. FOTUE Alain**, **Pr. Germaine DJUDJE**, **Pr. KENFACK JIOTSA Aurelien**, **Pr. MKAM TCHOUOBIAP Serges Eric**, **Pr. BODO Bertrand**, **Pr. Jacques HONA**, **Pr. NANA MBenjo**, **Pr. Conrad Bertrand TABI**, **Dr. MVOGO Alain**, and **Dr. MANDENG MANDENG Lucien** for their daily support and especially for their moral support when I was sometimes tempted to get discouraged by the criticism of some reviewers.

The fulfillment of my thesis is the work of the good atmosphere in my family. I would like to thank:

My brothers and sisters **MBOUMO NGUITEWO Anastasie** and her husband **TEDONGOLO Théophyl**, Mrs **MEJIOGUIN Anie Rose**, Mrs **DONGMO Anie Myriane**, **KENGNI Liliane** and her husband **GUEUTSA Pascal**, Ing. **FEUDJIO DAJIO Christian**, and **DJOMBA OUKABA** and all the 4th promotion of petroleum engineer of the University of Dschang. I thank all of them for their moral and financial supports and for all their prayers for me.

I thank all my uncles, aunts, cousins, nephews and nieces in particular **Mr. MAFFOUO TCHOFFO Basile** for his constant support. **Mr. TELLA SOBTEDJOU Sézar**, **Mr. NGUEUKENG Franck Boris**, **Mr. DONGMO Léonel**, **Mr. NOUBOUDEM Antoine** my primary school educator, who remains interested in my success. Thank you very much for your flawless coaching and advice. I do not forget here my friends **TCHOFFO Jean**, **KAMENI Simplice**, **SANDJA Ervé**, **KUPON Bruno**, **NGUIMFACK ZEUKENG Bertin**, **AZEMFACK Telesfor**, **TELLA MOMO Armand**, and **MEYOUG TINDO Rodrigue** for the constant affection and joy that they have always given me.

I cannot forget the warm hospitality of the administrative staff of the Department of Physics of my under graduate studies (University of Dschang) for the daily work that they do for the students under their responsibility..

I would also like to thank all my Ph.D mates of the Laboratory of Mechanics, Materials and Structures of the University Yaounde I for their contributions. A special thanks to **Dr. DJOKO Martin**, **Dr. BANSI KAMDEM Christel Delphin**, **Dr. TATSING Hurbert**,

Mr. HEUTEU Crépin Fleridas , **Mr. ZANGA Dieudonné**, **Dr. AWAKEM David**, **Mr. BITANG Daniel Cassidi**, **Mr. AWE Richard**, **Dr. TAPIMO Romuald**, **Mr. HISSEN**, **Mr. DJIOKO Jean Paul**, **Mme TSIAM Laure**, **Mme MBAKOP Caroline**, for playing a very important accompanying role since I started this thesis.

I am also thankful to all my committee members and international reviewers for their stimulating questions on this work. Thank you to have agreed to discuss and appreciate the results of this thesis.

I thank my love **GWENAE NGNIEGHE TAFAM Liliane** socle of my effort. Her patience, understanding and love over the long road leading to this point made the path seems much less rocky. Her encouragement and willingness to listen to my problems helped to sustain my effort. She who has always been able to support me in difficult times. Very tender and kind, you have always succeeded in establishing confidence in me. May God fill you with happiness.

Abstract

New classes of stable dissipative optical spatial solitons of the laser (2+1)-dimensional cubic-quintic complex Ginzburg-Landau equation, which describe the dynamics of class B lasers are investigated.

In order to reproduce the spatiotemporal dynamics of the large-aperture lasers, this laser nonlinear evolution equation has been derived by singular perturbation method, using the Maxwell-Bloch equations describing the propagation of slowly varying field envelope through a collection of two-levels atoms, and when the interaction of an electromagnetic field with matter in a laser cavity is considered without the assumption of a fixed direction of the transverse electric field. So, the propagation of such intense ultra-short pulses is affected by additional physical mechanisms that appear in the nonlinear models. These are coupling effects, cubic and quintic nonlinearities, and possible diffusion effects. Good agreement between analytical and numerical results has been observed when investigating the propagation and stabilization characteristics of those pulses that are modeled by such a reduced equations.

The study of the stability for spatially symmetric lattices and for nonsymmetric structures was carried out by drawing the curves giving the domains of the laser parameters: for which the stability of the laser system is realized. The curves of the effective potential of the laser system in each case have been presented. They reveal the generation of stable dissipative solitons. An agreement between theoretical derivations and the numerical study was also observed. In fact, the visualization of the domains of stability resulting from the analysis of the effective potential, and the Routh-Hurwitz method fits well with the numerical results.

Keywords: Laser, Complex Ginzburg-Landau equation, variational method, Split-Step Fourier Method, Dissipatifs Solitons.

Résumé

Nous étudions de nouvelles classes de solitons laser spatiaux optiques dissipatifs stables dans l'équation de Ginzburg-Landau complexe cubique-quintique à (2+1)-dimension, qui décrit la dynamique des lasers de classe B.

Afin de reproduire la dynamique spatio-temporelle des lasers à grande ouverture, cette équation d'évolution nonlinéaire des lasers a été dérivée par la méthode de perturbation singulière, en utilisant les équations de Maxwell-Bloch décrivant la propagation de l'enveloppe du champ lentement variable à travers une collection d'atomes à deux niveaux d'énergie. Nous supposons que l'interaction d'un champ électromagnétique avec la matière dans une cavité laser est considérée sans l'hypothèse d'une direction fixe du champ électrique transverse. Ainsi, la propagation de telles impulsions ultra-courtes intenses est affectée par des mécanismes physiques supplémentaires qui apparaissent dans les modèles non linéaires. Il s'agit des effets de couplage, des nonlinéarités cubiques et quintiques et des effets de diffusion. Un bon accord entre les résultats analytiques et numériques a été observé lors de l'étude des caractéristiques de propagation et de stabilisation de ces impulsions qui sont modélisées par des équations réduites.

L'étude de la stabilité pour les structures spatialement symétriques et pour les structures non symétriques a été réalisée en traçant les courbes donnant les domaines des paramètres laser, pour lesquels la stabilité du système laser est réalisée. Les courbes du potentiel effectif du système laser dans chaque cas ont été présentées. Elles révèlent la génération de solitons dissipatifs stables. Un lien entre les dérivations théoriques et l'étude numérique a également été observé. En fait, la visualisation des domaines de stabilité résultant de l'analyse du potentiel effectif, ou du critère de stabilité de Routh-Hurwitz cadre bien avec les résultats numériques.

Mots clés: Solitons dissipatifs, Laser, équation de Ginzburg-Landau complexe, Méthode variationnelle, Méthode de Fourier à pas divisé.

List of abbreviations

Acronym	Meaning
XPM:	Cross-Phase Modulation
SPM:	Self-Phase Modulation
1D:	one-dimensional
2D:	two-dimensional
3D:	three-dimensional
STS:	Spatiotemporal Solitons
GVD:	Group Velocity Dispersion
MB:	Maxwell-Bloch
CGL:	Complex Ginzburg-Landau
VCGL:	Vector Complex Ginzburg-Landau
CQ-CGL:	Cubic-quintic Complex Ginzburg-Landau
CEO:	Classical Electron Oscillator model
BECs:	Bose-Einstein Condensates
KdV:	Korteweg-de-Vries
IST:	Inverse Scattering Transform
NLS:	Nonlinear Schrödinger
R-H:	Routh-Hurwitz
SSFM:	Split-Step Fourier Method
MFSS-S:	Symmetrical Split-Step Fourier Method
RK4:	Fourth-Order Runge-Kutta
LEDs:	Light Emitting Diodes
WWW:	World Wide Web
ASE:	Amplified Spontaneous Emission

Acronyme	Signification
WDM:	Wavelength Division Multiplexed
DWDM:	Dense Wavelength Division Multiplexing
Maser:	Microwave Amplification by Stimulated Emission of Radiation
Laser:	Light Amplification by Stimulated Emission of Radiation
VCSEL:	Vertical Cavity Surface Emitting Laser
CW:	Continuous Wave
CV:	Collective Variable
DS:	Dissipative Soliton
PDE:	Partial Differential Equation
FODEs:	First-Order Differential Equations
ODEs:	Ordinary Differential Equations
RK:	Runge-Kutta
SVS:	Stabilized Vector Solitons
NDFA:	Normal Dispersion Fiber Amplifier

General Introduction

Since the operation of the first laser in 1960, literally hundreds of different laser varieties have been developed and the light that they produce is used in thousands of applications ranging from precision measurement, materials processing to medicine. Underlying all this variety, however, is a small set of basic physical principles upon which laser operation, laser beam propagation and the interaction of laser beams with matter depend. In order to cope with this preoccupying situation, since the discovery of the concept of laser in 1940 **[1]**, new theoretical approaches, experimental analyses, and systematic use of computer science have been developed. During the past 20 years, a lot of research works have been done in several types of lasers, which are very complex devices, having a rich temporal, spatial, and spatiotemporal dynamics **[2-6]**. These different types of lasers can be classified into **[7, 8]** Class A (for example, dye lasers) **[9-14]**, Class B (semiconductor lasers, CO_2 lasers, and solid-sate lasers) **[15-22]**, and Class C (the only example is the far-infrared lasers) **[23]**, depending on the decay rate of the photons, the carriers, and the material polarization. However, this classification is not applicable to inhomogeneously broadened lasers that included He-Ne, argon-ion, and Xe lasers, for example. Comparing these lasers, different dynamical features have been described, including instabilities, cascades of bifurcations, multistability, and sudden chaotic transitions **[2-6]**. Many other fascinating features and properties concerned with chaotic dynamics have been extensively addressed in relevant semiconductor laser systems, because of their potential applications in chaotic optical communications **[24-28]**. Further studies have suggested that optical cavities, also called cavity solitons, are present in a large variety of externally driven optical systems. However, their existence in laser systems is limited to the well-known laser with saturable absorbers, two-photon lasers, lasers with dense amplifying medium, or lasers pumped by squeezed vacuum **[29-41]**.

Dissipative structures are peculiar to nonequilibrium open systems. They are maintained by the balance of the influx of energy and matter with dissipation, and in many cases, they appear on a macroscopic scale. For this reason, the most natural theoretical description of these phenomena should begin with a consideration at a macro-level, nonlinear evolution equations such as the Navier-Stokes equation. Of course, one can argue that there exists the problem of determining the microscopic physical source of macroscopic dissipative structure. However, this problem is equivalent to that of determining the statistical mechanical basis of the behavior of the macroscopic evolution equations themselves. Following this line, questions regarding the microscopic physical source of dissipative phenomena can be separated from the study of dissipative phenomena. Such microscopic considerations are beyond the scope of this thesis.

Dissipative structures and other nonequilibrium patterns have become the subject of serious studies in physics only recently. Earnest research in this field did not begin until the 1970's. The approach used in the study of nonequilibrium patterns employs a phenomenological/qualitative manner of thinking which represents a bold departure from the physics that existed prior to this study, and as such, this approach represents an important success.

In the optical system, several models have been proposed to describe how the spatiotemporal dynamics emerges in large-aperture lasers. For example, the two-photon lasers have been the subject of continued theoretical attention since the early days of the laser era. The theoretical interest of the two-photon laser lies in the intrinsic nonlinear nature of the two-photon interaction. The most successful theoretical approach is given by the Maxwell-Bloch (MB) equations **[7, 8]**. In fact, the laser is a system where the number of photons is much larger than one, thus, allowing a semi-classical treatment of the electromagnetic field inside the cavity through the Maxwell equations, which has been developed by Lamb **[42, 43]** and independently by Haken **[44, 45, 46]**. The semi-classical laser theory ignores the quantum-mechanical nature of the electromagnetic field, and the amplifying medium is modeled quantum mechanically, as a

collection of two-level atoms through the Bloch equations **[42, 44, 46]**.

The linear analysis and numerical integration of the full MB equations **[47]** have been used to interpret the features of the experiment that cannot be fully understood with a perturbative model, such as the observed evolution from order to fully developed turbulence as the Fresnel number increases up to a critical control-parameter threshold **[48]**. In addition, it has been shown that the MB equations with homogeneous line broadening are appropriate for the description of the amplification of short pulses in the multilevel atomic iodine amplifier **[49]**. Some prototype of nonlinear evolution equations has been constructed by singular perturbation methods, using the MB equations as the starting point, in order to reproduce the spatiotemporal dynamics of the large-aperture lasers.

The first class of prototype equations which describe, for example, the class-A laser pattern dynamics, such as the multi-transverse-mode lasers, is the cubic complex Ginzburg-Landau (CGL) equation. In fact, the existence of a vortex solution of the laser equations, the stability of symmetric vortex lattices in the laser beams, the transition to nonsymmetric patterns dominated by titled waves, and to disordered spatial distribution have been well-reproduced by the cubic CGL equation **[50-53]**. To prevent the blowup of the solutions of the cubic CGL equation for negative detuning, the laser cubic CGL equation, which possesses fourth- and higher-order diffusion terms and which describes correctly the excitation of transverse modes and structure formation in a laser, has been derived **[54]**. It should also be mentioned that the adiabatic elimination of irrelevant variables has been shown to be very sensitive to the method used for the perturbation expansions in the case of partial differential equations which describe laser dynamics. That is why the center manifold theorem for the elimination of irrelevant variables has been used, leading to the cubic CGL equation in the small-field limit. The particular feature of the center manifold theory is that, it is a solid mathematical framework within which the fast variables as well as the characteristic scaling of the long-term dynamics are properly

determined **[52]**. It has also been shown that the cubic-quintic CGL equation is a continuous approximation to the dynamics of the field in a passively mode-locked laser **[55-59]**.

The second class of prototype equations which provides the generic description of transverse pattern formation in wide aperture, single longitudinal mode, two-level lasers, when the laser is operating near peak gain, is the complex Swift-Hohenberg equation for class A and C lasers **[60]**. Indeed, the complex Swift-Hohenberg equation comes naturally as a solvability condition for the existence of solutions to the MB laser equations in the form of asymptotic series in powers of the small detuning parameter **[60]**. In addition, when the laser pattern dynamics is sensitive to the degree of stiffness of the original physical problem, such as in the class-B lasers, the amplitude equations are the complex Swift-Hohenberg equation coupled to a mean flow **[60, 61]**, which is consistent with the observation that the population inversion variable in the MB laser equations acts as a weakly damped mode. Otherwise, the Swift-Hohenberg equation has been considered for a passive optical cavity driven by an external coherent field, valid close to the onset of optical bistability **[62]**. Moreover, theoretical studies of spatiotemporal structures of lasers with a large Fresnel number of the laser cavity have been successfully described in the cases in which two coupled fields are involved in the dynamics for class-B lasers. For example, it has been shown that the homogeneous steady-state solution may be destabilized by two generic instabilities. The first is a long wavelength instability which is related to the phase invariance of the electromagnetic field and is described by a scalar field obeying the Kuramoto-Shivasinsky equation. The second is a short wavelength instability which corresponds to a Hopf bifurcation and is described by a complex field which obeys a Swift-Hohenberg equation **[18, 19]**.

The third class of prototype equations which contains a phenomenological aspect and which is used in the theoretical description of the pulse dynamics in a mode-locked laser was pioneered by Haus and Mecozzi **[63]**. Assuming that only one polarization state plays a role and that the change of the pulse per round trip is small, so that one can replace the discrete laser components

with continuous approximations, Haus and Mecozzi **[63]** obtained a master equation which is nothing but the stationary version of the cubic CGL equation. The coefficients that appear in the model were related to the physical parameters in a rather phenomenological way **[63, 64]**.

All these three classes of prototype equations are scalar since it is usually considered that the polarization degree of freedom of the electromagnetic field is fixed either by material anisotropies or by experimental arrangement. Thus, the description of the dynamics is done in terms of a scalar field. It has been shown that the cavity-synchronous phase or amplitude modulation technique transforms passively mode-locked optical oscillators into actively mode-locked lasers **[65, 66]**. Mixing passive and active mode-locking in the same device results in a new class of optical oscillators capably of generating short pulses. To model this laser system, as an example, the scalar cubic-quintic CGL (CQ-CGL) equation has been used with terms corresponding to active mode-locking, in addition to the usual passive mode-locking terms **[67]**. However, the inclusion of a quintic saturating term in the scalar CQ-CGL equation was shown to be essential for the stability of pulsed solutions **[68-70]**. Since the scalar CQ-CGL equation is non-integrable, which means that general analytical solutions are not available, selected analytical solutions can only be found for specific relations between the equation parameters. Soliton pairs were studied extensively both theoretically **[71-74]** and experimentally **[75, 76]**. More complicated solutions for the CQ-CGL equations, such as pulsating, creeping, or exploding solutions have been reported numerically **[77]**. It is also well known that laser systems are made of several components, an accurate model then should involve consecutive sets of propagation equations. Models can be vectorial, when the polarization nature of light is involved, and can also include the delayed response of the saturable absorber and gain medium. The possibility of vectorial topological defects which are not predictable by the scalar theory were first analyzed by Gil **[78, 79]**. Using standard perturbative nonlinear analysis performed near the laser threshold, Gil **[78]** has derived a (3+1)-dimensional ((3+1)D) vectorial cubic CGL

equation by considering the interaction of an electromagnetic field with matter in a laser cavity without the assumption of a fixed direction of the transverse electric field. Different kinds of pattern formation are present in the dynamic states of the one-spatial dimension (localized structures) **[80-82]** and of the two-spatial dimensions (topological defects) **[83-89]** for the vectorial cubic CGL equation. Examples are the synchronization properties of spatiotemporally chaotic states **[86]**, the identification of a transition from a glass to a gas phase **[87]**, and the formation and annihilation processes leading to the different types of defects **[88]**. In addition, creation and annihilation processes of different kinds of vector defects, as well as a transition between different regimes of spatiotemporal dynamics have been described **[89]**. Semiconductor lasers are still developing, and stabilization both by the device structure and through external controls is currently an important research area.

It is well-known that in an optical communication system, the information is transported by solitons. The use of solitons in communications enhances the use of optical fibers since they carry a great deal of information generated by laser system over very long distances. Because of their robustness, dissipative solitons are appropriate objects to overcome the bandwidth challenge currently faced by medicine, industrial, particularly the telecommunications industry.

It is well-known that, in order to have a multi-level atomic system, we need the external perturbation system (a pumping process). Through external perturbations, semiconductor lasers are either stabilized or destabilized. The effects of such perturbations on laser dynamics include optical feedback, optical injection, and optoelectronic feedback. To stabilize laser oscillations, the disturbances may be weak or strong. The lasers can then be strongly stabilized under appropriate conditions of external parameters and operating conditions of the lasers **[90]**. Stabilization of semiconductor lasers is very important with regard to their application. For example, frequency stabilization, linewidth narrowing, power stabilization, polarization fixing, and beam shaping are very important in optical communications, optical data storage systems,

and optical measurements. In particular, ultrastabilized semiconductor lasers are expected in broad-band optical communications, high precision optical measurements, and standard light sources. Although laser technology has seen many advances, the laser remains a highly sought after area of research. The demand for some of these applications requires specific characteristics not available until now, such as power, and size.

The main objective:

The objective of this thesis is to make a contribution to the efforts undertaken by physicists specialized in nonlinear optics, to identify, clarify and classify the conditions for the generation, propagation, and stabilization of the impulses which are in the transverse dimensions of the space, as well as in the time domain. Although many works have been done in order to understand the physical process to be involved in the formation of stable solitons of dissipative systems, to the best of our knowledge, no work has been reported in the dynamics of optical solitons in the frame of multidimensional CGL equation with cubic-quintic nonlinearities, taking into account the contribution of the third-harmonic generation, the nonlinear polarization of one-photon-resonant and the two-photon-resonant processes.

Specifics objectives:

Our first specific objective is the derivation of a nonlinear dissipative model describing the dynamics of solitons cavity. In our second objective, we draw, and clarify the conditions of generation of the localized solutions in the laser cavity, describing a stable dynamic.

We first focus on the derivation of an equation, modeling the propagation of ultrashort vector optical dissipative solitons of laser systems with a linear gain/loss, cubic-quintic nonlinearities, diffraction in the presence of cubic and quintic cross-phase modulation, named the coupled (2+1)dimensional cubic-quintic complex Ginzburg-Landau ((2+1)D CQ-CGL) equation. The approach taken here is similar to that of Gil **[78]** for the vectorial cubic CGL equation. We start with the Maxwell-Bloch equations describing the propagation of a slowly varying field

envelope through a collection of two-level atoms when the interaction of an electromagnetic field with matter in a laser cavity is considered without the assumption of a fixed direction of the transverse electric field. Then, we report on the derivation of the laser (3+1)D vectorial CQ-CGL equation.

Furthermore, the theoretical treatment will allow us to establish a set of coupled first-order differential equations with the help of variational method (using the elliptic Gaussian pulse shape and the moving-Gaussian pulse as ansatz), whereas direct numerical simulations are carried out by means of fourth order Runge-Kutta method (RK4) and the split-step Fourier method (SSFM) to support our analytical results.

By means of the analysis of the effective potential that we have derived, the stability of the new types of dissipative solitons obtained have been investigated. A full direct numerical simulation of the coupled (2+1)D CQ-CGL equation confirms that the coupled multidimensional dissipative solitons can be self-trapped over a longer propagation time, even in the presence of random perturbations. Considering a well-known (2+1)D CQ-CGL equation **[91, 92]** describing the propagation of the information inside the nonlinear optical system, using the variational approach, it follows the stable propagation, in accordance with our stability analysis prediction.

The rest of the work is organized as follows.

Chapter 1 is devoted to the literature review on the generalities related to the laser theory. The following concepts will therefore be addressed: soliton, laser, class of laser, laser in optical communication systems, dispersive nonlinear effects in optical laser.

The chapter 2 is devoted to the models describing the dynamics in the laser cavity. Here, we also present some analytical and numerical methods used for our different studies.

Chapter 3 presents the main results of this thesis. These results concern the self-organization of dissipative soliton in the optical systems, model by the (2+1)D and the coupled (2+1)D cubic-quintic complex Ginzburg-Landau equation.

The present thesis ends with a general conclusion. We summarize our results and give some future directions that could be investigated.

Chapter I

Literature review on solitons, laser phenomena and wave propagation

1.1 Introduction

Dissipative structures and other non-equilibrium patterns are the subject of important study in physics. The name "dissipative system" was coined by Prigogine for systems considered in non-equilibrium thermodynamics. These systems are not isolated but are kept in contact with an external source that provides energy for the smaller sub-system. Thus, dissipation is essential for the transfer of pumped energy to a "cooler" part. Hence, the notion "dissipative system" is more complicated. It assumes that there is also an energy supply part, rather than just losses. A localized structure in such a system, i.e., a "dissipative soliton" truly deserves to be an established scientific keyword. Through this approach, a new theoretical framework has been developed, while new terms have arisen for the purpose of describing complex natural phenomena. Optical laser is one of the most interesting and important topics in the field of global and local nonequilibrium communication systems. The use of soliton in optical communication systems enhances the use of laser action, since they carry a great quantity of information. To understand why optical solitons are needed in optical communication systems, we should consider the problems that limit the distance and/or capacity of laser cavities. Optical systems inevitably have chromatic dispersion, losses (attenuation of the signal), and nonlinearity. Dispersion and nonlinearity can lead to the distortion of the signal. When soliton pulses are used as an information carrier, the effects of dispersion and nonlinearity balance (or compensate)

each other and thus, don't degrade the signal quality with the propagation distance. In such a regime, the pulses propagate through the optical system without changing their spectral and spatial shapes.

For a better understanding of the rest of our work, this chapter will bring out general information on solitons, laser system, dissipative solitons in communication systems (i.e. laser and optical fiber), and various effects that take place in optical communication system, due to the propagation of optical signal.

1.2 A brief history of soliton concept

It is well-known that many phenomena in the nature are nonlinear. In order to have a good understanding of those phenomena, many works have been done. The obtained results show some fascinating and important nonlinear phenomena: coherent nonlinear structures, and chaos phenomena. In particular, a category of coherent nonlinear structures called solitons, has been widely adopted as a fundamental datum for capturing and understanding the dynamic behavior of complex nonlinear systems. Solitons are localized large amplitude waves, which propagate with permanent shape and exhibit particle-like properties, emerging as a result of delicate balance between nonlinearity and dispersion or diffraction. The concept of solitons was enlightened first in the context of hydrodynamics, but was later extended to various scientific disciplines, with its most significant development reaped in optics and most recently, Bose-Einstein condensates (BECs). The birth to the modern study of soliton is since experiments conducted by John Scott Russell (1808-1882) **[93]**, to determine the most efficient design for canal boats, where he has discovered a phenomenon that he described as the wave translation. The discovery is described here in his own words **[93]**:

"*I was observing the motion of a boat which was rapidly drawn along a narrow channel by a pair of horses, when the boat suddenly stopped - not so the mass of water in the channel*

Figure 1.1: Recreation of a solitary wave on the Scott Russell Aqueduct on the Union Canal. Photograph courtesy of Heriot-Watt University **[93]**.

which it had put in motion; it accumulated round the prow of the vessel in a state of violent agitation, then suddenly leaving it behind, rolled forward with great velocity, assuming the form of a large solitary elevation, a rounded, smooth and well-defined heap of water, which continued its course along the channel apparently without change of form or diminution of speed. I followed it on horseback, and overtook it still rolling on at a rate of some eight or nine miles an hour, preserving its original figure some thirty feet long and a foot to a foot and a half in height. Its height gradually diminished, and after a chase of one or two miles I lost it in the windings of the channel. Such, in the month of August 1834, was my first chance interview with that singular and beautiful phenomenon which I have called "the Wave of Translation".

This experiment took place on the Union Canal at Hermiston, very close to the Riccarton campus of Heriot-Watt University, Edinburgh. In fluid dynamics, the wave is now called Russell's solitary wave. Example of the solitary wave is shown in Fig. 1.1.

In 1872, the French scientist Joseph Valentine de Boussinesq (1842-1929) **[94]**, and in 1895 the Dutch mathematicians Diederik Johannes Korteweg (1848-1941) and Gustav de Vries (1866-1934) **[95]**, proved theoretically the existence of solitary waves. Korteweg and de Vries derived

(known as the KdV equation) a model equation describing a far-field property of the surface wave in the lowest-order of dispersion and nonlinearity. This KdV equation is one of the prototype equations of solitons theory because it has remarkable mathematical properties. His study allows to understand the fundamental ideas of the concept of soliton. It is valid only if the fluid depth and the wave height are small compare with its width along the direction of propagation.

Later, in 1965, Martin Kruskal and Norman Zabusky **[96]** studied the KdV equation numerically and revealed the nature of these solitary waves that they could reemerge without change in shape and velocity even after the collision among themselves. They named these waves as solitons to sound like protons, electrons, photons in order to impress on their particle-like nature. The term "soliton" was justified when the KdV equation was solved analytically by means of Inverse Scattering Transform (IST) and the solution was described by a set of solitons **[97]**. Solitons are regarded as a fundamental unit of mode in nonlinear dispersive medium and play a role similar to the Fourier mode in a linear medium. In particular, a soliton being identified as an eigenvalue in IST supports its particle (Fermion) concept. Meanwhile, self-focusing in a Kerr medium was demonstrated and a spatially localized solution analogous to a soliton was found to emerge by the balance of the cubic nonlinearity and refraction **[98]**. The model equation, called the nonlinear Schrödinger equation (NLS), was later found to be integrable by Zakharov and Shabat **[99]**, also by means of the IST, and the solution is given by a set of solitons and dispersive waves.

1.3 Temporal soliton, spatial soliton and dissipative solitons

From a mathematical point of view, the ideal soliton is a solitary wave, exact solution of a nonlinear equation which propagates without deformation and without change of speed. In the ideal case (Hamiltonian), due to the strict mathematical integrability of the equation which

models the system, it retains its shape and its speed after collision.

However, because of the disturbances (defects, impurities, ...) which slightly modify the ideal properties of the soliton, physicists rather use the term "quasi soliton" which indicates a solitary wave or packet of energy propagating without deformation or modification too high of its speed. In view of all the soliton varieties and the rapid evolution of the field in optics, we will try to account for the variants linked to optical solitons. In the context of nonlinear optics, solitons are classified as being either temporal or spatial, depending on whether the confinement of light occurs in time or space during wave propagation **[100]**.

1.3.1 Temporal optical solitons

Temporal solitons represent optical pulses that maintain their shape during propagation. Their existence was predicted in 1973 in the context of optical fibers **[101]**. Since then, fiber solitons have been studied extensively and have even found applications in the field of fiber-optic communications **[102-111]**.

Temporal solitons inside optical fibers resulted from a balance between the group-velocity dispersion (GVD) and self-phase modulation (SPM) induced by the Kerr nonlinearity. The GVD broadens optical pulses during their propagation inside an optical fiber, except when the pulse is initially chirped in the right way. More specifically, a chirped pulse can be compressed during the early stage of propagation whenever the GVD parameter β_2 and the chirp parameter C happen to have opposite signs such that $\beta_2 C$ is negative **[112]**. The nonlinear phenomenon of SPM imposes a chirp on the optical pulse such that $C > 0$. Since $\beta_2 < 0$ in the $1.55\mu m$ wavelength region of silica fibers, the condition $\beta_2 C < 0$ is readily satisfied. Moreover, because the SPM-induced chirp is power dependent, it is not difficult to imagine that, under certain conditions, the SPM and GVD may cooperate in such a way that the SPM-induced chirp is just right to cancel the GVD-induced broadening of the pulse. SPM is one of the very iterating

manifestations of the optical Kerr effect and results in the accumulation of a nonlinear phase generated during propagation and which generates, unlike dispersion, a spectral widening of the pulse. The optical pulse would then propagate undistorted in the form of a soliton.

Let us consider the propagation of a light wave of field $\psi(z,t)$ in a nonlinear dispersive medium **[112]**:

$$i\frac{\partial\psi}{\partial z} - \frac{1}{2}\beta_2\frac{\partial^2\psi}{\partial t^2} + \gamma|\psi|^2\psi = 0, \tag{1.1}$$

where $\gamma(W^{-1}m^{-1})$ is the nonlinear coefficient and β_2 is the dispersion coefficient of the group velocity dispersion (GVD). This equation is the basis of many researches in the field of telecoms and was demonstrated in optical fibers in 1973 by Hasegawa and tappert **[101]**. The main features associated with temporal solitons can be summarized as follows. When an input pulse having an initial amplitude

$$\psi(0,t) = Nsech(t), \tag{1.2}$$

is launched into the fiber, its shape remains unchanged during propagation when $N = 1$, but follows a periodic pattern for integer values of $N > 1$ such that the input shape is recovered at $z = m\pi/2$, where m is an integer. The parameter N represents a dimensionless combination of two pulse parameters (peak power P_0 and width T_0); and is introduced as $N^2 = \gamma P_0 L_D = \gamma P_0 T_0^2/|\beta_2|$, where L_D is the dispersion length. This parameter governs the relative importance of the SPM and GVD effects on pulse evolution along the fiber. In fact, when $N << 1$, dispersion dominate, while SPM dominates for $N >> 1$. For $N \sim 1$, both SPM and GVD play an equally important role during pulse evolution.

Figure. 1.2 shows the pulse evolution for the first order ($N = 1$), second ($N = 2$) and third-order ($N = 3$) solitons for several values of z by plotting the pulse intensity $|\psi(z,t)|^2$. Only the fundamental temporal soliton (whose parameters satisfy the condition $N = 1$) propagates without deformation, all the other higher order solitons ($N > 1$) undergo a recurrent deformation movement during their propagation.

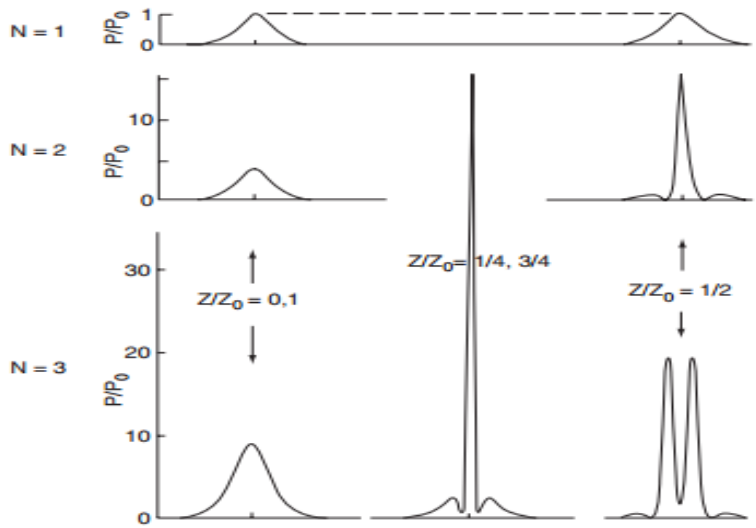

Figure 1.2: Behavior of the $N = 2$ and $N = 3$ solitons, compared with that of the fundamental ($N = 1$) soliton. Note that the vertical scale for the fundamental soliton has been magnified with respect to that of the other two, with $z_0 = \pi/2$. **[106, 107]**.

1.3.2 Spatial optical soliton

Spatial solitons represent self-guided beams that remain confined in the transverse directions orthogonal to the direction of propagation. In similar to the temporal soliton, they evolve from a nonlinear change in the refractive index of an optical material induced by the light intensity phenomenon known as the optical Kerr effect in the field of nonlinear optics **[108-110]**. The intensity dependence of the refractive index leads to spatial self-focusing (or self-defocusing) which is a major nonlinear effects that is responsible for the formation of optical solitons. A spatial soliton is formed when the self-focusing of an optical beam balances its natural diffraction-induced spreading (see Fig. 1.3).

Self-focusing and self-defocusing of continuous-wave (CW) optical beams in a bulk nonlinear medium has been studied extensively **[112]**. Self-trapping was not linked to the concept of spatial solitons immediately because of its unstable nature. During the 1980s, stable spatial solitons were observed using nonlinear media in which diffraction were limited to only one transverse dimension **[113]**. The formation of spatial solitons is based on the geometry of the

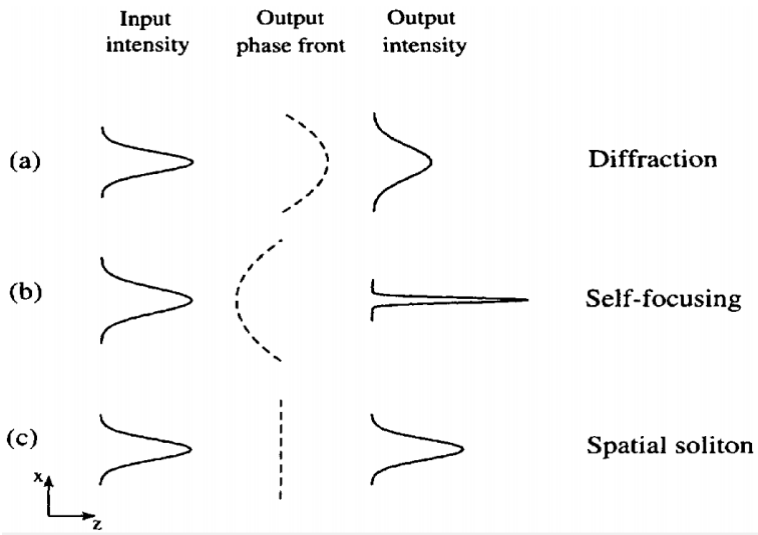

Figure 1.3: Schematic illustration of the lens analogy for spatial solitons. Diffraction acts as a concave lens while the nonlinear medium acts as a convex lens. A soliton forms when the two lenses balance each other such that the phase front remains plane. **[106]**.

waveguide and on the photo-induced phase shift **[106]**: Concerning the geometry of the induced waveguide, we know that a beam of limiting width obeys the laws of diffraction characterized by the Rayleigh length:

$$L_D = \frac{r}{\theta_D} = \frac{\pi n_0 r^2}{\lambda}, \tag{1.3}$$

where r is the mode radius ("waist"), n_0 the linear refractive index and λ the optical wavelength. The length of Rayleigh L_D is the propagation distance after which the size of the beam has increased by a factor $\sqrt{2}$ (its area doubled). In the presence of a positive nonlinearity medium ($\gamma > 0$), the beam induces an increase in index Δn, proportional to the intensity. The critical angle of total reflection between the two media, defined by $\theta_c = \sqrt{2\Delta n/n_0}$, allows to determine the characteristic length of nonlinearity (auto-focusing) in the approximation of small angles **[106]**,

$$L_{NL} = \frac{r}{\theta_c} = \frac{r}{\sqrt{2\Delta n/n_0}}. \tag{1.4}$$

The spatial soliton corresponds to a balance between diffraction and self-focusing. In this case, the two widths are equalized, so that $L_{NL} = L_D$ leads to $\theta_c = \theta_D$.

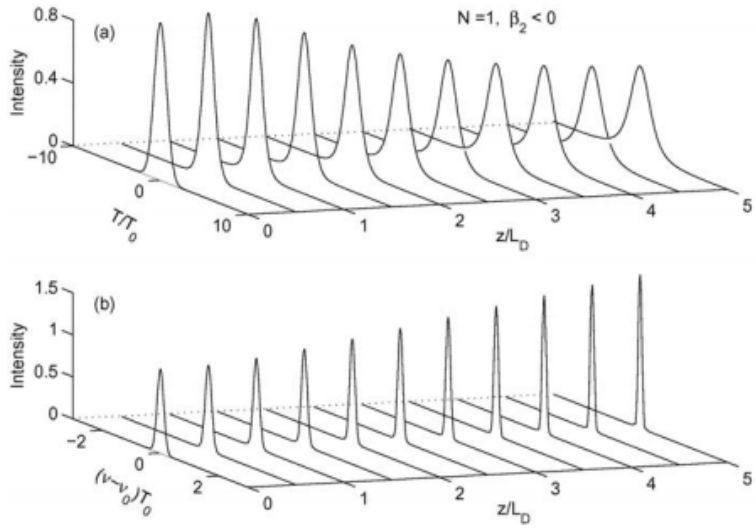

Figure 1.4: Evolution of (a): pulse shapes and (b): optical spectra over a distance of 5LD for an initially unchirped the Gaussian pulse propagates in the anomalous-dispersion regime ($\beta_2 < 0$ of the fiber. **[106]**.

As indicated by Zakharov and Shabat **[114]**, a continuous wave with (1+1)D with a sech profile and a prescribed relation between its width and its power can propagate as fundamental spatial soliton in a homogeneous Kerr medium, with exact balance between the Kerr effect and the diffraction. However, in the case with two transverse dimensions (2+1)D, the situation is quite different, marked by collapse; there is therefore no spatial Kerr soliton at (2+1)D. For an understanding of the evolution of the optical field in the optical system and consequently the resulting phenomena, it is necessary to consider the theory of electromagnetic wave propagation in dispersive nonlinear media. Like all electromagnetic phenomena, the propagation of optical fields in optical fibers is governed by Maxwell's equations. From the Maxwell's equations, the evolution of optical field inside the optical system, where the input electric field is assumed to propagate in the $+z$-direction and is polarized in the X-direction is described by the nonlinear Schrödinger (NLS) equation written as

$$i\frac{\partial\psi}{\partial z} + \eta\Delta\psi + \kappa|\psi|^2\psi = 0, \tag{1.5}$$

where η is the dispersion coefficient, κ in the nonlinear coefficient, $\psi(z, X)$ is the wave envelope,

$X = x_1, ..., x_d$, $\Delta = \sum_{l=1}^{d} \frac{\partial^2}{\partial x_l^2}$, and $d = 1$ or 2.

There is self-confinement of impulsions when $\kappa > 0$, and the opposite phenomenon when $\kappa < 0$. When $\kappa > 0$, Eq. (1.5) admits solutions which become singular after a finite time when $d = 2$ (critical case), or $d > 2$ (super-critical case). For $d = 1$, Eq. (1.5) is integrable and gives soliton solutions which result from the exact balance between diffraction and nonlinearity. For $d = 2$, in order to avoid the singularity in the wave function and thus, limit the risk of collapse of the pulses, it has been shown that the presence of a damping due to inhomogeneities in the structure of the fields and in the particle distribution function **[115]**, either by saturation of nonlinearity **[116]**, partial coherence **[117]**, or non-paraxiality of small beams **[116]** can be considered.

Therefore, in (2+1)D systems, the diffraction is not strong enough to overcome self-phase modulation. It then becomes difficult to find spatial solitons with (2+1)D stable over long distances **[118, 119]**. The disturbance effects which can modify or stop the "collapse" are dissipation, normal dispersion and the saturation of nonlinearity **[120]**. The most used alternative to obtain the formation of space solitons with more than one dimension, is to use dissipative media where the presence of gains and nonlinear losses allows to have more stable solitons and thus avoid the wave collapse.

1.3.3 Dissipative optical soliton

Observing nature, we can realize that "particles" are always submerged into dissipative media, which feed their continuous motion. The so-called conservative or Hamiltonian systems provide convenient models for basic mathematical analysis of simple motion, but they fail to describe real dynamics in longer time scales. In fact, for conservative Kerr media, the central issue is the problem of collapse. A cubic-quintic medium that features strong saturation of the Kerr effect could avoid collapse and provide confinement in several dimensions **[121, 122]**.

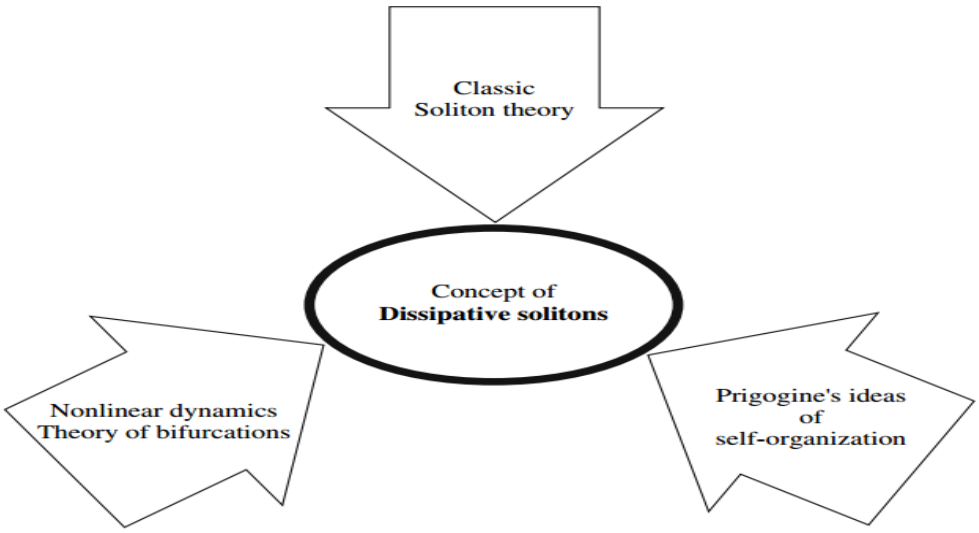

Figure 1.5: Three sources and three component parts of the concept of dissipative solitons.

Dissipative nonlinear systems suggest an interesting alternative. The additional balance between gain and loss in dissipative systems provides the necessary for the generation of stable dissipative soliton. Rosanov has showed that dissipative optical systems can admit solitons in one, two, and three dimensions **[123]**. These formations are stable during propagation, provided the system parameters are chosen in specific regions. Hence, the term "dissipative soliton" is used as the one that covers the majority of relevant phenomena in optics, biology and medicine. As a fuller explanation, it means "soliton in a dissipative system", where "dissipative system" is to be understood in Prigogine's sense as a sub-system with an external pump of energy, rather than a system with losses only. An optical laser is one of the examples of such subsystem in optics **[124]**. There is a significant difference between solitons in Hamiltonian systems and in dissipative ones. In Hamiltonian systems, soliton solutions appear as a result of a balance between diffraction (or dispersion) and nonlinearity. Diffraction spreads the beam, while nonlinearity focuses it and makes it narrower. In additional to the balance between diffraction/diffusion and nonlinearity, in systems with gain and loss, in order to have stationary solutions, gain and loss must be balanced in the first place. The two balances result in solutions which are fixed. The shape, amplitude and the width are all fixed and depend on the parameters of the equation.

The complex Ginzburg-Landau (CGL) equation was originally developed in the context of particle physics as a model of super-conductivity, and has since been widely used as a prototypical model for nonlinear wave propagation and pattern formation **[125, 126]**. The CGL equation may be viewed as an extension of the NLS equation. Accordingly, it can describe a broad range of behaviors suggested by the NLS dynamics, ranging from chaos and pattern formation **[127, 128]** to dissipative solitons **[129]**. In the paraxial wave approximation, the normalized propagation equation used to describe passively mode-locked lasers reads **[130]**

$$i\frac{\partial\psi}{\partial t}+\frac{D}{2}\frac{\partial^2\psi}{\partial x^2}+|\psi|^2\psi+\nu|\psi|^4\psi=i(\delta\psi+\varepsilon|\psi|^2\psi+\beta\frac{\partial^2\psi}{\partial x^2}+\mu|\psi|^4\psi), \tag{1.6}$$

in which t is the distance traveled inside the cavity, x is the retarded time, ψ is the normalized envelope of the field, D is the group velocity dispersion coefficient, with $D=\pm$, depending on whether the group velocity dispersion (GVD) is anomalous or normal, respectively, δ is the linear gain-loss coefficient, $i\beta\frac{\partial^2\psi}{\partial x^2}$ accounts for spectral filtering or linear parabolic gain ($\beta>0$), $\varepsilon|\psi|^2\psi$ represents the nonlinear gain (which arises, for example, from saturable absorption), the term with μ represents, if negative, the saturation of the nonlinear gain, while the one with ν corresponds, also if negative, to the saturation of the nonlinear refractive index. Since this cannot be solved exactly, depending on the field of application, a number of treatments have been adopted, namely the method of moments **[131]**, method of collective coordinates **[132-134]**, time-dependent variational method **[135]**, effective-particle method **[136]**, averaged Lagrangian description **[137]**, just to name a few.

In practice, one uses a trial function with a few parameters which depend on t. A suitable choice of trial function can be deduced from the general symmetries of the problem, and from results of experiments and numerical simulations. For example, consider a second trial function which is a combination of Gaussian and super-Gaussian types of functions **[130]**:

$$\psi(x,t)=A\exp(-\frac{x^2}{W^2}-\frac{x^4}{4mW^4}+iCx^2), \tag{1.7}$$

where $A(t)$, $W(t)$ and $C(t)$ are the amplitude, width and the chirp parameter. The constant m

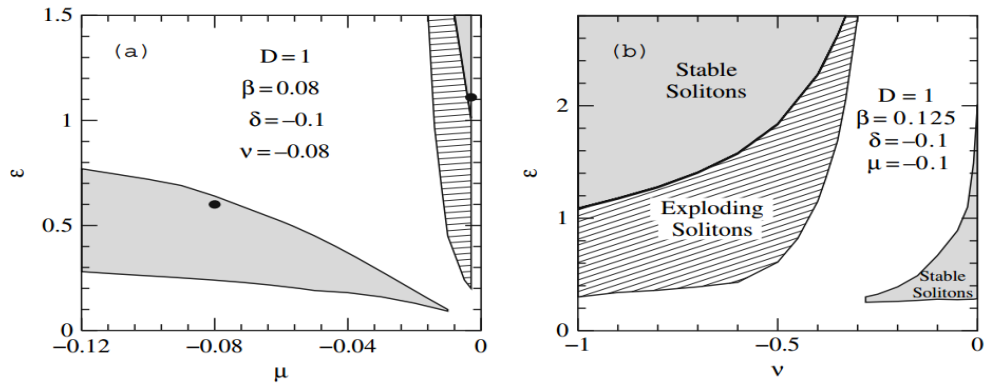

Figure 1.6: Regions of existence of the two types of solitons (gray) in (a) (ε, μ) and (b) (ε, ν) plane. In each case, the two separate regions are quite distinct. Parameters are shown in the plot. The hatched region corresponds to exploding solitons **[130]**.

can be chosen arbitrarily, but it is independent of t. The results of numerical simulations of the CGLE Eq. (1.6) is shown in Fig. 1.6. The gray regions correspond to stable stationary solitons while the hatched region corresponds to exploding solitons. Thus, explosive solitons in a simple model will be in the area of stable fixed points. The results for the exact field amplitude and phase profiles of the solutions for each region of existence of stable solitons are presented in Fig. 1.7. The solid lines represent the field amplitude of the solitons, while the dashed lines are their phase profiles. The upper curves (a) in Fig. 1.7 correspond to the upper-right thick black point in Fig. 1.6 (a) and vice versa: the lower curves (b) in Fig. 1.7 correspond to the lower-left thick black point. There are some obvious differences in the energies, widths and amplitudes of the two solitons. However, the most visible qualitative difference is in the soliton chirp. The phase profiles clearly show that the chirps in the two cases are of opposite signs. Due to this difference, the energy flows from the inside to the outside of the soliton in the first case while it flows inwards in the second case.

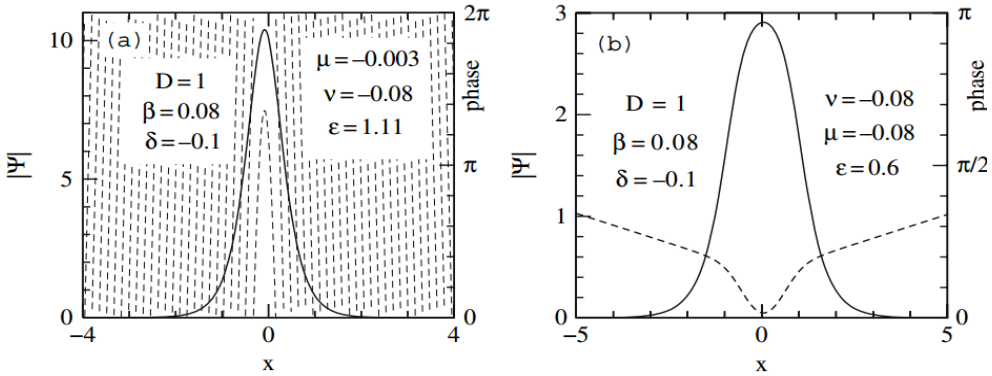

Figure 1.7: Exact soliton profiles (solid lines) of two examples in the (a) upper and (b) lower regions in Fig. 1.6 (b). They are marked by thick black dots in Fig. 1.6 (b). Dashed lines show their corresponding phase profiles **[130]**.

1.4 Overview on lasers

Lasers are devices that generate or amplify coherent radiation at frequencies in the infrared, visible, or ultraviolet regions of the electromagnetic spectrum **[138]**. The *laser* has become an important instrument, not only in physical research but for almost all fields of everyday life. The word laser has become a well-recognized word in everyday language, and is derived from its predecessor, the Maser, the acronym "*maser*" meaning "*microwave amplification by stimulated emission of radiation*". The laser is based on identical physical principles and is an optical maser, the abbreviation "*laser*" meaning "*light amplification by stimulated emission of radiation*". We basically regard a laser as a source of an intensive coherent light field.

From an electronics-engineering viewpoint, the developments that followed the operation of the first ruby laser in 1960 suddenly pushed the upper limit of coherent electronics from the millimeter-wave range, using microwave tubes and transistors, out to include the submillimeter, infrared, visible, and ultraviolet spectral regions (and soft X-ray lasers are now on the horizon). All the familiar functions of coherent signal generation, amplification, modulation, information transmission, and detection are now possible at frequencies up to a million times higher, or wavelengths down to a million times shorter, than previously. But it has also become possible

for engineers and scientists, in the fields of technology ranging from microbiology to auto manufacture, to perform an almost unlimited variety of new and unexpected functions made possible by the short wavelengths, high powers, ultrashort pulse widths, and other unique characteristics of these laser devices **[138]**.

The laser has historical roots in high-frequency and gas discharge physics. It was known from the maser that it was possible to construct an amplifier and oscillator for electromagnetic radiation with an inverted molecular or atomic system. In a famous publication A. Schawlow (1921-1999, nobel prize 1981) and C. Townes **[139]** (1915-, nobel prize 1964) had theoretically predicted the properties of an "optical maser", later called a laser.

1.4.1 What is a laser

Lasers, broadly speaking, are devices that generate or amplify light, just as transistors and vacuum tubes generate and amplify electronic signals at audio, radio, or microwave frequencies. Lasers come in a great variety of forms, using many different laser materials, many different atomic systems, and many different kinds of pumping or excitation techniques.

Most laser are constructed of three important elements:

(i) a laser medium (active medium) consisting of an appropriate collection of atoms, molecules, ions, or in some instances a semiconducting crystal. Also call gain material, it is the location of the energy states which participate in stimulated emission. The material can be:

Solid (Nd: YAG, ruby, GGG, GSGG, alexandrite, emerald, Cr: saphire, Ti: sapphir, AlGaAs/GaAs, etc.): crystals and glasses doped by special ions (solid-state lasers); the active medium of a solid-state laser is normally a rod with a circular cross-section, doped with special ions that play the role of active centres. A classical example of a solid lasing medium is a ruby rod 3 to 20 mm in diameter and 5 to 30 cm long. Ruby is crystalline alumina (Al_2O_3) doped with chromium ions (from 0.05 to 0.5$^0/_0$). Note that it is this impurity (dopant) that gives

ruby its typical colour (from pink to deep red) **[140]**. Those lasers are used, for example, as pump lasers for the excitation of tunable laser systems or for materials processing that demands intensive laser radiation with good spatial coherence properties.

Liquid (dye, chelate, etc.): Especially for wavelengths of 550-630 nm, the dyes laser is still a tunable light source without competition. In this range of spectrum, our color sensual perception changes quickly from green to yellow to red. For this reason, the light of dye lasers is superior to all solid-state lasers so far developed with regard to aesthetic and emotional quality. They are organic molecules with a carbon-carbon double bound. The dye molecules are dissolved (in alcohol or, if they ejected from nozzle space, in liquids with higher viscosity such as glycol). The electronic states have a vibration-rotation fine structure that is broadened to continuous bands because of the interaction with the solvent, similar to the vibronic ions. After absorption, the molecules relax rapidly to the upper band edge where the laser emission takes place. In complete analogy to two-electron atoms like helium, there are a singlet and a triplet system in dye molecules **[141]**, only the transitions between them (intercombination lines) are not as strongly suppressed. The lifetime of the triplet states is very long, however, so that the molecules accumulate there after several absorption-emission cycles and no longer take part in the laser process.

Gas (Krypton, argon, nitrogen, helium-neon, CO_2, KrF, $XeCl$, etc.) or plasma ($X-ray$, free-electron, etc.): gases and mixtures of gases (gas lasers); the active medium of a gas laser is a mixture of several gases, atoms or molecules of one of them are active centres while other gaseous components serve to produce population inversion on the lasing levels of the active centres. One possible mixture, for instance, is helium and neon (neon atoms are active centres). This mixture is placed in a gas discharge tube at low pressure: neon at a pressure of about 10 Pa and helium at about 100 Pa. Excitation in gas lasers is realized in the simplest manner by means of electric discharge in the active medium (typically glow discharge). In this case, the

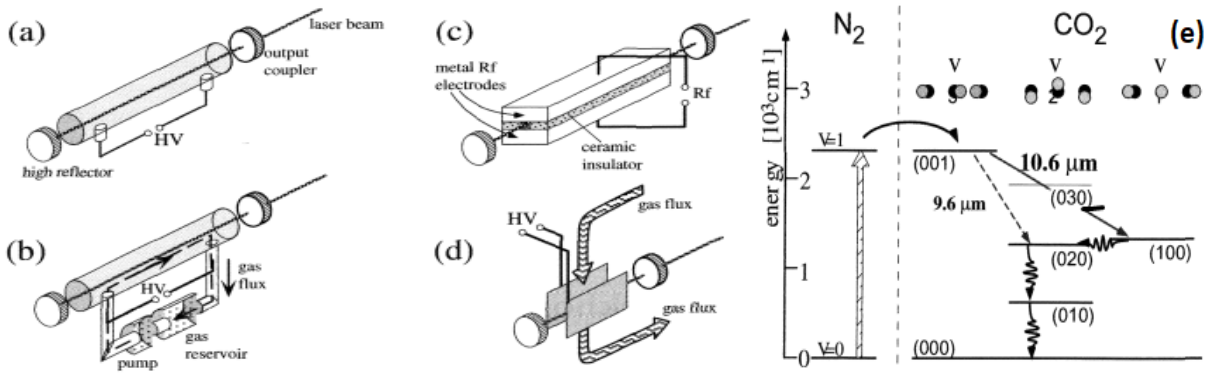

Figure 1.8: (a)-(d) are important configurations of CO_2 lasers, and (e) is the transitions relevant for the CO_2 laser **[141, 142]**.

energy of excitation is transferred to active centres as a result of collisions with particles in the gas discharge plasma **[140]**.

The carbon monoxide and dioxide CO_2 laser is the most important examples of the molecular gas lasers, and one of the most powerful lasers in general and thus plays an important role for material processing with lasers **[141, 142]**. The CO_2 lasers are excited by a discharge. They are most powerful and robust of all laser types. It makes available a high and focusable energy density that is highly favorable for contactless material processing and laser machining. Figures 1.8(a)-(d) show the important configurations of CO_2 lasers, and the relevant transitions. The conventional laser (see Fig. 1.8(a)) is operated with a sealed tube and longitudinal discharge. To increase the output power, a longitudinal gas flow (see Fig. 1.8(b)) or a radio-frequency waveguide laser (see Fig. 1.8(c)) can be used. The highest power can be achieved if the gas flow as well as the discharge are operated transversely to the laser beam (transversely excited, TE-laser) (see Fig. 1.8(d)). Figure 1.8(e) presents the molecular states involved in the laser process of the CO_2 laser. Asymmetric (V_1) and antisymmetric (V_3) stretching vibration as well as a bending vibration (V_2). Vibrational quantum states of the CO_2 molecule are identified by quantum numbers (V_1, V_2, V_3).

(ii) A pumping process to excite these atoms (molecules, etc.) into higher quantum-mechanical

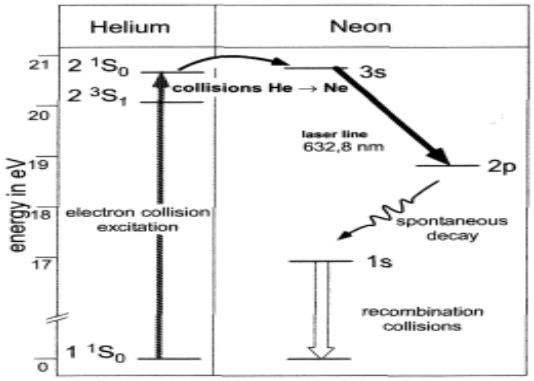

Figure 1.9: Energy levels of He and Ne atoms with the most prominent optical transition at 632.2nm. For nomenclature, the spectroscopic terms are used. For the energy levels, the lifetimes are given as well **[141]**.

energy levels (this system provides excitation of active centres, and inverted population of lasing levels builds up). The pumping source provides the energy to set up the energy states so that stimulated emission can occur (see Fig. 1.9). In Fig. 1.9, the helium-neon laser obtains its gain from an inversion in the metastable atomic excitations of the Ne atom (the luminescence of Ne atoms is also known due to the proverbial neon tubes). The Ne atoms are excited not directly by the discharge but by energy transfer from He atoms, which are excited to the metastable $^1S_0$ and $^3S_1$ levels by electron impact. The Ne atom has nearly energy levels so that an efficient energy transfer is enabled by resonant impact. Here, the excitation and the laser transition are split up into two different atomic systems, which is helpful for the realization of the desirable four-level system, though there is a problem at the lower laser level of the Ne atoms, which is metastable as well and cannot be emptied by radiative decay. In a narrow discharge tube, collisions with the wall lead to efficient depopulation of the lower laser level. There is, however, another possibility to excite neon atoms to level 3S: resonance transfer of energy from excited helium atoms to Ne atoms in the ground state, whereby the helium atom is de-excited while the neon atom undergoes a transition from the ground state to one of the excited levels. Taking into account collisions both with electrons and with excited helium atoms, level 3S must be

populated with higher probability than level 2P; hence, levels 2P and 3S in *Ne* atoms must be inversely populated.

The list of successful laser-pumping methods that have been demonstrated to date includes the following **[138, 142]**:

• Gas discharges, both dc, and pulsed, including glow discharges, hollow cathodes, arc discharges, and many kinds of pulsed axial and transverse discharges, and involving both direct electron excitation and two-stage collision pumping.

• Optical pumping, using flashlamps, arc lamps (pulsed or dc), tungsten lamps, semiconductor LEDs, explosions and exploding wires, other lasers, and even gas flames and direct sunlight.

• Chemical reactions, including chemical mixing, flash photolysis, and direct laser action in flames. It is instructive to realize that the combustion of one kg of fuel can produce enough excited molecules to yield several hundred kilojoules of laser output. A chemical laser burning one kg per second, especially if combined with a supersonic expansion nozzle, can thus provide several hundred kW of cw laser output from what becomes essentially a small "jet-engine laser."

• Direct electrical pumping, including high-voltage electron beams directed into high-pressure gas cells, and direct current injection into semi- conductor injection lasers.

• Nuclear pumping of gases by nuclear-fission fragments, when a gas laser tube is placed in close proximity to a nuclear reactor.

• Supersonic expansion of gases, usually preheated by chemical reaction or electrical discharge, through supersonic expansion nozzles, to create the so-called gasdynamic lasers.

• Plasma pumping in hot dense plasmas, created by plasma pinches, focused high-power laser pulses, or electrical pulses. There are also widely believed rumors that X-ray laser action has in fact been demonstrated in a rod of some laser material pumped by the ultimate high-energy pump source, the explosion of a nuclear bomb.

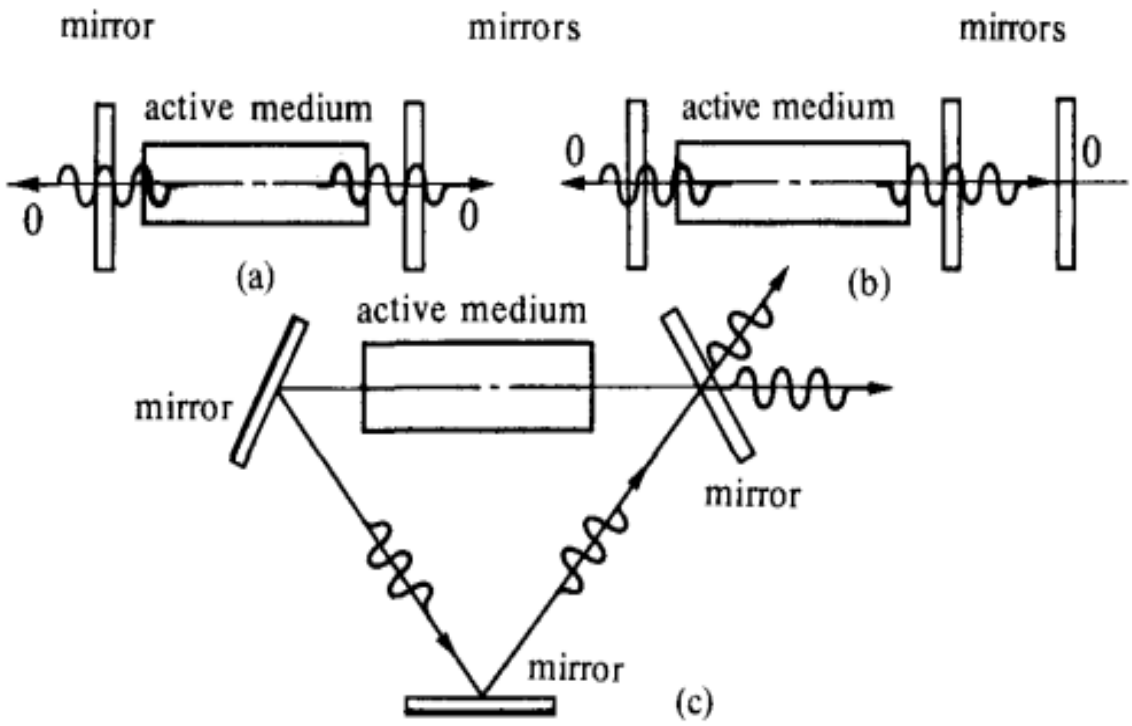

Figure 1.10: examples of optical resonators **[138]**.

(iii) An optical resonator is realized as a system of mirrors. In a more general sense, it includes not only a system of mirrors but also everything inside this system, including the active medium. Figure 1.10 schematically shows examples of optical resonators: (a)-a simple linear resonator; (b)-a coupled linear resonator; (c)-a ring resonator (00 - the optical axis of the laser, fixed in space by the system of resonator mirrors). In Fig. 1.10 suitable optical feedback elements "the optical resonator (together with some additional elements)" that allow a beam of radiation to either pass once through the laser medium (as in a laser amplifier) or bounce back and forth repeatedly through the laser medium (as in a laser oscillator). The resonant cavity provides a generative path for photons. In essence, the functions of the resonant cavity are to: 1) physically shorten the laser, and 2) tailor the profile of the electromagnetic mode **[142]**.

Mirrors may be coated with dielectric or metal layers. At least one of the mirrors must be partially transparent with respect to the emitted radiation; in the case of metal coating, the problem is solved by making a hole at the center of the mirror. So, by singles out a direction in

space for which the losses are minimized and the condition of generation is satisfied, the role of the optical resonator is to create a selectivity for photon states.

1.4.2 Laser model and Maxwell-Bloch equations in a ring resonator

The objective of this subsection is to describe the complete cavity-atom equations of motion for the laser, supposing that only a single cavity mode is significantly excited, as can often happen in real laser systems **[138, 140-142]**.

In a laser amplifier, the input signal will thus be amplified by the stimulated transitions. At the same time as can be see in Fig. 1.8(e) and Fig. 1.9, a small amount of the spontaneous emission (in essence, that portion traveling exactly parallel to the applied signal) will be added to the output signal by the spontaneous emission process. The spontaneous emission in this situation thus acts essentially like a small additive amplifier noise source insofar as the stimulated amplification process is concerned. Unless the applied signal is very small, approaching the noise limit of the laser amplifier, the added spontaneous-emission noise can normally be ignored in discussions of the basic stimulated amplification process **[141]**. There are actually two quite separate kinds of downward relaxation that occur in most atomic systems.

One mechanism is *radiative relaxation*, which is to say *spontaneous emission* or fluorescent radiation. It has been shown that atoms (or ion, or molecules) have quantum-mechanical energy levels; that atoms can be pumped or excited up into higher energy levels by various methods, emitting radiation at characteristic transition frequencies in the process. After being excited into upper energy levels, the atoms soon give up their excess energy by dropping down to lower energy levels, emitting spontaneous electromagnetic radiation in the process.

The other mechanism is what is commonly called the *stimulated* (upward and downward) transitions, that are the essential processes in all kinds of laser and maser action. During the process in which atoms spontaneously drop from an upper to a lower level while emitting elec-

tromagnetic and/or acoustic radiation at the transition frequency, such spontaneously emitted radiation has all the statistical properties of narrowly bandlimited gaussian noise, usually refer to an incoherent emission **[1, 15, 16, 138]**.

A real atomic system will, of course, have a very large number of energy levels E_i, with different time-varying populations $N_i(t)$. Although rate equations look complex, they are actually simple to set up. Writing them requires no more than careful accounting of the various state population **[1, 15-22, 138-143]**.

The laser equations of motion used in the scientific and engineering literature come in several slightly different forms and degrees of approximation. The most successful theoretical approach based on the "neoclassical formulation of laser theory", Classical Electron scillator model (CEO) to describe how the spatiotemporal dynamics emerges in large-aperture lasers is given by the Maxwell-Bloch (MB) equation **[138-143]**. Laser is a system where the number of photons is much larger than one. Thus a semi-classical treatment of the electromagnetic field inside the cavity, through the Maxwell equations, has been developed by Lamb **[43]** and independently by Haken **[46]**. The semi-classical laser theory ignores the quantum-mechanical nature of the electromagnetic field, and the amplifying medium is modeled quantum mechanically, as a collection of two-level atoms through the Bloch equations. The called "neoclassical formulation of laser theory" is based on a series of theoretical papers by Jaynes, since they represent the simplest form of semi-classical quantum theory (i.e., the atoms are quantized, but the electromagnetic field is not) as applied to a single cavity mode and a two-level atomic system. The MB equation connect the cavity mode amplitude $\mathbf{E}$, the atomic polarization amplitude $\mathbf{P}$, and the population difference $\Delta N(t)$ relevant to that particular cavity mode **[1, 15-22, 138-143]**.

These equations consist of the cavity equation, the atomic polarization equation, and the population difference equation **[138, 144]**

$$\frac{\partial^2 \mathbf{E}}{\partial t^2} = -\mu_0 c^2 \frac{\partial^2 \mathbf{P}}{\partial t^2} + c^2 \nabla^2 \mathbf{E} - \kappa \frac{\partial \mathbf{E}}{\partial t}, \tag{1.8a}$$

$$\frac{\partial^2 \mathbf{P}}{\partial t^2} = -\gamma_\perp \frac{\partial \mathbf{P}}{\partial t} - w_a^2 \mathbf{P} - gD\mathbf{E}, \tag{1.8b}$$

$$\frac{\partial D}{\partial t} = -\gamma_\parallel (D - D_0) + \frac{2}{\hbar w}\left(\mathbf{E}.\frac{\partial \mathbf{P}}{\partial t}\right). \tag{1.8c}$$

The used symbols have the following meaning:

-$\nabla = \frac{\partial}{\partial x}\boldsymbol{i} + \frac{\partial}{\partial y}\boldsymbol{j} + \frac{\partial}{\partial z}\boldsymbol{k}$ and $\nabla^2 = \frac{\partial^2}{\partial x^2} + \frac{\partial^2}{\partial y^2} + \frac{\partial^2}{\partial z^2}$, with $\boldsymbol{i}$, $\boldsymbol{j}$ and $\boldsymbol{k}$ the spatial directions;

- $\mathbf{E}$ is the envelope of the electric field;

- $\mathbf{P}$ is the envelope variable of the atomic polarization;

- $D \equiv \Delta N$ is the population inversion;

- μ_0 is the magnetic susceptibility;

- c is the velocity of light;

- $\gamma_\perp$ and $\gamma_\parallel$ are the relaxation rates for the polarization and the population inversion, respectively;

- κ is the cavity damping coefficient;

- $\hbar$ is Planck's constant;

- w is the electric field frequency;

- w_a the atomic frequency;

- g is the coupling constant between the electric field and the population inversion;

- D_0 is the pumping term;

- Assuming that the electric field frequency w is very close to the atomic frequency w_a, it follows that $\hbar w$ is the energy gap between the two atomic levels.

These three equations are used as the starting point for a great many laser analyses in the literature. This particularly simple form for the ideal two-level case with fixed total population turns out to be very useful and important for describing a great variety of laser and maser phenomena.

1.5 Dissipative solitons in physical systems

Dissipative soliton (DS) is a localized structure which exists for an extended period of time, even though parts of the structure experience gain and loss of energy and/or mass. This "structure" could be a profile of light intensity, temperature, magnetic field, etc. These solitons exist in "open" systems which are far from equilibrium. Thus, energy and matter can flow into the system through its boundaries. The structure exists indefinitely in time, as long as the parameters in the system stay constant. It may evolve (i.e. change its shape periodically or otherwise) but it disappears when the source of energy or matter is switched off, or if the parameters of the system move outside the possible range of existence of the soliton **[145-147]**.

In contrast to solitons in conservative systems, solitons in systems far from equilibrium are dynamical objects that have non-trivial internal energy flows. Since they are produced by dissipative systems, they depend strongly on an energy supply from an external source. Even if it is a stationary object, a DS continuously redistributes energy between its parts. A pump of energy is essential, and this means that the structures are defined by the rules of the system (gain, loss, dispersion, nonlinearity, etc.), rather than by the initial conditions **[145-147]**. Stationary solitons (pulses, fronts, etc.) can form where the overall gain and loss are balanced. These structures will typically appear in biochemical, optical and thermal systems, as they are "generic" and do not require particular formations to create them.

Throughout the definition of DS, we are dealing with an infinite-dimensional dynamical system governed by the cubic-quintic complex Ginzburg-Landau (CQ-CGL) equation which in optics has been widely used to describe the pulsed operation of passively mode-locked lasers and all-optical long-haul soliton transmission lines. Generally, the CQ-CGL equation has a wide range of applications in various branches of physics, chemistry and biology. An extensive list of applications can be found in the review paper by Aranson and Kramer **[148]**. This enormous sphere of knowledge has been dubbed "The world of the Ginzburg-Landau equation" **[148]**.

The CQ-CGL equation has so many different types of solutions, this area of expertise is a whole world by itself.

1.5.1 Scalar CGL model

Dissipative solitons (DSs) have been found in a variety of systems, including chemical reactions**[149, 150]**, gas discharges **[151]**, and fluids **[68]**. They are also found in optical cavities due to the interplay of different effects, such as diffraction, nonlinearity, driving, and dissipation **[152-156]**. Instead, a cavity soliton is unique once the parameters of the system have been fixed. This fact makes these structures potentially useful in optical (i.e., fast and spatially dense) storage and processing of information **[154,156-159]**. An optical cavity filled with a nonlinear Kerr medium can be described by the model introduced by Lugiato and Lefever **[160]**. This prototype model, obtained by averaging the dependence of the field along the propagation direction, was first introduced to study pattern formation in this system. Later studies showed that this model also exhibits DSs in some parameter regions **[161, 162]**. In the paraxial limit, after suitably rescaling the variables, the dynamics of the intra-cavity slowly varying amplitude of the electromagnetic field $E(\mathbf{x}, t)$, where $\mathbf{x} = (x, y)$ is the plane transverse to the propagation direction, is given by

$$\frac{\partial E}{\partial t} = -\left(1 + i\theta\right) E + i\nabla^2 E + E_I + i|E|^2 E. \tag{1.9}$$

The first term on the right-hand side describes cavity losses (which make the system dissipative), E_I is the input field, θ is the cavity detuning with respect to E_I, and $\nabla^2 = \frac{\partial^2}{\partial x^2} + \frac{\partial^2}{\partial y^2}$ is the transverse Laplacian which models diffraction. The sign of the cubic term indicates the so-called self-focusing case.

When neither loss nor input field is present, the intra-cavity field can be rescaled to $E \to Ee^{i\theta t}$ to remove the detuning term and Eq. (1.9) becomes the nonlinear Schrödinger equation (NLSE). For the NLS equation in two spatial dimensions, an initial condition with sufficient

energy collapses, so energy accumulates at a point in space, leading to the divergence of the solution at a finite time **[163]**. Dissipation, such as that originating from the cavity losses, can prevent this collapse **[164]**. In any case, in the parameter region in which DSs are stable, their dynamics is closely related to the collapse regime. In this system, the above mechanism, which combines collapse and cavity losses, is also responsible for various instabilities arising in regular patterns which lead to complex spatiotemporal dynamical behavior, including the existence of optical turbulence **[165]**. The stability of this has been obtained using the modulational instability (MI), and showed the existence of stable DSs that appear when suitable (localized) transient perturbations are applied.

In a mode-locked laser, the existence of stable soliton pairs was first predicted in 1997 **[166]**, by using a CQ-CGL equation model, which is a generic equation that has been used in many areas of nonlinear physics. In this context, the CQ-CGL equation takes the form of a normalized propagation equation, as follows:

$$\frac{\partial E}{\partial z} + \frac{D}{2}\frac{\partial^2 E}{\partial t^2} + |E|^2 E + \nu |E|^4 E = i(\delta E + \beta \frac{\partial^2 E}{\partial t^2} + \varepsilon |E|^2 E + \mu |E|^4 E), \tag{1.10}$$

where z is the normalized distance of propagation, t is the time in the moving pulse frame, and E is the normalized envelope of the electric field. The left-hand side of Eq. (1.10) contains the conservative terms, including chromatic dispersion (with coefficient D), the nonlinear Kerr effect, and its possible saturation, if ν is taken as negative. In the normalized form, the dispersion coefficient is taken to be $D = +1$ for propagation in anomalous dispersive medium, and $D = -1$ in the case of normal dispersion. The right-hand side of Eq.(1.10) contains respectively the linear loss term, with a negative coefficient δ, the nonlinear gain, with a positive coefficient ε, which is required to favor pulses over continuous waves, a Gaussian spectral filter with positive coefficient β, and a saturation of the nonlinear gain term which is required for the stabilization of the amplitude of pulses and is associated with a negative coefficient μ.

1.5.2 The vector CGL model for laser emission from wide-aperture resonators

The previous described model is scalar. The scalar CGL equation is considered as a paradigm model for the qualitative description of general nonlinear oscillatory media **[161, 162, 166]**. The vector CGL equation **[78, 79]** plays the same role when the order parameter is of vector character, as is the case for the electromagnetic field when the polarization is not fixed. For example, the vector CGL equation is an appropriate model for laser emission from wide-aperture resonators close to the lasing threshold **[167]** in the absence of polarization-selecting cavity features. For systems where the relevant unstable mode is of vectorial character, a CGL equation is generalized to the vector CGL equation **[78]**

$$\frac{\partial \mathbf{E}}{\partial z} = \mathbf{E} + (1 + i\alpha)\,\nabla^2\mathbf{E} - (1 + i\beta)\left[(\mathbf{E}.\mathbf{E}^*)\,\mathbf{E} + \frac{1}{2}(\gamma - 1)\,(\mathbf{E}.\mathbf{E})\,\mathbf{E}^*\right]. \tag{1.11}$$

In the simplest case, the amplitude $\mathbf{E}$ has two complex components. This is precisely the case of optical systems, for which, $\mathbf{E} = (E_x, E_y)$ describe the complex slowly varying amplitude of the electric field, where E_x and E_y are the cartesian components. The right and left circularly polarized components $\mathbf{E} = (E_+, E_-)$ are related to them via the relations $\mathbf{E}_x = (E_+ + E_-)/\sqrt{2}$ and $\mathbf{E}_y = (E_+ - E_-)/i\sqrt{2}$. In terms of the circular components, Eq. (1.11) reads **[168]**

$$\frac{\partial E_\pm}{\partial z} = E_\pm + (1 + i\alpha)\,\nabla^2 E_\pm - (1 + i\beta)\left(|E_\pm|^2 + \gamma|E_\mp|^2\right)E_\pm. \tag{1.12}$$

The coefficient γ, which in general can be complex, gives the coupling between the components. α is related to the strength of diffraction, and β to the nonlinear frequency detuning. Different kinds of localized structures **[78, 79, 169]** are present in the dynamic states of the two-dimensional vector CGL equation. These objects carry topological properties which endorse them with a characteristic stability and robustness. The qualitative behavior for the vector complex Ginzburg-Landau equation Eq. (1.12) for $|\gamma| < 1$ is rather different from the

one for $|\gamma| > 1$. In the second case the nonlinear competition between E_+ and E_- tends to favor one of them against the other, so that in regions where E_+ is developed, E_- generally vanishes, and vice versa **[169]**.

The principles that made possible the observation of stable temporal soliton "molecules" in mode-locked lasers could be extended to the spatiotemporal case, at least in principle. Theoretically, the CGL equation model can be easily extended to multi-dimensions with the inclusion of the transverse Laplacian operator to take into account spatial diffraction in the paraxial approximation.

1.5.3 Dissipative solitons of (D+1)-dimensional CQ-CGL equation

In the present context of this work about dissipative solitons, gain and loss are important, and this statement requires a further comment. Dissipative solitons derive their stability from a balanced flow of energy into and out of the soliton **[170-172]**. Their description requires generalized versions of the NLS equation, e.g., the complex Ginzburg-Landau (CGL) equation. Dissipative systems described by the CGL equation driven far from thermal equilibrium support solitonlike localized states, referred to as "dissipative solitons" **[173]**. Exact solutions for the cubic CGL equaion are available **[174-176]** but they are unstable. The problem of instabilities, leading to the collapse, and which depend on the number of space dimensions and strength of nonlinearity has attracted the attention, and the most straightforward modification of the model, which opens the way to the stable solitary pulse, is the introduction of the cubic-quintic (CQ) nonlinearity, with linear gain and cubic loss in the cubic CGL equation **[129]**. Dynamics of dissipative solitons can be described by a (D+1)-dimensional CQ-CGL equation **[91, 92, 166]**

$$i\frac{\partial E}{\partial z} + \Delta E + |E|^2 E - \nu |E|^4 E = \mathbf{Q}, \tag{1.13}$$

with

$$\mathbf{Q} = i\left[\delta E + \mu |E|^4 E + \varepsilon |E|^2 E + \beta \Delta E\right]. \tag{1.14}$$

The left-hand-side of Eq. (1.13) contains the conservative terms. E is the normalized complex envelope of the optical field, and $\Delta = r^{1-D}\frac{\partial}{\partial r}\left(r^{1-D}\frac{\partial E}{\partial r}\right)$ is the D-dimensional Laplacian describing beam diffraction and/or anomalous group velocity dispersion. Therefore, cubic and quintic nonlinearities have to be in opposite signs; i.e., parameter ν is negative. Dissipative terms are denoted by $\mathbf{Q}$ given in Eq. (1.14). Depending on the sign of the parameter δ, the first term is either linear gain or loss. $\beta > 0$ accounts for diffusive coefficient. The cubic and quintic gain-loss parameters are respectively ε and μ.

In optical transmission systems, the CGL equation has been the subject of considerable studies, and it has been found that, the diffusivity in the transverse plane is a necessary ingredient to get stable dissipative structures even in the lack of bandwidth limited gain.

1.6 Conclusion

In this chapter, we have pointed out some generalities about soliton, laser, dissipative solitons in laser systems and in optical fibers. It follows that the CGL model is promising equation to study the solitons of all optical device.

The introduction of a new concept dissipative soliton, has been a promising solution for optimizing performance and eliminating propagation losses. Although we have found that nonlinearity in optical systems is used to cope with dispersion in conservative system, the problem of collapse can also be solved using, the balance between gain and loss in dissipative optical system.

Rapid progress in ultrashort time laser technology has made it possible that, optical pulses with durations comparable to the carrier oscillation cycle can be generated. The propagation of such dissipative soliton is then affected by additional physical mechanisms like diffusion, cubic and quintic nonlinearities, where especially mixture effects, and nonlinear effects become important. These aspects of the problem will be investigated throughout this work. In the next

chapter, we will present the methodology of investigations used to obtain our results.

Chapter II

Model and methodology of investigations

2.1 Introduction

Nowadays, research in physics devotes much attention to nonlinear phenomena, in dissipative systems. What is the reason for this? In fact, most physical phenomena are intrinsically nonlinear, also, much systems in our environment is dissipative.

However, the mathematical techniques used in the study of these problems in lasers-cavities systems remained generally scalar.Considering a vectorial nature of the electric field, and after some assumptions, Gil **[78]** first developed a 3D vectorial Ginzburg-Landau (CGL) equation describing the behavior of the electric field in a dielectric. This model has been the subject of many works, but it is important to mention that at least all the obtained results showing the generation of pattern formation include the solution of defect type **[78, 79, 169]**.

For the laser system, the vector (3+1)D CQ-CGL equation, take into account the self-phase modulation (SPM), and the cross-phase modulation (XPM) that has not yet been investigated in relation with the dissipative solitons. This model equation has been derived for the first time in this thesis. Dissipative soliton stability depends crucially on the energy balance and exists as long as there is a continuous energy supply to the system.

Our main objective is to investigate new types of dissipative and nonlinear dynamics and thus, contribute to the understanding of 3D dissipative optical solitons. In order to accomplish our aims, we employ some analytical and numerical methods, which lead to many behaviors of the solutions. The numerical methods are used to consolidate the analytical results. In the first

part of this chapter, we derive the vector (3+1)D CQ-CGL equation in the physical context of laser cavity. In the second part, we give general information about our analytical methods and the third part is devoted to the presentation of numerical methods.

2.2 Derivation of the vector (3+1)-dimensional cubic-quintic complex Ginzburg-Landau equation

As presented in chapter I, a lasing medium consists of atoms or molecules, in which transition between two different energy levels occur. These transitions can be caused by light (absorption or stimulated emission), by collisions or by spontaneous emission. We use the model of two-level atoms, which is treated in a semiclassical way, i.e. the atoms are treated quantum-mechanically and the light field classically (quantum fluctuations are neglected). The geometry is that of the ring laser. Let us recall the MB equations (see Eqs.(1.8a)-(1.8c)) (for derivation, see **[138]**) described the ring lasers, and write as follows:

$$\frac{\partial^2 \mathbf{E}}{\partial t^2} = -\mu_0 c^2 \frac{\partial^2 \mathbf{P}}{\partial t^2} + c^2 \left[\nabla^2 \mathbf{E} - \nabla(\nabla.\mathbf{E})\right] - \kappa \frac{\partial \mathbf{E}}{\partial t}, \tag{2.1a}$$

$$\frac{\partial^2 \mathbf{P}}{\partial t^2} = -\gamma_\perp \frac{\partial \mathbf{P}}{\partial t} - w_a^2 \mathbf{P} - gD\mathbf{E}, \tag{2.1b}$$

$$\frac{\partial D}{\partial t} = -\gamma_\parallel (D - D_0) + \frac{2}{\hbar w}\left(\mathbf{E}.\frac{\partial \mathbf{P}}{\partial t}\right), \tag{2.1c}$$

To better understand the derivation of the vector (3+1)D CQ-CGL equation, a laborious nonlinear analysis has been fulfill by the use of the well known perturbative nonlinear analysis near the laser threshold; and the expansion multimodal method. In fact, it is not trivial to take into account the nonlinear effects inside the MB system Eqs. (2.1). The development multimodal method is one approach adopted for such analysis, which consider the contribution of all higher harmonics of the electric field and the polarization, proportional to a small parameter ϵ.

It would be advisable to start with the derivation of the vector (3+1)D CGL equation equation which accounts for the cubic nonlinearity and the coupled term.

2.2.1 Modeling of the laser vector (3+1)D cubic complex Ginzburg-Landau equation

i) Multimodal development method

The field of nonlinear optics is complex and encompasses myriads of interesting effects and practical applications. In spite of its richness, most of the effects can be described accurately with just a few equations. This introduction to nonlinear optics is therefore limited to a simple analysis of Maxwell's Bloch (MB) equations (Eq. (2.1)) which govern the interaction between the electric field and the material inside the laser cavity.

On a fundamental level, the origin of nonlinear response is related to anharmonic motion of bound electrons under the influence of an applied field. As a result, the total polarization $\mathbf{P}$ induced by electric dipoles is not linear in the electric field $\mathbf{E}$, but satisfies the more general relation **[112]**

$$\mathbf{P} = \varepsilon_0(\chi^1.\mathbf{E} + \chi^2 : \mathbf{EE} + \chi^3 : \mathbf{EEE} + ...), \tag{2.2}$$

where ε_0 is the vacuum permittivity and $\chi^{(l)}(l = 1, 2, 3, ...)$ is lth order susceptibility. In general, $\chi^{(l)}$ is a tensor of rank $l+1$. The linear susceptibility $\chi^{(1)}$ is the contribution to $\mathbf{P}$, representing the dominant contribution to $\chi^{(l)}(l > 1)$ that are responsible for such nonlinear effects as higher-harmonic generation and sum-frequency generation **[112]**.

However, as it is not trivial to take into account nonlinear effects in the MB system, the multimodal development method **[177]** is one of the approaches adapted to take into account nonlinear effects in the MB system Eqs. (2.1). To remind, it considers the contributions of all the higher harmonics of the fields and polarizations, proportional to a small parameter ϵ. This parameter can be linked to the intensity of the fundamental frequency mode ω. To apply this

theory, we must therefore seek solutions of the system (2.1) of the form

$$\mathbf{E} = \sum_{j=1}^{\infty} \in^{j} \sum_{n=-j}^{+j} \mathbf{E}_j^n(r) \exp(inwt),, \tag{2.3a}$$

$$\mathbf{P} = \sum_{j=1}^{\infty} \in^{j} \sum_{n=-j}^{+j} \mathbf{P}_j^n(r) \exp(inwt), \tag{2.3b}$$

$$D = \sum_{j=1}^{\infty} \in^{j} \sum_{n=-j}^{+j} D_j^n(r) \exp(inwt), \tag{2.3c}$$

under the conditions $\mathbf{E}_j^{-n} = (\mathbf{E}_j^n)^*$, $\mathbf{P}_j^{-n} = (\mathbf{P}_j^n)^*$, and $D_j^{-n} = (D_j^n)^*$. We assume a permanent electric field, that leads to $\forall j > 0$, $\mathbf{E}_j^0 = 0$.

We focus our study to the case of $\mathbf{E} = \mathbf{E}_1^1$, $D_1^0 = D_0$. In the presence of the intense field in the system, we have $D_0 << \frac{2}{\hbar w_a}\left(E \cdot \frac{\partial P}{\partial t}\right)$. Inserting the relation of $\mathbf{P}$ and D given from Eqs. (2.3a)-(2.3c) into Eqs. (2.1a)-(2.1c), it comes, for any $e^{inw_a t}$, the following relations:

From Eq. (2.2), the linear polarization takes the form

$$\mathbf{P}_1 = \mathbf{P}_1^1 = \frac{1}{\mu_0 c^2}\left(-1 + \frac{ik}{w_a}\right)\mathbf{E}_1^1, \tag{2.4}$$

and from Eqs. (2.1b) and (2.1c), it comes, for any $e^{inw_a t}$, the following relations:

$$\omega_a\left[\left(1-n^2\right)\omega_a + i\gamma_\perp\right]\left(\epsilon^1\mathbf{P}_1^n + \epsilon^2\mathbf{P}_2^n + ...\right) = -g\sum_{p+q=n}\left(\epsilon^1 D_1^q + \epsilon^2 D_2^q + ...\right)\left(\epsilon^1\mathbf{E}_1^p + \epsilon^2\mathbf{E}_2^p + ..\right) \tag{2.5a}$$

$$\left(\gamma_\parallel + in\omega_a\right)\left(\epsilon^1 D_1^n + \epsilon^2 D_2^n + ...\right) = \frac{2i}{\hbar}\sum_{p+q=n} q\left(\epsilon^1\mathbf{E}_1^p + \epsilon^2\mathbf{E}_2^p + ...\right)\left(\epsilon^1\mathbf{P}_1^q + \epsilon^2\mathbf{P}_2^q + ...\right), \tag{2.5b}$$

where p and q can take the negative values, and $p + q = n$. For any power of ϵ, solving these equation, we have obtained the following at different orders:

$$\epsilon^1, n = 0: \quad \mathbf{P}_1^0 = 0, \quad D_1^0 = D_0, \tag{2.6a}$$

$$\epsilon^1, n = 1: \quad \mathbf{P}_1^1 = \frac{1}{\mu_0 c^2}\left(-1 + \frac{ik}{w_a}\right)\mathbf{E}_1^1, \quad D_1^1 = 0, \tag{2.6b}$$

$$\epsilon^2, n = 0: \quad \mathbf{P}_2^0 = 0, \quad D_2^0 = \frac{2i}{\hbar\gamma_\parallel}\left(\mathbf{P}_1^1\mathbf{E}_1^{-1} - \mathbf{P}_1^{-1}\mathbf{E}_1^1\right), \tag{2.6c}$$

$$\epsilon^2, n=1: \quad \mathbf{P}_2^1 = \frac{ig}{\gamma_\perp w_a}\left(D_1^0 \mathbf{E}_1^1\right), \quad D_2^1 = 0, \tag{2.6d}$$

$$\epsilon^2, n=2: \quad \mathbf{P}_2^2 = 0, \quad D_2^2 = \frac{2i}{\hbar\left(\gamma_\parallel + 2iw_a\right)}\left(\mathbf{P}_1^1 \mathbf{E}_1^1\right), \tag{2.6e}$$

$$\epsilon^3, n=0: \quad \mathbf{P}_3^0 = 0, \quad D_3^0 = \frac{2i}{\hbar\gamma_\parallel}\left(\mathbf{P}_2^1 \mathbf{E}_1^{-1} - \mathbf{P}_2^{-1} \mathbf{E}_1^1\right), \tag{2.6f}$$

$$\epsilon^3, n=1: \quad \mathbf{P}_3^1 = \frac{ig}{\gamma_\perp w_a}\left(D_2^0 \mathbf{E}_1^1 + D_2^2 \mathbf{E}_1^{-1}\right), \qquad D_3^1 = 0, \tag{2.6g}$$

$$\epsilon^3, n=2: \quad \mathbf{P}_3^2 = 0, \quad D_3^2 = \frac{2i}{\hbar\left(\gamma_\parallel + 2iw_a\right)}\left(\mathbf{P}_2^1 \mathbf{E}_1^1\right), \tag{2.6h}$$

$$\epsilon^3, n=3: \quad \mathbf{P}_3^3 = \frac{ig}{\left(8w_a - 3i\gamma_\perp\right)}\left(D_2^2 \mathbf{E}_1^1\right), \quad D_3^3 = 0. \tag{2.6i}$$

The atomic polarization properties of the two-level atoms can be expanded as

$$\mathbf{P} = \epsilon \mathbf{P}_1 + \epsilon^2 \mathbf{P}_2 + \epsilon^3 \mathbf{P}_3, \tag{2.7}$$

Hence, From the MB equation, we see more inside the electric field and the laser cavity. $\mathbf{P}_1 = \mathbf{P}_1^1$ and $\mathbf{P}_2 = \mathbf{P}_2^1$ which describe the linear polarization. The interaction of a beam of light with a nonlinear optical medium is describe in terms of the nonlinear polarization $\mathbf{P}_3 = \mathbf{P}_3^1 + \mathbf{P}_3^3$. These result can also be rewrite as: $\mathbf{P}_3 = a(\mathbf{E}\cdot\mathbf{E}^*)\mathbf{E} + b(\mathbf{E}\cdot\mathbf{E})\mathbf{E}^* + d(\mathbf{E}\cdot\mathbf{E})\mathbf{E}$, with a, b and d are the complex parameters depending on the laser system parameters. We see that the nonlinear polarization consists of three contributions. These contributions have very different physical characters, since the first contribution has the vector nature of $\mathbf{E}$, whereas the second contribution has the vector nature of $\mathbf{E}$. The first contribution thus produces a nonlinear polarization with the same handedness as $\mathbf{E}$, whereas the second contribution produces a nonlinear polarization with the opposite handedness, and the third contribution describe the case of third-harmonic generation **[178]**. The origin of the different physical characters of the tree contributions to $\mathbf{P}_3$ can be understood in terms of the energy level diagrams shown in Figs. 2.1(a)- (c).

This result can help to describe the nonlinear refractive index of an isotropic material. The relative magnitude of the coefficients a, b and d depends upon the nature of the physical process that produces the optical nonlinearity **[178]**.

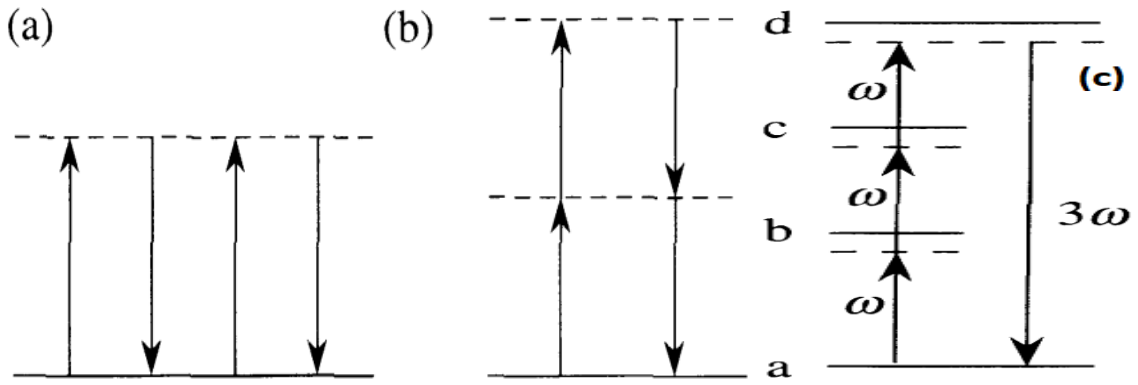

Figure 2.1: Diagrams (a) and (b) represent the resonant contributions to the nonlinear coefficients a and b, respectively. Diagram (c) represent the resonant nonlinear optical response describing third-harmonic generation **[178]**.

ii) Perturbative nonlinear analysis

Focussing ourself on the MB equations (Eqs. (2.1a)-(2.1c)) which is the starting point of this analysis, we assume that the traveling waves are lasing with frequency w_a and critical vector k_c=$\pm w_a/c$. In addition, the longitudinal direction $\mathbf{z}$ is selected by the geometry of the laser medium or the mirrors. The direction of propagation is given by $\mathbf{K}_c = k_c\mathbf{z}$, though a priori both directions of propagation are equiprobable. Once the atomic polarizability is known, the well-established perturbative nonlinear analysis is performed near the laser threshold by introducing a small parameter ($\epsilon << 1$) defined by **[78]**

$$D_0 = D_{OC} + \epsilon^2 \widetilde{D}_0, \tag{2.8}$$

where D_{OC} is a critical value given by **[78]**

$$D_{OC} = \frac{\kappa\gamma_\perp}{\mu_0 c^2 g}.$$

Now, the laser variable will also depend on two slow spatial and temporal scales, respectively,

$$X = \epsilon x, \qquad Y = \epsilon y, \tag{2.9a}$$

and

$$Z = \epsilon^2 z, \qquad T = \epsilon^2 t. \tag{2.9b}$$

Then, close enough to the laser threshold, we look for solutions ($\mathbf{E}$, $\mathbf{P}$, D) of Eqs. (2.6) in the form of a power series expansion in the small parameter ϵ as follows

$$\begin{pmatrix} \mathbf{E} \\ \partial_t \mathbf{E} \\ \mathbf{P} \\ \partial_t \mathbf{P} \\ D \end{pmatrix} = \begin{pmatrix} 0 \\ 0 \\ 0 \\ 0 \\ D_0 \end{pmatrix} + \epsilon \begin{pmatrix} \mathbf{E}_1 \\ \partial_t \mathbf{E}_1 \\ \mathbf{P}_1 \\ \partial_t \mathbf{P}_1 \\ D_1 \end{pmatrix} + \epsilon^2 \begin{pmatrix} \mathbf{E}_2 \\ \partial_t \mathbf{E}_2 \\ \mathbf{P}_2 \\ \partial_t \mathbf{P}_2 \\ D_2 \end{pmatrix} + ... \tag{2.10}$$

with

$$\begin{pmatrix} \mathbf{E}_1 \\ \partial_t \mathbf{E}_1 \\ \mathbf{P}_1 \\ \partial_t \mathbf{P}_1 \\ D_1 \end{pmatrix} = \begin{pmatrix} \mathbf{A} \\ i w_a \mathbf{A} \\ \frac{1}{\mu_0 c^2}(-1 + \frac{ik}{w_a})\mathbf{A} \\ \frac{i w_a}{\mu_0 c^2}(-1 + \frac{ik}{w_a})\mathbf{A} \\ 0 \end{pmatrix} \mathrm{e}^{i(w_a t - k_c z)} + c.c., \tag{2.11}$$

with $\mathbf{A} \perp \mathbf{Z}$, where $\mathbf{A}$ is slowly varying field amplitude in space and time. With the transformation of Eqs. (2.9a) and (2.9b), the operators reduce to

$$\frac{\partial}{\partial t} \to \frac{\partial}{\partial t} + \epsilon^2 \frac{\partial}{\partial T}; \quad \frac{\partial}{\partial z} \to \frac{\partial}{\partial z} + \epsilon^2 \frac{\partial}{\partial Z}, \tag{2.12a}$$

$$\nabla_{1x} \to \nabla_{1x} + \epsilon \nabla_{1X}, \quad \nabla_{1x} = (\frac{\partial}{\partial x}, \quad \frac{\partial}{\partial y}), \quad \nabla_{1X} = (\frac{\partial}{\partial X}, \quad \frac{\partial}{\partial Y}), \tag{2.12b}$$

After inserting Eqs. (2.6) into the MB equations Eqs. (2.1), taking into account Eqs. (2.4) and (2.12), the Eq. (2.1) now reads

$$\left(\ell_0 + \epsilon \ell_1 + \epsilon^2 \ell_2\right)\left(\epsilon \mathbf{E}_1 + \epsilon^2 \mathbf{E}_2 + \epsilon^3 \mathbf{E}_3 + ...\right) = -\mu_0 c^2 \left(\frac{\partial^2}{\partial t^2} + 2\epsilon^2 \frac{\partial}{\partial t}\frac{\partial}{\partial T}\right)\left(\epsilon \mathbf{P}_1 + \epsilon^2 \mathbf{P}_2 + \epsilon^3 \mathbf{P}_3 + ...\right), \tag{2.13a}$$

$$\begin{aligned} \left(\tfrac{\partial^2}{\partial t^2} + 2\epsilon^2 \tfrac{\partial}{\partial t}\tfrac{\partial}{\partial T}\right)\left(\epsilon \mathbf{P}_1 + \epsilon^2 \mathbf{P}_2 + \epsilon^3 \mathbf{P}_3 + ...\right) = &-\left(\gamma_\perp \left(\tfrac{\partial^2}{\partial t^2} + 2\epsilon^2 \tfrac{\partial}{\partial t}\tfrac{\partial}{\partial T}\right) + w_a\right)\left(\epsilon \mathbf{P}_1 + \epsilon^2 \mathbf{P}_2 + \epsilon^3 \mathbf{P}_3 + ...\right) \\ &-g\left(D_{0c} + \epsilon^2\left(\tilde{D}_0 + D_2\right) + \epsilon^3 D_3 + ...\right)\left(\epsilon \mathbf{E}_1 + \epsilon^2 \mathbf{E}_2 + \epsilon^3 \mathbf{E}_3 + ...\right) \end{aligned}, \tag{2.13b}$$

$$\left(\frac{\partial}{\partial t}+\epsilon^2\frac{\partial}{\partial T}\right)\left(\epsilon^2 D_2+\epsilon^3 D_3+...\right)=-\gamma_{\parallel}\left(\epsilon^2 D_2+\epsilon^3 D_3+...\right)+\frac{2}{\hbar w_a}(\epsilon\mathbf{E}_1+\epsilon^2\mathbf{E}_2 +\epsilon^3\mathbf{E}_3+...)\left(\frac{\partial}{\partial t}+\epsilon^2\frac{\partial}{\partial T}\right)\left(\epsilon\mathbf{P}_1+\epsilon^2\mathbf{P}_2+\epsilon^3\mathbf{P}_3+...\right), \tag{2.13c}$$

where the nonlinear terms involve fast and slow scales, and the zero indices correspond to the fast scale. The following operators are defined:

$$\ell_0=\frac{\partial^2}{\partial t^2}+\kappa\frac{\partial}{\partial t}-c^2\left(\nabla_{\perp 0}^2+\frac{\partial^2}{\partial z^2}\right), \tag{2.14a}$$

$$\ell_1=\nabla_{\perp 0}\nabla_{\perp}\ , \tag{2.14b}$$

$$\ell_2=2\frac{\partial}{\partial t}\frac{\partial}{\partial T}+\kappa\frac{\partial}{\partial T}-c^2\left(\nabla_{\perp}^2+2\frac{\partial}{\partial z}\frac{\partial}{\partial Z}\right). \tag{2.14c}$$

One identify at each other the terms of equations. It follows for the ϵ order that, marginal solutions are $\mathbf{E}_1$, and $\mathbf{P}_1$, and related by:

$$\ell_0\mathbf{E}_1=-\mu_0 c^2\frac{\partial^2\mathbf{P}_1}{\partial t^2}, \tag{2.15a}$$

$$\frac{\partial^2\mathbf{P}_1}{\partial t^2}=-\gamma_{\perp}\frac{\partial\mathbf{P}_1}{\partial t}-\omega_a^2\mathbf{P}_1-gD_{0c}\mathbf{E}_1. \tag{2.15b}$$

for ϵ^2 order, the marginal solutions are $\mathbf{E}_2$, and $\mathbf{P}_2$, is given by:

$$\ell_0\mathbf{E}_2=-\mu_0 c^2\frac{\partial^2\mathbf{P}_2}{\partial t^2}, \tag{2.16a}$$

$$\frac{\partial^2\mathbf{P}_2}{\partial t^2}=-\gamma_{\perp}\frac{\partial\mathbf{P}_2}{\partial t}-\omega_a^2\mathbf{P}_2-gD_{0c}\mathbf{E}_2\ , \tag{2.16b}$$

$$\frac{\partial D_2}{\partial t}=-\gamma_{\parallel}D_2+\frac{2}{\hbar\omega_a}\left(\mathbf{E}_1.\frac{\partial\mathbf{P}_1}{\partial t}\right). \tag{2.16c}$$

and D_2 is obtained by solving Eq. (2.16c).

For ϵ^3 order, the solvability condition of the marginal solutions $\mathbf{E}_3$, $\mathbf{P}_3$, is given by:

$$\kappa\frac{\partial\mathbf{E}_1}{\partial T}=-2iw_a\frac{\partial\mathbf{E}_1}{\partial T}-2iw_a c\left(\frac{\partial}{\partial Z}+\frac{i}{2k_c}\nabla_{\perp}^2\right)\mathbf{E}_1-\mu_0 c^2\left(2\frac{\partial}{\partial T}\frac{\partial\mathbf{P}_1}{\partial t}\right), \tag{2.17a}$$

$$2\frac{\partial}{\partial T}\frac{\partial\mathbf{P}_1}{\partial t}=-\gamma_{\perp}\frac{\partial\mathbf{P}_1}{\partial t}-g\left(\tilde{D}_0+D_2\right)\mathbf{E}_1\ , \tag{2.17b}$$

$$\frac{\partial D_3}{\partial t} = -\gamma_{\parallel} D_3 + \frac{2}{\hbar\omega_a}\left(\mathbf{E}_2.\frac{\partial \mathbf{P}_1}{\partial t} + \mathbf{E}_1.\frac{\partial \mathbf{P}_2}{\partial t}\right). \tag{2.17c}$$

From Eqs. (2.17a) and (2.17b), and by combining Eqs. (2.5a) and (2.5b), we obtain

$$\frac{\partial \mathbf{E}_1}{\partial T} = \frac{2c(\gamma_\perp - iw_a)}{k - \gamma_\perp + 2iw_a}\left(\frac{\partial}{\partial Z} + \frac{i}{2k_c}\nabla_\perp^2\right)\mathbf{E}_1 + \frac{\mu_0 c^2 g}{k - \gamma_\perp + 2iw_a}\left(\tilde{D}_0 + D_2\right)\mathbf{E}_1. \tag{2.18}$$

The nonlinearities come from the interaction between the population inversion and the electric field. In order to analyze the higher order diffusive term in this system, the higher-order correction $\gamma_\perp^2 \frac{\partial^2 \mathbf{P}_1}{\partial T^2}$ is needed to the polarization equation Eq.(2.16b).

Substituting the modifying Eq.(2.17b) into Eq.(2.17a); we obtain the following amplitude equation (vector (3+1)D cubic CGL equation) derived by Gil **[78]**:

$$\frac{\partial}{\partial T}\mathbf{A} = C_1 A + C_2\left(\frac{\partial}{\partial Z} + \frac{i}{2k_c}\nabla_\perp^2\right)\mathbf{A} + C_3\left(\frac{\partial}{\partial Z} + \frac{i}{2k_c}\nabla_\perp^2\right)^2\mathbf{A} + C_4\left(\mathbf{A}\cdot\mathbf{A}^*\right)\mathbf{A} + C_5\left(\mathbf{A}\cdot\mathbf{A}\right)\mathbf{A}^*, \tag{2.19}$$

with

$$C_1 = \frac{\mu_0 c^2 g \tilde{D}_0\left(\kappa - \gamma_\perp + 2iw_a\right)}{\left((\kappa - \gamma_\perp)^2 + 4w_a^2\right)}, \tag{2.20a}$$

$$C_2 = -\frac{2c\left(\gamma_\perp(\gamma_\perp - \kappa) + 2w_a^2 + iw_a(\kappa - 3\gamma_\perp)\right)}{\left((\kappa-\gamma_\perp)^2 + 4w_a^2\right)}, \tag{2.20b}$$

$$C_3 = -\frac{4c^2\gamma_\perp\left(\gamma_\perp^2(2\kappa - \gamma_\perp) + \kappa\left(\kappa\gamma_\perp - 4w_a^2\right) - i\gamma_\perp\left(3\gamma_\perp^2 + 4w_a^2 - \kappa\left(2\gamma_\perp^2 - \kappa\right)\right)\right)}{\left((\kappa-\gamma_\perp)^2 + 4w_a^2\right)^2}, \tag{2.20c}$$

$$C_4 = \frac{4kg(-(\kappa-\gamma_\perp) + 2iw_a)}{\hbar w_a \gamma_\parallel\left((\kappa-\gamma_\perp)^2 + 4w_a^2\right)}, \tag{2.20d}$$

$$C_5 = \frac{2g\left(\gamma_\parallel\left(2w_a^2 + \kappa\left(\kappa - \gamma_\parallel^2\right)\right) - 2w_a^2(\kappa + \gamma_\perp) - iw_a\left(\gamma_\parallel(\kappa + \gamma_\perp) + 2\kappa(\kappa - \gamma_\perp) + 4w_a^2\right)\right)}{\hbar w_a\left(\gamma_\parallel^2 + 4w_a^2\right)\left((\kappa-\gamma_\perp)^2 + 4w_a^2\right)}, \tag{2.20e}$$

Since the derivation of this model, it has been the subject of many works, leading to the generation of different forms of patterns.

2.2.2 Modeling of the laser vector (3+1)D cubic-quintic complex Ginzburg-Landau equation

In order to analyze higher order nonlinearities in the system, the nonlinear polarization term $\mathbf{P}_3$ is needed. Therefore, the second correction is needed, taking into account the nonlinear polarization into the population inversion equation (Eq.(2.16c)).

For ϵ^3 order, the solvability condition of the marginal solutions $\mathbf{E}_3$, $\mathbf{P}_3$,is given by:

$$\kappa\frac{\partial\mathbf{E}_1}{\partial T}=-2iw_a\frac{\partial\mathbf{E}_1}{\partial T}-2iw_ac\left(\frac{\partial}{\partial Z}+\frac{i}{2k_c}\nabla_\perp^2\right)\mathbf{E}_1-\mu_0c^2\left(2\frac{\partial}{\partial T}\frac{\partial\mathbf{P}_1}{\partial t}\right), \tag{2.21a}$$

$$2\tfrac{\partial}{\partial T}\tfrac{\partial\mathbf{P}_1}{\partial t}=-\gamma_\perp\tfrac{\partial\mathbf{P}_1}{\partial t}+\gamma_\perp^2\tfrac{\partial^2\mathbf{P}_1}{\partial T^2}-g\left(\tilde{D}_0+D_2\right)\mathbf{E}_1\ , \tag{2.21b}$$

$$\tfrac{\partial D_2}{\partial t}=-\gamma_\parallel D_2+\tfrac{2}{\hbar w_a}\left(\mathbf{E}_1.\tfrac{\partial(\mathbf{P}_1+\mathbf{P}_3)}{\partial t}\right). \tag{2.21c}$$

Let recall that $\mathbf{P}_3=\mathbf{P}_3^1+\mathbf{P}_3^3$. D_2 is again obtained by solving Eq. (2.21c):

$$D_2=D_{20}+D_{22}e^{2i(w_at-k_cz)}+D_{22}^*e^{-2i(w_at-k_cz)}+D_{24}e^{4i(w_at-k_cz)}+D_{24}^*e^{-4i(w_at-k_cz)}, \tag{2.22}$$

with

$$\begin{aligned}D_{20}=&\frac{4}{\hbar\mu_0c^2w_a\gamma_\parallel}(-k\mathbf{A}\mathbf{A}^*+\frac{kg\mathbf{A}^2\mathbf{A}^{*2}}{\hbar w_a\gamma_\perp}(\frac{4}{\gamma_\parallel}+\frac{1}{(\gamma_\parallel-2iw_a)}+\frac{1}{(\gamma_\parallel+2iw_a)})\\&+\frac{ig\mathbf{A}^2\mathbf{A}^{*2}}{\hbar w_a\gamma_\perp}(\frac{1}{(\gamma_\parallel+2iw_a)}-\frac{1}{(\gamma_\parallel-2iw_a)})),\end{aligned} \tag{2.23a}$$

$$\begin{aligned}D_{22}=&\frac{2}{\hbar\mu_0c^2w_a\left(\gamma_\parallel+2iw_a\right)}(-\mathbf{A}^2(k+iw_a)+\frac{2g\mathbf{A}^3\mathbf{A}^*}{\hbar}(\frac{k}{\gamma_\perp w_a}(\frac{1}{(\gamma_\parallel+2iw_a)}+\frac{2}{\gamma_\parallel})\\&+\frac{3}{\left(\gamma_\parallel+2iw_a\right)\left(8w_a-3i\gamma_\perp\right)}+\frac{i}{\left(\gamma_\parallel+2iw_a\right)}(\frac{1}{\gamma_\perp}-\frac{3k}{w_a\left(8w_a-3i\gamma_\perp\right)}))),\end{aligned} \tag{2.23b}$$

$$D_{24}=\frac{12g\mathbf{A}^4}{\hbar^2\mu_0c^2w_a\left(\gamma_\parallel+4iw_a\right)\left(8w_a-3i\gamma_\perp\right)}\left(1-\frac{ik}{w_a}\right). \tag{2.23c}$$

Substituting Eq.(2.22) into Eq.(2.21b), and after some algebra, we obtain the following (3+1)D vectorial CQ-CGL equation

$$\begin{aligned}\frac{\partial\mathbf{A}}{\partial T}=&z_1\mathbf{A}-z_2\left(\frac{\partial}{\partial\mathbf{Z}}+\frac{i}{2k_c}\nabla_\perp^2\right)\mathbf{A}+z_3\left(\frac{\partial}{\partial Z}+\frac{i}{2k_c}\nabla_\perp^2\right)^2\mathbf{A}-z_4\left(\mathbf{A}\cdot\mathbf{A}^*\right)\mathbf{A}\\&-z_5\left(\mathbf{A}\cdot\mathbf{A}\right)\mathbf{A}^*+z_6\left(\mathbf{A}^2\cdot\mathbf{A}^{*2}\right)\mathbf{A}+z_7\left(\mathbf{A}^3\cdot\mathbf{A}^*\right)\mathbf{A}^*,\end{aligned} \tag{2.24}$$

with

$$z_1=\frac{\mu_0c^2g\tilde{D}_0\left(k-\gamma_\perp+2iw_a\right)}{\left(k-\gamma_\perp\right)^2+4w_a^2}, \tag{2.25a}$$

$$z_2=\frac{2c\left(2w_a^2+\gamma_\perp\left(\gamma_\perp-k\right)+iw_a\left(k-3\gamma_\perp\right)\right)}{\left(k-\gamma_\perp\right)^2+4w_a^2}, \tag{2.25b}$$

$$z_3 = \frac{4c^2\gamma_\perp \begin{pmatrix} \gamma_\perp^2(2\kappa-\gamma_\perp)+\kappa\left(\kappa\gamma_\perp-4w_a^2\right) \\ -i\gamma_\perp\left(3\gamma_\perp^2+4w_a^2-\kappa(2\gamma_\perp-\kappa)\right) \end{pmatrix}}{\left(\kappa-\gamma_\perp\right)^2+w_a^2}, \tag{2.25c}$$

$$z_4 = \frac{4kg\left((k-\gamma_\perp)-2iw_a\right)}{\hbar w_a\gamma_\parallel\left(\left(k-\gamma_\perp\right)^2+4w_a^2\right)}, \tag{2.25d}$$

$$z_5 = \frac{2g \begin{pmatrix} \gamma_\parallel(\kappa(\kappa-\gamma_\perp^2)+2w_a^2)-2w_a^2(\kappa+\gamma_\perp) \\ -iw_a\left(\gamma_\parallel(\kappa+\gamma_\perp)+\kappa(\kappa-\gamma_\perp)+42w_a^2\right) \end{pmatrix}}{\hbar w_a\left(\left(\kappa-\gamma_\perp\right)^2+w_a^2\right)\left(\gamma_\parallel^2+4w_a^2\right)}, \tag{2.25e}$$

$$z_6 = \frac{8kg^2\left(\gamma_\parallel\left(k+2\gamma_\parallel\right)+10w_a^2\right)(k-\gamma_\perp-2iw_a)}{\hbar^2w_a^2\gamma_\perp\gamma_\parallel^2\left(\left(k-\gamma_\perp\right)^2+4w_a^2\right)\left(\gamma_\parallel^2+4w_a^2\right)} \tag{2.25f}$$

$$z_{7r} = \frac{4g^2 \begin{pmatrix} (\gamma_\parallel(k(3\gamma_\parallel^2+4w_a^2)+4w_a^2\gamma_\parallel)(9\gamma_\perp^2+64w_a^2)+3\gamma_\perp\gamma_\parallel((8w_a^2 \\ +3k\gamma_\perp)(\gamma_\parallel^2-4w_a^2)+4\gamma_\parallel w_a^2(-8k+3\gamma_\perp)))(k-\gamma_\perp) \\ +2w_a^2(((\gamma_\parallel^2-4w_a^2-4k\gamma_\parallel)\gamma_\parallel-4k(\gamma_\parallel^2+4w_a^2))(9\gamma_\perp^2+64w_a^2) \\ +3\gamma_\parallel\gamma_\perp((-8k+3\gamma_\perp)(\gamma_\parallel^2-4w_a^2)-4(8w_a^2+3k\gamma_\perp)\gamma_\parallel)) \end{pmatrix}}{\hbar^2w_a^2\gamma_\perp\gamma_\parallel(\gamma_\parallel^2+4w_a^2)^2(9\gamma_\perp^2+64w_a^2)((k-\gamma_\perp)^2+4w_a^2)} \tag{2.25g}$$

$$z_{7i} = \frac{4g^2 \begin{pmatrix} (w_a(((\gamma_\parallel^2-4(w_a^2+k\gamma_\parallel))-4k(\gamma_\parallel^2+4w_a^2))(9\gamma_\perp^2+64w_a^2) \\ +3\gamma_\parallel\gamma_\perp((-8k+3\gamma_\perp)(\gamma_\parallel^2-4w_a^2)-4\gamma_\parallel(8w_a^2+3k\gamma_\perp)))(\mathrm{k}-\gamma_\perp \\ )-2(\gamma_\parallel(\mathrm{k}(3\gamma_\parallel^2+4w_a^2)+4w_a^2\gamma_\parallel)(9\gamma_\perp^2+64w_a^2)+3w_a\gamma_\parallel\gamma_\perp((8w_a^2 \\ +3k\gamma_\perp)(\gamma_\parallel^2-4w_a^2)+4w_a^2\gamma_\parallel(3\gamma_\perp-8k))) \end{pmatrix}}{\hbar^2w_a^2\gamma_\perp\gamma_\parallel(\gamma_\parallel^2+4w_a^2)^2(9\gamma_\perp^2+64w_a^2)((k-\gamma_\perp)^2+4w_a^2)}, \tag{2.25h}$$

where $\nabla_\perp^2 = \frac{\partial^2}{\partial X^2}+\frac{\partial^2}{\partial Y^2}$ represents a two-dimensional Laplacian operator and the asterisk $(*)$ stands for the complex conjugate. Eq. (2.24) describes the behavior of the electric field in the dielectric medium. When coefficients $z_6 = z_7 = 0$, in Eq. (2.24), we recover the laser $(3+1)D$ vectorial cubic CGL equation that was introduced early by Gil **[78]** as a vector order parameter for an unpolarized laser and its vectorial topological defects.

Due to the highly nonlinear nature of Eq. (2.24), we introduce a number of useful simplifications: (i) we use the traditional uniform field limit which requires that both the mirror transmissivity

and the gain per pass of the active medium be small, while their ratio may be arbitrary but finite; (ii) a large free spectral range; (iii) the number of modes that are significantly excited is manageably small **[179]**; (iv) the fourth-order derivative has been neglected **[78]**. In this way, the new field amplitude obeys the equation of motion

$$\mathbf{A} = \mathbf{B}\left(X, Y, T\right) \exp\left(-i\Delta Z\right), \tag{2.26}$$

where the amplitude $B(X, Y, T)$ is governed by the equation

$$\frac{\partial \mathbf{B}}{\partial T} = c_1\mathbf{B} + c_2\nabla^2\mathbf{B} - c_3\left(\mathbf{B}\cdot\mathbf{B}^*\right)\mathbf{B} - c_4\left(\mathbf{B}\cdot\mathbf{B}\right)\mathbf{B}^* + c_5\left(\mathbf{B}^2\cdot\mathbf{B}^{*2}\right)\mathbf{B} + c_6\left(\mathbf{B}^3\cdot\mathbf{B}^*\right)\mathbf{B}^*, \tag{2.27}$$

where $c_1 = z_1 + \Delta\left(-\Delta z_3 + iz_2\right)$, $c_2 = \frac{(2\Delta z_3 - iz_2)}{2k_c}$, $c_3 = z_4$; $c_4 = z_5$, $c_5 = z_6$, $c_6 = z_7$, and $\mathbf{B} \perp \mathbf{Z}$. Considering the case where $\mathbf{B}$ has two complex components such as $\mathbf{B} = (B_x, B_y)$ (cartesian components), describing the complex slowly varying amplitudes of the electric field **[169]**, the right and left circularly polarized components (B_+, B_-) are related to the cartesian components by the relations $B_x = (B_+ + B_-)/\sqrt{2}$ and $B_y = (B_+ - B_-)/i\sqrt{2}$. We then obtain the coupled equations describing the dynamics of the circular components after usual scaling transformations **[168]**

$$\begin{aligned} i\frac{\partial\psi_+}{\partial t} &+ \psi_+ + \Delta\psi_+ + |\psi_+|^2\psi_+ + \gamma_r|\psi_-|^2\psi_+ + \nu|\psi_+|^4\psi_+ + \delta_r\left(|\psi_-|^2 + 2|\psi_+|^2\right)|\psi_-|^2\psi_+ \\ &= i\left[\delta\psi_+ + \beta\Delta\psi_+ + \varepsilon|\psi_+|^2\psi_+ + \mu|\psi_+|^4\psi_+ + \delta_i\left(|\psi_-|^2 + 2|\psi_+|^2\right)|\psi_-|^2\psi_+\right], \end{aligned} \tag{2.28a}$$

$$\begin{aligned} i\frac{\partial\psi_-}{\partial t} &+ \psi_- + \Delta\psi_- + |\psi_-|^2\psi_- + \gamma_r|\psi_+|^2\psi_- + \nu|\psi_-|^4\psi_- + \delta_r\left(|\psi_+|^2 + 2|\psi_-|^2\right)|\psi_+|^2\psi_- \\ &= i\left[\delta\psi_- + \beta\Delta\psi_- + \varepsilon|\psi_-|^2\psi_- + \mu|\psi_-|^4\psi_- + \delta_i\left(|\psi_+|^2 + 2|\psi_-|^2\right)|\psi_+|^2\psi_-\right], \end{aligned} \tag{2.28b}$$

where

$$\begin{aligned} &\delta = -c_{1i}/c_{1r}, \;\; \beta = c_{2i}/c_{2r}, \;\; \varepsilon = c_{3i}/c_{3r}, \;\; \mu = c_{5i}/c_{5r}, \quad \gamma_r = (c_{3r} + 2c_{4r})/c_{3r}, \\ &\gamma_i = (c_{3i} + 2c_{4i})/c_{3r}, \;\; \delta_r = -(c_{5r} + 3c_{6r})/2c_{5r}, \;\; \delta_i = -(c_{5i} + 3c_{6i})/2c_{5r}, \end{aligned} \tag{2.29}$$

with $\nu = sign(c_{5r}/c_{3r}^2)$, $t \to T$, $(x, y) \to \sqrt{c_{2r}}(X, Y)$, $\psi_\pm \to B_\pm/\sqrt{c_{3r}}$. In Eqs. (2.28), $\nabla^2\psi_+$ and $\nabla^2\psi_-$ represent two-dimensional Laplacian operators describing diffraction in the transverse $(x,\ y)$-plane, $|\psi_+|^2\psi_+$ and $|\psi_-|^2\psi_-$ denote the cubic self-phase modulation (SPM), $|\psi_-|^2\psi_+$

and $|\psi_+|^2\psi_-$ correspond to the cubic cross-phase modulation (XPM), $|\psi_+|^4\psi_+$ and $|\psi_-|^4\psi_-$ denote the quintic SPM, $|\psi_-|^2|\psi_+|^2\psi_+$ and $|\psi_+|^2|\psi_-|^2\psi_-$ represent the mixed quintic XPM, and $|\psi_-|^4\psi_+$ and $|\psi_+|^4\psi_-$ denote the quintic XPM. In the following ε, μ, γ_r, γ_i, δ_r, and δ_i are real parameters of SPM and XPM terms of Eqs. (2.28). δ is related to the linear loss ($\delta < 0$) or gain ($\delta > 0$). β denotes the strength of diffraction, and ε to the nonlinear frequency detuning. μ stands for the saturation of the nonlinear frequency detuning, γ_r and γ_i are the nonlinear cross coefficients related to the cubic XPM, δ_r and δ_i are the nonlinear cross coefficients describing the quintic XPM, ν represents the nonlinear coefficient for the quintic SPM.

2.3 Analytical methods

It is well known that the CGL equation is a nonlinear partial differential equations that could not be solved, at least not exactly. However, in order to study the dynamics of such system, many technics (include analytical, and numerical) have been developed. Now several significant (1+1)D, (2+1)D and (3+1)D models, such as (2+1)D CQ-CGL equation **[92]**, (3+1)D CQS-CGL equation **[171]**, the method of collective coordinates **[170]**, the variational method **[92, 171]** have been investigated and some special types of localized solutions for these have also been obtained by means of different approaches.

In this thesis, a set of evolution equations and expression for potential function have been derived using a variational method. The variational method allows us to obtain physical insight in terms of a few relevant parameters. After the derivation of the fixed point from the obtained variational system, we use the Routh-Hurwitz stability criterium, to study the stability of our solutions. We recall that this variational method has been successfully used to address a variety of nonlinear problems. The motivations of our choice are based on the advantages of this method. Among them, we have: (1) The variational analysis leads to the fact that the pulse propagation can be completely characterized although approximately without having to know

the exact pulse field, that is without having to solve the multidimensional CQ-CGL equation; (2) The variational analysis gives a detailed qualitative picture of the role and mode of action of each perturbation (such as XPM, SPM, loss/gain, or diffusion) on the pulse.

In order to investigate new types of multidimensional dissipative optical light bullets, our first consideration based on the variational approximation, takes into account the most popular Gaussian pulse shape as the starting point of view and then, we also investigated through variational method, the propagation characteristics and stabilization of moving-Gaussian pulse. We examine their stability by means of both the rigorous analysis of linearized equations for small perturbations, and in direct numerical simulations to support our analytical results.

In what follows, we will present some of the above cited methods, and those that will be applied directly in Chapter 3.

2.3.1 Variational method

Variational methods are commonly used to describe the dynamics of nonlinear waves in nonlinear optics, and atomic physics. Originally, the variational approach is widely used for the analysis of conservative systems and the method has been extended to dissipative systems **[179-182]**.

These methods rely on a well-informed ansatz substituted in the Lagrangian or Hamiltonian formulation of a complex, infinite dimensional system. This ansatz reduces an original partial differential equation (PDE) model to a few degrees of freedom establishing equations describing the approximate dynamics appropriately projected into the solution space spanned by the ansatz. Since the laser's advent, nonlinear optics has become a particularly interesting field for its theoretical context as well as its practical consequences on technology, in particular, on nonlinear optical fiber and waveguide systems. Here, the variational method has been widely applied to obtain approximated solutions for problems concerning pulse and/or beam

propagation within the framework of the nonlinear Schrödinger equation and nonlinear dissipative pulses, which applies to problems involving one or more transverse dimensions besides the propagation dimension.

Here, we briefly outline the basic concepts of the variational method. Consider a given (2+1)-dimensional cubic-quintic complex Ginzburg-Landau equation of the form **[91, 92]**

$$i\frac{\partial\psi}{\partial z} + (\frac{\partial^2\psi}{\partial x^2} + \frac{\partial^2\psi}{\partial y^2}) - |\psi|^2\psi + \nu|\psi|^4\psi = Q, \tag{2.30}$$

where ψ is the normalized complex envelope of the optical field. The Laplacian with respect to x and y describes the beam diffraction. In order to prevent the wave collapse, the saturating nonlinearity is required. As a consequence, cubic and quintic nonlinearities need to have opposite signs, i.e., parameter ν is negative. Dissipative terms are denoted by Q

$$Q = i\{\gamma\psi + \varepsilon|\psi|^2\psi + \mu|\psi|^4\psi + \beta_0(\frac{\partial^2\psi}{\partial x^2} + \frac{\partial^2\psi}{\partial y^2})\}. \tag{2.31}$$

The first term with parameter γ is linear loss. The cubic and quintic gain-loss terms contain respectively parameters ε and μ. The last term accounts for the parabolic gain, if $\beta_0 > 0$.

In order to establish the variational approach for CQ-CGL equation, we construct the total Lagrangian $L = L_c + L_Q$ of the system described by Eq. (2.30) containing both, a conservative part

$$l_c = \frac{i}{2}(\psi^*\frac{\partial\psi}{\partial z} - \psi\frac{\partial\psi^*}{\partial z}) + \left|\frac{\partial\psi}{\partial x}\right|^2 + \left|\frac{\partial\psi}{\partial y}\right|^2 + \frac{1}{2}|\psi|^4 - \frac{\nu}{3}|\psi|^6, \tag{2.32}$$

and the dissipative one

$$l_Q = i(\delta|\psi|^2 + \beta(\left|\frac{\partial\psi}{\partial x}\right|^2 + \left|\frac{\partial\psi}{\partial y}\right|^2) + \frac{\varepsilon}{2}|\psi|^4 + \frac{\mu}{3}|\psi|^6). \tag{2.33}$$

With the asymmetrical trial function given by **[92]**

$$\psi(x, y, z) = A\exp(-\frac{x^2}{2X^2} - \frac{y^2}{2Y^2} + iCx^2 + iSy^2 + i\phi), \tag{2.34}$$

as a functional of amplitude A, spatial widths X and Y, wave front curvatures C and S, and phase ϕ, all function of the independent variable z. Optimization of each of these functions gives one of six Euler-Lagrange equations averaged, together with conservative Lagrangian $\ell_c = \int\int L_c dxdy$, over transverse coordinates x and y

$$\frac{d}{dz}(\frac{\partial \ell_c}{\partial \dot{\eta}}) - \frac{\partial \ell_c}{\partial \eta} = 2R_e \int\int dxdyQ\frac{\partial \psi^*}{\partial \eta}, \tag{2.35}$$

where R_e denotes the real part.

The application of the variational approach to the partial differential (2+1)D CQ-CGL equation leads to a set of six coupled first-order differential equations (FODEs) resulting from the variation with respect to the amplitude A, widths X, and Y, wave front curvatures C, S and ϕ. These equations show the pulse parameters changes during the propagation inside a waveguide and how they are coupled with each other.

2.3.2 Routh-Hurwitz stability analysis method

The Routh stability criterion **[184]** is an analytical procedure for determining if all the roots of a polynomial have negative real parts **[185, 186]**.

In order to ascertain the stability of a linear time-invariant system, it is necessary to determine if any of the roots of its characteristics equation have negative real parts. A. Hurwitz and E. J. Routh independently published the method of investigating the sufficient conditions of stability of a system **[184]**. In this work, we consider the characteristic equation of a linear system is given by

$$f(z) = a_n z^n + a_{n-1} z^{n-1} + ...a_1 z + a_0 = 0, \tag{2.36}$$

where the coefficients $a_i (i = 0, 1, 2, ..., n)$ are real constants. To define the n Hurwitz matrices

using the coefficients a_i of the characteristic polynomial, the table is constructed in the form

$$\begin{array}{cccccc} z^n & a_n & a_{n-2} & a_{n-4} & \dots & \dots \\ z^{n-1} & a_{n-1} & a_{n-3} & a_{n-5} & \dots & \dots \\ z^{n-2} & b_{n-1} & b_{n-3} & b_{n-5} & \dots & \dots \\ z^{n-3} & c_{n-1} & b_{n-3} & b_{n-5} & \dots & \dots \\ \dots & \dots & \dots & \dots & \dots & \dots \\ z^0 & h_{n-1} & \dots & \dots & \dots & \dots \end{array}, \tag{2.37}$$

where

$$\begin{array}{c} b_{n-1} = \frac{-1}{a_{n-1}} \begin{vmatrix} a_n & a_{n-2} \\ a_{n-1} & a_{n-3} \end{vmatrix} = \frac{a_{n-1}a_{n-2} - a_n a_{n-3}}{a_{n-1}} \\ b_{n-3} = \frac{-1}{a_{n-1}} \begin{vmatrix} a_n & a_{n-4} \\ a_{n-1} & a_{n-5} \end{vmatrix} \quad c_{n-1} = \frac{-1}{b_{n-1}} \begin{vmatrix} a_{n-1} & a_{n-3} \\ b_{n-1} & b_{n-3} \end{vmatrix} \end{array}. \tag{2.38}$$

To be a stable fixed point within the linearized analysis, all the eigenvalues must have negative real parts. Using the Routh-Hurwitz criterion, the necessary and sufficient conditions for Eq. (2.36) to have $\Re(z_{1,2,3,\dots,n}) < 0$ ($\Re$ represents the real part) are:

▷ Necessary and sufficient condition that depends only on a_i

• **Requirement for system stability**

All the coefficients are positive or they have the same sign. If one of the coefficients is zero or negative, and at least one other coefficient is positive, there is at least one imaginary root with a positive real part.

• **Sufficient condition for system stability**

All the elements in the first column of Routh are positive or they have the same sign. The necessary and sufficient condition for the stability of the system is that the coefficients of the characteristic polynomial and the elements of the first Routh-Hurwitz column must be positive or must have the same sign **[185-188]**.

2.4 Numerical methods

Since the CQ-CGL equation is generally not solvable analytically, in order to confirm the prediction of the approximative analytical approach, numerical simulations methods are needed. Some numerical method used in this thesis are presented in this section.

2.4.1 Split-step method

In order to face the questions of non-integrability of the propagation equations, numerical methods have been developed. In this stage of our thesis, we limit ourselves to the propagation of ultrashort pulses in nonlinear and dispersive optical fibers described by the CGL equation **[188]**, written in the form:

$$\psi_z = (\gamma_r + i\gamma_i)\,\psi - (p_i - ip_r)\,\psi_{tt} - (q_i - iq_r)\,|\psi|^2\psi, \tag{2.39}$$

This equation can be written as

$$\frac{\partial\psi(z,t)}{\partial z} = (\hat{D} + \hat{N})\psi(z,t), \tag{2.40}$$

where $\hat{D}$ represents the linear operator, and the nonlinear operator is $\hat{N}$, defined by: relation:

$$\hat{D} = (\gamma_r + i\gamma_i) - \frac{\partial^2}{\partial t^2}, \tag{2.41a}$$

$$\hat{N}(\psi(z,t)) = -\,(q_i - iq_r)\,|\psi|^2. \tag{2.41b}$$

The symmetrical Fourier Split-Step method (MFSS-S) is one of the most widely used pseudo-spectral methods for studying the propagation of pulses in non-linear and dispersive media **[188-195]**.

$$exp(h\hat{D}/2)exp(h\hat{N})exp(h\hat{D}/2), \tag{2.42a}$$

In this method, the propagation length is subdivided into intervals of lengths h. If the value of h is sufficiently low, we can approximate the solution by assuming that along each interval, the operators of dispersion $\hat{D}$ and nonlinear $\hat{N}$ act independently.

From the strang formula Eq. (2.42a), the dispersion effects act continuously on the two halves of the length segment h: $[z, z+h/2[$ and $]z+h/2, z+h]$; while the nonlinear effects are inserted at the point $z+h/2$ in the middle of the segment. In this way the variations of the nonlinear operator $\hat{N}$ in the meantime $[z+h]$ can be overlooked.

The formal solution of the amplitude of the variable field $\psi(z+h,t)$ as a function of $\psi(z,t)$, is given by the equation:

$$\psi(z+h,t) = \exp(\frac{h\hat{D}}{2})\exp(h\hat{N})\exp(\frac{h\hat{D}}{2})\psi(z,t)\cdot \tag{2.43}$$

The dispersion operator, comprising partial time derivatives Eq. (2.41a) will be calculated in the spectral domain using the Fourier transforms. The differential operator $\frac{\partial}{\partial t}$ is replaced by $i\omega$ and we calculate each partial derivative of order n as follows: $\frac{\partial^n}{\partial t^n} \overset{F}{\leftrightarrow} (i\omega)^n$, where F denotes the Fourier transform. The same calculation principle is applied to the last two terms of the non-linear operator Eq. (2.41b), which represent the Self-Steepening effect and the Raman effect and which also have time derivatives. However, since N depends on z through $\psi(z,t)$, it is then replaced, along a segment, by its integral which can be approximated using the trapezoid method:

$$\int_{z}^{z+h} \hat{N}(z')dz' \approx \frac{h}{2}\left[\hat{N}(z) + \hat{N}(z+h)\right]. \tag{2.44}$$

Note that $\psi(z+h,h)$ is not known when we want calculate $\hat{N}(z)$, we must therefore proceed by iterations in order to estimate $\hat{N}(z+h)$ and we have several possibilities for choosing the initial value, this is what will bring us to the proposition and to the study of two implementations.

Further, an algorithm based on MFSS-S is developed for solving CQ-CGL equation and the soliton switching is studied in the fiber and in the laser cavity system.

2.4.2 Fourth-order Runge-Kutta method

Runge-Kutta method is a numerical technique used to solve ordinary differential equation of the form

$$\frac{dy}{dx} = f(x, y),. \tag{2.45}$$

with $y(x_0) = y_0$.

Runge-Kutta 4th was first developed to solve first order ordinary differential equation. Later it was adapted to solve to solve higher order ordinary differential equations or coupled (simultaneous) differential equations. It is based on the following

$$y_{i+1} = y_i + (a_1k_1 + a_2k_2 + a_3k_3 + a_4k_4), \tag{2.46}$$

where knowing the value of $y = y_i$ at x_i, we can find the value of $y = y_{i+1}$ at x_{i+1}, and $h = x_{i+1} - x_i$.

Equation (2.45) is equivalent to the first five terms of Taylor series

$$\begin{aligned}\tfrac{dy}{dx} &= y_i + \tfrac{dy}{dx}\Big|_{x_i,y_i}(x_{i+1} - x_i) + \tfrac{1}{2!}\tfrac{d^2y}{dx^2}\Big|_{x_i,y_i}(x_{i+1} - x_i)^2 + \tfrac{1}{3!}\tfrac{d^3y}{dx^3}\Big|_{x_i,y_i}(x_{i+1} - x_i)^3 \\ &+ \tfrac{1}{4!}\tfrac{d^4y}{dx^4}\Big|_{x_i,y_i}(x_{i+1} - x_i)^4\end{aligned} \tag{2.47}$$

Knowing that $\frac{dy}{dx} = f(x, y)$ and $h = x_{i+1} - x_i$

$$y_{i+1} = y_i + hf(x_i, y_i) + \frac{h^2}{2!}f'(x_i, y_i) + \frac{h^3}{3!}f''(x_i, y_i) + \frac{h^4}{4!}f'''(x_i, y_i).. \tag{2.48}$$

Based on equating Eq. (2.47) and (2.48), the solutions are obtained such as

$$y_{i+1} = y_i + \frac{h}{6}(k_1 + 2k_2 + 2k_3 + k_4), \tag{2.49}$$

where

$$k_1 = f(x_i, y_i), \tag{2.50a}$$

$$k_2 = f(x_i + \frac{h}{2}, y_i + \frac{hk_1}{2}), \tag{2.50b}$$

$$k_3 = f(x_i + \frac{h}{2}, y_i + \frac{hk_2}{2}), \tag{2.50c}$$

$$k_4 = f(x_i + h, y_i + hk_3). \tag{2.50d}$$

The RK4 method makes four estimates of $f(x, y)$ per segment, each estimate is refined by the previous one; the first at the starting point x, the second and the third at the point $x+h/2$, from the middle of the segment and the last at the end point $x + h$.

2.5 Conclusion

This chapter was devoted to the methods used in this thesis. Helped by the theory of nonlinear perturbation, and the multimodal method, we have derivative the vector $(3 + 1)$ CQ-CGL equation, from where the coupled system $(2 + 1)$D CQ-CGL equation. Other analytical methods (variational method) and numerical methods (the Split-Step Fourier method and the Runge-Kutta method of order 4) have been presented, and some of these Methods have been used to study the dynamics of the signal in the nonlinear optical system. In the next chapter, we will present our results.

Chapter III

Results and Discussions

3.1 Introduction

The preceding chapters were devoted to generalities on the theory of solitons, laser, dissipative soliton in dissipative optical systems (laser cavity and optical fiber) modeled by the complex Ginzburg-Landau equations. From the Maxwell-Bloch model, we have derived a new equation which models the propagation of the optical soliton in the laser cavity, called "the coupled (2+1)-dimensional CQ-CGL equation". This new model which takes into account cubic-quintic non-linearities, diffraction and two coupled terms, refering to cubic cross-phase modulation and quintic cross-phase modulation (XPM), is an originality in the study of the propagation of dissipative solitons based on the model Ginzburg-Landau complex. This model is an advance in this field of study and represents one of the most important contributions of this thesis.

In order to achieve other objectives, we have highlighted some analytical methods which have been proposed to describe the main characteristics of the evolution of impulses such as the variational method, and methods of studying stability like that of Routh-Hurwitz (R-H) and the analysis of the effective potential. To confirm the different results obtained from the analytical methods, we also make use of numerical study, by considering the RK4 method and the Split-Step Fourier method.

The obtained results deal with the stability of solitons of the dissipative system describe by the (2+1)D CQ-CGL equation Eq. (2.30), and the generation associated to the stability of dissipative solitons of the coupled laser (2+1)D CQ-CGL equation. These results can find their

application in the field of telecommunications, medicine and industry.

3.2 Stable soliton of the (2+1)D cubic-quintic complex Ginzburg-Landau equation

Physical system which exchange energy with the environment (dissipative systems) possess a dynamics including various phenomena, such as the saturable loss, nonlinear gain, dispersive loss, dispersion and other effects. A rich variety of structure can be obtained due to the interaction between such phenomena **[92, 171, 197]**, and dissipative soliton is a typical example. It has been shown that their parameters particularly depend on the system parameters.

3.2.1 Variational equations

The main idea of this section is to map the parameters of the (2+1)D CQ-CGL model Eq. (2.30), for which new types of localized waves appear, belonging to the class of dissipative solitons. However although this model is not analytically solvable, it is difficult to have exact solutions. In order to obtain a better understanding of the dynamics which influence the behavior of the impulse during its propagation, the impulse field ψ was approached by a test function which can easily be expressed according to the physical parameters of the soliton. Thus, from the variational approach, the equation of propagation of the field (Eq. (2.30)) is transformed into a system of ordinary differential equations describing the evolution of the pulse during the propagation.

For our study, the following ansatz has been used **[137,170,197-199]**.

$$\psi = A\exp\left\{-\frac{(x-X_2)^2}{2X^2} - \frac{(y-X_2)^2}{2Y^2} + iC(x-X_2)^2 + iS(y-X_2)^2 + iY_2(x-X_2) + iY_2(y-X_2) + i\phi\right\}, \tag{3.1}$$

where A is the amplitude, X and Y are the spatial widths, C and S are the unequal wavefront curvature, X_2 the central position, ϕ is the phase and Y_2 accounts for the velocity of the soliton

along the direction of x and y, all function of the independent variable z.

The application of the variational approach to the partial differential (2+1)D CQ-CGL equation leads to a set of eight coupled first-order differential equations (FODEs) resulting from the variation with respect to the linear frequency, unequal spatial widths, the unequal wavefront curvature, the amplitude, the central position and the phase respectively:

$$\frac{dY_2}{dz} = -\frac{2\beta Y_2}{Y^2} + \delta Y_2 - \frac{2\beta Y_2}{X^2} - 2\beta C^2 X^2 Y_2 - 2\beta S^2 Y^2 Y_2, \tag{3.2a}$$

$$\frac{dX}{dz} = 4CX - 2\beta C^2 X^3 - \frac{\varepsilon}{4} A^2 X + \frac{2\beta}{X} + \frac{\delta}{2} X - \frac{2\mu}{9} A^4 X, \tag{3.2b}$$

$$\frac{dY}{dz} = 4SY - 2\beta S^2 Y^3 - \frac{\varepsilon}{4} A^2 Y + \frac{2\beta}{Y} + \frac{\delta}{2} Y - \frac{2\mu}{9} A^4 Y, \tag{3.2c}$$

$$\frac{dC}{dz} = -\frac{1}{3}\frac{A^2}{X^2} + \frac{4}{X^4} + \frac{4\nu}{9}\frac{A^4}{X^2} - 4C^2 - 8\beta\frac{C}{X^2}, \tag{3.2d}$$

$$\frac{dS}{dz} = -\frac{1}{3}\frac{A^2}{Y^2} + \frac{4}{Y^4} + \frac{4\nu}{9}\frac{A^4}{Y^2} - 4S^2 - 8\beta\frac{S}{Y^2}, \tag{3.2e}$$

$$\begin{aligned}\frac{dA}{dz} = -2A(C+S) + \frac{8\mu}{9}A^5 + \frac{5\varepsilon}{4}A^3 - 4\beta A Y_2^2 - 3\beta\frac{A}{Y^2} \\ + \frac{\delta}{2}A - 3\beta\frac{A}{X^2} - \beta A C^2 X^2 - \beta A S^2 Y^2,\end{aligned} \tag{3.2f}$$

$$\frac{dX_2}{dz} = 2Y_2 - \beta C X^2 Y_2 - \beta S Y^2 Y_2, \tag{3.2g}$$

$$\frac{d\phi}{dz} = \frac{1}{2}A^2 - \frac{2}{X^2} - \frac{2}{Y^2} - \frac{5\nu}{9}A^4 + 2\beta C + 2\beta S + 2Y_2^2 - 2\beta C X^2 Y_2^2 - 2\beta S Y^2 Y_2^2. \tag{3.2h}$$

As can be seen, the additional parameters X_2 and Y_2 (central position and the speeds) influence the dynamics of the other parameters of the soliton through Eqs. (3.2a-3.2h)(in comparison to some previous works [92]). Consequently, it is the dynamics of the entire soliton which can be greatly affected during propagation in the system. However, explicit information regarding the different solutions and their stability can not be gained at this stage of the analytical procedure.

Looking for steady state solutions of the system given by Eqs. (3.2a-3.2f), the derivatives of soliton parameters with respect to z are set equal to zero. Thus, after some algebra we obtained the steady state amplitude (Eq. (3.6)) with two discrete values A_+ and A_- steady

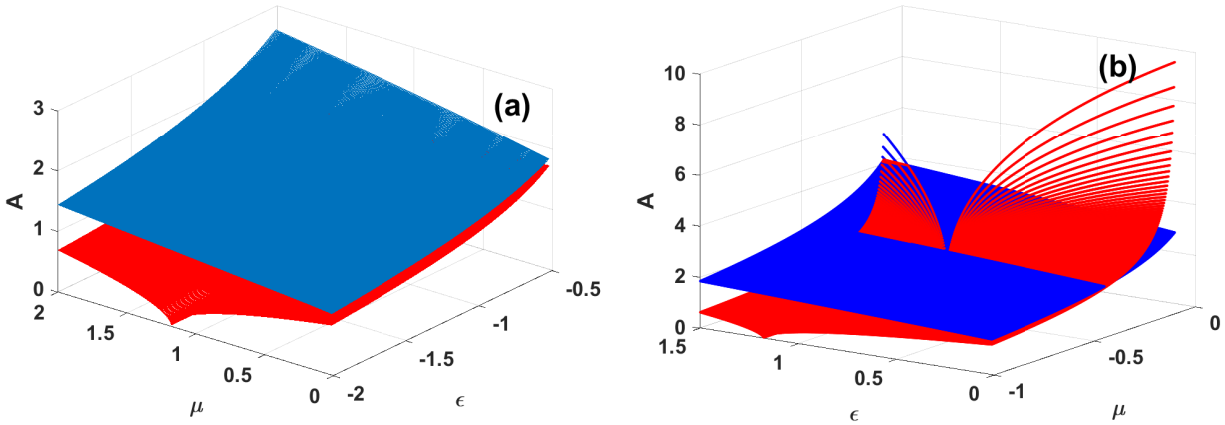

Figure 3.1: Double steady state solution $A-$(red) and $A+$ (blue). (a): $\nu = 0.72$, $\beta = 0.5$, $\delta = -0.1$; (b): $\nu = 0.72$, $\beta = 0.05$, $\delta = -1$.

state solutions. We note that only the symmetric steady state solutions, with equal widths ($X = Y$) and spatial chirps ($C = S$) have been considered.

Figure 3.1 presents the region of existence of the stationary solutions in the space of the dissipative parameters respectively in the case of $\beta = 0.5$, $\delta = -0.1$, $\nu = 0.72$ (see Fig. 3.1(a)) and the case of $\beta = 0.05$, $\delta = -1$, $\nu = 0.72$ (see Fig. 3.1(b)) in the plane of (μ, ε) parameters.

From the above equations, we obtained the width

$$X = \frac{2\sqrt{2+2\beta^2}}{\sqrt{\frac{4}{9}(\beta\nu-\mu)A^4 + (\frac{1}{2}+\frac{1}{3}\beta\varepsilon)A^2 + \frac{\delta}{\beta}}}, \tag{3.3}$$

the linear frequency

$$Y_2 = \frac{1}{6}\sqrt{\frac{9A^2\varepsilon}{\beta} + \frac{6A^4\mu}{\beta}}, \tag{3.4}$$

the chirp

$$C = \frac{4}{9}(\beta\nu+\mu)A^4 + \left(\frac{1}{2}\varepsilon - \frac{1}{3}\beta\right)A^2. \tag{3.5}$$

and the amplitude

$$A\pm = \left(\beta(\tfrac{4}{3}+2\beta\varepsilon) \pm \sqrt{\Delta_1}\right)^{1/2}\left(\tfrac{92\beta}{\beta}(-\beta\mu+\nu)\right)^{-1/2} + 0\left(\theta^2\right), \tag{3.6}$$

with $\Delta_1 = \beta^2(\frac{4}{3}+2\beta\varepsilon)^2 - \frac{256\delta\beta}{9}(1+2\beta^2)(-\beta\mu+\nu)$.

It is important to point out that the balance between the gain/loss and the diffraction with saturating nonlinearity can lead to a fixed steady state solution only for non zero curvature, which is not the case with conservative systems **[137, 189, 200]**.

Considering the physical situation where the central positions and the soliton speed may be taken different in the two transverse axis x and y, the following solution is used

$$\psi = A\exp\left\{-\tfrac{(x-X_2)^2}{2X^2} - \tfrac{(y-Y_{22})^2}{2Y^2} + iC(x-X_2)^2 + iS(y-Y_{22})^2 + iX_3(x-X_2) + iY_2(y-Y_{22}) + i\phi\right\}, \tag{3.7}$$

where additional parameters Y_{22} account for the central position coordinate in the y direction, and X_3 the speed in the x direction. Following the same analytical approach, we obtain

$$\frac{dX_3}{dz} = -8\beta X_3(C^2X^2 - \frac{1}{X^2}), \tag{3.8a}$$

$$\frac{dY_2}{dz} = -8\beta Y_2(S^2Y^2 - \frac{1}{Y^2}), \tag{3.8b}$$

$$\frac{dX}{dz} = 4XC + 4\beta(\frac{1}{X^2} - C^2X^3) - \frac{\varepsilon}{4}XA^2 - \frac{2\mu}{9}XA^4, \tag{3.8c}$$

$$\frac{dY}{dz} = 4YS + 4\beta(\frac{1}{Y^2} - S^2Y^3) - \frac{\varepsilon}{4}YA^2 - \frac{2\mu}{9}YA^4, \tag{3.8d}$$

$$\frac{dC}{dz} = -\frac{4\beta}{X^2}(5C+S) + \frac{3}{4}\frac{A^2}{X^2} - \frac{2\nu}{9}\frac{A^4}{X^2} + \frac{4}{X^4} - 4C^2, \tag{3.8e}$$

$$\frac{dS}{dz} = -\frac{4\beta}{Y^2}(C+5S) + \frac{3}{4}\frac{A^2}{Y^2} - \frac{2\nu}{9}\frac{A^4}{Y^2} + \frac{4}{Y^4} - 4S^2, \tag{3.8f}$$

$$\frac{dA}{dz} = \frac{3\varepsilon}{4}A^3 + \frac{5\mu}{9}A^5 + \delta A - 2A(S+C) - 2\beta A(\frac{1}{X^2} + \frac{1}{Y^2}) - \beta A(X_3^2 + Y_2^2), \tag{3.8g}$$

$$\frac{dX_2}{dz} = 2X_3(1 - 2\beta CX^2), \tag{3.8h}$$

$$\frac{dY_{22}}{dz} = 2Y_2(1 - 2\beta SY^2), \tag{3.8i}$$

$$\frac{d\varphi}{dz} = 12\beta(S+C) - \frac{7}{4}A^2 + \frac{5\nu}{9}A^4 - 4(\frac{1}{X^2} + \frac{1}{Y^2}) + X_3^2 + Y_2^2 - 4\beta(X^2X_3^2C + Y^2Y_3^2S). \tag{3.8j}$$

We noted that, the soliton speed parameters (X_3, Y_2) and the central positions (X_2, Y_{22}) respectively influence the dynamics of the other parameters as we observed in Eqs. (3.2a-3.2h). However, some relevant new characteristics appear concerning the dynamics of the new

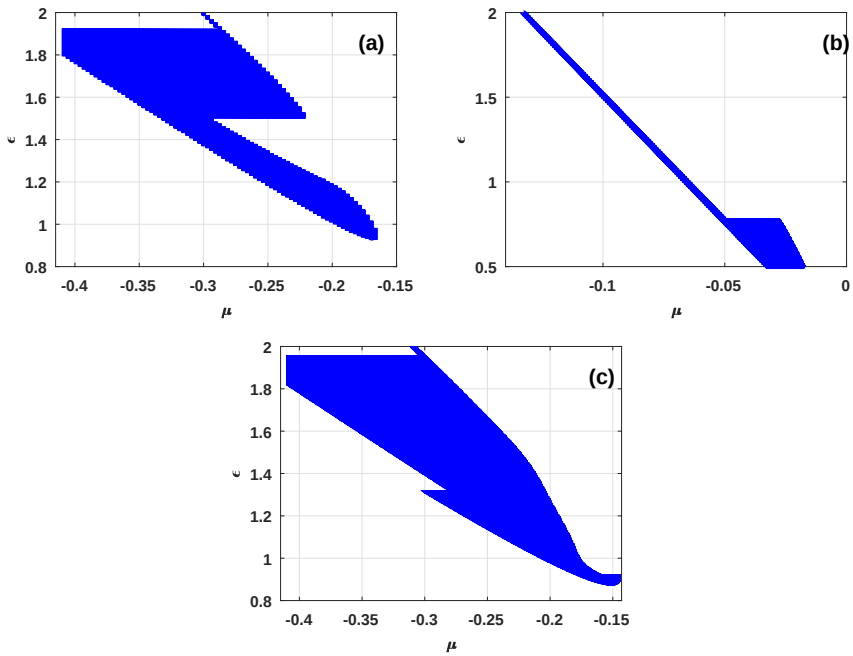

Figure 3.2: Domain of stable solutions with $X_3 = Y_2$. (a) $\nu = 0.72$, $\beta = 0.5$, $\delta = -0.1$, (b) $\nu = 0.2$,$\beta = 0.5$, $\delta = -0.01$ and (c) $\nu = 0.72$, $\beta = 0.5$, $\delta = -1$. We can observe the great influence of the parameters system on the stability domain.

parameters (X_3, Y_2) and (X_2, Y_{22}). We noted that the parameter δ do not affected the dynamics of the linear frequencies, and it also appears that the dynamics of the central positions X_3 and Y_2 respectively for x and y directions are influenced by the soliton parameters respectively for the same directions. Another relevant result is related to the interaction between the unequal wavefront curvature in their dynamics. The steady state solutions arising from equations Eqs. (3.8a)-(3.2g) are obtained by considering $X = Y$, $C = S$, $X_3 = Y_2$. Then, after some algebra, we have:

the steady amplitude

$$A_{\pm} = \sqrt{\frac{-b \pm \sqrt{b^2 - 4ac}}{2a}}, \tag{3.9}$$

with

$$a = -\frac{64}{81}\left[(6\beta^2(18\beta^2+1)-2)\mu^2 + 20\beta\nu(1+6\beta)\mu + \beta^2\nu^2(1-12\beta^2) + \frac{\nu^2}{2}\right]$$

$$b = \frac{1}{9}\left[(32(1-3\beta^2(1+6\beta^2))\varepsilon + \frac{80}{3}\beta(1+6\beta^2))\mu^2 - 80\beta\nu(1+6\beta^2)\varepsilon + 48\beta^2\nu(1+12\beta) + 24\nu\right]$$

$$c = 2(-3\beta^2(1+18\beta^2)+1)\varepsilon^2 + 30\beta(1+6\beta^2)\varepsilon + 9\beta^2(12\beta^2-1)\varepsilon - \frac{9}{2}.$$

The width

$$X = \left(2A^2\frac{3(2\beta\varepsilon-1)+2(6\beta\mu+1)A^2}{(6\beta^2+1)}\right)^{-1/2}, \tag{3.10}$$

the wavefront curvature

$$C = \frac{\left(\frac{1}{2}(3\beta+\varepsilon)+\frac{4}{9}(\mu-\beta\nu)A^4\right)A^2}{8(6\beta^2+1)}, \tag{3.11}$$

and the linear frequency

$$X_3 = \sqrt{\frac{\frac{2}{3}\left((8\beta^2+1)\mu+\frac{1}{3}\beta\nu\right)A^4+\left((\frac{15}{2}\beta^2+1)\varepsilon-\frac{3}{4}\beta\right)A^2+2\delta\left(6\beta^2+1\right)}{2\beta(6\beta^2+1)}}. \tag{3.12}$$

3.2.2 Stability analysis and numerical results

An important criterium that gives necessary and sufficient conditions for the stability of the roots of the characteristic polynomial (with real coefficients) to lay in the left half of the complex plane are known as the Routh-Hurwitz (R-H) criteria **[185, 201]**. The stable stationary solutions of Eq. (2.30) are determined by the analysis of the eigenvalues λ_j $(j = 1, \ldots, 6)$ of the matrix $M_{ij} = \frac{\partial\dot{\eta}_i}{\partial\eta_j}$ given as follows:

$$\lambda^6 + a_1\lambda^5 + a_2\lambda^4 + a_3\lambda^3 + a_4\lambda^2 + a_5\lambda + a_6 = 0, \tag{3.13}$$

where $\eta = A, X, Y, Y_2, C$ or S, $\dot{\eta} = \frac{d\eta}{dz}$, with a_i $(i = 1, \ldots, 6)$ depending on the system parameters and the fixed points. To be a stable fixed point according to Lyapunov method, all the eigenvalues must have negative real parts **[92, 148]**. Using the Routh-Hurwitz criterion, the necessary and sufficient conditions for Eq. (3.13) to have $\mathrm{Re}(\lambda_i) < 0$, $i = 1, \ldots, 6$ are given as follows:

$$a_i > 0, \quad b_1 > 0, \quad c_1 > 0, \quad d_1 > 0, \quad e_1 > 0, \tag{3.14}$$

with

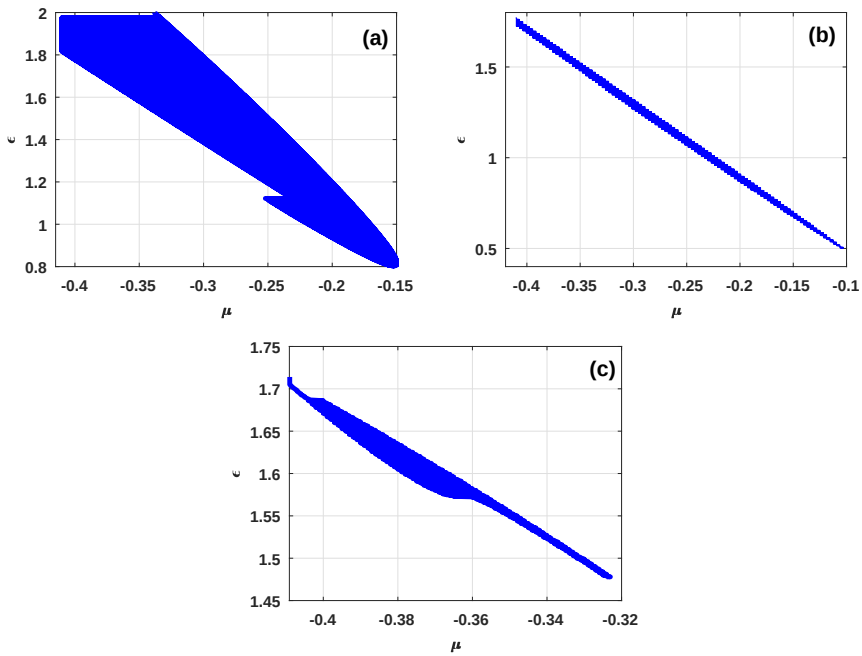

Figure 3.3: Domain of stable solutions with $\delta = -1$ and $\nu = 0.72$, for (a) $\beta = 0.5$, $X_3 = Y_2/2$, (b) $\beta = 0.5$, $X_3 = Y_2/5$; (c) $\beta = 1.5$, $X_3 = Y_2/5$.

$$b_1 = \frac{-1}{a_1}(a_3 - a_2 a_1), \qquad b_3 = \frac{-1}{a_1}(a_5 - a_1 a_4)$$

$$c_1 = \frac{-1}{b_1}(a_1 b_3 - b_1 a_3), \qquad c_3 = \frac{-1}{b_1}(a_1 a_6 - b_1 a_5)$$

$$d_1 = \frac{-1}{c_1}(b_1 c_3 - c_1 b_3), \qquad e_1 = \frac{-1}{d_1}(c_1 a_6 - c_3 d_1).$$

It follows that solutions with amplitudes A_- satisfied the above stability conditions as we can see in Fig. 3.2. showing the influence of the dissipative parameters on the stability domain of the solutions when the speed has the same value in transverse directions x and y.

Considering the ansatz (Eq. (3.7)), the stable stationary solutions of Eq. (2.30) are determined by the analysis of the eigenvalues λ_j $(j = 1, \ldots, 7)$ of (7X7) matrix given by:

$$\lambda^7 + \alpha_1\lambda^6 + \alpha_2\lambda^5 + \alpha_3\lambda^4 + \alpha_4\lambda^3 + \alpha_5\lambda^2 + \alpha_6\lambda + \alpha_7 = 0, \tag{3.15}$$

where $\alpha_i (i = 1, .., 7)$ depend on the system parameters and the stationary solutions related to Eqs. (3.9)-(3.12). The necessary and sufficient conditions for the stability are given by:

$$\alpha_i > 0, \quad \beta_{11} > 0, \quad \beta_{21} > 0, \quad \beta_{31} > 0, \quad \beta_{41} > 0 \quad and \quad \beta_{51} > 0, \tag{3.16}$$

where

$\beta_{11} = \alpha_2 - \frac{\alpha_3}{\alpha_1}$ $\quad \beta_{13} = \alpha_4 - \frac{\alpha_5}{\alpha_1}$ $\quad \beta_{15} = \alpha_6 - \frac{\alpha_7}{\alpha_1}$

$\beta_{21} = \alpha_3 - \frac{\beta_{13}\alpha_1}{\beta_{11}}$ $\quad \beta_{23} = \alpha_5 - \frac{\beta_{15}\alpha_1}{\beta_{11}}$

$\beta_{31} = \beta_{13} - \frac{\beta_{11}\beta_{23}}{\beta_{21}}$ $\quad \beta_{33} = \beta_{15} - \frac{\beta_{11}\alpha_7}{\beta_{21}}$

$\beta_{41} = \beta_{23} - \frac{\beta_{21}\beta_{33}}{\beta_{31}}$ $\quad \beta_{51} = \beta_{33} - \frac{\beta_{31}\alpha_7}{\beta_{41}}$.

Numerical results lead to numerous stability domains (see Fig. 3.3) and the solutions satisfying these conditions behave stable during long distance of propagation (see Fig. 3.5). For $Y_2 = X_3$, the stable domain of dissipative solution (see Fig. 3.2) is given for different set of dissipative parameters. For $\delta = -0.1$, $\beta = 0.5$ and $\nu = 0.72$, Fig. 3.2(a) shows a blue stability domain. When $\delta = -.01$, $\beta = 0.5$, $\nu = 0.2$, Fig. 3.2(b) shows a decrease of the stability domain, and for $\delta = -1$, $\beta = 0.5$ and $\nu = 0.72$, Fig. 3.2(c) shows an increase of the stability domain. As observed in Figs. 3.2(a) to 3.2(c), for different values of the system parameters, the stability domain do not remaind the same. We can then conclude that the stability of the solutions is influenced by the parameters of the system. These results correspond to those given by the previous variational equations (see Eqs. (3.2a)-(3.2h), and Eqs. (3.8a)-(3.8j)).

For the case of solution given by Eq. (3.7), Fig. 3.3 presents the blue stability domains, for some particular cases of the ratio between the soliton speeds X_3 and Y_2 (corresponding to the x and y transverse axis). The Fig. 3.3(a) showing a wide domain of the stability solution is obtained for $\beta = 0.5$, $\delta = -1$, $\nu = 0.72$ and $X_3 = Y_2/2$. Using the same previous dissipative values as in Fig. 3.3(a), with $X_3 = Y_2/5$, the stability domain decreases as can be seen in Fig. 3.3(b). For $\beta = 1.5$ $\delta = -1$, $\nu = 0.72$ and $X_3 = Y_2/5$, the corresponding stability domain (Fig. 3.3(c)) is considerably reduced. From Fig. 3.3, we notice that the components of the soliton speed as well as the amplitude, the widths, the chirps are greatly dependent on the dissipative parameters of the system, and consequently, the stability of the stationary solution. The evolution of the steady state amplitudes A_+ and A_- (Eq. (3.6)) as function of the cubic nonlinearity has been analyzed through the bifurcation diagram for the case of

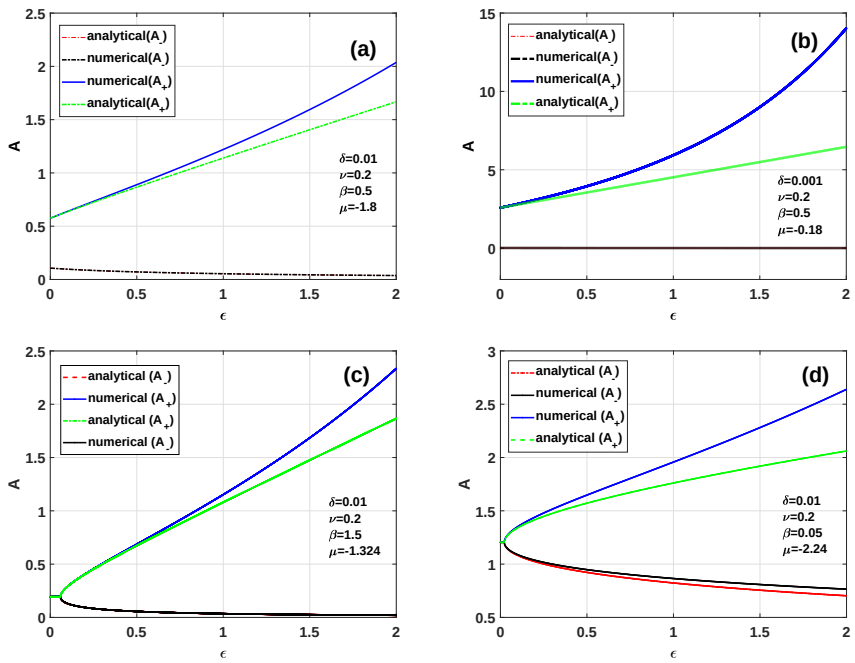

Figure 3.4: Bifurcation diagrams of stable A_- and unstable A_+ solutions with $\nu = 0.2$ in (a): $\beta = 0.05$, $\delta = 0.01$, $\mu = -1.324$; (b): $\beta = 0.05$, $\delta = 0.001$, $\mu = -0.18$; (c): $\beta = 1.5$, $\delta = 0.01$, $\mu = -1.324$; (d): $\beta = 0.05$, $\delta = 0.01$, $\mu = -2.24$.

solution given by Eq. (3.9). Then, in Fig. 3.4, typical bifurcation diagrams are shown where the amplitude of the steady state solution is plotted as a function of the parameter ε. As it is known, the valid variationally obtained analytical curves corresponding to Fig. 3.4 must be a good approximation of the numerical obtained results. In Fig. 3.4, we have shown the comparison between analytical and numerical bifurcation diagrams.

At this stage of our analysis, we have noted several behaviors of the comparison between analytical and numerical results of the amplitudes A_- and A_+. It can be seen in Figs. 3.4(a) and (b) that the solutions amplitude A_+ (numerical and analytical) present a good agreement for smaller values of the nonlinear parameter ε, associated with some discrepancies for increasing values of the amplitude.

At the same time, the solutions A_- present a good agreement for small amplitude (Fig. 3.4(a)) and zero amplitude (Fig. 3.4(b)). When varying the parameters β and μ, the comparison of bifurcation diagrams are shown in Figs. 3.4(c) and (d), where a good agreement is also noted

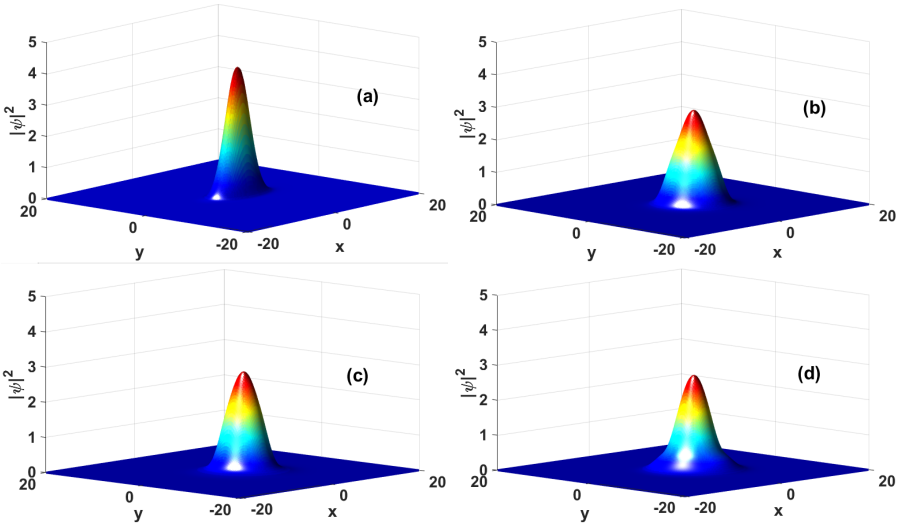

Figure 3.5: Profiles of the steady state solution at different positions along the propagation distance with parameters $\nu = 0.72$, $\beta = 0.5$, $\delta = -1$, $\varepsilon = 1.349$, $\mu = -0.3$. (a) z=0, (b) z=10, (c) z=100 and (d) z=4000.

between the solution A_- of lower amplitudes on the lower branch and the solution A_+ of the upper branch.

It is important to point out that the results in Fig. 3.4(d) are similar as those obtained by Skarka et al. **[92, 137]**. Therefore, our work presents a more general behavior of the dynamics of solutions A_+ and A_- in the very large space of parameters, where the cross compensation between the linear/nonlinear and loss/gain parameters is necessary to obtain the stability of the soliton solutions.

We are now interested on the global evolution of the solution, with the system parameters taken in the stable domain obtained in Figs. 3.3. Dealing with Eq. (3.7), we have noted an evolution of the initial solution as depicted in Fig. 3.5(a) with $\nu = 0.2$, $\beta = 0.5$, $\delta = -1$, $\varepsilon = 1.349$, $\mu = -0.3$. During this evolution, we have observe the shifting of the central position for some values of the parameters system, as has been analytically predicted. Also, the soliton intensity remains practically constant around an average value for different propagation distances (see Fig. 3.5(b) to 3.5(d)). From the dynamics depicted in Figs. 3.5, we can clearly noted the influence of the additional parameters stabilizing the dynamics of propagation, in

comparison to the work reported by Skarka et al. **[92]**. From this analysis, the stability of the solutions A_- and A_+ is a necessary condition to obtain a soliton after self-organizing evolution as reported also in Refs. **[92, 137, 202, 203]**.

It appears that the variational analysis associated to the Routh-Hurwitz conditions are useful treatments for the study of stability criteria for the propagation of dissipative solitons in nonlinear media. Due to the large parameters space, more detailed numerical simulations of both the variational equations and the CQ-CGL equation lead to a great variety of behaviors of the solutions.

3.3 Analysis of the coupled (2+1)D cubic-quintic complex Ginzburg-Landau equation

Let us recall that nonlinear dissipative systems modeled by the scalar cubic quintic CGL equation admit optical stable soliton solutions in one **[170]**, or several dimensions **[92, 171]**. The cubic-quintic complex equation has so many different types of solutions that this area of expertise is a whole world by itself. Even if we restrict ourselves to localized solutions, i.e., dissipative solitons of CGL equation, the variety of these objects is still not known in its full complexity although the regions of soliton existence have been studied quite extensively. Besides, the coupled CQ-CGL equation that we have derived is new in this area, and offers a wide range of localized solutions that we could not obtain from the scalar cubic quintic CGL equation or from the coupled kerr model derived by Gil **[78]**.

In our notation, the coupled (2+1)D CQ-CGL equation is

$$\begin{aligned} i\frac{\partial\psi_+}{\partial t} &+ \psi_+ + \Delta\psi_+ + |\psi_+|^2\psi_+ + \gamma_r|\psi_-|^2\psi_+ + \nu|\psi_+|^4\psi_+ + \delta_r\left(|\psi_-|^2 + 2|\psi_+|^2\right)|\psi_-|^2\psi_+ \\ &= i\left[\delta\psi_+ + \beta\Delta\psi_+ + \varepsilon|\psi_+|^2\psi_+ + \mu|\psi_+|^4\psi_+ + \delta_i\left(|\psi_-|^2 + 2|\psi_+|^2\right)|\psi_-|^2\psi_+\right], \end{aligned} \tag{3.17a}$$

$$\begin{aligned} i\frac{\partial\psi_-}{\partial t} &+ \psi_- + \Delta\psi_- + |\psi_-|^2\psi_- + \gamma_r|\psi_+|^2\psi_- + \nu|\psi_-|^4\psi_- + \delta_r\left(|\psi_+|^2 + 2|\psi_-|^2\right)|\psi_+|^2\psi_- \\ &= i\left[\delta\psi_- + \beta\Delta\psi_- + \varepsilon|\psi_-|^2\psi_- + \mu|\psi_-|^4\psi_- + \delta_i\left(|\psi_+|^2 + 2|\psi_-|^2\right)|\psi_+|^2\psi_-\right], \end{aligned} \tag{3.17b}$$

this model is derived in chapter II, where $\Delta = \frac{\partial^2}{\partial x^2} + \frac{\partial^2}{\partial y^2}$. The optical envelope $\psi_\pm(x, y, t)$ is the normalized complex function of three real variables x, y and t, where x and y are the normalized two transverse coordinates and t is the normalized propagation time. All the parameters of Eq. (3.17), i.e., ν, δ, ε, γ_r, γ_i, μ, δ_r and δ_i are real constants, and the pump profile parameter related to $\psi_\pm$ is normalized to unity **[204]**. The negative coefficient ν is the saturation of the Kerr nonlinearity, and the quintic coefficient $\delta_r < 0$ is the saturation of the cubic coupling absorption γ_r. The dissipative term δ is the linear loss/gain coefficient, β is the diffusion coefficient, ε is the cubic gain, μ is the quintic loss, γ_i and δ_i respectively denote the cubic and the quintic coupled coefficients. This model also finds its application in Bose-Einstein condensates, moreover a similarity result, but to (1+1)D had been derived by Bélobo et al. **[205, 206]**, Describing the dynamics of soltons in BECs, hence , this turns out to be an extension.

3.3.1 Variational approach for coupled (2+1)D cubic-quintic complex Ginzburg-Landau model for nonsymmetric structures

Due to its complexity, the coupled (2+1)D cubic-quintic CGL equation does not allow exact analytical solutions. Therefore, we extend the variational approach to dissipative systems described by the coupled (2+1)D CQ-CQL equations **[91, 92]**. The set of Euler-Lagrange equations characterize the solutions depending on the various dissipative parameters.

In this step of our analysis, Eqs. (3.17a) and (3.17a)are rewrite as the follows:

$$i\frac{d\psi_\pm}{dt} + \psi_\pm + \Delta\psi_\pm + |\psi_\pm|^2\psi_\pm + \gamma_r\,|\psi_\mp|\,\psi_\pm + \nu|\psi_\pm|^4\psi_\pm + \delta_r(|\psi_\mp|^2 + 2|\psi_\pm|^2)|\psi_\mp|^2\psi_\pm = \mathcal{Q}_\pm, \tag{3.18}$$

with

$$\mathcal{Q}_\pm = i(\delta\psi_\pm + \beta\Delta\psi_\pm + \varepsilon|\psi_\pm|^2\psi_\pm + \gamma_i\,|\psi_\mp|\,\psi_\pm + \mu|\psi_\pm|^4\psi_\pm + \delta_i(|\psi_\mp|^2 + 2|\psi_\pm|^2)|\psi_\mp|^2\psi_\pm). \tag{3.19}$$

The left-hand-side of Eq. (3.18) contains the conservative terms, where $\Delta = \frac{\partial^2}{\partial x^2} + \frac{\partial^2}{\partial y^2}$. The optical envelope $\psi_\pm(x, y, t)$ is the normalized complex function of three real variables x, y

and t, where x and y are the normalized two transverse coordinates and t is the normalized propagation time. The pump profile parameter related to $\psi_\pm$ is normalized to unity **[204]**. The right term $\mathcal{Q}_\pm$ of Eq. (3.18), given by Eq. (3.19), stands for the dissipation..

The variational method for dissipative systems is used in the following, with the objective to obtain more physical insight in terms of a few relevant parameters and then present numerical simulations that confirm the analytical predictions. Then the left-hand-side of Eq. (3.18) is derived from the Lagrangian density **[92, 206]** given by

$$\mathcal{L} = \frac{i}{2}\left(\psi_-^*\frac{\partial\psi_-}{\partial t} - \psi_-\frac{\partial\psi_-^*}{\partial t} + \psi_+^*\frac{\partial\psi_+}{\partial t} - \psi_+\frac{\partial\psi_+^*}{\partial t}\right) + \left|\frac{\partial\psi_\mp}{\partial x}\right|^2 + \left|\frac{\partial\psi_\mp}{\partial y}\right|^2 + \frac{1}{2}|\psi_\pm|^4 + \frac{\nu}{3}|\psi_\pm|^6 + \gamma_r|\psi_\mp|^2|\psi_\pm|^2 + \delta_r\left(|\psi_\pm|^4|\psi_\mp|^2 + |\psi_\pm|^2|\psi_\mp|^4\right), \tag{3.20}$$

where $\psi_\pm^*$ stands for the complex conjugate of $\psi_\pm$. Of course, the knowledge of the special characteristics of the propagation of laser beams through optical systems has to be one of the keystones of optical engineers and researchers working on optics, and the clear definition of their characteristic parameters has an important impact in the success of the applications of laser sources **[207]**. Gaussian beams play such an important role in optical lasers as well as in longer wavelength systems that they have been extensively analyzed. Almost every text on optical systems discusses Gaussian beam propagation in some detail, and several comprehensive review articles are available **[92, 170, 171, 188]**.

In order to extend our study to the characterization of the dissipative soliton during the propagation in the medium, we adopt the following Gaussian trial function **[92, 171, ?]**

$$\psi_\pm = A\exp\left\{-\frac{(x\pm X_m)^2}{2X^2} - \frac{y^2}{2Y^2} + iC(x\pm X_m)^2 + iSy^2 + i\phi\right\}, \tag{3.21}$$

where A is the amplitude, X and Y are the unequal spatial widths, C and S are the unequal wavefront curvature, X_m is the central position, and ϕ is the phase of the light bullet, all of which are functions of the independent variable t.

In order to proceed to the analytical treatment of the model and characterize the solutions depending on the various dissipative parameters, the equations for the motions of the variational parameters η are obtained through the Euler-Lagrange equations **[92, 206]**

$$\frac{d}{dt}\left(\frac{\partial \mathbf{L}}{\partial \dot{\eta}}\right) - \frac{\partial \mathbf{L}}{\partial \eta} = 2R_e \int\int dxdy \left(\mathcal{Q}_- \frac{\partial \psi_-^*}{\partial \eta} + \mathcal{Q}_+ \frac{\partial \psi_+^*}{\partial \eta}\right), \tag{3.22}$$

where $\dot{\eta} = \frac{d\eta}{dt}$. Here, η represents the parameters A, X, Y, C, S, X_m and ϕ in the ansatz, while

$$\mathbf{L} = \int\int \mathcal{L} dxdy \tag{3.23}$$

is the average Lagrangian of the conservative system obtained by substituting Eq. (3.21) into Eq. (3.20) and taking out integration over coordinates x and y. Thus, with the aim of the Euler-Lagrange equation **[171]**, we obtain the following set of differential equations describing the dynamics of the seven relevant parameters of the trial solution Eq. (3.21):

$$\begin{aligned}\frac{dA}{dt} =& 2A\left(S+C\right) - \delta A - \frac{3}{4}\varepsilon A^3 - \frac{5}{9}\mu A^5 + \beta A\left(\frac{1}{X^2}+\frac{1}{Y^2}\right) + \gamma_i A^3 e^{-\frac{2X_m^2}{X^2}}\left(-1+\frac{1}{4X^2}+\frac{1}{4Y^2}+\frac{X_m^2}{2X^2}\right)\\ &+ A^5\delta_i e^{-\frac{8X_m^2}{3X^2}}\left(-1+\frac{1}{4X^2}+\frac{1}{4Y^2}+\frac{4X_m^2}{9X^2}\right),\end{aligned} \tag{3.24a}$$

$$\begin{aligned}\frac{dX}{dt} =& 4CX\left(\beta CX^2-1\right) - \frac{\beta}{X^2} + XA^2\left(\frac{\varepsilon}{4}+\frac{2\mu A^2}{9}\right) + \gamma_i A^2 e^{-\frac{2X_m^2}{X^2}}\left(-\frac{X_m^2}{X}-\frac{1}{X}+\frac{X}{2}\right)\\ &+ \delta_i A^4 e^{-\frac{8X_m^2}{3X^2}},\end{aligned} \tag{3.24b}$$

$$\begin{aligned}\frac{dY}{dt} =& 4SY\left(\beta SY^2-1\right) - \frac{\beta}{Y^2} + YA^2\left(\frac{\varepsilon}{4}+\frac{2\mu A^2}{9}\right) + \gamma_i A^2 e^{-\frac{2X_m^2}{X^2}}\left(-\frac{1}{Y}+\frac{Y}{2}\right)\\ &+ \delta_i A^4 e^{-\frac{8X_m^2}{3X^2}}\left(-\frac{1}{2Y}+\frac{Y}{2}\right),\end{aligned} \tag{3.24c}$$

$$\begin{aligned}\frac{dC}{dt} =& 4C^2 + \frac{1}{X^2}\left(4\beta C - \frac{A^2}{4} - \frac{2\nu A^4}{9} - -\frac{1}{X^2}\right) + \frac{\gamma_r A^2}{4X^2} e^{-\frac{2X_m^2}{X^2}}\left(\frac{4X_m^2}{X^2}-1\right)\\ &+ \frac{2\delta_r A^4}{3X^2} e^{-\frac{8X_m^2}{3X^2}}\left(\frac{8X_m^2}{3X^2}-1\right),\end{aligned} \tag{3.24d}$$

$$\frac{dS}{dt} = 4S^2 + \frac{1}{Y^2}\left(4\beta S - \frac{A^2}{4} - \frac{2\nu A^4}{9} - \frac{1}{Y^2}\right) - \frac{\gamma_r A^2}{4Y^2} e^{-\frac{2X_m^2}{X^2}} - \frac{2\delta_r A^4}{3Y^2} e^{-\frac{8X_m^2}{3X^2}}, \tag{3.24e}$$

$$\frac{dX_m}{dt} = A^2 X_m\left(\gamma_i e^{-\frac{2X_m^2}{X^2}} + \frac{8\delta_i A^2}{9} e^{-\frac{8X_m^2}{3X^2}}\right), \tag{3.24f}$$

$$\frac{d\phi}{dt} = -1 - 2\beta\left(C+S\right) + \frac{1}{X^2} + \frac{1}{Y^2} + A^2\left(\frac{3}{4} + \frac{5\nu A^2}{9}\right) + \frac{\gamma_r A^2}{2} e^{-\frac{2X_m^2}{X^2}}\left(-\frac{X_m^2}{X^2} + \frac{3}{2}\right) + \frac{\delta_r A^4}{3}\left(-\frac{8X_m^2}{3X^4} + 5\right) e^{-\frac{8X_m^2}{3X^2}}. \tag{3.24g}$$

Eqs. (3.24a)-(3.24g) represent the coupled equations that show how pulse parameters change during propagation. Looking for steady state solutions of the system of Eqs. (3.24a)-(3.24g) after vanishing derivatives of amplitude, width, curvature, and central position, we focus our study to the symmetric steady state solutions, with $X_m = 0$, equal widths ($X = Y$) and spatial chirps ($C = S$). The corresponding steady state amplitude has two discrete values A^+ and A^- given by

$$A^{\pm} = \sqrt{\frac{9\beta\left(-4\beta(1+\beta\varepsilon+\gamma_r)\pm\sqrt{\Delta}\right)}{2(\beta\mu+4\nu+4\delta_r)}}, \tag{3.25}$$

with $\Delta = \frac{(1+\beta\varepsilon+\gamma_r)^2}{16\beta^2} - \frac{4\delta(\beta\mu+4\nu+4\delta_r)}{9\beta}$. We also obtain the width,

$$X = \left(\left(\left(\frac{\mu}{3} + \frac{\delta_i}{2}\right) A^4 + \frac{1}{2}(\varepsilon+\gamma_i)A^2 + \delta\right)/\beta\right)^{-1/2} + 0(\theta^2), \tag{3.26}$$

and the chirp

$$C = \frac{C_4 A^4 + C_2 A^2 + \delta}{4\beta^2}, \tag{3.27}$$

with $C_4 = \frac{1}{3}(2\mu + 3\delta_i + 4\beta(\delta_r + \frac{\nu}{3}))$, and $C_2 = \frac{1}{4}(2(\varepsilon+\gamma_i) + \beta(1+\gamma_r))$. The variational equations show clearly how the pulse parameters change during the propagation inside a waveguide and how they are coupled with each other.

To study the dynamical stability of the vector light bullet solution given above, we first derive the effective potential. An important criterion for the stability of our stationary solution is to investigate the possibility of light bullets to be trapped in the well. We examine the dynamical behaviors of a light bullet using the initial conditions given by Eqs. (3.25)-(3.27), from its symmetric equilibrium. Integration of variational Eqs. (3.24a)-(3.24g) gives **[171, 189, 208]**

$$\frac{1}{4}\left(\frac{dX}{dt}\right)^2 + \frac{1}{4}\left(\frac{dY}{dt}\right)^2 + U(X,Y) = U(X_0, Y_0), \tag{3.28}$$

where $U(X,Y)$ is the effective potential given in Appendix A. Eq. (3.28) describes the dynamics of the widths and shows a competition among diffraction and nonlinearity, and can be adopted

to study the stability of the optical light bullet through the medium. The existing stationary solution describes the motion of a particle located at the bottom of the potential well. Given the effective potential $U(X, Y)$, we have the equations

$$\frac{d^2X}{dt^2} = -2\frac{\partial U(X,Y)}{\partial X}, \tag{3.29a}$$

$$\frac{d^2Y}{dt^2} = -2\frac{\partial U(X,Y)}{\partial X}, \tag{3.29b}$$

which are equivalent to those describing the dynamics of a particle in two-dimensional potential well.

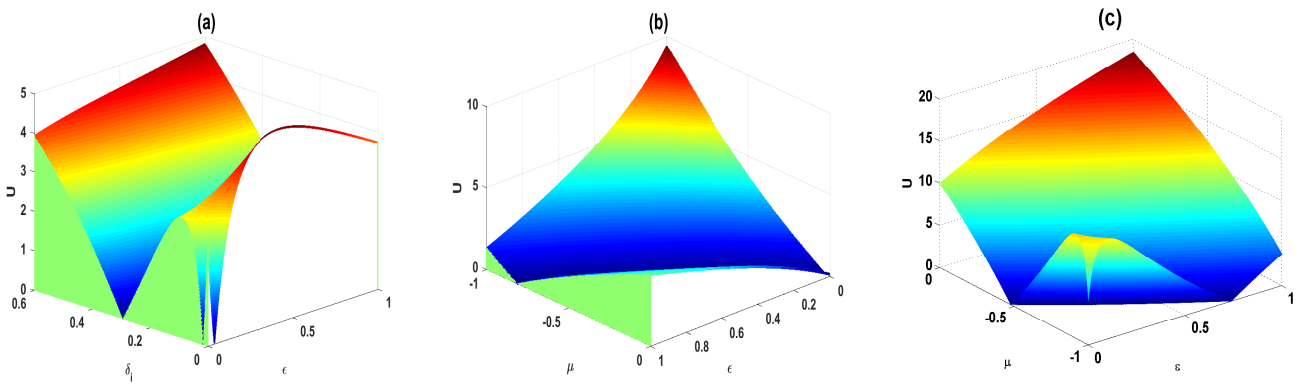

Figure 3.6: Effective potential U versus $(\varepsilon,\ \delta_i)$ in panel (a), and versus (ε, μ) in panels (b) and (c) for the parameters $\delta = -0.01059$, $\beta = 0.49$, $\gamma_i = 0.25118$, $\nu = -1$, and: (a) $\gamma_r = 1.1087$, $\delta_r = -0.5074$, $\mu = -.9$, $X_m = 1.3$, (b) $\gamma_r = 0.9$, $\delta_r = -0.5074$, $\delta_i = 0.04289$, $X_m = 1.3$, (c) $\gamma_r = 0.9$, $\delta_r = -0.35074$, $\delta_i = 0.04289$, $X_m = 0.05$.

When the nonlinearity exactly balances the diffraction, the curve of the potential shows an extremum, which is an equilibrium solution **[189]**. In such a direction, the obtained effective potential U, in the plane of nonlinear dissipative parameters, is depicted in Fig. 3.6, where panel (a) describes the effective potential versus (ε, δ_i), while panels (b) and (c) show U versus (ε,μ), confirming that the effective potential has a global minimum. This reveals the existence of a stable stationary light bullet. This confirms as well the existence of the stationary soliton solution corresponding to the optical dissipative soliton located at the bottom of the effective potential well. From Figs. 3.6, we observe that the shape of the effective potential depend to

the dissipative parameters as well as the soliton parameters. However, from Figs. 3.6(a)-3.6(c), the blue domains of the potential well corresponding to the bottom of the effective potential well (minima) are the domains of parameters for which the soliton can be trapped, and then, a stable propagation can be achieved. These confirm the analytical predictions form Eqs. (3.24a)-(3.24g). Fig. 3.6 presents two extrema, minima and maxima. Therefore, depending on the dissipative parameters and the central position, the beam will be either trapped or diffracted. The beam with initial condition corresponding to the point lying on the potential curve below the maximum will always be trapped, therefore generating a light bullet **[189]**. Using the variational method, it can be predicted that all beams initially around the minimum of the potential well will form light bullets around its equilibrium condition, with initial condition focusing until the turning point at the bottom region. The analysis of the potential well reveals the existence of a stable equilibrium which plays the role of an attractor **[171, 206]**.

Computer simulations are performed using the laser (2+1)D vectorial CQ-CGL equations Eq. (3.17) by means of the split-step Fourier Method (SSFM).

In order to confirm the analytical predictions, the coupled (2+1)D cubic-quintic CGL Eqs. (3.17) have been numerically solved by means of split-step Fourier method (SSFM) with a time-step $\Delta t = 10^{-3}$, on a mesh of size 100×100, with space-steps $\Delta x = \Delta y = 0.01$. The used initial conditions are Gaussian trial function given by Eq. (3.21), with amplitude $A = A^{-}$ (see Eq. (3.25)), the unequal spatial widths X given by Eq. (3.26) and $Y = X/3$, the unequal wavefront curvature C given by Eq. (3.27) and $S = C$.

For a good choice of dissipative parameters in the vicinity of the effective potential of Figs. 3.6, Figs. 3.7(a) and 3.7(d) show the spatial transverse profiles of the initial asymmetric dissipative light bullets with corresponding values of parameters taken around the bottom of the effective potential of Fig. 3.6(c), with $\delta_r = -0.35074$, $\epsilon = 0.456$, and $\mu = -0.98047$. During the evolution, we note a regular change from asymmetrical to a symmetrical light bullet for each

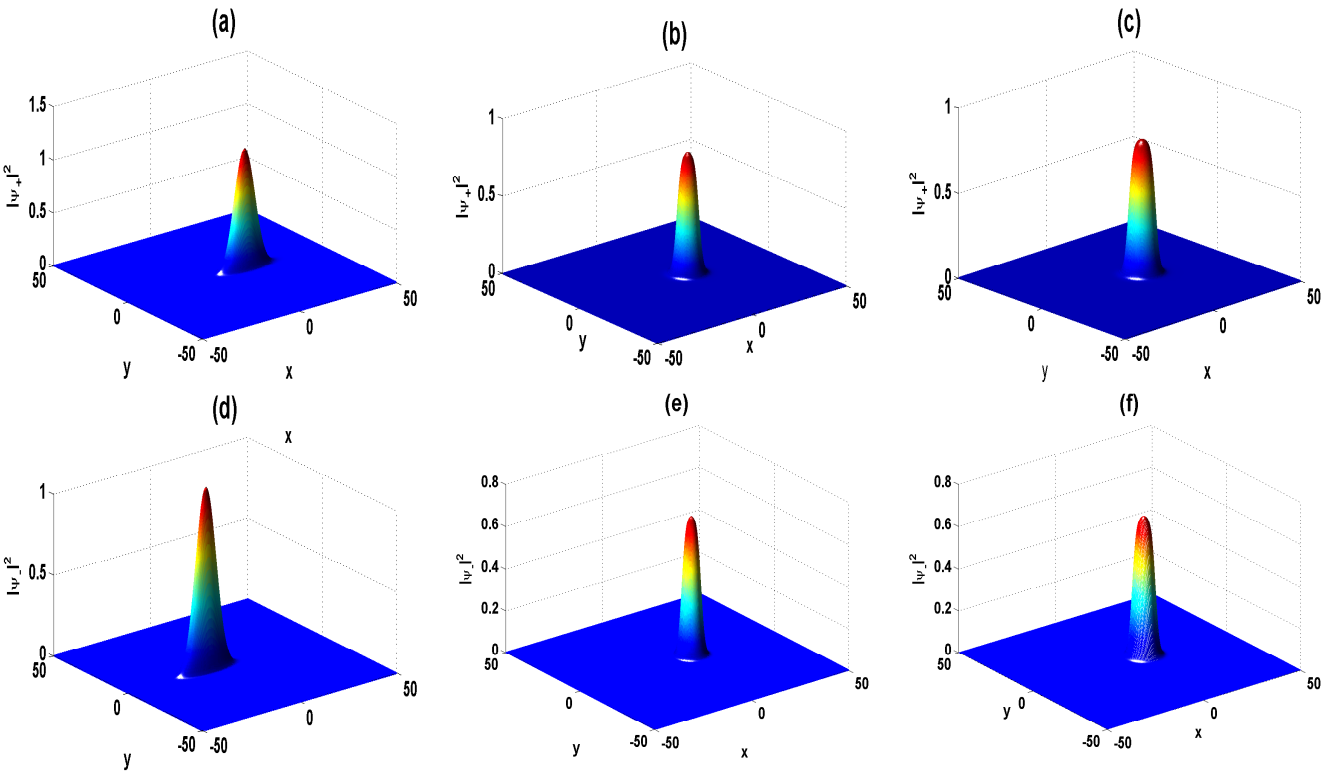

Figure 3.7: Spatial profile of $\psi_+(x, y)$ (panels (a) to (c)) and $\psi_-(x, y)$ (panels (d) to (f)). (a) and (d) correspond to $t = 0$, (b) and (e) correspond to $t = 100$, while (c) and (f) have been recorded at time $t = 50000$, with the parameters: $\delta = -0.01059$, $\beta = 0.45$, $\varepsilon = 0.456$, $\gamma_r = 0.9$, $\gamma_i = 0.25118$, $\delta_i = 0.04289$, $\delta_r = -0.35074$, $\nu = -1$, $\mu = -0.98047$, and $X_m = 10$.

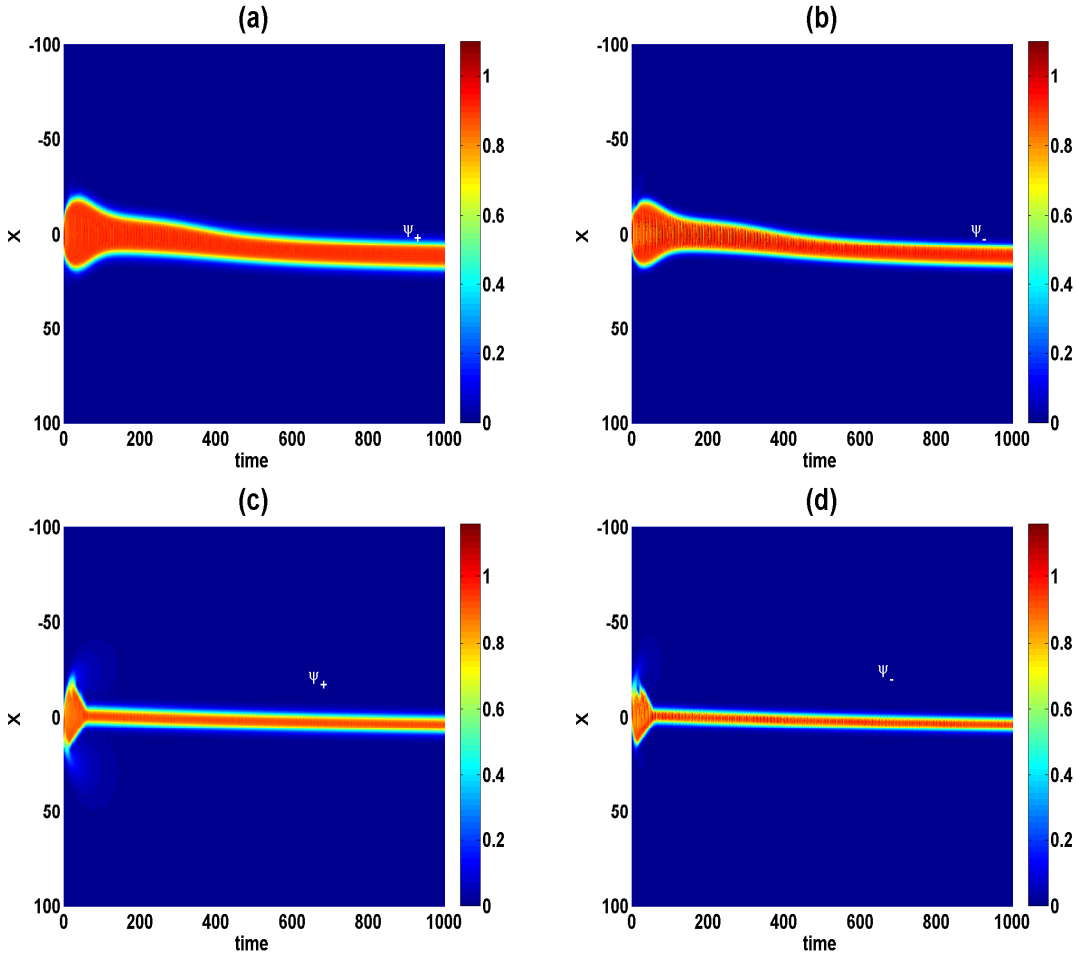

Figure 3.8: The density profiles of the space-time behavior of ψ_+ (panels (a) and (c)) and ψ_- (panels (b) and (d)). (a) and (b) correspond to $X_m = 0.5$ and $\gamma_r = 0.9$, while (c) and (d) give the results related to $X_m = 5$ and $\gamma_r = 1.109$. The rest of parameters remains the same as in Fig. 3.7.

solution ψ_+ and ψ_- (see Figs. 3.7(c) and 3.7(f)). We also observe a small shift of the central position, accompanied with a reduction of the intensity of the solution during a short time of propagation. Thereafter a stable propagation for longer time is observed. Figures 3.7(b) and 3.7(e) have been recorded at $t = 100$, and Figs. 3.7(c) and 3.7(f) correspond to $t = 50000$. Follows these results, we can deduce that the analysis of the possibility of the soliton trapped in the bottom of the effective potential can be a good criterium of the numerous important method, that can helps to analyze the stability of the soliton solution of the coupled multi-dimensional CQ-CGL equation.

In order to evaluate the influence of dissipative parameters on the stable dynamics of our predicted soliton solutions, the results of Figs. 3.8(a) and 3.8(b) have been obtained for $\gamma_r = 0.9$, $\delta_r = -0.3074$, $\varepsilon = 0.456$, $\mu = -0.98047$, $X_m = 1.5$ (values of other parameters are the same as in Fig. 3.7). Similarly to Fig. 3.7, we observe a small shift of the central position, a decreasing of the widths and also a small reduction of the intensity during a short-time of propagation. Stable dynamics for longer time of propagation is achieved as can observed in the figures. In order to better appreciate the influence of the coupled terms on the light bullet stability, Figs. 3.8(c) and 3.8(d) have been obtained for $\gamma_r = 1.109$, (values of other parameters are the same as in Figs. 3.8(a) and 3.8(b)). A regime of stable evolution of solutions ψ_+ (see Fig. 3.8(c)) and ψ_- (see Fig. 3.8(d)) is obtained in comparison to Figs. 3.8(a) and 3.8(b) for this value of coupled coefficient.

Secondly, we evaluated the influence of the quintic-coupled term, and the results are summarized in Fig. 3.9. Figures. 3.9(a) and 3.9(b) display the evolution of the cross-section of the

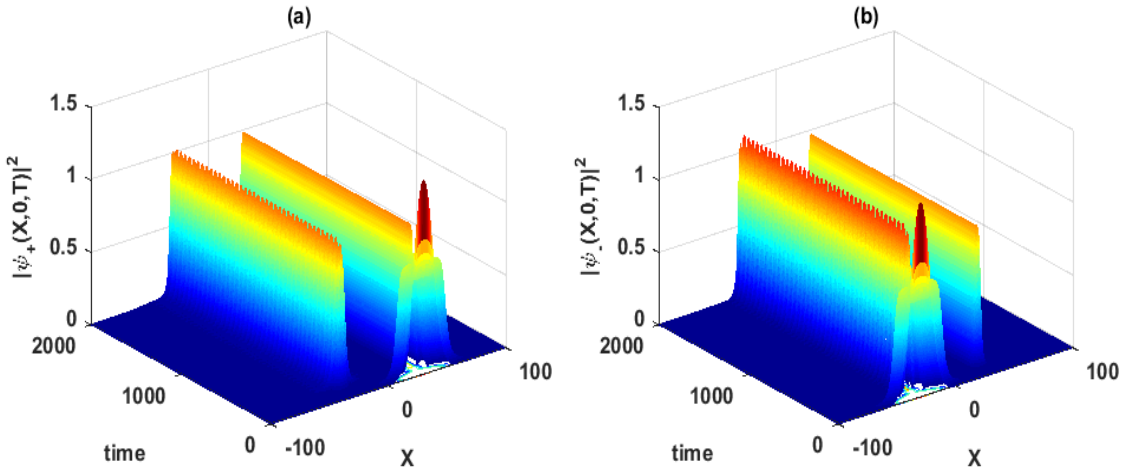

Figure 3.9: Wave space-time dynamics, which corroborates the stability of the dissipative light bullets (a) $\psi_+(x,0,t)$ and (b) $\psi_-(x,0,t)$ obtained for the $\gamma_r = 1.109$ and $\delta_r = -0.15074$, with the other parameters keeping the similar values as in Fig. 3.7.

dissipative light bullets obtained from direct numerical simulations of the full coupled (2+1)D CQ-CGL equation for $\delta_r = -0.15074$, $\varepsilon = 0.49$, $\mu = -0.9$, $X_m = 10$ while the other pa-

rameters remain the same as in Figs. 3.8(c) and 3.8(d). Figs. 3.9(a) and 3.9(b) show the generation of the second couple of light bullets with stable evolution. We depict the generation of the second pulse when the stable regime started. The stable evolution of those coupled soliton solutions is an illustration of the stable characteristic of our sustem. In order to have a stable evolution of the coupled dissipative light bullets, we need the balance between gain/loss, diffraction/nonlinearity and, as shown our analysis, the balance between the coupled effects.

In Fig. 3.10, we have summarized the stable evolution the dissipative light bullets. The obtained (2+1)D stable coupled spatial dissipative light bullets are among new interesting dynamical aspects of laser optics. We have realized through numerical simulations that the intensity of the initially generated asymmetric light bullets (see Figs. 3.10(a) and 3.10(b)) decreases in the beginning (see Figs. 3.10(c) and 3.10(d)), which is followed thereafter by the reconstitution of the coupled light bullets when the coupling changes (see Figs. 3.10(e) and 3.10(f)). This gets more pronounced when time increases and remains very sensitive to the coupling parameters, leading to a stable evolution of the light bullets over longtime propagation (see Figs. 3.10(g) and 3.10(h)).

We have reported the comprehensive analysis of the formation of vector light bullets in an optical nonlinear medium described by a set of (2+1)D cubic-quintic CGL equations. Through the variational method, we have performed the theoretical analysis using a Gaussian trial function as solution, and we have obtained seven coupled first-order differential equations whose solutions have been discussed. Such analytical results have been confronted to direct numerical simulations via the the split-step Fourier method, where we have successfully shown that the system is able to interchange energy to keep both light bullets bounded, this under the balance between gain/losses, dispersion/diffraction and nonlinearities. Under such conditions, we have noticed the emergence of asymmetric dissipative light bullets and their disintegration on one hand, and stable evolution of the coupled dissipative light bullets on the other hand. Moreover,

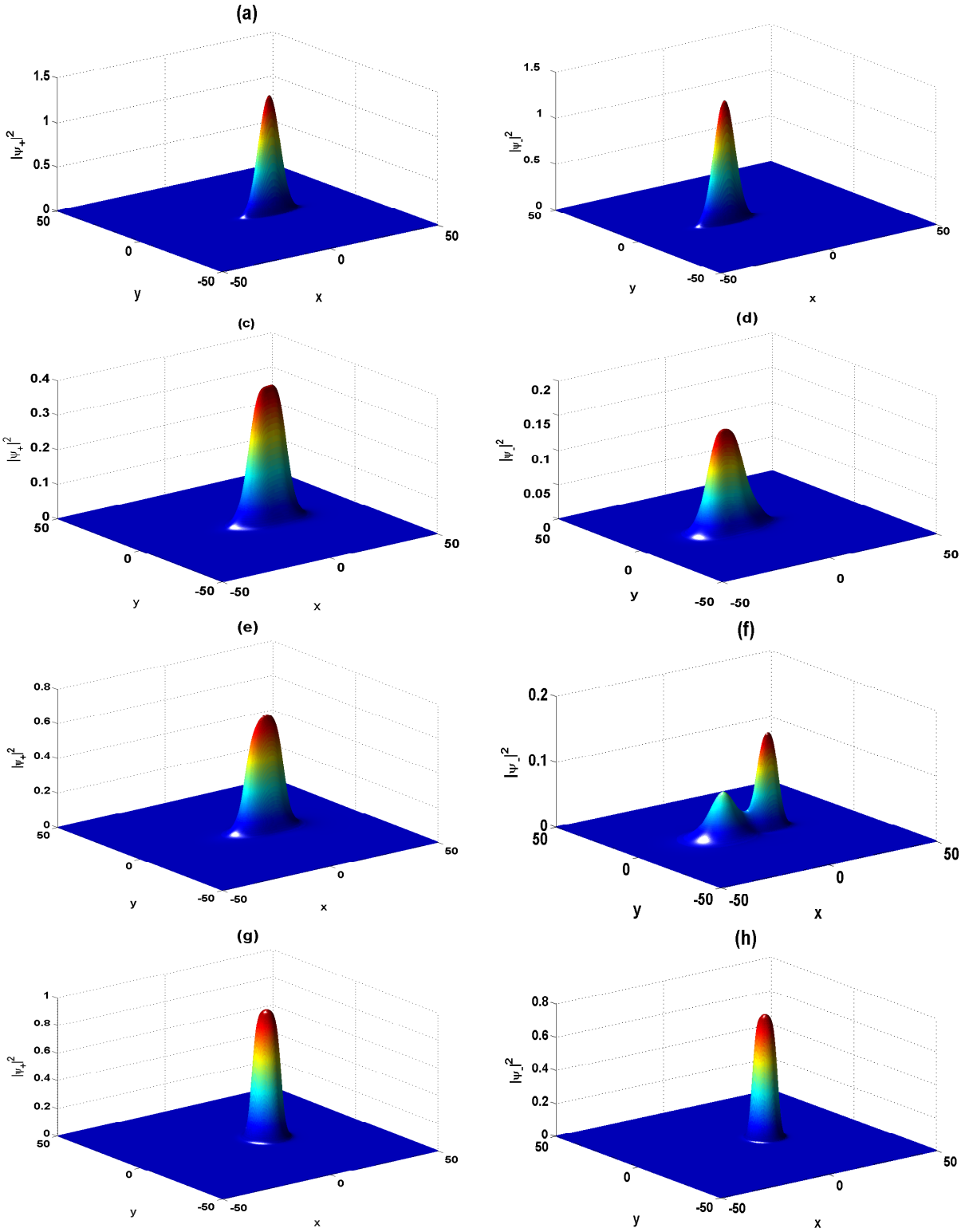

Figure 3.10: (2+1)D spatial profiles of the light bullet intensities $|\psi_+(x,y)|^2$ (left column) and $|\psi_-(x,y)|^2$ (right column) obtained from direct simulation of Eq. (3.18) at times $t = 0$ [(a) and (b)], $t = 10$ [(c) and (d)], $t = 25$ [(e) and (f)], and $t = 50000$ [(g) and (h)], with the set of parameters: $\delta = -0.01059$, $\beta = 0.45$, $\varepsilon = 0.49$, $\gamma_r = 0.9$, $\gamma_i = 0.25118$, $\delta_i = 0.04289$, $\delta_r = -0.25074$, $\nu = -1$, $\mu = -0.9$, and $X_m = 10$.

the formation of (2+1)D stable coupled spatial dissipative light bullets has been detected. They have been found to be very sensitive to coupling parameters, whose impact on the long-time dynamics was pronounced. However, this implies new interesting dynamical aspects of laser optics, since the involved coupling mechanism can be adopted as a tool to generate appropriate stabilized vector light bullets which could be otherwise difficult to obtain.

3.3.2 Variational approach for coupled (2+1)D cubic-quintic complex Ginzburg-Landau model for a moving symmetric lattices

We also investigate the propagation characteristics and stabilization of moving-Gaussian pulse in laser media in order to understand the dynamical properties of the vector moving dissipative solitons for several dynamical regimes of the coupled (2+1)D CQ-CQGL equation **[199]**. The theoretical method to investigate the two spin components of a coupled (2+1)D CQGL equation is the variational approach. Therefore, we look for solutions of Eq. (3.18) in the symmetric gaussian form **[170, 199, 206]**, as

$$\psi_{\pm} = A \exp\left\{ -\frac{(x \pm X_0)^2 + y^2}{2X^2} + i[2C((x \pm X_0)^2 + y^2) \pm N(x \pm X_0) + \varphi] \right\}, \tag{3.30}$$

where A is the amplitude, X is the spatial width, C is the unequal wavefront curvature, X_0 is the central position, φ is the phase and N accounts for the motion of the soliton along the transverse direction.

Hence, the corresponding set of six Euler-Lagrange equations are

$$\begin{aligned}\frac{dA}{dt} &= -\frac{3}{4}A^3\varepsilon + \frac{2A^2\beta}{X^2} - \frac{5}{9}A^5\mu + 4AC + A\beta N^2 - \delta A + \left(-1 + \frac{1}{2X^2} + \frac{X_0^2}{X^2}\right) A^3\gamma_i e^{-\frac{2X_0^2}{X^2}} \\ &+ \left(\frac{8X_0^2}{9X^2} - 1 + \frac{1}{2X^2}\right) A^5\delta_i e^{-\frac{8X_0^2}{3X^2}},\end{aligned} \tag{3.31a}$$

$$\frac{dX}{dt} = -\frac{1}{4}A^2X\varepsilon - \frac{\beta}{X} + \frac{2}{9}A^4X\mu + 4XC\left(\beta CX^2 - 1\right) + \frac{1}{2}\left(-X + \frac{1}{X} + \frac{2X_0^2}{X}\right)A^2\gamma_i e^{-\frac{2X_0^2}{X^2}} + \left(\frac{16X_0^2}{9X} - 1 + \frac{1}{X}\right)A^4\delta_i e^{-\frac{8X_0^2}{3X^2}}, \tag{3.31b}$$

$$\frac{dC}{dt} = -\frac{1}{4X^2}A^2 - \frac{2}{9X^2}A^4\nu + \frac{4\beta C}{X^2} + \frac{\gamma_r A^2}{X^2}\left(\frac{X_0^2}{X^2} - \frac{1}{4}\right)e^{-\frac{2X_0^2}{X^2}} + \frac{2\delta_r A^4}{3X^2}\left(\frac{8X_0^2}{9X^2} - 1\right)e^{-\frac{8X_0^2}{3X^2}} - \frac{1}{X^4} + 4C^2, \tag{3.31c}$$

$$\frac{dN}{dt} = 2N\beta\left(\frac{1}{X^2} + 4X^2C^2\right) + (2\gamma_i C - \frac{\gamma_r}{X^2})A^2X_0e^{-\frac{2X_0^2}{X^2}} + \left(\delta_i C - \frac{\delta_r}{X^2}\right)\frac{16A^4X_0}{9}e^{-\frac{8X_0^2}{3X^2}}, \tag{3.31d}$$

$$\frac{dX_0}{dt} = 2N\beta\left(-1 + 2X^2C\right) + \gamma_i A^2X_0e^{-\frac{2X_0^2}{X^2}} + \frac{8\delta_i A^4X_0}{9}e^{-\frac{8X_0^2}{3X^2}}, \tag{3.31e}$$

$$\frac{d\varphi}{dt} = 1 + 4\beta C\left(NX^2 - 1\right) + \frac{5}{9}A^4\nu + \frac{3}{4}A^2 + \frac{2}{X^2} - N^2 + \left(\gamma_i NX_0 + \frac{3\gamma_r}{4} - \frac{\gamma_r X_0^2}{X^2}\right)A^2e^{-\frac{X_0^2}{X^2}} + \frac{1}{3}\left(\frac{8\delta_i NX_0}{3} + 5\delta_r - \frac{16\delta_r X_0^2}{3X^2}\right)A^4e^{-\frac{8X_0^2}{3X^2}}. \tag{3.31f}$$

Evidently, the variational technique reveals the interaction between the symmetric gaussian waves and the laser system, including the additional relevant effects, during propagation. The dynamics of the entire soliton can be greatly affected during the propagation.

However, as well as the theoretical analysis shows the influence of the system on the dissipative soliton dynamics, explicit information related to the different solutions and their stability cannot be obtained at this stage of the analytical procedure.

The steady-state solutions of the system of Eqs. (3.31a) to (3.31e) are obtained by setting the derivatives of soliton parameters with respect to *time*, to zero. Taking $X_0 = 0$, for more simplicity, and after some algebra, we obtain the following solutions that give:

i) the amplitude

$$A = \frac{3}{2}\sqrt{-\frac{1+\gamma_r}{2(\nu + 3\delta_r)}}, \tag{3.32}$$

ii) the width

$$X = \left[\frac{((18\beta\delta_i + 24\delta_r) + 8(\beta\mu - \nu))A^4 + 9(\beta(\varepsilon - \gamma_i) - 1 - \gamma_r)A^2}{36(2(1+\beta^2) + \frac{\beta A^2}{2}(\gamma_i + A^2\delta_i))} \right]^{-1/2}, \tag{3.33}$$

iii) the soliton velocity

$$N = \sqrt{\frac{\delta + \frac{1}{2}(\gamma_i + \varepsilon)A^2 + (\frac{\delta_i}{2} + \frac{\mu}{3})A^4}{\beta}}, \tag{3.34}$$

iv) the unequal wavefront curvature

$$C = \frac{1}{2\beta X^2}, \tag{3.35}$$

necessary to build the steady-state solution.

The stability analysis of the moving dissipative soliton is performed through the effective potential (see Appendix B).Doing so, we first investigate the possibility of the soliton trapped at the bottom of the effective potential well.

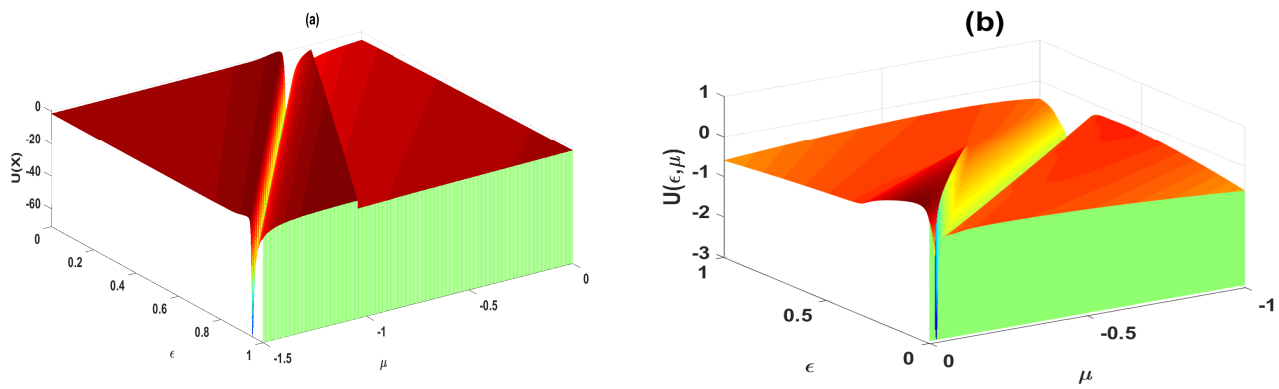

Figure 3.11: Potential $U(\varepsilon, \mu)$ for the following set of parameters: $\nu = -1$, $X_0 = 12.5$; (a) $\delta = -0.159$, $\gamma_r = 1.1087$, $\gamma_i = 0.2118$, $\beta = 0.0159$, $\delta_i = 0.1289$, $\delta_r = -0.5074$, (b) $\delta = -0.13761$, $\gamma_r = 1.0535$, $\gamma_i = 0.1001$, $\beta = 0.1761$, $\delta_i = 0.43$, $\delta_r = -0.5016$.

The analysis of the possibility of the soliton to be trapped in the well is presented in Fig. 3.11. The used parameters correspond to the population inversion decay rate $\gamma_{||} = 10^7 s^{-1}$, polarization decay rate $\gamma_\perp = 3.9 \times 10^9 s^{-1}$, the cavity loss $\kappa = 9.9 \times 10^7 s^{-1}$ and the lasing wavelength $\lambda = 10.6\ \mu m$ **[209]**, together with the atomic transition frequency $\omega_a = 0.2 \times 10^8 s^{-1}$ for Fig. 3.11(a), and $\omega_a = 2.5 \times 10^8 s^{-1}$ for Fig. 3.11(b). From Figs. 3.11(a) and 3.11(b), we

can observe the appearance of two domains of instability (plane domain with zero potential and the domain of maximum potential), and the stability domain with minimum values of the effective potential, where the soliton can be trapped. For a good choice of dissipative parameters, belonging to the stable domain (bottom of the effective potential), the generated symmetric gaussian input solution will be self-trapped and will shows a stable propagation.

The time evolution of the solution parameters has been numerically investigated by means of the fourth-order Runge-Kutta computational method.The results displayed in Figs. 3.12(a)and 3.12(b) show that the amplitude A, the width X, the velocity N, and the unequal wavefront curvature C evolve with a slight change at the beginning of their propagation. From Figs. 3.12(c) and 3.12(d) (showing the input/output of the two solutions), one sees the increasing of the widths, slight decrease of the intensities and the shift of the central position corresponding to the two solutions. Despite this slight difference, the variational analysis gives a qualitative detailed picture of the role and mode of action of each perturbation (such as coupled, diffraction, self-phase modulation, loss or gain) on the pulse during propagation. Using parameters corresponding to the stable domain of Fig. 3.11(b) (bottom of the effective potential), we obtain Figs. 3.13(a) and 3.13(b). They present a stable evolution of the intensities of the coupled moving dissipative solitons ψ_- and ψ_+ during propagation in the space-time domain. In fact, each profile carry some information that is given by it spectral profile. The spectral profile Figs. 3.13(c) and 3.13(d) show the corresponding spectral evolution of Figs. 3.13(a) and 3.13(b). Albeit the initial shift of their central position, which is in agreement with the analytical predictions (see Eqs. (3.31a)-(3.31f)) concerning particularly the influence of the dissipative parameters on the solitons central position and the speed parameters, together with Fig. 3.11, solitons remain stable during propagation. However, as we have noted, a continuous shift of the initial central position during propagation, the corresponding spectral dynamics presents constant central position (see Figs. 3.13(c) and 3.13(d)).

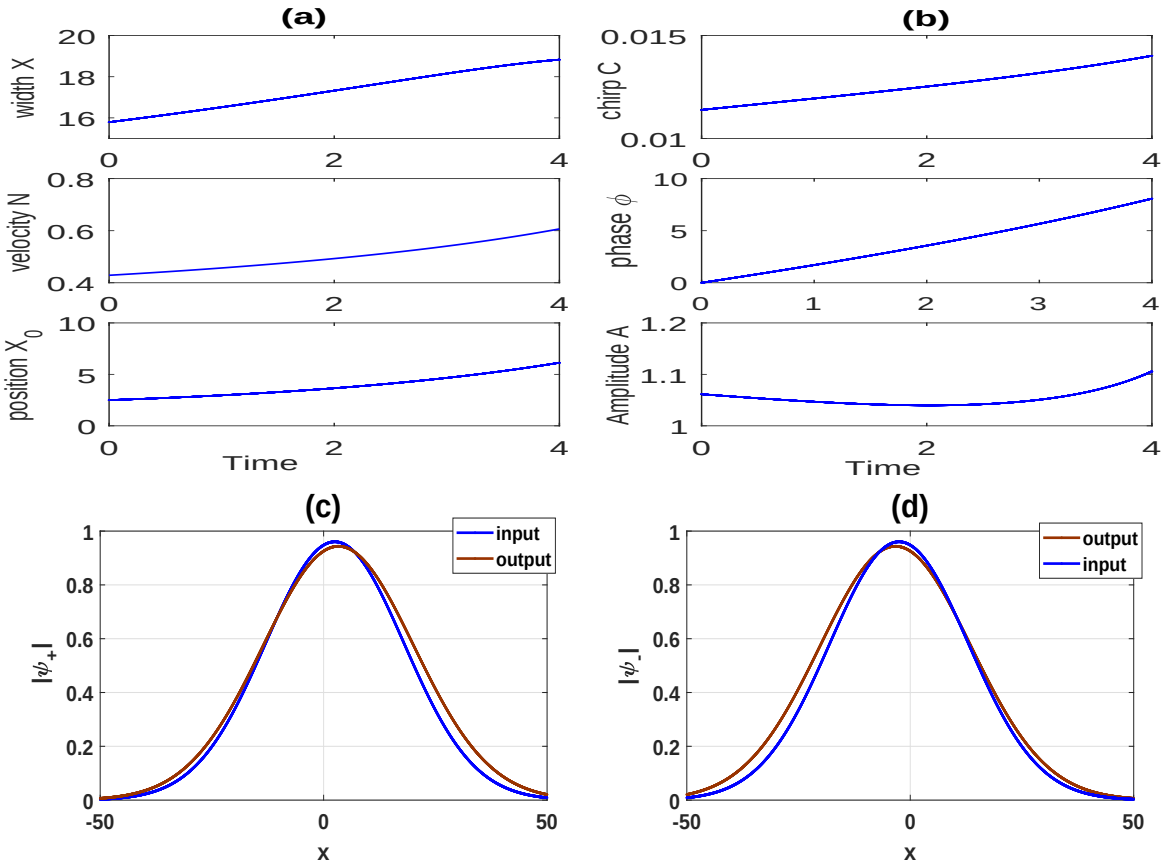

Figure 3.12: Panels (a) and (b) display the evolution of the amplitude, the pulse widths, the chirp, the unequal wavefront curvatures, the velocity, the central position and the phase with respect to t. Panels (c) and (d) depict the input/output profiles of the solutions ψ_+ and ψ_- for the following set of parameters: $\delta = -0.159$, $\gamma_r = 1.1087$, $\gamma_i = 0.2118$, $\nu = -1$, $\beta = 0.0159$, $\delta_i = 0.1289$, $\delta_r = -0.5074$, and the initial central position $X_0 = 2.5$.

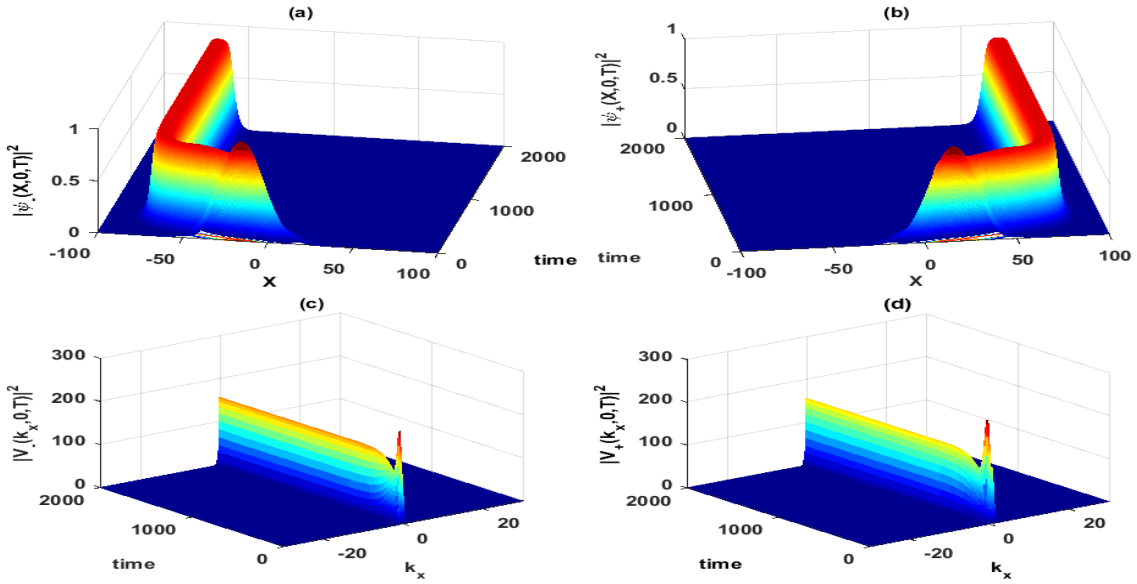

Figure 3.13: Panels (a) and (b) show the three dimensional spatial evolution as predicted by the stability of the dissipative soliton trapped in the potential well. Panels (c) and (d) display their corresponding spectral evolution V_- and V_+, respectively for the values of parameters $\varepsilon = 0.72$, $\mu = -0.728$ and $X_0 = 15.5$.

It is well known that, in the case of the CQ-CGL equation, there can be several stable solutions existing for the same set of parameters. It means that the characteristics of this behavior are also given by the parameters of the system. Here we restrict ourselves to localized solutions, i.e., dissipative solitons of CGL equation, the variety of these objects is still not known in its full complexity although the regions of soliton existence have been studied quite extensively **[130]**. Stable harmonic time evolution of solutions ψ_+ and ψ_- are shown in Figs. 3.14(a) and 3.14(b). So the results are confirmed by the prediction of Haken **[210]**, showing that the lasers are stable systems. Fig. 3.14(b) with its corresponding spectral evolution shown in Fig. 3.14(d) reveal the moving harmonic dynamics. On the other hand, Figs. 3.14(a) and the corresponding spectral evolution (see Fig. 3.14(c)), related to the solution ψ_+, show a stationary harmonic evolution with large period, compared to ψ_- solution. This coherent evolution is an important property of laser systems, and are used in some applications such as holography and interferometry **[211, 212]**. When carefully adjusting the nonlinear parameters

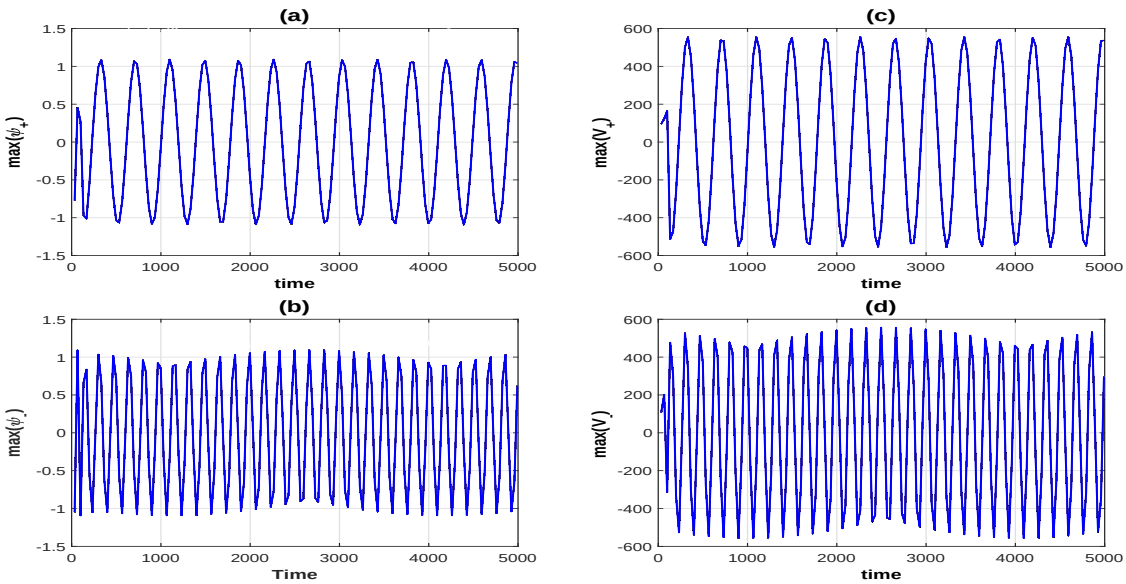

Figure 3.14: Panels (a) and (b) are the periodic evolution of $max(\psi_+(t))$ and $max(\psi_-(t))$ of the dissipative soliton obtained by direct numerical simulation of Eq. (13). The corresponding spectral evolution $max(V_+(t))$ and $max(V_-(t))$ are presented in panels (c) and (d), with $\delta_r = -0.25016$, $\varepsilon = 0.72$, and $\mu = -0.73$, while the rest of parameters remains the same in Figs. 3.11(b).

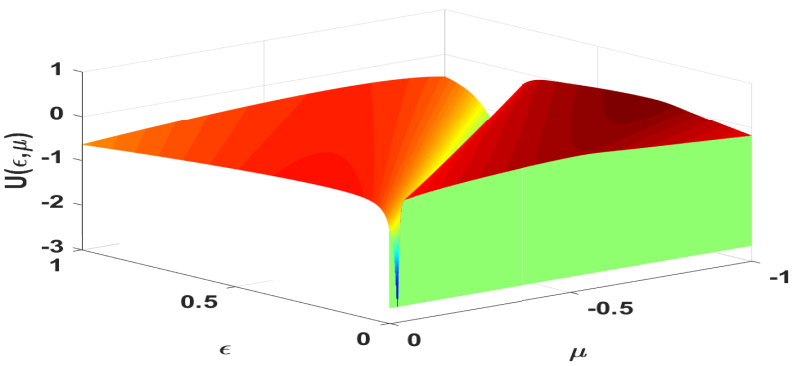

Figure 3.15: Potential $U(\varepsilon, \mu)$, as a function ε and μ, for $\delta_r = -0.25016$. The other parameters remain unchanged as in Fig. 3.11(b).

around the bottom of the effective potential well, a typical optical evolution of the solution is depicted and displayed in Figs. 3.16(a) and 3.16(b), for the maximum values of ψ_+ and ψ_-, respectively. Their corresponding spectral evolutions are given in Figs. 3.16(c) and 3.16(d). The variational results shows that, during the dynamic, the central position is affected by the dissipative parameters, and the the soliton parameter. Also, the analysis of the effective potential shown that the soliton can be traps in the bottom of the effective potential. Figs. 3.14 and 3.16 leads to a good agreement both for analytical and numerical results. In fact, a periodic evolution is noted in Fig. 3.14 using parameters taken from the bottom of the potential well. When shifting such values,we observe a gradually change of periodicity of the solutions ψ_+ and ψ_-, which indicates a gradually lost of stability as presented in Fig. 3.16. Interestingly, similar result was experimentally obtained by Cohen et al. **[213]**, using a semiconductor laser with quasi-periodic dynamics induced by external optical feedback from a cavity with two arms, also known as the T-cavity. They showed the existence of frequency shifts in the spectrum occurring in the optical domain, therefore given the way for the development of novel laser-feedback-based devices with the capability for subwavelength, nanoscale, multidimensional position sensing.

Figures. 3.17(a), 3.17(c) and 3.17(e) for $|\psi_+(x,y)|^2$, and Figs. 3.17(b), 3.17(d) and 3.17(f) for $|\psi_-(x,y)|^2$ present the three-dimensional evolution of the dynamics given in Figs. 3.14(a) and 3.14(b), and reveal the formation of alternate structures, that had been predicted and observed in the CO_2 laser **[214]**.

Fig. 3.18 presents profiles of dissipative solitons at different propagation times. The obtained 3D stable spatiotemporal optical solitons, by direct numerical simulations,are among new interesting dynamical aspects of dissipative optical solitons. The results are obtained with $X_0 = 12.5$, $\delta_r = -0.3$, and the rest of parameters are the same as those of Fig. 3.17. We observe that when carefully adjusting the value of δ_r, the initial symmetric solution (see Figs. 3.18(a) and 3.18(b)) evolves toward a new stable formation with a non-smooth vertex top

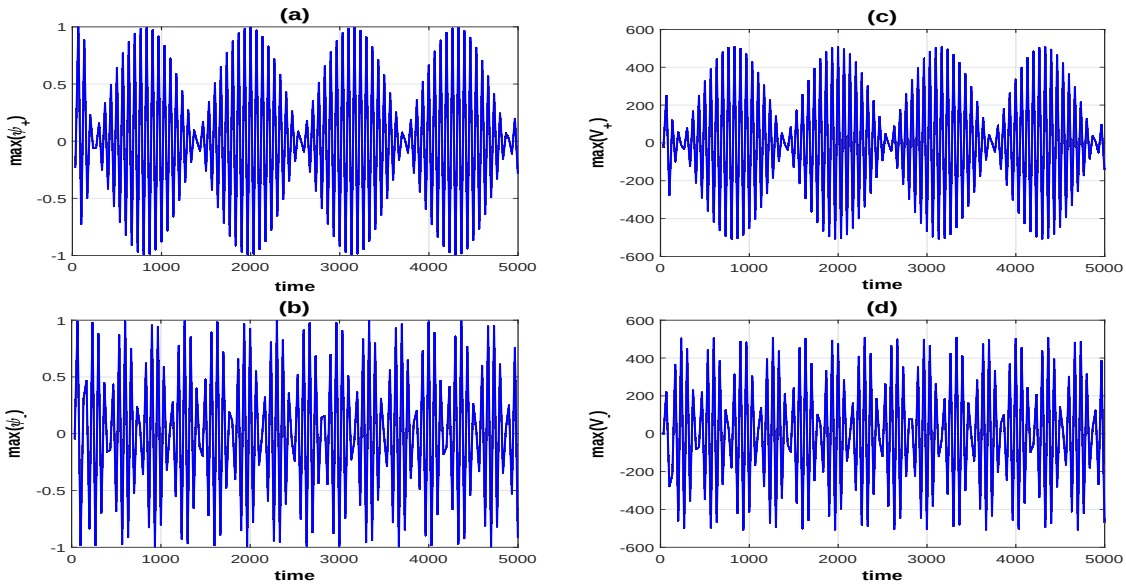

Figure 3.16: Panels (a) and (b) show the quasi-periodic evolution of $max(\psi_+(t))$ and $max(\psi_-(t))$ of the dissipative soliton by direct numerical simulation of Eq. (13). The corresponding spectrals evolution $max(V_+(t))$ and $max(V_-(t))$ are presented in panels (c) and (d), with $\delta_r = -0.25016$, $\varepsilon = 0.63051$ and $\mu = -0.728$. The rest of parameters are taken from Fig. 3.11(b).

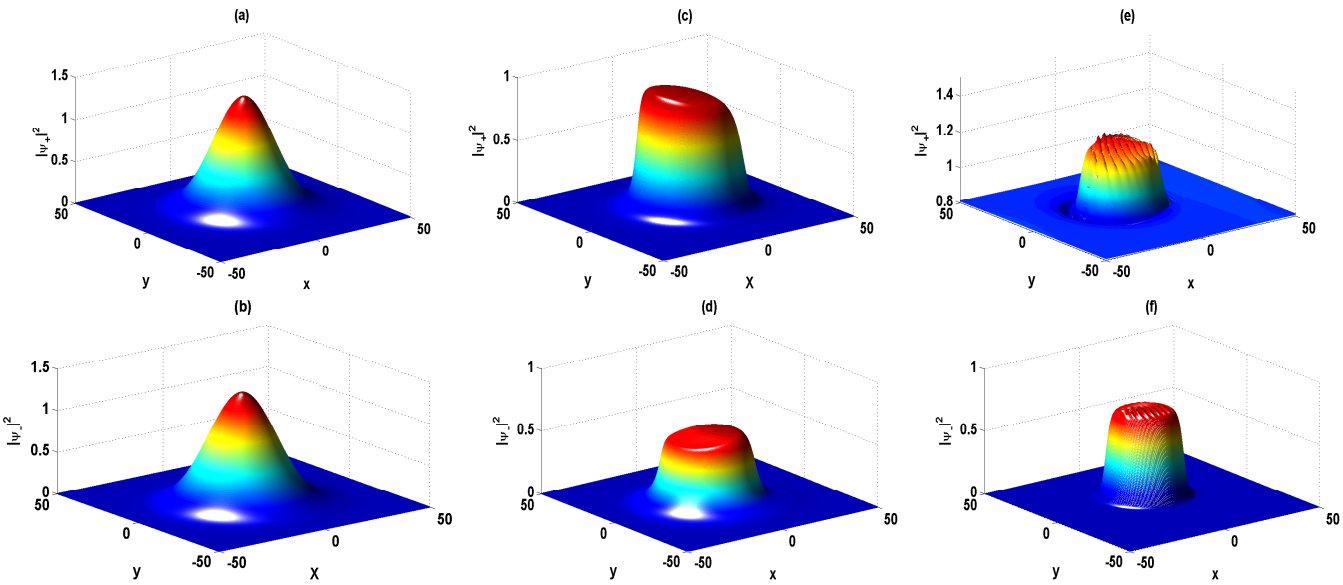

Figure 3.17: Spatial profiles of the solution $\psi_+(x, y)$ (upper line) and $\psi_-(x, y)$ (bottom line) at different steps of the evolution: (a) and (b) $T = 0$, (c) and (d) $T = 4$, (e) and (f) $T = 10000$, using the following parameters: $\delta = -0.13761$, $\beta = 0.1761$, $\varepsilon = 0.7$, $\gamma_r = 1.0535$, $\gamma_i = 0.1001$, $\delta_i = 0.043$, $\delta_r = -0.25016$, $\nu = -1$, $\mu = -0.73$, and $X_0 = 2.5$.

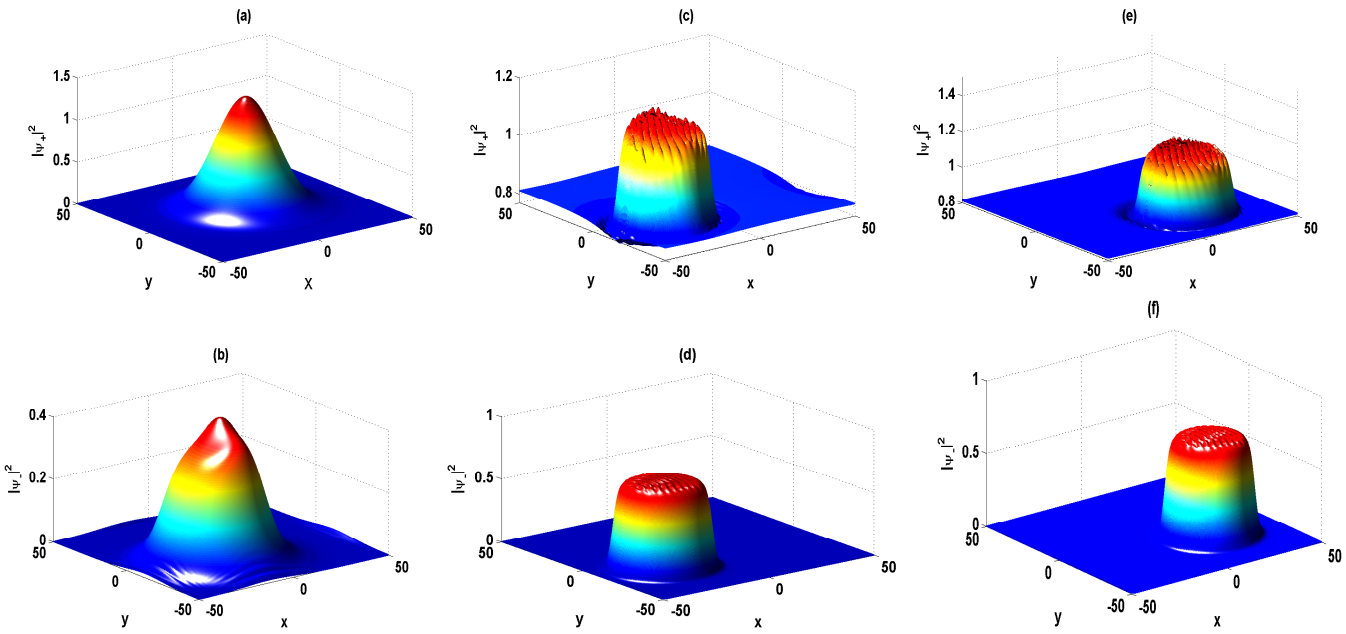

Figure 3.18: Spatial profile of the solution $\psi_+(x,y)$ (upper line) and $\psi_-(x,y)$ (bottom line) at different steps of the evolution: (a) and (b) $T = 0$, (c) and (d) $T = 15000$, (e) and (f) $T = 30000$, using the following parameters values: $\delta = -0.13761$, $\beta = 0.1761$, $\varepsilon = 0.7$, $\gamma_r = 1.0535$, $\gamma_i = 0.1001$, $\delta_i = 0.043$, $\delta_r = -0.3$, $\nu = -1$, $\mu = -0.73$, and $X_0 = 12.5$.

profile. Recently, a similar result was obtained by Djoko et al. **[215]**. They showed that such profiles are stable and can be considered as potential objet for long-distance transmission in communication systems. These stable structures can be a good candidates for laser devices.In order to confirm the results of Fig. 3.18, Fig. 3.19 displays the spectral evolution of the solution given in Fig. 3.18, and it follows that, in spite of the non-smooth vertex top profile, those profiles remain stable. These structures can be a good candidates for class B laser devices.

By the means of the effective potential of the system, we have shown that solitons can be trapped in the potential well, leading to a good agreement between analytical and numerical results. In such dissipative systems, Cross-compensation involving self-focusing, loss/gain and coupled effects appear as a stabilization mechanism of the controllable behavior of induced optical vector moving solitons during propagation. As the stability criterium is based on the possibility of the soliton trapped in the bottom of the potential well, an appropriate choice

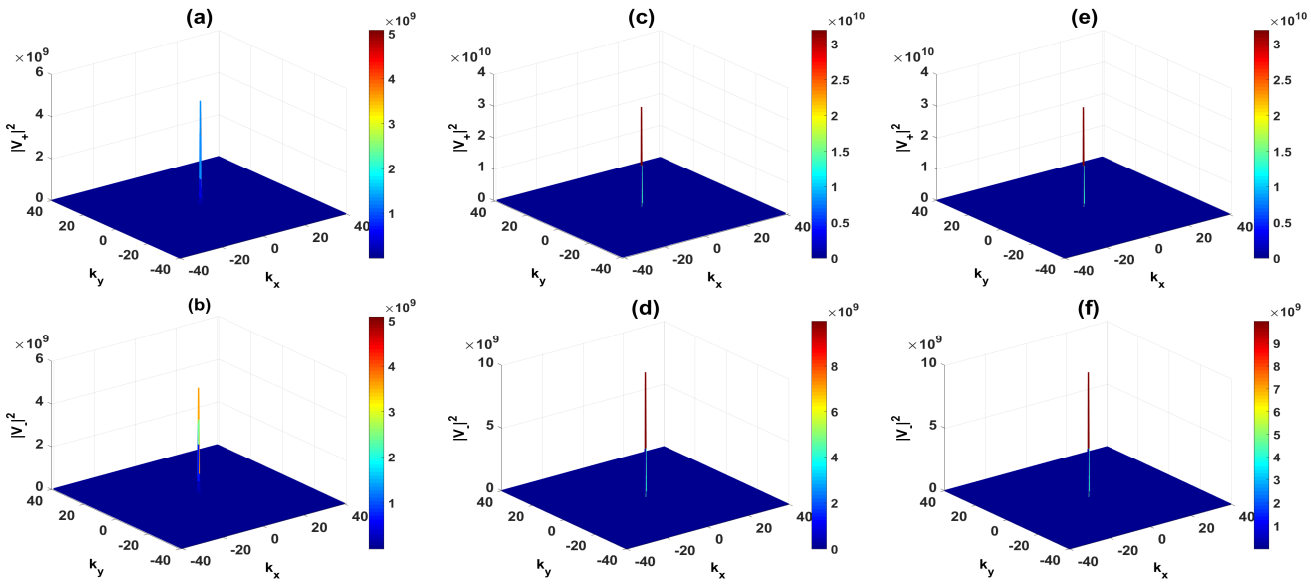

Figure 3.19: Spectral profile $|V_+|^2$ (upper line) and $|V_-|^2$ (bottom line) of the results of Fig. 8, at different steps of the evolution: (a) and (b) $T = 0$, (c) and (d) $T = 15000$, (e) and (f) $T = 30000$.

of parameters in the bottom of the effective potential leads to the generation light bullet, harmonic, and quasi-periodic stable evolution, characteristic of laser system. Consequently, the generation of the coupled moving dissipative solitons is well described by the coupled CQGL.

Since the results obtained in this work revealed the formation of alternate structures (pulse and pulse trains, periodic and quasi-periodic dynamic), that had been predicted and observed in the CO_2 laser, and the coherent evolution which are known to be an important property of the laser system, they could be of great importance for technology advances related to the laser systems in order to increase their capabilities. In addition, they allow the development of novel laser-feedback-based devices with the capability for subwavelength, nanoscale, multidimensional position sensing. Also, since the obtained non-smooth vertex top profile have been proved to be stable during propagation,these structures could also be considered as potential candidates for laser devices.

3.4 Conclusion

In this chapter, we have performed a detailed analytical and numerical studies of dissipative optical soliton in optical media modeled by the (2+1)D CQ-CGL equation, and the coupled (2+1)D CQ-CGL equation with SPM and XPM. By the variational approximation method accompanied by the stability method (the RH criterion, effective potential), we have obtained a set of parameters, for which the system can generate and propagate a multidimensional stable solitons. The direct numerical simulations of the CQ-CGL model present a good agreement with the analytical prediction, and reveal the stable propagation of light bullet,periodic, and pseudo-periodic dynamic, and the generation of stable pulse trains. The variational approach has been performed, first by the use of the standard Gaussian pulse, after the moving Gaussian solution. The stability analysis based on the possibility of the soliton trapped in the bottom of the effective potential showed a good agreement with direct numerical simulations of the coupled (2+1D CQ-CGL equation. The original results reported in this thesis are timely and relevant for long-haul communication systems. The opportunity to treat analytically and numerically asymmetrical input pulses propagating toward stable and robust dissipative soliton, opens possibilities for diverse practical applications for conception of all-optical transmission systems, signal processing, and mode-locked laser generating ultrashort pulses.

General Conclusion

In this thesis, we have studied the formation and stability of new classes of spatial/spatiotemporal optical dissipative solitons. This has been done in the framework of the (2+1)-dimensional cubic-quintic complex Ginzburg-Landau[(2+1)D CQ-CGL], and coupled (2+1)D CQ-CGL equation that we have derived. The first equation ((2+1)D CQ-CGL equation), which modeled the propagation of ultrashort optical soliton in laser system, includes the effects of two-dimensional transverse diffraction of the beam, and its evolution along the laser system. By means of the variational approach associated to a good choice of two moving non symmetrical gaussian solutions, we have derived a set of ordinary differential equations describing the pulse parameters evolution inside the optical system. The equations have been solved for the particular symmetric case, and by means of the Routh-Hurwith stability criterium, the stability condition has been derived. From the parameters belonging to the stability domain, the numerical simulations of the (2+1)D CQ-CGL equation showed the generation of localized solution, that move stably during the propagation.

In the second step, starting with the well-known Maxwell-Bloch equation modeling the interaction between the electric wave and the material inside the laser cavity, by considering the vectorial characteristic of the electric wave, we have first derived the vectorial (3+1)-dimensional CQ-CGL equation. After some approximations, the model is transformed to a coupled (2+1)D CQ-CGL equation describing the circular polarized components of the electric wave inside the laser cavity. The coupled (2+1)D CQ-CGL model include: third-, and fourth- order coupling

terms, the cubic-, quintic nonlinearities, the diffusion, in addition to the linear loss/gain terms.

To investigate the possibility of solitons formation, our numerical investigations of the evolution of the pulse along a laser cavity have been carried out first by the means of the variational approximation method, which with the help of the numerical method, allows us to investigate the stability domains of parameters by which, our system can propagate. Moreover, a fully direct numerical simulation of the coupled (2+1)D CQ-CGL equation using the split-step Fourier method, finally tests the results of the stability analysis. The fourth-order Runge-Kutta method, allows us to integrate the system of first order differential equations obtained by the variational approach. The obtained variational equations show clearly how the pulse parameters are affected by the physical system during the propagation. Moreover, a fully direct numerical simulation of the coupled (2+1)D CQ-CGL equation using the split-step Fourier method, finally tests the results of the variational approach. The different cases obtained, also permitted us to realize that the analytical and numerical treatment reveal the balance between gains and losses, interplay between coupled, diffraction and nonlinearities. Then, the vector dissipative light bullet can propagate in laser cavity due to the balance between nonlinearities and coupled.

To achieve our goals in this second step of our work, we used the variational approach with the standard non symmetric Gaussian form of the spatiotemporal optical field to obtain a set of differential equations characterizing the variation of the pulse parameters in laser cavity. Secondly, we have investigated the propagation characteristics and stabilization of the symmetric and elliptic moving-Gaussian pulse in coupled cubic-quintic nonlinear media with third-, and fourth- order cross terms.

For some choice of parameters, in the case of the Gaussian form of the pulse, both dissipative light bullets and double-bullet for coupled regime were obtained, by using extensive numerical simulations. Then, by studying the propagation characteristics and stabilization of generalized-Gaussian pulse based on coupled (2+1)-dimensional cubic-quintic complex Ginzburg-Landau

equation, we have presented new numerical solutions of 3D stable vectorial optical bullets.

Also, with a symmetric moving Gaussian form of the spatiotemporal optical field, by extensive analytical and numerical simulations, we have observed the generation one, two- shifting soliton, and the formation with a non-smooth vertex top profile, periodic and pseudo-periodic dynamics by the coupled (2+1)-dimensional CQ-CGL equation. We have discussed the theoretical generation of dissipative solitons and have made extensive use of numerical simulations with various parameters to discuss the various structures that arise from the higher dimensional CQ-CGL equation. The stability analysis have been done using the plot of the potential function of the problem to show the existence of a stable stationary soliton.

The results have confirmed that, dissipative optical solitons that have been formed under the combined interplay between diffusion, gain, loss, cubic and quintic coupled effect, and cubic-quintic nonlinearities are good candidates for CO_2 laser, and found application in the industrial treatment, such as thermal treatment, cutting, etc.

This work may be interesting for all those, whether professionals or not, who want to refresh their knowledge and obtain information or find the appropriate keys for the better understanding of dissipative solitons.

Open problems and future directions

At the end of this work, numerous points related to this topic remain unsolved, and then may be subject to future investigations.

-The numerical simulation of the Maxwell-Bloch equations,

- the generation of patterns formations such as the topological defect,

- the criterium of the generation of stable vortex solutions,

- and the analysis of the effect of non-locality inside the laser cavity.

The analysis can also be applied for other type of class B laser such as

- HeNe: $\lambda = 633nm$, GaAs: $\lambda = 904$,

- YAG:Nd: $\lambda = 1064$ or $532nm$, etc.., that found application in medicine, communication, industry (laser printer, smoke detector, etc...). where λ is the laser wavelength.

Appendices

Appendix A:

In this Appendix, we present the effective potential derived from Eqs. (3.24a)-(3.24g):

$$
\begin{aligned}
U = & \left(\left(\left(5-\frac{3}{2Y^2}\right)X^2+\frac{55}{336}+\frac{9}{224X_m^2}+\frac{43}{252}X_m^2-\frac{\frac{4X_m^4}{9}+\frac{17X_m^2}{36}+\frac{1}{8}}{X^2}\right)\delta_i\gamma_i A^6-\frac{1}{2}A^2\ln(X)\right)e^{-\frac{14X_m^2}{3X^2}} \\
& +\left(\frac{1}{8}\left(\left(\frac{7}{2}-\frac{1}{Y^2}\right)X^2+\frac{3}{16X_m^2}+\frac{7}{9}\right)+\frac{8X_m^2}{81}-\frac{\frac{1}{16}+\frac{16}{81}X_m^4+\frac{2X_m^2}{9}}{X^2}\right)\delta_i^2A^8e^{-\frac{16X_m^2}{X^2}} \\
& +\left(\left(\left(4-\frac{1}{2Y^2}\right)X^2+\frac{8X_m^2}{9}+\frac{1}{2}\right)\frac{\mu\delta_iA^8}{9}+\left(\left(7-\frac{1}{2Y^2}\right)\frac{X^2}{8}+\frac{X_m^2}{9}+\frac{1}{16}\right)\varepsilon\delta_iA^6\right. \\
& +\left(\left(\frac{\delta}{2}-S+\left(C^2-\frac{1}{2Y^2}+\frac{16C^2X_m^2}{9}+\frac{4}{3}C\right)\beta\right)\delta_iX^2+\delta_i\left(\frac{2}{3}-\frac{16CX_m^2}{9}-C\right)\right. \\
& \left.\left.+\beta\delta_i\left(\frac{7}{12}+\frac{3}{16X_m^2}-C^2X^4-\frac{\frac{1}{4}+\frac{4X_m^2}{9}}{X^2}\right)\right)A^4\right)e^{-\frac{8X_m^2}{3X^2}} \\
& +\left(\left(\left(\left(3-\frac{1}{Y^2}\right)X^2+1+X_m^2+\frac{1}{4X_m^2}\right)-\frac{\frac{1}{4}+X_m^2+X_m^4}{2X^2}\right)\gamma_i^2A^4+\frac{\beta\gamma_iA^2}{2}\right)e^{-\frac{4X_m^2}{X^2}} \\
& +\left(\left(\frac{11}{2}-\frac{1}{Y^2}\right)\frac{X^2}{18}+\frac{X_m^2}{9}+\frac{1}{18}\right)\mu\gamma_iA^6+\left(\left(1-\frac{1}{32Y^2}\right)\frac{X^2}{4}+\frac{X_m^2}{8}+\frac{1}{16}\right)\varepsilon\gamma_iA^4 \\
& +\left(\left(-C^2X^4+\frac{1}{8X_m^2}-\frac{1+2X_m^2}{4X^2}\right)\beta\gamma_i-\gamma_iC(1+2X_m^2)\right. \\
& \left.+\frac{\gamma_r}{2}+\left(\gamma_i\frac{\delta-2S-2C}{4}+\beta\gamma_i\left(\frac{C}{2}+2C^2X_m^2+C^2+\frac{1}{4Y^2}\right)\right)A^2+\frac{1}{X^2}\right)e^{-\frac{2X_m^2}{X^2}} \\
& +\left(X^2+Y^2\right)\left(\frac{\mu^2A^8}{9}+\frac{5\varepsilon\mu A^6}{24}\right)+\left(-\frac{4}{9}\{(\nu+\beta\mu)(\ln(X)+\ln(Y))+\beta\mu\left(C^2X^4+S^2Y^4\right)\}\right. \\
& \left.+\frac{5\varepsilon^2}{64}(X^2+Y^2)+\left(4\beta C\nu+2\mu\delta-4\mu S-\frac{2\beta\mu}{Y^2}\right)\left(\frac{X^2}{9}\right)+\left(4\beta S\nu+2\mu\delta-4\mu C-\frac{2\beta\mu}{X^2}\right)\left(\frac{Y^2}{9}\right)\right)A^4 \\
& +\left(-\frac{\beta\varepsilon}{2}(C^2X^4+S^2Y^4)-(\ln(X)+\ln(Y))\left(\frac{2+\beta\varepsilon}{4}\right)+\left(-\frac{\beta\varepsilon}{Y^2}+2\varepsilon C+4\delta\varepsilon-2\varepsilon S\right)\frac{X^2}{8}\right. \\
& \left.+\left(4\beta S+2\varepsilon S-2\varepsilon C+\delta\varepsilon-\frac{\beta\varepsilon}{X^2}\right)Y^2\right)A^2-4\beta^2(C^4X^6+S^4Y^6)+4\beta(S^3Y^4+C^3Y^4) \\
& -6\beta^2(C^2X^2+S^2Y^2)+12\beta(S\ln(Y)+C\ln(X))-\frac{\beta^2}{4}\left(\frac{1}{X^2}+\frac{1}{Y^2}\right)
\end{aligned}
$$

Appendix B:

The effective potential derived from Eqs. (3.31a) to (3.31e).

$$
\begin{aligned}
U(X) =&(\frac{32X_0^4}{81X^2}+\frac{1}{X^2}-\frac{28X_0^2}{81}+\frac{4X_0^2}{9X^2}-\frac{13}{36}+\frac{3}{128X_0^2})A^8\delta_i^2e^{-\frac{16X_0^2}{X^2}}+(\frac{8X_0^4}{X^2}\\
&+\frac{1}{4X^2}+(\frac{17}{18X^2}-\frac{79}{126})X_0^2-\frac{5X^2}{4}-\frac{53}{84}-\frac{9}{56X_0^2})A^6\delta_i\gamma_ie^{-\frac{14X_0^2}{3X^2}}\\
&+((-\frac{1}{8}(7X^2+\frac{15}{8X_0^2})\delta_i^2-\frac{1}{9}(1+8X^2+\frac{16}{9}X_0^2)\delta_i\mu)A^8-(1+2X_0^2\\
&+7X^2)A^6\varepsilon\delta_i+(\frac{8}{9}(4C+\frac{\beta}{X^2}-4\beta\delta_iC^2X^2)X_0^2\delta_i-\frac{16}{9}(1\\
&+5\beta CX^2)\delta_iNX_0^2-\frac{8\beta\delta_rCX^2}{3}+2\beta\delta_iC^2X^2(X^2-1)+2\delta_iC\\
&-\frac{4}{3}\delta_r+2\delta_iCX^2+\delta_i\beta N^2X^2-\delta\delta_iX^2+\frac{\beta\delta_i}{2X^2}-\frac{11}{6}\beta\delta_i-\frac{\delta_iN}{X_0}\\
&-\frac{3\beta\delta_i}{4X_0^2})A^4)e^{-\frac{8X_0^2}{X^2}}+(-(1+2X_0^2-\frac{11}{2}X^2)\mu\gamma_iA^6-(1+4X^2+\\
&2X_0^2)A^4+(-\gamma_r-\frac{3}{2}\gamma_i\beta+2\gamma_iC+4\gamma_iCX_0^2-2\gamma_iNX_0+2\beta\gamma_iC^2X^4\\
&-\frac{\gamma_iN}{X_p}-\frac{\gamma_i\beta}{2X_0^2}+\frac{\beta\gamma_i}{2X^2}+\frac{\gamma_i\beta X_0^2}{X^2})A^2-(\frac{\gamma_i\delta}{2}+8\beta\gamma_iCX_0N+2\beta\gamma_iC^2\\
&+\beta\gamma_rC+4\beta\gamma_iC^2X_0^2-\frac{\beta\gamma_iN}{2}))e^{-\frac{2X_0^2}{X^2}}+(\frac{\gamma_i^2X_0^2}{2X^2}+\frac{\gamma_i^2}{8X^2}-\frac{\gamma_i^2}{4}-\\
&\frac{3}{32}\gamma_i^2X^2-\frac{\gamma_i^2}{16X_0^2}-\frac{\gamma_i^2X_0^2}{4}+\frac{\gamma_i^2X_0^2}{2X^2})e^{-\frac{4X_0^2}{X^2}}-\frac{2\mu^2X^2A^8}{9}-\frac{5\mu\varepsilon X^2A^6}{12}\\
&+4\beta^2C^2X^2(2C^2X^4+3)-\frac{2}{X^2}+\frac{\beta^2}{2X^2}-8\beta C^3X^4-24\beta C\ln(X)\\
&+(\frac{X^2\varepsilon}{4}(\beta N^2-\delta)+\beta CX^2(-1+\varepsilon CX^2)+(1+\beta\varepsilon)\ln(X))A^2
\end{aligned}
$$

Bibliography

[1] V. A. Fabrikant, referenced Jeft Hecht, Laser pioneers, revised ed. (San Diego, CA:Academic Press, 1992), pp. 5-6, as being cited in mMario Bertolotti, Masers and Lasers: Ahistorical Approach (Bristol, England: Adam Hilger Ltd., 1982).

[2] H. Haken, Synergetics: An Introduction, Springer, Berlin, 1977.

[3] M. C. Cross, P. C. Hohenberg, Rev. Mod. Phys. **65** 851 (1993).

[4] A. C. Newell and J. V. Moloney, Nonlinear Optics (Addison-Wesley, Reading; MA, 1993).

[5] Y. I. Khanin, Principles of Laser Dynamics, North-Holland, Amsterdam, 1995.

[6] F. Tito Arecchi, Stefano Boccaletti, Pier Luigi Ramazza, Physics Reports **318** 1 (1999).

[7] F. T. Arecchi, G. L. Lippi, G. P. Puccioni and J. R. Tredicce, Opt. Commun. **51** 308 (1984).

[8] J. R. Tredicce, F. T. Arecchi, G. L. Lippi, and G. P. Puccioni, J. Opt. Soc. Am. B **2** 173 (1985).

[9] S. Ciuchi, F. de Pasquale, M. San Miguel, and N.B. Abraham, Phys. Rev. A 44, 7657 (1991).

[10] E. Hernandez-Garcia, R. Toral, and M. San Miguel, Phys. Rev. A 42, 6823 (1990).

[11] S. G. Chuartzman, D. Krygier, and A. A. Hnilo, Opt. Commun. 121, 1 (1995).

[12] D. M. Fondevilla and A. A. Hnilo, Opt. Commun. 162, 324 (1999).

[13] V. M. Perez-Garcia, I. Pastor, and J. M. Guerra, Phys. Rev. A 52, 2392 (1995).

[14] C. Mayol, R. Toral, and C. R. Mirasso, Phys. Rev. A 59, 4690 (1999).

[15] G. P. Agrawal and N. K. Dutta, Long-Wavelength Semiconductor Lasers (Van Nostrand Reinhold, New York, 1986).

[16] C. O. Weiss and R. Vilaseca, Dynamics of Lasers (VCH Publishers, Weinheim, 1991).

[17] D. Dangoisse, D. Hennequin, C. Lepers, E. Louvergneaux, and P. Glorieux, Phys. Rev. A 46, 5955 (1992).

[18] G. Huyet, M. C. Martinoni, J. R. Tredicce, and S. Rica, Phys. Rev. Lett. 75, 4027 (1995).

[19] G. Huyet and J. Tredicce, Physica D 96, 209 (1996).

[20] A. Labate, M. Ciofini, R. Meucci, S. Boccaletti, and F. Arecchi, Phys. Rev. A 56, 2237 (1997).

[21] S. P. Hegarty, G. Huyet, J. G. McInerney, and K. D. Choquette, Phys. Rev. Lett. 82, 1434 (1999).

[22] O. Hess, S. Koch, and J. V. Moloney, IEEE J. Quantum Electron. 31, 35 (1995).

[23] F. Strumia, in: Advances in laser spectroscopy, eds. F.T. Arecchi, F. Strumia and H. Walther (Plenum Press, New York, 1983) p. 267.

[24] P. Colet and R. Roy , J. Opt. Lett. **19**, 2056 (1994).

[25] Argyris A and Syvridis D., J. Lightwave Technol. **22**, 1272 (2004).

[26] Buldu J. M, Ojalvo J. G., and Torrent M. C., IEEE J. Quantum Electron. **41** 164, (2005).

[27] Chen H. F. and Liu J. M., IEEE J. Sel. Top Quantum Electron. **10**, 918 (2005).

[28] Wu L and Zhu Q. W., Chin. Phys. **12**, 300 (2003).

[29] N. Rosanov and G. Khodova, J. Opt. Soc. Am. B **7**, 1057 (1990).

[30] S. Wabnitz, IEEE J. OF Quantum Electron. **32**, (1996) 925.

[31] M. Brambilla, L. Lugiato, and M. Stefani, Chaos **6**, 368 (1996).

[32] S. Barland, J. Tredicce, M. Brambilla, L. Lugiato, S. Balle, M. Giudici, T. Maggipinto, L. Spinelli, G. Tissoni, T. Knödl et al., Nature (London) **419**, 699 (2002).

[33] X. Hachair, S. Barland, L. Furfaro, M. Giudici, S. Balle, J. Tredicce, M. Brambilla, T. Maggipinto, I. Perrini, G. Tissoni et al. , Phys. Rev. A **69**, 043817 (2004).

[34] P. Del'Haye, A. Schliesser, O. Arcizet, T. Wilken, R. Holzwarth, and T. Kippenberg, Nature (London) **450**, 1214 (2007).

[35] T. Ackemann, W. J. Firth, and G.-L. Oppo, Adv. At. Mol. Opt. Phys. **57**, 323 (2009).

[36] F. Leo, S. Coen, P. Kockaert, S.-P. Gorza, P. Emplit, and M. Haelterman, Nat. Photonics **4**, 471 (2010).

[37] F. Prati, L. A. Lugiato, G. Tissoni, and M. Brambilla, Phys. Rev. A **84**, 053852 (2011).

[38] L. Lugiato, F. Prati, and M. Brambilla, Nonlinear Optical Systems (Cambridge University Press, Cambridge, U.K., 2015).

[39] F. Gustave, L. Columbo, G. Tissoni, M. Brambilla, F. Prati, B. Kelleher, B. Tykalewicz, and S. Barland, Phys. Rev. Lett. **115**, 043902 (2015).

[40] F. Gustave, C. Rimoldi, P. Walczak, L. Columbo, M. Brambilla, F. Prati, G. Tissoni, and S. Barland, Eur. Phys. J. D **71**, 154 (2017).

[41] Shayesteh Rahmani Anbardan, Cristina Rimoldi, Reza Kheradmand, Giovanna Tissoni, and Franco Prati, Phys. Rev. E **97**, 032208 (2018).

[42] M. Sargent III, M. O. Scully, and W. E. Lamb, Jr., Laser Physics (Addison-Wesley Publ. Co., Reading, MA, 1974).

[43] W. E. Lamb, Jr., Phys. Rev. **134**, A1429 (1964).

[44] H. Haken, Light Vol. 2, Laser Light Dynamics (North-Holland, Amsterdam, 1985).

[45] H. Haken and H. Sauermann, Z. Phys. **173**, 261 (1963).

[46] H. Haken, Laser Theory (Springer-Verlag, Berlin, 1984).

[47] I. Leyva and J. M. Guerra, Phys. Rev. A **66**, 023820 (2002).

[48] F. Encinas-Sanz, I. Leyva, and J. M. Guerra, Phys. Rev. Lett. **84**, 883 (2000).

[49] M. Riley, T. D. Padrick, and R. Palmer, IEEE J. Quantum Electr. QE **15**, 178 (1979).

[50] L. A. Lugiato, C. Oldano, and L. M. Narducci, J. Opt. Soc. Am. B 5, 879 (1988).

[51] P. Coullet, L. Gil, F. Rocca, Opt. Commun. 73 (1989) 403.

[52] G. L. Oppo, G. D'Alessandro, W. J. Firth, Phys. Rev. A 44 (1991) 4712.

[53] K. Staliunas, C.O. Weiss, Physica D 81 (1995) 79.

[54] K. Staliunas, Phys. Rev. A 48 (1993) 1573.

[55] J. D. Moores, Opt. Commun. 96, 65 (1993).

[56] E. P. Ippen, H. A. Haus, and L. Y. Liu, J. Opt. Soc. Am. B 6, 1736 (1989).

[57] C.-J. Chen, P. K. A. Wai, and C. R. Menyuk, Opt. Lett. 19, 198 (1994).

[58] C.-J. Chen, P. K. A. Wai, and C. R. Menyuk, Opt. Lett. 20, 350 (1995).

[59] J. M. Soto-Crespo, N. N. Akhmediev, and V. V. Afanasjev, J. Opt. Soc. Am. B 13 (1996) 1439.

[60] J. Lega, J.V. Moloney, A.C. Newell, Phys. Rev. Lett. 73 (1994) 2978.

[61] J. Lega, J.V. Moloney, A.C. Newell, Physica D 83 (1995) 478.

[62] M. Tlidi, M. Giorgiou, and P. Mandel, Phys. Rev. A 48, 4605 (1993).

[63] H. A. Haus and A. Mecozzi, IEEE J. Quantum Electron. 29, 983 (1993).

[64] C. R. Menyuk, J. K. Wahlstrand, J. Willits, R. P. Smith, T. R. Schibli, and S. T. Cundiff, Opt. Express 15 (2007) 6677.

[65] W.-W. Hsiang, C.-Y. Lin, M. Tien, and Y. Lai, Opt. Lett. 30 (2005) 2493.

[66] W.-W. Hsiang, C.-Y. Lin, and Y. Lai, Opt. Lett. 31 (2006) 1627.

[67] Wonkeun Chang, Nail Akhmediev, and Stefan Wabnitz, Phys. Rev. A 80, 013815 (2009).

[68] Thual, O. and Fauve S. , J. Phys. France 49, 1829?1833 (1988).

[69] Soto-Crespo, J. M., Akhmediev, N. and Afanasjev, V., J. Opt. Soc. Am. 13, 1439 (1996).

[70] Kutz, J. N. Mode-locked soliton lasers. SIAM Rev. 48, 629 (2006).

[71] H. R. Brand and R. J. Deissler, Phys. Rev. Lett. 63, 2801 (1989).

[72] B. A. Malomed, Phys. Rev. A 44, 6954 (1991).

[73] N. N. Akhmediev, A. Ankiewicz, and J. M. Soto-Crespo, J. Opt. Soc. Am. B 15, 515 (1998).

[74] D. Turaev, A. G. Vladimirov, and S. Zelik, Phys. Rev. E 75, 045601(R) (2007).

[75] J. M. Soto-Crespo, N. Akhmediev, Ph. Grelu, and F. Belhache, Opt. Lett. 28, 1757 (2003).

[76] Ph. Grelu and N. Akhmediev, Opt. Express 12, 3184 (2004).

[77] J. M. Soto-Crespo, N. Akhmediev, and A. Ankiewicz, Phys. Rev. Lett. 85, 2937 (2000).

[78] L. Gil, Phys. Rev. Lett. 70 (1993) 162.

[79] L. Gil, Int. J. Bif. Chaos 3 (1993) 573.

[80] E. Hernández-Garcia, M. Hoyuelos, P. Colet, M. San Miguel, R. Montagne, Int. J. Bif. Chaos 9 (1999) 2257

[81] A. Amengual, E. Hernández-Garcia, R. Montagne, M. San Miguel, Phys. Rev. Lett. 78 (1997) 4379.

[82] R. Montagne, E. Hernández-Garcia, Phys. Lett. A 273 (2000) 239.

[83] L. M. Pismen, Phys. Rev. Lett. **72** 2557 (1994).

[84] L. M. Pismen, Physica D **73** 244 (1994).

[85] M. San Miguel, Phys. Rev. Lett. **75** 425 (1995).

[86] E. Hernández-Garcia, M. Hoyuelos, P. Colet, M. San Miguel, R. Montagne, Int. J. Bif. Chaos **9** 2257 (1999).

[87] M. Hoyuelos, E. Hernández-Garcia, P. Colet, M. San Miguel, Comp. Phys. Comm. **121** 414 (1999).

[88] E. Hernández-Garcia, M. Hoyuelos, P. Colet, M. San Miguel, Phys. Rev. Lett. **85** 744 (2000).

[89] Miguel Hoyuelos, Emilio Hernández-Garcia, Pere Colet, Maxi San Miguel, Physica D **174** 176 (2003).

[90] K. Zhang, L. Yi-zeng, Ji Lin, and Hui-jun Li, Phys. Rev. A. **97** 023844 (2018).

[91] L.-C. Crasovan, B.A. Malomed, D. Mihalache: Phys. Lett. A **289** 59-65 (2001).

[92] V. Skarka, D. V. Timotijevic and N. B. Aleksic: J. Opt. A: Pure appl. Opt. **10** 075102 (2008).

[93] J. S. Russell, Rep. 14th Meet. British Assoc, Adv. Sci. (John Murray, London, 1844), p. 311.

[94] J. Boussinesq , « Théorie des ondes et des remous qui se propagent le long d'un canal rectangulaire horizontal, en communiquant au liquide contenu dans ce canal des vitesses sensiblement pareilles de la surface au fond », *Journal de Mathématiques Pures et Appliquées* **17**, 55-108 (1872).

[95] D. J. Korteweg and G. Devries, Philos. Mag., Ser. **5**, 422 (1895).

[96] N. J. Zabusky and M. D. Kruskal, Phys. Rev. Lett. **15**, 240 (1965).

[97] C. S. Gardner, J. M. Greene, M. D. Kruskal, and R. M. Miura, Phys. Rev. Lett. **19**, 1095 (1967).

[98] R. Y. Chiao, E. Garmire, and C. H. Towns, Phys. Rev. Lett. **13**, 479 (1964).

[99] V. E. Zakharov and A. B. Shabat, Sov. Phys. JETP **34**, 62 (1972).

[100] T. Dauxois and M. Peyrard, "Physics of Solitons", (2006).

[101] A. Hasegawa and F. Tappert, Appl. Phys. Lett. **23**, 142 (1973).

[102] A. Hasegawa and Y. Kodama, *Solitons in Optical Communications*, (Clarendon, Oxford University Press, Oxford, (1995)).

[103] H. A. Haus and W. S. Wong, Rev. Mod. Phys. **68**, 423 (1996).

[104] L. F. Mollenauer, J. P. Gordon, and P. V. Mamyshev, *Optical Fiber Telecommunications III*, I. E Kaminow and T. L. Koch, Eds. (Academic Press, San Diego, CA, 1997), Chap. 12.

[105] G. P. Agrawal, *Applications of Nonlinear Fiber Optics* (Academic, San Diego, CA, 2001).

[106] Y. S. Kivshar and G. P. Agrawal, *optical solitons* (2003).

[107] L.F. Mollenauer, J.P. Gordon, *Solitons in Optical Fibers: Fundamentals and Applications* (2006).

[108] Y. R. Shen, Principles of Nonlinear Optics (Wiley, New York, 1984).

[109] P. N. Butcher and D. N. Cotter, The Elements of Nonlinear Optics (Cambridge University Press, Cambridge, UK, 1990).

[110] R. W. Boyd, *Nonlinear Optics* (Academic Press, San Diego, CA, 1992).

[111] D. Mihalache, D. Mazilu, Boris A. Malomed, L. Torner: Opt. Comm. **152** 136-170 (1998).

[112] G. P. Agrawal, *Fiber-Optic Communication Systems*, (3rd Ed. New York: Wiley, (2002)).

[113] R. Y. Chiao, E. Garmire and C. H. Townes: phys. Rev. Lett. **13** 479 (1964).

[114] V. E. Zakharov, and A. B. Sharab, *Exact theory of two-dimensional self-focosing and one-dimensional self-modulation of waves in nonlinear media.* Sov. Phys. JETP, **34**, 62-69 (1972).

[115] V. NTsytovich, and R. Bingham, *Arrest of wave collaps and transitional damping*, Comments Plasma Phys. Controlled Fusion 14, 361-368 (1992).

[116] G. Fibich, and G. Papanicolaou, *Self-focusing in the perturbed and unperturbed nonlinear Schrödinger equation in critical dimension*, SIAM J. Appl. Math. **60** 183-240 (1999).

[117] O. Bang, D. Edmundson, and W. Krolikowski, *Collapse of incoherent light beam in inertial bulk Kerr media*, Phys. Rev. Lett. **83** 5479-5482 (1999).

[118] J. T. Manassah, *Collapse of the two-dimensional spatial soliton in a parabolic-index media*, Opt., Lett. **17** 1259-1261 (1992).

[119] C. Sun, C. Barsi, and J. W. Fleischeur, *Peakon profiles and collapse-bounce cycles in sef-focusing Spatial beamd*, Opt. Express 16 20676-20686 (2008).

[120] C. Sulem and P. L. Sulem, *The nonlinear Schrödinger equation: self-focusing and wave collapse*,(Springer-Verlag, New York, (1999))

[121] D. E. Edmundson and R. H. Enns, Phys. Rev. A **51**, 2491 (1995).

[122] C. Josserand and S. Rica, Phys. Rev. Lett. **78**, 1215 (1997)

[123] N. N. Rosanov, *Spatial Hysteresis and Optical Patterns* (Springer, Berlin, (2002), Chap. 6).

[124] H. Haken, *Synergetics*, (Springer-Verlag, Berlin, 1983). 4

[125] V. E. Zakarov and A. B. Shabat: Phys. JETP **37** 823 (1973).

[126] I. S. Aranson and L. Kramer: Rev. Mod. Phys. **74** 99 (2002).

[127] M. C. Cross and P. C. Hohenberg: Rev. Mod. Phys. **65** 851 (1993).

[128] P. Mandel and M. Tlidi: J. Opt. B: Quantum Semiclass. Opt. **6** R60-R75 (2004).

[129] N. Akhmediev, A. Ankiewicz, (eds.): **Dissipative Solitons**, Springer Lect. Notes Phys. **661**. Springer, Berlin, Heidelberg (2005).

[130] N. Akhmediev, and A. Ankiewicz (Eds.), *Dissipative Solitons: From Optics to Biology and Medicine*, Springer Lect. Notes Phys. **751** (Springer, Berlin, Heidelberg (2008)).

[131] P. T. Dinda, A. B. Moubissi and K. Nakkeeran, Phys. Rev. E **64** (2001) 016608.

[132] B. G. O. Essama , J. Atangana, F. B. Motto, B. Mokhtari, E. C. Noureddine and T. C. Kofané, Phys. Rev. E **90** (2014) 032911.

[133] J. Fan and S. Jiang, Appl. Math. Lett. **16** (2003) 435.

[134] G. D. Montesinos, M. I. Rodas-Verde, V. M. Pérez-García and H. Michinel, Chaos **15** (2005) 033501.

[135] A. Ankiewicz, N. Akhmediev and N. Devine, Opt. Fiber Technol. **13** (2007) 91.

[136] P. M. Morse and H. Feshbach, *Methods of theoretical physics*, McGraw-Hill (1953).

[137] V. Skarka and N. B. Aleksic: Phys. Rev. Lett. **96** 013903 (2006).

[138] A. E. Siegman, *Lasers* (University Science Books, Mill Valley, 1986).

[139] A. Schawlow, C. Townes, *Infrared and optical masers.* Phys. Rev. **112**, 1940 (1958).

[140] L. V. Tarasov, *Laser age in Optics* (Mir Publishers (1977) Russian edition. First published (1981).).

[141] D. Meschede, ***Optics, Light and Laser*** *The practical Approach to Modern Aspect of Photonics and Laser Physics* (Wiley-VCH (2004)).

[142] K. J. Kuhn, *LASER ENGINEERING* (PrenticeHall (1988)).

[143] A. Javan, W. R. J. Bennet, D. Herriott, *Population Inversion and Continuous Optical Maser Oscillation in a Gas Discharge Containing a He-Ne Mixture*, Phys. Rev. Lett. **6**, 106 (1961).

[144] L. W. Davis, *Semiclassical treatment of the optic maser*, Proc. IEEE **51**, 76-80 (1963).

[145] N. Akhmediev and A. Ankiewicz, Solitons around us: Integrable, Hamiltonian and dissipative systems, in Optical Solitons: Theoretical and Experimental Challenges, Edited by

K. Porsezian and V.C. Kurakose, (Springer, Berlin-Heidelberg, (2003)), pp. 105-126. 1, 5, 6.

[146] N. Akhmediev and A. Ankiewicz, Solitons of the complex Ginzburg-Landau equation, in Spatial Solitons 1, Edited by S. Trillo and W.E. Toruellas, (Springer, Berlin-Heidelberg, (2001)), pp. 311-342. 1.

[147] N. Akhmediev, General theory of solitons, in Soliton-Driven Photonics, edited by A.D. Boardman and A.P. Sukhorukov, (Kluver Academic Publishers, Netherlands, (2001)), pp. 371-395. 1.

[148] N. Akhmediev, J.M. Soto-Crespo, and G. Town, Phys. Rev. E **63**, 056602 (2001).

[149] J. E. Pearson, Science **261**, 189 (1993).

[150] K.J. Lee and H.L. Swinney, Science **261**, 192 (1993).

[151] I. Müller, E. Ammelt, and H. G. Purwins, Phys. Rev. Lett. **82** 3428 (1999).

[152] N. N. Rosanov, Progress in Optics, (Elsevier, Amsterdam, (1996)), Vol. **35**. 114

[153] Feature Section on Cavity Solitons, edited by L. A. Lugiato, IEEE J. Quantum Electon. **39**, 2 (2003). 114

[154] W.J. Firth and C.O. Weiss, Opt. Photon. News **13**, 55 (2002).

[155] M. Tlidi, P. Mandel, and R. Lefever, Phys. Rev. Lett. **73**, 640 (1994).

[156] S. Barland, et al., Nature (London) **419**, 699 (2002).

[157] W. J. Firth and A. J. Scroggie, Phys. Rev. Lett. **76**, 1623 (1996).

[158] P. Coullet, C. Riera, and C. Tresser, Phys. Rev. Lett. **84**, 3069 (2000).

[159] P. Coullet, C. Riera, and C. Tresser, Chaos **14**, 193 (2004).

[160] L. A. Lugiato and R. Lefever, Phys. Rev. Lett. **58**, 2209 (1987).

[161] W. J. Firth, A. Lord, and A. J. Scroggie, Physica Scripta **67**, 12 (1996).

[162] W. J. Firth and A. Lord, J. Mod. Optic. **43**, 1071 (1996).

[163] J. J. Rasmussen and K. Rypdal, Phys. Scr. **33**, 481 (1986).

[164] M. V. Goldman, K. Rypdal, and B. Hafizi, Phys. Fluids **23**, 945 (1980).

[165] D. Gomila, and P. Colet, Phys. Rev. A **68**, 011801 (R) (2003).

[166] N. Akhmediev, A. Ankiewicz, and J.M. Soto-Crespo, Phys. Rev. Lett. **79**, 4047 (1997).

[167] J. Yang, Y. Tan, Phys. Rev. Lett. **85**, 3624 (2000), and references.

[168] Y. Kuramoto: *in Chemical Oscillations, Waves and Turbulence*, ed. by H. Haken, Springer Series in Synergetics Vol. **19** (Springer, Berlin, (1984)).

[169] Mi. Hoyuelos, E. Hernández-Garcia, P. Colet, and M. S Miguel, Physica D **174**, 176-197 (2003).

[170] S. I. Fewo, T. C. Kofane, Opt. Commun. **281**, 2893 (2008).

[171] M. Djoko, T.C. Kofane: Commun Nonlinear Sci Numer Simulat **48** 179-199 (2017).

[172] M. Djoko and T.C. Kofane: Commun Nonlinear Sci Numer Similar **68** 169-187 (2019).

[173] F. Ndzana, A. Mohamadou, and T. C. Kofane, Phys. Rev. E **79**, 056611 (2009).

[174] F. Ndzana, A. Mohamadou, and T. C. Kofane, Phys. Rev. E **79**, 056611 (2009).

[175] J. M. Weiss, M. Tabor, and G. Carnevale, J. Math. Phys. **24**, 522 (1983).

[176] R. Conte and M. Musette, Physica D **69**, 1 (1993),

[177] H. Leblonb, j. Phys. B: At. Mol. Opt. Phys. **41** 043001 (2008).

[178] R. W. Boyd *Nonlinear Optics "second Edition"* (Academic Press, (2003)).

[179] L. A. Lugiato, G. L. Oppo, J. R. Tredicce, L. M. Narducci, and M. A. Pernigo, J. Opt. Soc. Am. B **7**, 1019 (1990),

[180] S. Chavez Cerda, S.B. Cavalcanti and J. M. Hickmann, Eur. Phys. J. D **1**, 313 (1998).

[181] B. A. Malomed, Prog. Opt. **43**, 71 (2002).

[182] A. Scott, *Nonlinear Science. Emergence and Dynamics of Coherent Structures* (Oxford University Press, Oxford, (2003)).

[183] P. Coullet, T. Frish and F. Plaza, *Sources and sinks of wave patterns* Physica D **62**, 75-79 (1993).

[184] A. Lepschy, *Comments on Polynomial Factorization using Routh Criterion*, IEEE Proceedings, (1972).

[185] R. N. Clark: IEEE Control Systems Magazine **12** 3 (1992).

[186] M. Gopal, *Control Systems Principles and Design*, (Tata McGraw Hill, Second edition, (2000)) **[184]**.

[187] E. X. DeJesus, and C. Kaufman, *Routh-Hurwitz criterion in the examination of eigenvalues of a system of nonlinear ordinary differential equations*, Phys. Rev. A **35**, 5288-5290 (1987).

[188] S. I. Fewo, J. Atangana, A. Kenfack-Jiotsa and T. C. Kofane: Opt. Comm. **252** 138-149 (2005).

[189] V. Skarka, V. I. Berezhehiani and R. Mmiklaszewski, Phys. Rev. E. **56** (1997) 1080.

[190] H. Ghafouri-Shiraz, M. Nagata, P. Shum, *A novel method for analysis of soliton propagation in optical fibers*, IEEE J. Quantum Electron, **31**, 190-200 (1995).

[191] T. R. Taha, M. J. Ablowitz, *Analytical and numerical aspects of certain nonlinear evolution equation. II Numerical nonlinear Schrödinger equation*, J. Computing Physics, **55**, 203-230 (1984).

[192] S. Yu, S. Zhao, G.W. Wei, *Local spectral time splitting method for first- and second-order partial differential equations*, J. Comp. Phys., **206**, 727-780 (2005).

[193] P.W. White, J.A.C Weideman, *Numerical simulation of solitons and dromions in the Davey-Stewartson system*, Math. Comput. Simul. *37*, 469-479 (1994).

[194] W. Bao, S. Jin, P. A. Markowich, *On Time-splitting spectral approximations for the Schrödinger equation in the semiclassical regime*, J. Comp. Phys. **175**, 487-524 (2002).

[195] G. Strang, *On the construction and comparison of difference schemes*, SIAM Journal on Numerical Analysis, **5**, 506-517 (1968).

[196] G. P. Agrawal, *Nonlinear Fiber Optics*, (4th ed., Academic Press, Boston, (2007)).

[197] G. Nicolis, and I. Prigogine, *Self organization in nonequilibrium systems-From dissipative structures to order through fluctuations*. John Wiley and sons, New York, (1977).

[198] B. K. Esbensen, M. Bache, O Biang, and W. Krolikowski: Phys. Rev. A **86** 033838 (2012).

[199] W. Zhu and Y. He: Opt. Express **18**(16) 1753 (2010).

[200] V. Skarka, V. I. Berezhehiani and R. Mmiklaszewski: Phys. Rev. E. **59** 1270 (1999).

[201] Y. S. Apte, M.Tech.: IEE-IERE Proceedings - India **7** 4 (1969).

[202] V. V. Afanasjev, N. Akhmediev and J. M. Soto-Crespo: Phys. Rev. E **53** 2 (1996).

[203] P. C. Bressloff and Z. P. Kilpatrick: Phys. Rev. E **78** 041916 (2008).

[204] K. Staliunas, Opt. Comm. **90** (1992) 123.

[205] D. B. Belobo, G. H. Ben-Bolie and T. C. Kofane, Int. J. Mod. Phys. B **28**, 1450003 (2014).

[206] M. D. Mboumba, A. B. Moubissi, T. B. Ekogo, G. H. Ben-Bolie and T. C. Kofané, Int. J. Mod. Phys. B **29** (2015) 1550202.

[207] V. A. Zhdanovskii, and V. N. Snopko, Measurement Techniques **45**, 369-373 (2002).

[208] M. Shen, Q. kong, J. Shi and Q. wang, Phys. Rev. A **77** (2008) 015811.

[209] F. Encinas-Sanz, S. Melle, and O. G. Galderón: Phys. Rev. Lett. **93** 2139-1 (2004).

[210] J. Ohtsubo: ***Semicondoctor Lasers*** *Stability, Instability and Chaos* (Springer in Optical Sciences 111, (2013)).

[211] K. J. Kuhn: *Laser Engineering* (PRentice Hall, (1998)).

[212] H. Kapteyn, O. Cohen, I. Christov, M. Murnane, Science **317**, 775 (2007).

[213] S. D. Cohen, A. Aragoneses, D. Rontani, M. C. Torrent, C. Masoller, and D. J. Gauthier, Opt. Lett. **38**, 4331 (2013).

[214] D. Dangoisse, D. Hennequin, C. Lepers, E. Louvergneaux and P. Gloriex, Phys. Rev. A **46**, 5955 (1992).

[215] M. Djoko and T. C. Kofane: Opt. Comm. **416** 190-201 (2018).

List of Publications

[1] Alain Djazet, Serge I. Fewo, Elvis B. Ngompé Nkouankam, and Timoléon C. Kofané, "*Stability analysis for moving dissipative solitons in two-dimensional dynamical model*", Eur. Phys. J. D **74**, 67 (2020).

[2] Alain Djazet, Conrad B. Tabi, Serge I. Fewo, and Timoléon C. Kofané, "*Vector dissipative light bullets in optical laser beam*", Applied Physics B **126**, 74 (2020).

Eur. Phys. J. D (2020) 74: 67
https://doi.org/10.1140/epjd/e2020-100467-7

THE EUROPEAN PHYSICAL JOURNAL D

Regular Article

Stability analysis for moving dissipative solitons in two-dimensional dynamical model

Alain Djazet[1,2], Serge I. Fewo[1,a], Elvis B. Ngompé Nkouankam[3], and Timoléon C. Kofané[1,2]

[1] Laboratory of Mechanics, Materials and Structure, Department of Physics, Faculty of Science, University of Yaounde I, P.O. Box 812, Yaounde, Cameroon
[2] Centre d'Excellence Africain en Technologies de l'Information et de la Communication (CETIC), University of Yaounde I, Yaounde, Cameroon
[3] Research Innovation Entrepreneurship Pole, University Institute of the Coast, P.O. Box 3001, Douala, Cameroon

Received 24 September 2019 / Received in final form 9 February 2020
Published online 9 April 2020
© EDP Sciences / Società Italiana di Fisica / Springer-Verlag GmbH Germany, part of Springer Nature, 2020

Abstract. Pulse propagating in inhomogeneous nonlinear media with linear/nonlinear gain and loss described by the asymmetrical $(2+1)$-dimensional cubic-quintic Ginzburg-Landau equation is considered. The evolution and the stability of the dissipative optical solitons generated from an asymmetric input with respect to two transverse coordinates x and y are studied. Our approach is based on the variational method. This approach allows us to analyze the influence of various physical parameters on the dynamics of the propagating signal and its relevant parameters. According to the parameters of the system and a suitable choice of the test function, a domain of dissipative parameters for stable solitonic solutions is determined. Bifurcation diagrams related to the existence of the stationary solutions presented show a good agreement between analytical and numerical results.

1 Introduction

Since the word solitons was coined in 1965, the field of solitons in general and the one of optical solitons in particular have grown enormously. In the context of nonlinear optics, solitons are classified as being either temporal or spatial, depending on whether the confinement of light occurs in time or space during wave propagation [1]. The temporal solitons are the optical pulses that maintain their shape in the temporal domain [2,3], whereas spatial solitons represent self-guide beams that remain confined in the transverse directions orthogonal to the direction of propagation [4–6]. The earliest example of spatial solitons corresponds to the 1964 discovery of the nonlinear phenomenon of self-trapping of continuous-wave (CW) optical beams in a bulk nonlinear medium [7,8]. Self-trapping was not linked to the concept of spatial solitons immediately because of its unstable nature. During the 1980s, stable spatial solitons were observed using nonlinear media in which diffraction was limited to only one transverse dimension [8]. On the other hand, solitons in Bose-Einstein condensates represent coherent atomic structures due to the competition between the spreading caused by its kinetic energy and the attracting interaction potential [9,10]. The uniqueness of solitons lies in the fact that they are robust objects exhibiting particle-like properties during the collisions [11,12]. Such solitons, originating from integrable nonlinear models, collide elastically [13]. It should be specified that dissipative systems in nonlinear optics admit stable solitons in one, two, and three dimensions [14–17]. Dissipative solitons have been widely studied in nonlinear optics, from fundamental point of view and due to the clear physical meaning in applications. Among others, several important applications of dissipative solitons are reachable in passively mode-locked laser systems and optical transmission lines.

The complex Ginzburg-Landau Equation (CGLE) was originally developed in the context of particle physics as a model of super-conductivity, and has since been widely used as a prototypical model for nonlinear wave propagation and pattern formation [14,15,18]. The CGLE may be viewed as an extension of the nonlinear Schrödinger (NLS) equation. Accordingly, it can describe a broad range of behaviors suggested by the NLS dynamics, ranging from chaos and pattern formation [19,20] to dissipative solitons [21]. While solitons in conservative systems are supported by the balance between the linear effects and the nonlinearity, dissipative solitons require an additional balance between linear/nonlinear loss and gain [22,23]. Thus, they do not form continuous families, but represent isolated attractors. Recently, considerable efforts were focused on the prediction of setting supporting stable multidimensional localized patterns [16,17,24–27]. The CGLE with a potential term as a model of dissipative solitons has been

[a] e-mail: sergefewo@yahoo.fr

used recently to study stable two-dimensional localized structures existing due to balance between gain and loss in nonlinear systems far from equilibrium. New mechanism of replication of both dissipative solitons and dissipative vortices has been performed [28]. Moreover, a mechanism performing nontrivial topological transformations by applying an external potential which changes topological characteristics of dissipative vortices in a controllable way is proposed. It is found that, in a highly nonequilibrium state, driven by an external potential, various topological excitations emerge and decay. In addition, fascinating transformations of topological structures are possible due to the fact that the energy of the vortex excitations is not conserved [29].

The properties and conditions of their existence have been studied extensively [25,30–33]. Some recent works have analyzed the effect of competing dissipative parameters on the existence and stability of solitons. It has been shown that the simultaneous presence of linear/nonlinear loss and gain leads to the stabilization of complex solitons structures [16,17,25,34–38]. The main purpose of this work is to extend the stability analysis of the moving asymmetrical dissipative solitons taking into consideration two additional relevant parameters in the definition of the function of study, accounting for the central position and the motion of the soliton. They are put together in addition to the usually used parameters such as the amplitude, spatial width, unequal wavefront curvature and phase [33].

This paper is organized as follows: the derivation of the dynamical equations of the solution parameters, and the analytical stationary solution of the system are presented in Section 2. In Section 3, we present the general stability condition of the solutions of the dynamical equations based on the Routh-Hurwitz method. Section 4 is devoted to the numerical investigations. Particularly, analytical results are numerically solved leading to the observation of the domain of stability/instability of dissipative solitons, for various parameters of the dissipative system. Moreover, bifurcation diagrams of the stationary solution are also obtained numerically and compared to the analytical results, which showed a good agreement. Finally, Section 5 concludes the paper.

2 Analytical treatment

We consider the propagation of a two-dimensional beam with the slowly varying envelope $\psi = \psi(x, y, z)$, where x, y and z are transverse and longitudinal coordinates, respectively. The model of dissipative soliton is the $(2+1)$ dimensional CQGLE which describes a wide range of physical phenomena in various systems. This model takes into account the cubic and the quintic nonlinearities, and the spatial diffraction in the transverse coordinates. In the paraxial wave approximation, the normalized propagation equation reads [32,33]:

$$i\frac{\partial\psi}{\partial z} + \frac{\partial^2\psi}{\partial x^2} + \frac{\partial^2\psi}{\partial y^2} + |\psi|^2\psi - \nu|\psi|^4\psi = \mathbf{Q}, \qquad (1)$$

with

$$\mathbf{Q} = i\left[\delta\psi + \mu|\psi|^4\psi + \varepsilon|\psi|^2\psi + \beta\left(\frac{\partial^2\psi}{\partial x^2} + \frac{\partial^2\psi}{\partial y^2}\right)\right]. \qquad (2)$$

The left-hand-side of equation (1) contains the conservative terms. The parameter ν is the saturation coefficient of the Kerr nonlinearity. The right hand side of equation (1) accounts for the dissipative terms. The parameter δ represents the linear gain/loss depending on the sign ($\delta < 0$ for linear loss) and $\beta > 0$ accounts for diffusive coefficient. The cubic and quintic gain-loss parameters are respectively ε and μ. The last term in equation (2) accounts for the diffusive term. The generation of dissipative solitons needs as prerequisite a simultaneous balance of the diffraction with the self-focusing as well as gain and loss. The present paper deals with the study of the existence of the stationary solution, including additional relevant parameters (the central position, and the linear frequency) in comparison with some commonly used analytical soliton solutions. This is performed in some aspects using a similar approach reported by Skarka et al. [33]. Moreover, we extend our study in the characterization of the evolution of the single parameters of the dissipative solitons as it propagates in the medium. This leads to a general picture of the stability conditions of the solitons as a function of the several dissipative parameters.

In order to describe the dynamics of the pulse evolution, various analytical treatments have been proposed, including the variational method [16,17,38,39]. Since the nonlinear propagation model (Eq. (1)) cannot be solved exactly, the most commonly used direct method is the so-called variational approach. This approach for optical solitons is applied by considering the averaged Lagrangian of the conservative system, where the conservative Lagrangian density is given by,

$$l_c = \frac{i}{2}(\psi^*\frac{\partial\psi}{\partial z} - \psi\frac{\partial\psi^*}{\partial z}) + \left|\frac{\partial\psi}{\partial x}\right|^2 + \left|\frac{\partial\psi}{\partial y}\right|^2 + \frac{1}{2}|\psi|^4 - \frac{\nu}{3}|\psi|^6, \qquad (3)$$

and the dissipative one

$$l_Q = i(\delta|\psi|^2 + \beta(\left|\frac{\partial\psi}{\partial x}\right|^2 + \left|\frac{\partial\psi}{\partial y}\right|^2) + \frac{\varepsilon}{2}|\psi|^4 + \frac{\mu}{3}|\psi|^6). \qquad (4)$$

Since the main objective of the present work is to analyze the influence of the central position and the linear frequency on the stability of the 2D spatial optical dissipative solitons, the following ansatz has been used [40–42].

$$\psi = A\exp\left\{-\frac{(x-X_2)^2}{2X^2} - \frac{(y-X_2)^2}{2Y^2} + iC(x-X_2)^2 + iS(y-X_2)^2 + iY_2(x-X_2) + iY_2(y-X_2) + i\phi\right\}, \qquad (5)$$

where A is the amplitude, X and Y are the spatial widths, C and S are the unequal wavefront curvature, X_2 the central position, ϕ is the phase and Y_2 account for the motion of the soliton along the direction of x and y, all function of the independent variable z.

We now focus on the analytical technique in order to perform the analytical description of the model, and then

characterize the solutions depending on the various dissipative parameters. Optimization of each function in equation (5) gives an Euler-Lagrange equation over transverse coordinates x and y [39,43–46]

$$\frac{d}{dz}\frac{\partial L_c}{\partial \dot{\eta}} - \frac{\partial L_c}{\partial \eta} = 2\Re_e \int\int dxdxQ\frac{\partial \psi^*}{\partial \eta}, \tag{6}$$

where $L_c = \int\int l_c dxdy$ is the conservative Lagrangian, $\Re_e$ denotes the real part and (*) denotes the complex conjugate, while $\eta = A, X, Y, C, S, Y_2, X_2, \varphi$ and $\dot{\eta} = \frac{d\eta}{dz}$.

The application of the variational approach to the partial differential (2+1)D CQCGL equation leads to a set of eight coupled first-order differential equations (FODEs) resulting from the variation with respect to the linear frequency, unequal spatial widths, the unequal wavefront curvature, the amplitude, the central position and the phase respectively:

$$\frac{dY_2}{dz} = -\frac{2\beta Y_2}{Y^2} + \delta Y_2 - \frac{2\beta Y_2}{X^2} - 2\beta C^2X^2Y_2 - 2\beta S^2Y^2Y_2, \tag{7}$$

$$\frac{dX}{dz} = 4CX - 2\beta C^2X^3 - \frac{\varepsilon}{4}A^2X + \frac{2\beta}{X} + \frac{\delta}{2}X - \frac{2\mu}{9}A^4X, \tag{8}$$

$$\frac{dY}{dz} = 4SY - 2\beta S^2Y^3 - \frac{\varepsilon}{4}A^2Y + \frac{2\beta}{Y} + \frac{\delta}{2}Y - \frac{2\mu}{9}A^4Y, \tag{9}$$

$$\frac{dC}{dz} = -\frac{1}{3}\frac{A^2}{X^2} + \frac{4}{X^4} + \frac{4\nu}{9}\frac{A^4}{X^2} - 4C^2 - 8\beta\frac{C}{X^2}, \tag{10}$$

$$\frac{dS}{dz} = -\frac{1}{3}\frac{A^2}{Y^2} + \frac{4}{Y^4} + \frac{4\nu}{9}\frac{A^4}{Y^2} - 4S^2 - 8\beta\frac{S}{Y^2}, \tag{11}$$

$$\frac{dA}{dz} = -2A(C+S) + \frac{8\mu}{9}A^5 + \frac{5\varepsilon}{4}A^3 - 4\beta AY_2^2 - 3\beta\frac{A}{Y^2} + \frac{\delta}{2}A - 3\beta\frac{A}{X^2} - \beta AC^2X^2 - \beta AS^2Y^2, \tag{12}$$

$$\frac{dX_2}{dz} = 2Y_2 - \beta CX^2Y_2 - \beta SY^2Y_2, \tag{13}$$

$$\frac{d\phi}{dz} = \frac{1}{2}A^2 - \frac{2}{X^2} - \frac{2}{Y^2} - \frac{5\nu}{9}A^4 + 2\beta C + 2\beta S + 2Y_2^2 - 2\beta CX^2Y_2^2 - 2\beta SY^2Y_2^2. \tag{14}$$

As can be seen, the additional parameters X_2 and Y_2 (central position and the speeds) influence the dynamics of the other parameters of the soliton (in comparison to some previous works [33]). Consequently, it is the dynamics of the entire soliton which can be greatly affected during propagation in the system. However, explicit information regarding the different solutions and their stability can not be gained at this stage of the analytical procedure.

Looking for steady state solutions of the system given by equations (7)–(12), the derivatives of soliton parameters with respect to z are set equal to zero. Thus, after some algebra we obtained the steady state amplitude (Eq. (15)) with two discrete values A_+ and A_- steady state solutions. We note that only the symmetric steady state solutions, with equal widths ($X = Y$) and spatial chirps ($C = S$) have been considered. For convenience reasons, the higher coupled term has been neglected, and the dissipative parameters are considered as $\theta = max(\beta, \delta, \varepsilon, \mu)$.

$$A\pm = \left(\beta\left(\frac{4}{3} + 2\beta\varepsilon\right) \pm \sqrt{\beta^2\left(\frac{4}{3} + 2\beta\varepsilon\right)^2 - \frac{256\delta\beta}{9}(1+2\beta^2)(-\beta\mu+\nu)}\right)^{1/2} \left(\frac{92\beta}{\beta}(-\beta\mu+\nu)\right)^{-1/2} + 0\left(\theta^2\right). \tag{15}$$

Figure 1 presents the region of existence of the stationary solutions in the space of the dissipative parameters respectively in the case of $\beta = 0.5$, $\delta = -0.1$, $\nu = 0.72$ (see Fig. 1a) and the case of $\beta = 0.05$, $\delta = -1$, $\nu = 0.72$ (see Fig. 1b) in the plane of (μ, ε) parameters. We obtained the width

$$X = \frac{2\sqrt{2+2\beta^2}}{\sqrt{\frac{4}{9}(\beta\nu-\mu)A^4 + (\frac{1}{2} + \frac{1}{3}\beta\varepsilon)A^2 + \frac{\delta}{\beta}}}, \tag{16}$$

the linear frequency

$$Y_2 = \frac{1}{6}\sqrt{\frac{9A^2\varepsilon}{\beta} + \frac{6A^4\mu}{\beta}}, \tag{17}$$

and the chirp

$$C = \frac{4}{9}(\beta\nu+\mu)A^4 + \left(\frac{1}{2}\varepsilon - \frac{1}{3}\beta\right)A^2. \tag{18}$$

It is important to point out that the balance between the gain/loss and the diffraction with saturating nonlinearity can lead to a fixed steady state solution only for non zero curvature, which is not the case with conservative systems [47–49].

Using the previous equations, the steady state power ($P = \int\int |\psi|^2 dxdy = A^2XY$) is therefore defined as:

$$P = 8A^2(1+\beta)\left(\frac{4}{9}(\beta\mu-\nu)A^4 + \left(\frac{1}{2} + \frac{\beta\varepsilon}{3}\right)A^2 + \frac{\delta}{\beta}\right)^{-1}. \tag{19}$$

It is important to point out that the used ansatz (Eq. (5)) is a simplification of a general form (Eq. (20)) where the central positions and the soliton speed may be taken different in the two transverse axis x and y. Therefore, we consider the following solution

$$\psi = A\exp\left\{-\frac{(x-X_2)^2}{2X^2} - \frac{(y-Y_{22})^2}{2Y^2} + iC(x-X_2)^2 + iS(y-Y_{22})^2 + iX_3(x-X_2) + iY_2(y-Y_{22}) + i\phi\right\}, \tag{20}$$

where additional parameters Y_{22} account for the central position coordinate in the y direction, and X_3 the speed in the x direction. Following the same analytical approach, we obtain

$$\frac{dX_3}{dz} = -8\beta X_3(C^2X^2 - \frac{1}{X^2}), \tag{21}$$

$$\frac{dY_2}{dz} = -8\beta Y_2(S^2Y^2 - \frac{1}{Y^2}), \tag{22}$$

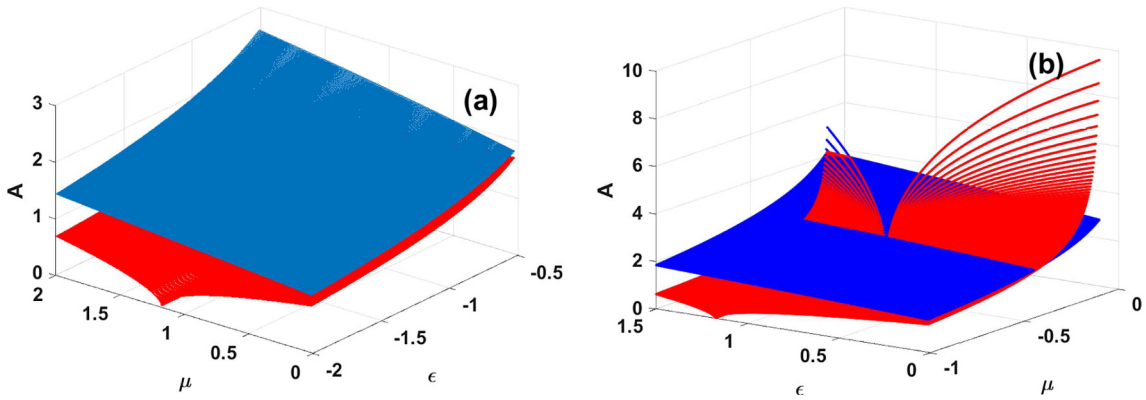

Fig. 1. Double steady state solution $A-$(red) and $A+$ (blue). (a): $\nu = 0.72$, $\beta = 0.5$, $\delta = -0.1$; (b): $\nu = 0.72$, $\beta = 0.05$, $\delta = -1$.

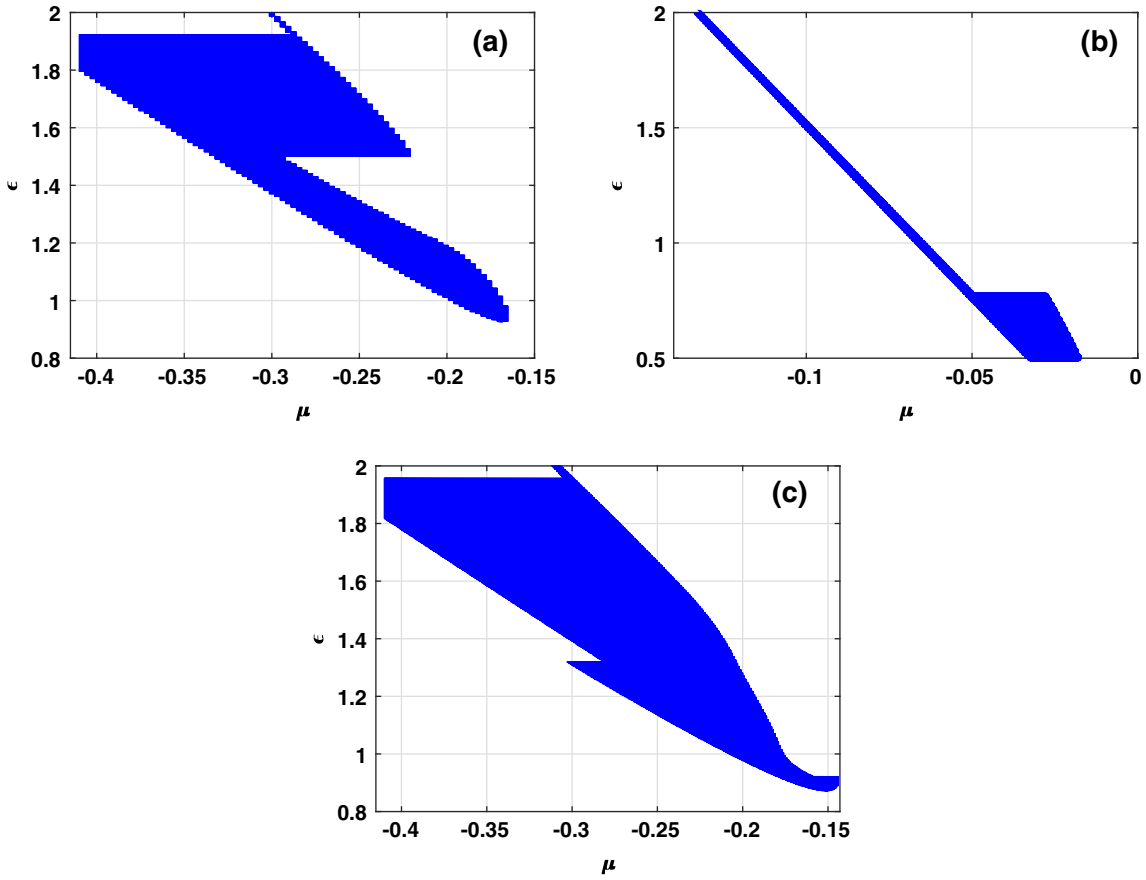

Fig. 2. Domain of stable solutions with $X_3 = Y_2$. (a) $\nu = 0.72$, $\beta = 0.5$, $\delta = -0.1$, (b) $\nu = 0.2$,$\beta = 0.5$, $\delta = -0.01$ and (c) $\nu = 0.72$, $\beta = 0.5$, $\delta = -1$. We can observe the great influence of the system on the stability domain.

$$\frac{dX}{dz} = 4XC + 4\beta(\frac{1}{X^2} - C^2X^3) - \frac{\varepsilon}{4}XA^2 - \frac{2\mu}{9}XA^4, \tag{23}$$

$$\frac{dY}{dz} = 4YS + 4\beta(\frac{1}{Y^2} - S^2Y^3) - \frac{\varepsilon}{4}YA^2 - \frac{2\mu}{9}YA^4, \tag{24}$$

$$\frac{dC}{dz} = -\frac{4\beta}{X^2}(5C + S) + \frac{3}{4}\frac{A^2}{X^2} - \frac{2\nu}{9}\frac{A^4}{X^2} + \frac{4}{X^4} - 4C^2, \tag{25}$$

$$\frac{dS}{dz} = -\frac{4\beta}{Y^2}(C + 5S) + \frac{3}{4}\frac{A^2}{Y^2} - \frac{2\nu}{9}\frac{A^4}{Y^2} + \frac{4}{Y^4} - 4S^2 \tag{26}$$

$$\frac{dA}{dz} = \frac{3\varepsilon}{4}A^3 + \frac{5\mu}{9}A^5 + \delta A - 2A(S + C) - 2\beta A(\frac{1}{X^2} + \frac{1}{Y^2}) - \beta A(X_3^2 + Y_2^2), \tag{27}$$

$$\frac{dX_2}{dz} = 2X_3(1 - 2\beta CX^2), \tag{28}$$

$$\frac{dY_{22}}{dz} = 2Y_2(1-2\beta SY^2), \tag{29}$$

$$\frac{d\varphi}{dz} = 12\beta(S+C) - \frac{7}{4}A^2 + \frac{5\nu}{9}A^4 - 4\left(\frac{1}{X^2}+\frac{1}{Y^2}\right) + X_3^2 + Y_2^2 - 4\beta(X^2X_3^2C + Y^2Y_3^2S). \tag{30}$$

We noted that, the speeds (X_3, Y_2) and the central positions (X_2, Y_{22}) respectively influence the dynamics of the other parameters as we observed in equations (7)–(14). However, some relevant new characteristics appear concerning the dynamics of the new parameters (X_3, Y_2) and (X_2, Y_{22}). In comparison to equations (7)–(14), we noted that the parameter δ do not affected the dynamics of the linear frequencies, and it also appears that the dynamics of the central positions X_3 and Y_2 respectively for x and y directions are influenced by the soliton parameters respectively for the same directions. Another relevant result is related to the mismatch between the unequal wavefront curvature in their dynamics.

The steady state solutions arising from equations (21)–(27) are obtained by considering $X = Y$, $C = S$, $X_3 = Y_2$. Then, after some algebra, we have:
the steady amplitude

$$A_\pm = \sqrt{\frac{-b \pm \sqrt{b^2-4ac}}{2a}}, \tag{31}$$

with

$$a = -\frac{64}{81}\left[(6\beta^2(18\beta^2+1)-2)\mu^2 + 20\beta\nu(1+6\beta)\mu + \beta^2\nu^2(1-12\beta^2) + \frac{\nu^2}{2}\right]$$

$$b = \frac{1}{9}\left[(32(1-3\beta^2(1+6\beta^2))\varepsilon + \frac{80}{3}\beta(1+6\beta^2))\mu^2 - 80\beta\nu(1+6\beta^2)\varepsilon + 48\beta^2\nu(1+12\beta) + 24\nu\right]$$

$$c = 2(-3\beta^2(1+18\beta^2)+1)\varepsilon^2 + 30\beta(1+6\beta^2)\varepsilon + 9\beta^2(12\beta^2-1)\varepsilon - \frac{9}{2}.$$

The width

$$X = \left(2A^2\frac{3(2\beta\varepsilon-1)+2(6\beta\mu+1)A^2}{(6\beta^2+1)}\right)^{-1/2}, \tag{32}$$

the wavefront curvature

$$C = \frac{\left(\frac{1}{2}(3\beta+\varepsilon)+\frac{4}{9}(\mu-\beta\nu)A^4\right)A^2}{8(6\beta^2+1)}, \tag{33}$$

and the linear frequency

$$X_3 = \sqrt{\frac{\frac{2}{3}\left((8\beta^2+1)\mu+\frac{1}{3}\beta\nu\right)A^4 + \left((\frac{15}{2}\beta^2+1)\varepsilon - \frac{3}{4}\beta\right)A^2 + 2\delta\left(6\beta^2+1\right)}{2\beta(6\beta^2+1)}}. \tag{34}$$

In the third part of this work, we analyze their stabilities.

3 Stability analysis

As it is well-known, the CGLE admits localized solutions which are dissipative solitons [21,40]. The stability of these solitary waves has been widely investigated [7,50,51]. This investigation is extended in many domains of research including plasma, fluids, optics, Bose-Einstein condensates, and so on [25,50,51]. We are looking for a stable steady state that can evolve towards a soliton.

An important criterion that gives necessary and sufficient conditions for the stability of the roots of the characteristic polynomial (with real coefficients) to lay in the left half of the complex plane is known as the Routh-Hurwitz (R-H) criterion [52,53]. The stable stationary solutions of equation (1) are determined by the analysis of the eigenvalues λ_j $(j = 1, \ldots, 6)$ of the matrix $M_{ij} = \frac{\partial \dot{\eta}_i}{\partial \eta_j}$ given as follows:

$$\lambda^6 + a_1\lambda^5 + a_2\lambda^4 + a_3\lambda^3 + a_4\lambda^2 + a_5\lambda + a_6 = 0, \tag{35}$$

where $\eta = A, X, Y, Y_2, C$ or S, $\dot{\eta} = \frac{d\eta}{dz}$, with a_i $(i = 1, \ldots, 6)$ depending on the system parameters and the fixed points. To be a stable fixed point according to Lyapunov method, all the eigenvalues must have negative real parts [51]. Using the Routh-Hurwitz criterion, the necessary and sufficient conditions for equation (35) to have $\mathrm{Re}(\lambda_i) < 0$, $i = 1, \ldots, 6$ are given as follows:

$$a_i > 0, \quad b_1 > 0, \quad c_1 > 0, \quad d_1 > 0, \quad e_1 > 0, \tag{36}$$

with

$$b_1 = \tfrac{-1}{a_1}(a_3 - a_2a_1), \qquad b_3 = \tfrac{-1}{a_1}(a_5 - a_1a_4)$$

$$c_1 = \tfrac{-1}{b_1}(a_1b_3 - b_1a_3), \qquad c_3 = \tfrac{-1}{b_1}(a_1a_6 - b_1a_5)$$

$$d_1 = \tfrac{-1}{c_1}(b_1c_3 - c_1b_3), \qquad e_1 = \tfrac{-1}{d_1}(c_1a_6 - c_3d_1).$$

It follows that solutions with amplitudes A_- satisfied the above stability conditions as we can see in Figure 2. Figure 2 shows the influence of the dissipative parameters on the stability domain of the solutions when the speed has the same value in transverse directions x and y.

For the symmetric case, equation (35) is reduced to the polynomial of degree 4 as:

$$\lambda^4 + a_3\lambda^3 + a_2\lambda^2 + a_1\lambda + a_0 = 0, \tag{37}$$

with

$$a_3 > 0,\ a_0 > 0,\ a_3a_2 - a_1 > 0 \text{ and } a_1b_1 - a_3a_0 > 0. \tag{38}$$

This symmetric case, with the stability condition given in equation (38) had been study by Zhu [42] for the CQ CGL equation, including a linear potential.

Considering the ansatz (Eq. (20)), the stable stationary solutions of equation (1) are determined by the analysis of the eigenvalues λ_j $(j = 1, \ldots, 7)$ of (7X7) matrix given by:

$$\lambda^7 + \alpha_1\lambda^6 + \alpha_2\lambda^5 + \alpha_3\lambda^4 + \alpha_4\lambda^3 + \alpha_5\lambda^2 + \alpha_6\lambda + \alpha_7 = 0, \tag{39}$$

where $\alpha_i (i = 1, .., 7)$ depend on the system parameters and the stationary solutions related to equations (31)–(34). The necessary and sufficient conditions for the stability are given by:

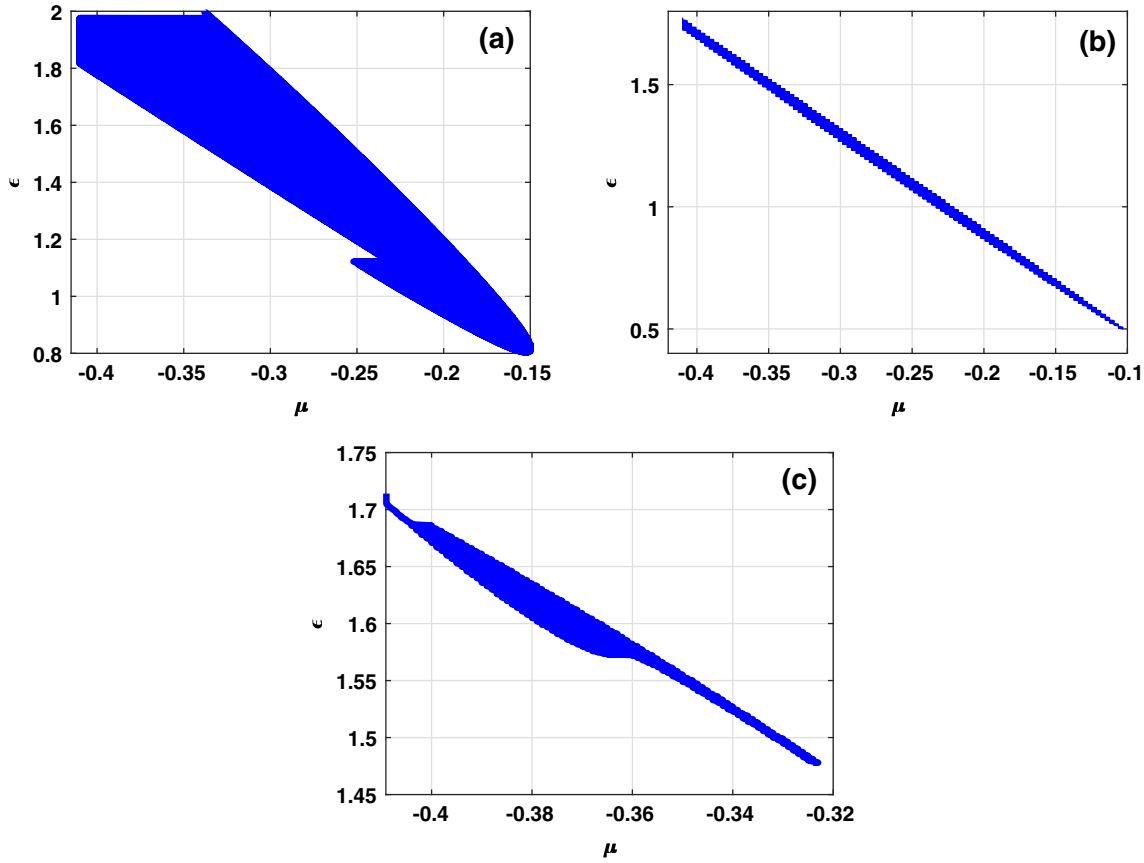

Fig. 3. Domain of stable solutions with $\delta = -1$ and $\nu = 0.72$, for (a) $\beta = 0.5$, $X_3 = Y_2/2$, (b) $\beta = 0.5$, $X_3 = Y_2/5$; (c) $\beta = 1.5$, $X_3 = Y_2/5$.

$$\alpha_i > 0, \quad \beta_{11} > 0, \quad \beta_{21} > 0, \quad \beta_{31} > 0, \quad \beta_{41} > 0 \quad \text{and} \quad \beta_{51} > 0, \tag{40}$$

where

$$\beta_{11} = \alpha_2 - \frac{\alpha_3}{\alpha_1} \qquad \beta_{13} = \alpha_4 - \frac{\alpha_5}{\alpha_1} \qquad \beta_{15} = \alpha_6 - \frac{\alpha_7}{\alpha_1}$$

$$\beta_{21} = \alpha_3 - \frac{\beta_{13}\alpha_1}{\beta_{11}} \qquad \beta_{23} = \alpha_5 - \frac{\beta_{15}\alpha_1}{\beta_{11}}$$

$$\beta_{31} = \beta_{13} - \frac{\beta_{11}\beta_{23}}{\beta_{21}} \qquad \beta_{33} = \beta_{15} - \frac{\beta_{11}\alpha_7}{\beta_{21}}$$

$$\beta_{41} = \beta_{23} - \frac{\beta_{21}\beta_{33}}{\beta_{31}} \qquad \beta_{51} = \beta_{33} - \frac{\beta_{31}\alpha_7}{\beta_{41}}.$$

Numerical result reads to numerous stability domains (see Fig. 3) and the solution satisfied these conditions behave stable during long distance of propagation (see Fig. 7).

4 Numerical results

In order to check the predictions of our analytical approach concerning the appearance of the stable stationary solutions, the numerical simulations of equation (1) are carried out by the use of the Split-Step Fourier Method.

For $Y_2 = X_3$, the stable domain of dissipative solution (see Fig. 2) is given for different set of dissipative parameters. For $\delta = -0.1$, $\beta = 0.5$ and $\nu = 0.72$, Figure 2a shows a blue stability domain. When $\delta = -.01$, $\beta = 0.5$, $\nu = 0.2$, Figure 2b shows a decrease of the stability domain, and for $\delta = -1$, $\beta = 0.5$ and $\nu = 0.72$, Figure 2c shows an increase of the stability domain. As observed in Figures 1a and 1b, Figure 2 confirms that the stability of the solutions is influenced by the parameters of the system. These results correspond to those given by the previous variational equations (see Eqs. (7)–(14) and (21)–(29)).

For the case of solution given by equation (20), Figure 3 presents the blue stability domains, for some particular cases of ratio between the soliton speeds X_3 and Y_2 (corresponding to the x and y transverse axis). Figure 3a showing a wide domain of the stability solution is obtained for $\beta = 0.5$, $\delta = -1$, $\nu = 0.72$ and $X_3 = Y_2/2$. Using the same previous dissipative values as in Figure 3a, with $X_3 = Y_2/5$, the stability domain decreases as can be seen in Figure 3b. For $\beta = 1.5$ $\delta = -1$, $\nu = 0.72$ and $X_3 = Y_2/5$, the corresponding stability domain (Fig. 3c) is considerably reduced. From Figure 3, we notice that the components of the soliton speed as well as the amplitude, the widths, the chirps are greatly dependent on the dissipative parameters of the system, and consequently, the stability of the stationary solution.

The evolution of the steady state amplitudes as function of the cubic nonlinearity has been analyzed through the bifurcation diagram for the case of solution given by

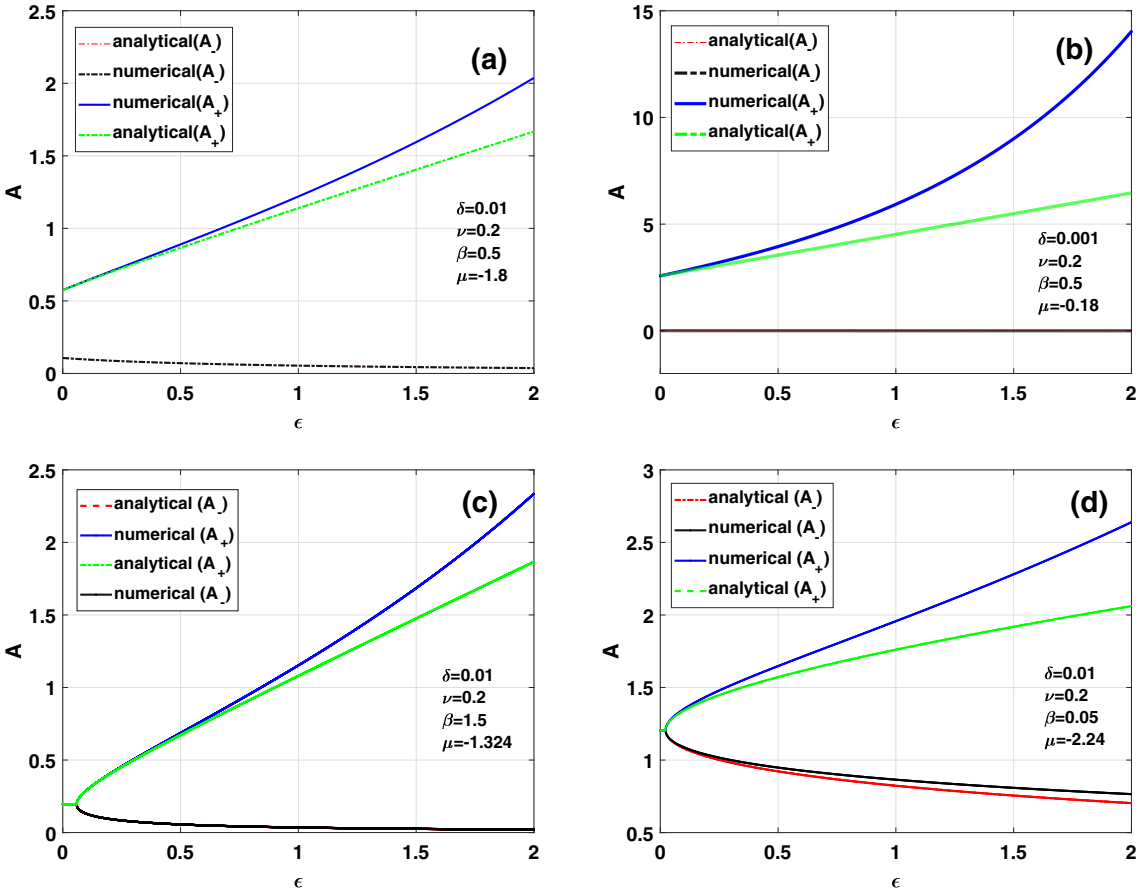

Fig. 4. Bifurcation diagrams of stable A_- and unstable A_+ solutions with $\nu = 0.2$ in (a): $\beta = 0.05$, $\delta = 0.01$, $\mu = -1.324$; (b): $\beta = 0.05$, $\delta = 0.001$, $\mu = -0.18$; (c): $\beta = 1.5$, $\delta = 0.01$, $\mu = -1.324$; (d): $\beta = 0.05$, $\delta = 0.01$, $\mu = -2.24$.

equation (5). Then, in Figure 4, typical bifurcation diagrams are shown where the amplitude of the steady state solution is plotted as a function of the parameter ε. As it is known, the valid variationally obtained analytical curves corresponding to Figure 4 must be a good approximation of the numerical obtained results. In Figure 4, we have shown the comparison between analytical and numerical bifurcation diagrams.

At this stage of our analysis, we have noted several behaviors of the comparison between analytical and numerical results of the amplitudes A_- an A_+. It can be seen in Figures 4a and 4b that the solutions amplitude A_+ (numerical and analytical) present a very good agreement for smaller values of the nonlinear parameter ε, associated with some discrepancies for increasing values of the amplitude. At the same time, the solutions A_- present a very good agreement for small amplitude (Fig. 4a) and zero amplitude (Fig. 4b). When varying the parameters β and μ, the comparison of bifurcation diagrams is shown in Figures 4c and 4d, where a good agreement is also noted between the solution A_- of lower amplitudes on the lower branch and the solution A_+ of the upper branch. It is important to point out that the results in Figure 4d are similar as those obtained by Skarka et al. [33,49]. Therefore, our work presents a more general behavior of the dynamics of solutions A_+ and A_- in the very large space of parameters, where the cross compensation between the linear/nonlinear and loss/gain parameters is necessary to obtain the stability of the soliton solutions.

We are now interested on the global evolution of the solution taken in some stable domain obtained in Figures 2 and 3. As an initial input solution at position $z = 0$ (Fig. 5a), the steady state amplitude A_- is considered with parameters system $\nu = 0.2$, $\beta = 0.05$, $\delta = 0.01$, $\varepsilon = 1.3$, $\mu = -0.15$. The evolution of the propagation of this solution is depicted in Figures 5b–5d where we observed that the shape of the solution is practically maintained, but associated to a decrease of its amplitude. We can also mention the effect of the speed on the central position of the dynamics of the soliton which has been analytically predicted by means of the variational approach. Considering the set of parameters system $\nu = 0.2$, $\beta = 0.005$, $\delta = 0.001$, $\varepsilon = 1.349$, $\mu = -0.4996$, the propagation of the steady state solution A_+ is represented in Figure 5 for some positions along the propagation distance z. From the initial input solution (Fig. 6a), we can also observe that the shape of the propagating solution is maintained with a considerable reduction of the amplitude. The central position (as for the case of the solution A_-) is also affected during the propagation as can be seen in Figures 6b–6d. When dealing with equation (20), we have noted an evolution of the initial solution as depicted

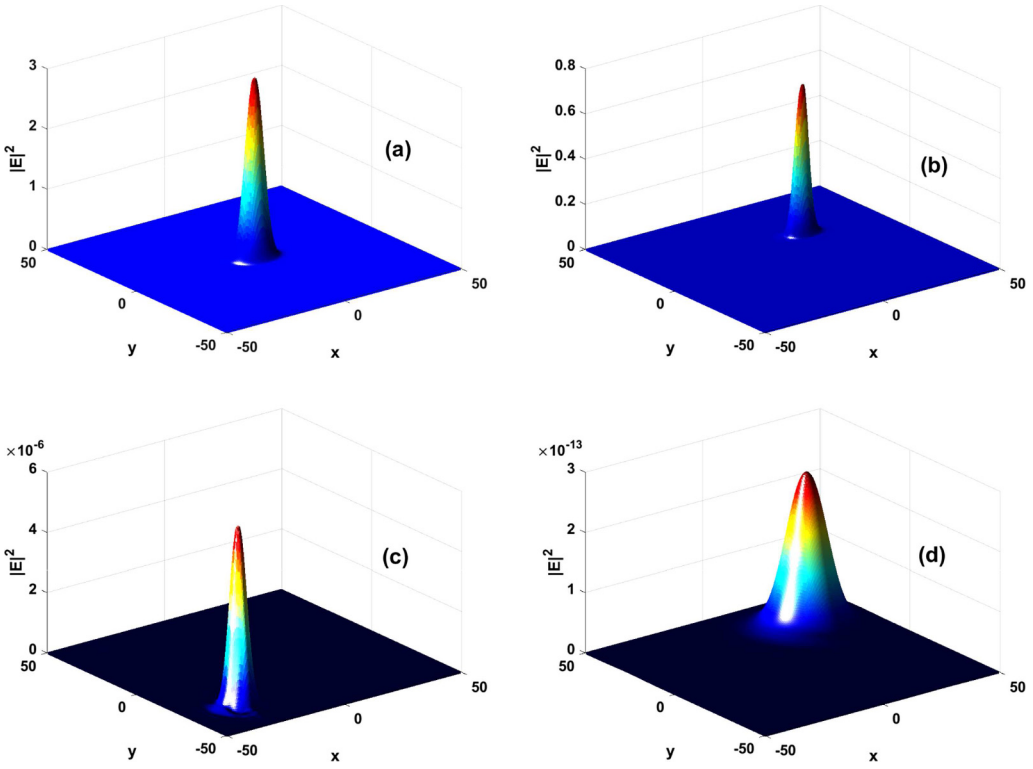

Fig. 5. Profiles of the steady state solution (which amplitude is A_-) at different positions along the propagation distance with parameters $\nu = 0.2$, $\beta = 0.05$, $\delta = 0.01$, $\varepsilon = 1.3$, $\mu = -1.8$. (a) ($z = 0$), (b) ($z = 1$), (c) ($z = 5$), (d) ($z = 12$).

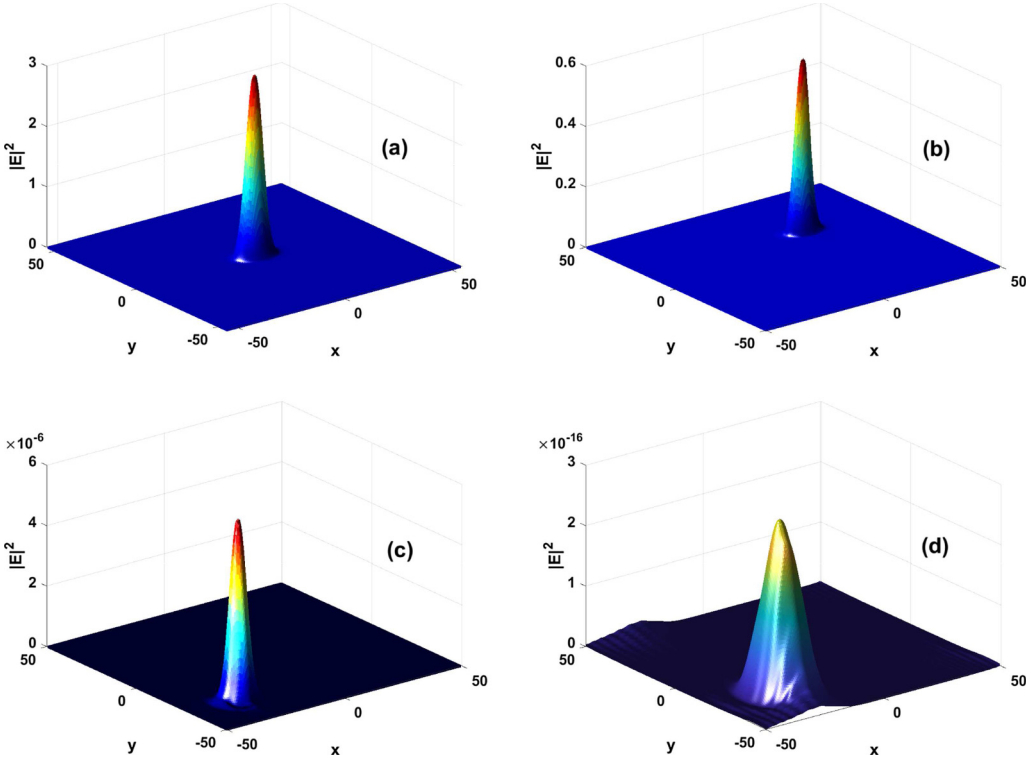

Fig. 6. Profiles of the steady state solution (which amplitude is A_+) at different positions along the propagation distance with parameters $\nu = 0.2$, $\beta = 0.005$, $\delta = 0.001$, $\varepsilon = 1.349$, $\mu = -0.4996$. (a) $z = 0$, (b) $z = 1$, (c) $z = 5$ and (d) $z = 12$.

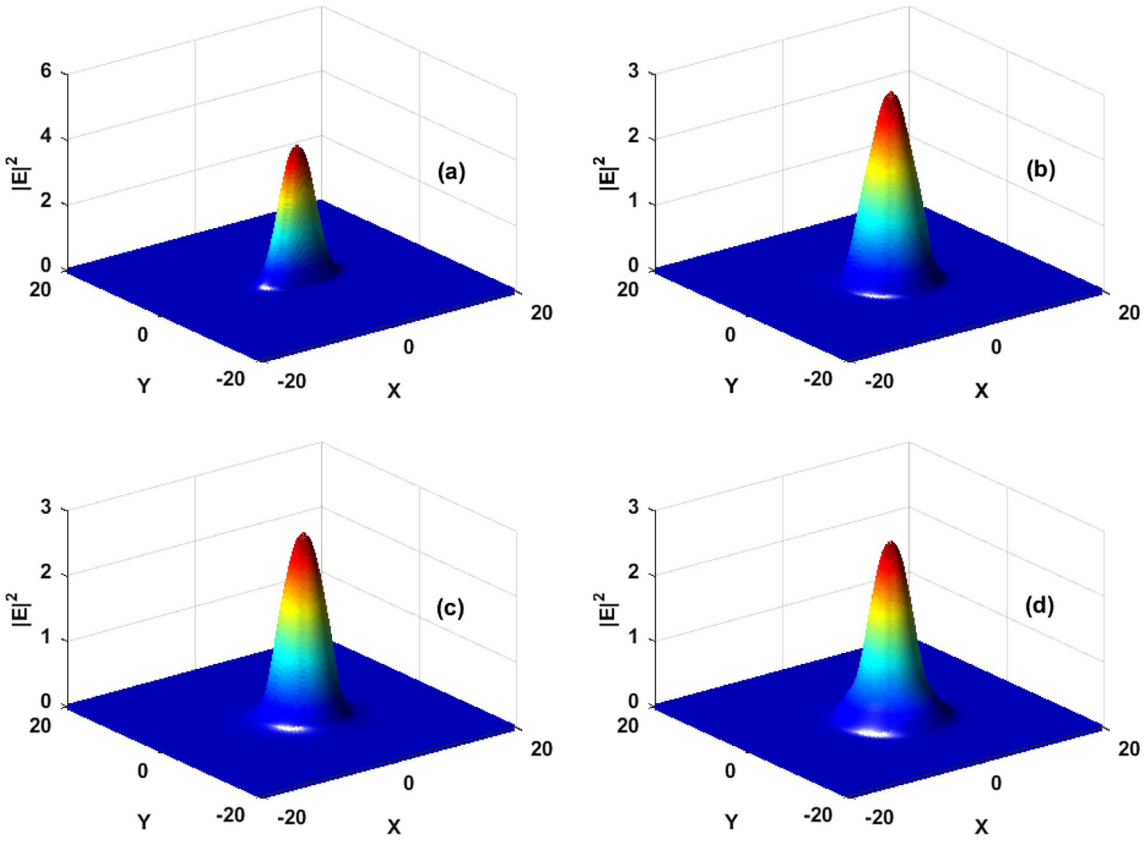

Fig. 7. Profiles of the steady state solution at different positions along the propagation distance with parameters $\nu = 0.72$, $\beta = 0.5$, $\delta = -1$, $\varepsilon = 1.349$, $\mu = -0.3$. (a) $z = 0$, (b) $z = 10$, (c) $z = 100$ and (d) $z = 4000$.

in Figure 7 with $\nu = 0.2$, $\beta = 0.5$, $\delta = -1$, $\varepsilon = 1.349$, $\mu = -0.3$. During this evolution, the soliton intensity remains practically constant around an average value for different propagation distances.

From the dynamics depicted in Figures 5–7, we can clearly note the influence of the additional parameters during the propagation, in comparison with the work reported by Skarka et al. [33]. From this analysis, the stability of the solutions A_- and A_+ is a necessary condition to obtain a soliton after self-organizing evolution as reported also in references [33,35,36,49].

It appears that the variational analysis associated to the Routh-Hurwitz conditions is a useful treatment for the study of stability criteria for the propagation of dissipative solitons in nonlinear media. Due to the large parameters space, more detailed numerical simulations of both the variational equations and the CQGLE lead to a great variety of behaviors of the solutions.

5 Conclusion

Based on the joint variational approach and numerical simulations, we have successfully carried out analytical and numerical studies on the stability of dissipative solitons modeled by the cubic-quintic CGLE. We have clearly established that the system admits two steady state amplitudes for which domains of stability/instability are well defined in function of dissipative parameters of the system. Remarks on the comparison with some parallel works earlier performed are worth mentioning in the literature. An interesting effect here is the chirped soliton stabilities indicated by Skarka et al. [33], showing that chirped solitons are stable for a positive β diffusive parameter.

Another result concerned the influence of the wave speed on the soliton stability. This impractical restriction has been overcome by Esbensen et al. [41] who performed a perturbed variational approach using the Gaussian ansatz type pulse to obtain a dynamical system due to the five characteristic parameters of interest for the pulse, namely the amplitude, the initial phase, the spatial position, the spatial width and the speed. We have recovered some of the previously mentioned results of Skarka et al. [33], as concerning the steady state amplitudes assuming some approximations. We have noted the great influence of the speed on the stability of the stationary solution (see Fig. 3a), where $X_3 = Y_2/2$, and Figure 3b for $X_3 = Y_2/5$. Through the bifurcation diagrams, we have also characterized the evolution of the steady state amplitudes as a function of the nonlinearity. A very good agreement between the analytical and numerical results has been obtained. Then, assuming an initial input solution, the steady state amplitude solution evolves towards a self-organized dissipative soliton for various values of dissipative parameters in the stable domain. Another relevant result obtained in this work is that we have also shown the influence

of the speed on the evolution of the steady state solutions as reported in Figures 5–7. Thus, additional relevant parameters of the Gaussian solution lead to a more general behavior of the dynamics of the dissipative solitons in the system.

The authors (S.I. Fewo, A. Djazet and T.C. Kofané) would like to thank the *CETIC* (University of Yaoundé I, Cameroon) for their helpful support.

Author contribution statement

Alain Djazet performed the calculs, elaborated the numerical code and drafted the manuscript. Serge I. Fewo designed the study, participated in the elaboration of the numerical code, the writing and editing of the paper. Elvis B. Ngompé Nkouankam helped in the calculs and writing the manuscript. Timoléon C. Kofané supervised the whole study. All authors read the manuscript.

Publisher's Note The EPJ Publishers remain neutral with regard to jurisdictional claims in published maps and institutional affiliations.

References

1. Y.S. Kivshar, G.P. Agrawal, *Optical Solitons* (2003)
2. N. Efremidis, K. Hizanidis, J. Opt. Soc. Am. B **19**, 1 (2002)
3. S. Shwetanshumala, Prog. Electromagn. Res. Lett. **3**, 17 (2008)
4. Z. Chen, M. Segev, D.N. Christodoulides, Rep. Prog. Phys. **75**, (2012)
5. M. Segev, Opt. Quantum Electron. **30**, 503 (1998)
6. E.A. Ultanir, G.I. Stegeman, C.H. Lange, F. Lederer, Opt. Lett. **29**, 3 (2004)
7. G.A. Askar'yan, Sov. Phys. JETP **15**, 1088 (1962)
8. R.Y. Chiao, E. Garmire, C.H. Townes, Phys. Rev. Lett. **13**, 479 (1964)
9. A. Barthelemy, S. Maneuf, G. Froehly, Opt. Commun. **55**, 201 (1985)
10. K.E. Strecker, G.B. Patridge, A.G. Truscott, R.G. Hulet, Nature **417**, 150 (2002)
11. L. Khaykovich, F. Scherck, G. Ferrari, T. Bourdel, J. Cubizolles, L.D. Carr, Y. Castin, C. Salomon, Science **296**, 1290 (2002)
12. P.L. Knight, A. Miller, in *Optical solitons - theory and experiment*, edited by J.R. Taylor (Cambridge University Press, Cambridge, UK, 1992)
13. G.I. Stegeman, M. Segev, Science **286**, 1518 (1999)
14. V.E. Zakarov, A.B. Shabat, Phys. JETP **37**, 823 (1973)
15. N.N. Rosanov, *Spatial Hysteresis and Optical Patterns* (Springer, Berlin, 2002)
16. M. Djoko, T.C. Kofane, Commun. Nonlinear Sci. Numer. Simul. **48**, 179 (2017)
17. M. Djoko, T.C. Kofane, Commun. Nonlinear Sci. Numer. Simul. **68**, 169 (2019)
18. I.S. Aranson, L. Kramer, Rev. Mod. Phys. **74**, 99 (2002)
19. M.C. Cross, P.C. Hohenberg, Rev. Mod. Phys. **65**, 851 (1993)
20. P. Mandel, M. Tlidi, J. Opt. B: Quantum Semiclass. Opt. **6**, R60 (2004)
21. N. Akhmediev, A. Ankiewicz (eds), *Dissipative solitons*, in *Lecture notes in physics* (Springer, Berlin, 2005), Vol. 661
22. A.M. Sergeev, V.I. Petviashvili, Dokl. Akad. Nauk SSSR **276**, 1380 (1984)
23. A.M. Sergeev, V.I. Petviashvili, Sov. Phys. Dokl. **29**, 493 (1984)
24. B.A. Malomed, D. Mihalache, F. Wise, L. Torner, J. Opt. B: Quantum Semiclass. Opt. **7**, R53 (2005)
25. D. Mihalache, D. Mazilu, F. Lederer, Y.V. Kartashov, L.C. Crasovan, L. Torner, B.A. Malomed, Phys. Rev. Lett. **97**, 073904 (2006)
26. A.S. Desyatnikov, Y.S. Kivshar, L. Torner, Prog. Opt. **47**, 291 (2005)
27. B.A. Malomed, Eur. Phys. J. Special Topics **225**, 2507 (2016)
28. B.A. Kochetov, V.R. Tuz, Phys. Rev. E **98**, 062214 (2018)
29. B.A. Kochetov, O.G. Chelpanova, V.R. Tuz, A.I. Yakimenko, Phys. Rev. E **100**, 0632202 (2019)
30. O.V. Borovkova, Y.V. Kartashov, L. Torner, Phys. Rev. A **81**, 063806 (2010)
31. L.A. Lugiato, F. Prati, M.L. Gorodetsky, T.J. Kippenberg, Philos. Trans. R. Soc. A **376**, 0113 (2018)
32. L.C. Crasovan, B.A. Malomed, D. Mihalache, Phys. Lett. A **289**, 59 (2001)
33. V. Skarka, D.V. Timotijevic, N.B. Aleksic, J. Opt. A: Pure Appl. Opt. **10**, 075102 (2008)
34. B.A. Malomed, Physica D **29**, 155 (1987)
35. V.V. Afanasjev, N. Akhmediev, J.M. Soto-Crespo, Phys. Rev. E **53**, 2 (1996)
36. P.C. Bressloff, Z.P. Kilpatrick, Phys. Rev. E **78**, 041916 (2008)
37. S. Wang, A. Docherty, B.S. Marks, C.R. Menyuk, J. Opt. Soc. Am. B **30**, 11 (2013)
38. V. Skarka, N.B. Aleksic, V.I. Berezhiani, Phys. Rev. A **81**, 045803 (2010)
39. D. Anderson, Phys. Rev. A **27**, 3135 (1983)
40. S.I. Fewo, C.M. Ngabireng, T.C. Kofane, J. Phys. Soc. **7**, 074401 (2008)
41. B.K. Esbensen, M. Bache, O. Biang, W. Krolikowski, Phys. Rev. A **86**, 033838 (2012)
42. W. Zhu, Y. He, Opt. Express **18**, 1753 (2010)
43. A. Anderson, M. Lisak, A. Berntson, J. Phys. **57**, 917 (2001)
44. B. Malomed, Prog. Opt. **43**, 71 (2002)
45. A. Scott, *Nonlinear Science. Emergence and Dynamics of Coherent Structures* (Oxford University Press, Oxford, 2003)
46. S. Chavez Cerda, S.B. Cavalcanti, J.M. Hickmann, Eur. Phys. J. D **1**, 313 (1998)
47. V. Skarka, V.I. Berezhehiani, R. Mmiklaszewski, Phys. Rev. E. **56**, 1080 (1997)
48. V. Skarka, V.I. Berezhehiani, R. Mmiklaszewski, Phys. Rev. E. **59**, 1270 (1999)
49. V. Skarka, N.B. Aleksic, Phys. Rev. Lett. **96**, 013903 (2006)
50. J.M. Soto-Crespo, N. Akhmediev, A. Ankiewicz, Phys. Rev. Lett. **85**, 2937 (2000)
51. N. Akhmediev, J.M. Soto-Crespo, G. Town, Phys. Rev. E **63**, 056602 (2001)
52. R.N. Clark, IEEE Control Syst. Mag. **12**, 3 (1992)
53. Y.S. Apte, IEE-IERE Proc. – India **7**, 4 (1969)

Applied Physics B (2020) 126:74
https://doi.org/10.1007/s00340-020-07422-7

Applied Physics B
Lasers and Optics

Vector dissipative light bullets in optical laser beam

Alain Djazet[1] · Conrad B. Tabi[2] · Serge I. Fewo[1] · Timoléon C. Kofané[1,2,3]

Received: 24 October 2019 / Accepted: 17 March 2020
© Springer-Verlag GmbH Germany, part of Springer Nature 2020

Abstract

The dynamics of light bullets propagating in nonlinear media with linear/nonlinear, gain/loss and coupling described by the (2+1)-dimensional vectorial cubic–quintic complex Ginzburg–Landau (CGL) equations is considered. The evolution and the stability of the vector dissipative optical light bullets, generated from an asymmetric input with respect to two transverse coordinates x and y, are studied. We use the variational method to find a set of differential equations characterizing the variation of the light bullet parameters in the laser cavity. This approach allows us to analyze the influence of various physical parameters on the dynamics of the propagating beam and its relevant parameters. Then, we solve the original coupled (2+1)D cubic–quintic CGL equation using the split-step Fourier method. Numerical results and analytical predictions are confronted, and a good agreement between the two approaches is obtained.

1 Introduction

Solitons, which are fascinating nonlinear wave phenomena, are self-trapped light beams or pulses supported by the balance between diffraction and/or dispersion (in the spatial and/or temporal domain) and nonlinearities of various types [1–6]. The generation, propagation and interaction of optical vortices in nonlinear media have attracted much attention and have been the subject of extensive studies in recent years. In the single-mode fibers (SMFs), in which the soliton formation has drawn a lot of attention, the light propagation is governed by the nonlinear Schrödinger equation (NLS) equation [7] and, when considering the vectorial nature of light, its propagation in the SMF is governed by a set of coupled NLS equations [8], whose characteristics and dynamics are richer than those of the scalar NLS equation.

In laser systems, the formation and dynamics of transverse light patterns in nonlinear resonator remains a field of intense research [9–12]. Assuming that the direction of the electric field is constant and applying the slowly varying envelope approximation to the Maxwell–Bloch (MB) equations helped to establish the relationship between nonlinear optics and the cubic complex Ginzburg–Landau (CGL) equation [12, 13]. Considering the interaction of an electromagnetic field with matter in a laser cavity without the assumption of a fixed direction of the transverse electric field, Gil [9], using the standard perturbative nonlinear analysis, exclusively proposed that the MB equations could be reduced to a vectorial cubic CGL equation. Although this later formulation has been widely adopted, soliton solutions in this context are usually not stable, both for anomalous [14] and normal dispersions [15], except if higher-order nonlinear (quintic) terms are introduced, leading to the so-called cubic–quintic CGL equation. The competition between the cubic and quintic nonlinearities may open new possibilities with a broad range of behaviors, characterized by different kinds of patterns formation in one-(localized structures) [16–18] and two-spatial dimensions (topological defects) [16, 19–24] for the vectorial cubic CGL equation. Motivated by these, we recently adopted the same procedure as Gil and rather derived a vectorial cubic–quintic CGL equation from which

✉ Conrad B. Tabi
tabic@biust.ac.bw

Alain Djazet
djazet.alain@yahoo.fr

Serge I. Fewo
sergefewo@yahoo.fr

Timoléon C. Kofané
tckofane@yahoo.com

1 Laboratoire de Mécanique, Département de Physique, Faculté des Sciences, Université de Yaoundé I, B.P. 812, Yaoundé, Cameroun

2 Department of Physics and Astronomy, Botswana International University of Science and Technology, Private Bag 16, Palapye, Botswana

3 Centre d'Excellence Africain en Technologies de l'Information et de la Communication (CETIC), Université de Yaoundé I, Yaoundé, Cameroun

Published online: 03 April 2020

we obtained that the modulational instability (MI) mechanism may lead to localized modes with interesting and new behaviors, strongly related to the change in the laser cavity parameters [25]. However, the MI technique becomes obsolete when it comes to describe the main characteristics of individual pulse evolution, namely its amplitude, temporal and spatial widths, position of the maximum, unequal wavefront curvatures, chirp parameters and phase shift. Depending on the field of application, a number of treatments have been adopted, namely the method of moments [26], method of collective coordinates [27–29], time-dependent variational method [30], effective-particle method [31], averaged Lagrangian description [32], just to name a few. Particularly, the variational method has been successfully applied to address a variety of nonlinear problems through the use of the Lagrange density and its relation to the Euler–Lagrange equations [33]. Besides, the fundamental advantage of the variational approach is that it provides an outline under the field dynamics during propagation [34, 35]. A potential well is generated into a stationary point due to the exact balance between repulsive and attractive potentials, justifying the formation of stable optical solitons. In the present work, to investigate the generation of the vector light bullets of the laser coupled cubic–quintic CGL equation, and their stability for several dynamical regimes, we make use of the variational method to obtain physical insight in terms of a few important parameters and then propose numerical simulations that confirm qualitatively our analytical predictions.

The rest of the paper is organized as follows. In Sect. 2, we present the propagation model of the optical light bullet which includes the cubic and quintic coupling terms, diffraction terms, cubic and quintic nonlinearity terms. In addition, with the help of the variational method involving trial function, the set of variational equations resulting from the Euler–Lagrange equations is obtained. In Sect. 3, the average equations for the effective potential function is derived along with the numerical treatment of the analytical results. Section 4 is devoted to some concluding remarks.

2 Model and analytical treatment using variational approach

In the good cavity limit, when both the induced polarization and population inversion are enslaved by a slowly varying vector electromagnetic field of a multi-transverse-mode laser (MTM), a general form of the equations describing vector soliton process is reduced to the coupled (2+1)D cubic–quintic CGL equation [25]

$$\begin{aligned} i\frac{\mathrm{d}\psi_\pm}{\mathrm{d}t} &+ \psi_\pm + \Delta\psi_\pm + |\psi_\pm|^2\psi_\pm \\ &+ \gamma_r|\psi_\mp|\psi_\pm + \nu|\psi_\pm|^4\psi_\pm \\ &+ \delta_r(|\psi_\mp|^2 + 2|\psi_\pm|^2)|\psi_\mp|^2\psi_\pm = \mathcal{Q}_\pm, \end{aligned} \tag{1}$$

with

$$\begin{aligned} \mathcal{Q}_\pm = i(&\delta\psi_\pm + \beta\Delta\psi_\pm + \varepsilon|\psi_\pm|^2\psi_\pm + \gamma_i|\psi_\mp|\psi_\pm \\ &+ \mu|\psi_\pm|^4\psi_\pm \\ &+ \delta_i(|\psi_\mp|^2 + 2|\psi_\pm|^2)|\psi_\mp|^2\psi_\pm). \end{aligned} \tag{2}$$

The left-hand-side of Eq. (1) contains the conservative terms, where $\Delta = \frac{\partial^2}{\partial x^2} + \frac{\partial^2}{\partial y^2}$. The optical envelope $\psi_\pm(x, y, t)$ is the normalized complex function of three real variables x, y and t, where x and y are the normalized two transverse coordinates and t is the normalized propagation time. All the parameters of Eqs. (1) and (2), i.e., ν, δ, ε, γ_r, γ_i, μ, δ_r and δ_i, are real constants, and the pump profile parameter related to $\psi_\pm$ is normalized to unity [36]. The negative coefficient ν is the saturation of the Kerr nonlinearity, and the quintic coefficient $\delta_r < 0$ is the saturation of the cubic coupling absorption γ_r. The right term $\mathcal{Q}_\pm$ of Eq. (1), given by Eq. (2), stands for the dissipation, where δ is the linear loss/gain coefficient, β is the diffusion coefficient, ε is the cubic gain, μ is the quintic loss, γ_i and δ_i, respectively, denote the cubic and the quintic coupling coefficients.

Due to its complexity, the coupled (2+1)D cubic–quintic CGL equation does not allow exact analytical solutions. Therefore, the use of an approximated analytical approach is needed, which includes for example the collective coordinate method [37], the moment method [38], the variational method [34, 35, 39, 40], and so on. Solutions are in general analyzed by considering trial Gaussian [34] functions with a few free parameters such as the amplitude, spatial pulse widths, the central position of the pulse maximum, the unequal wavefront curvatures, and the phase shift, which depend on the propagation time t. In this respect, the variational method for dissipative systems is used in the following, with the objective to obtain more physical insight in terms of a few relevant parameters and then present numerical simulations that confirm the analytical predictions. In so doing, the left-hand side of Eq. (1) is derived from the Lagrangian density given by

$$\begin{aligned} \mathcal{L} = &\frac{i}{2}\left(\psi_-^*\frac{\partial\psi_-}{\partial t} - \psi_-\frac{\partial\psi_-^*}{\partial t} + \psi_+^*\frac{\partial\psi_+}{\partial t} - \psi_+\frac{\partial\psi_+^*}{\partial t}\right) \\ &+ \left|\frac{\partial\psi_\mp}{\partial x}\right|^2 + \left|\frac{\partial\psi_\mp}{\partial y}\right|^2 + \frac{1}{2}|\psi_\pm|^4 + \frac{\nu}{3}|\psi_\pm|^6 \\ &+ \gamma_r|\psi_\mp|^2|\psi_\pm|^2 + \delta_r\left(|\psi_\pm|^4|\psi_\mp|^2 + |\psi_\pm|^2|\psi_\mp|^4\right), \end{aligned} \tag{3}$$

where $\psi_\pm^*$ stands for the complex conjugate of $\psi_\pm$. To extend our study to the characterization of the evolution of

the single parameters of the dissipative light bullet during propagation in the medium, we adopt the following Gaussian trial function

$$\psi_{\pm} = A\exp\left\{-\frac{(x\pm X_m)^2}{2X^2}-\frac{y^2}{2Y^2} + iC(x\pm X_m)^2 + iSy^2 + i\phi\right\}, \tag{4}$$

where A is the amplitude, X and Y are the unequal spatial widths, C and S are the unequal wavefront curvature, X_m is the central position, and ϕ is the phase of the light bullet, all of which are functions of the independent variable t.

To proceed to the analytical treatment of the model and characterize the solutions depending on the various dissipative parameters, the equations for the motions of the variational parameters η are obtained through the Euler–Lagrange equations [34, 35]

$$\frac{\mathrm{d}}{\mathrm{d}t}\left(\frac{\partial \mathbf{L}}{\partial \dot{\eta}}\right) - \frac{\partial \mathbf{L}}{\partial \eta} = 2R_e\int\int \mathrm{d}x\mathrm{d}y\left(\mathcal{Q}_-\frac{\partial\psi_-^*}{\partial\eta} + \mathcal{Q}_+\frac{\partial\psi_+^*}{\partial\eta}\right), \tag{5}$$

where $\dot{\eta} = \frac{\mathrm{d}\eta}{\mathrm{d}t}$. Here, η represents the parameters A, X, Y, C, S, X_m and ϕ in the ansatz, while

$$\mathbf{L} = \int\int \mathcal{L}\mathrm{d}x\mathrm{d}y \tag{6}$$

is the average Lagrangian of the conservative system obtained by substituting Eqs. (4) into (3) and taking out integration over coordinates x and y. Thus, we make use of the Euler–Lagrange equation [40] and obtain the following set of differential equations describing the dynamics of the seven relevant parameters of the trial solution (4):

$$\begin{aligned}\frac{\mathrm{d}A}{\mathrm{d}t} =& 2A(S+C) - \delta A - \frac{3}{4}\varepsilon A^3 - \frac{5}{9}\mu A^5 \\ &+ \beta A\left(\frac{1}{X^2}+\frac{1}{Y^2}\right) \\ &+ \gamma_i A^3 e^{-\frac{2X_m^2}{X^2}}\left(-1+\frac{1}{4X^2}+\frac{1}{4Y^2}+\frac{X_m^2}{2X^2}\right) \\ &+ A^5\delta_i e^{-\frac{8X_m^2}{3X^2}}\left(-1+\frac{1}{4X^2}+\frac{1}{4Y^2}+\frac{4X_m^2}{9X^2}\right),\end{aligned} \tag{7a}$$

$$\begin{aligned}\frac{\mathrm{d}X}{\mathrm{d}t} =& 4CX\left(\beta CX^2-1\right) - \frac{\beta}{X^2} + XA^2\left(\frac{\varepsilon}{4}+\frac{2\mu A^2}{9}\right) \\ &+ \gamma_i A^2 e^{-\frac{2X_m^2}{X^2}}\left(-\frac{X_m^2}{X}-\frac{1}{X}+\frac{X}{2}\right) + \delta_i A^4 e^{-\frac{8X_m^2}{3X^2}},\end{aligned} \tag{7b}$$

$$\begin{aligned}\frac{\mathrm{d}Y}{\mathrm{d}t} =& 4SY\left(\beta SY^2-1\right) - \frac{\beta}{Y^2} + YA^2\left(\frac{\varepsilon}{4}+\frac{2\mu A^2}{9}\right) \\ &+ \gamma_i A^2 e^{-\frac{2X_m^2}{X^2}}\left(-\frac{1}{Y}+\frac{Y}{2}\right) \\ &+ \delta_i A^4 e^{-\frac{8X_m^2}{3X^2}}\left(-\frac{1}{2Y}+\frac{Y}{2}\right),\end{aligned} \tag{7c}$$

$$\begin{aligned}\frac{\mathrm{d}C}{\mathrm{d}t} =& 4C^2 + \frac{1}{X^2}\left(4\beta C - \frac{A^2}{4} - \frac{2\nu A^4}{9} - -\frac{1}{X^2}\right) \\ &+ \frac{\gamma_r A^2}{4X^2}e^{-\frac{2X_m^2}{X^2}}\left(\frac{4X_m^2}{X^2}-1\right) \\ &+ \frac{2\delta_r A^4}{3X^2}e^{-\frac{8X_m^2}{3X^2}}\left(\frac{8X_m^2}{3X^2}-1\right),\end{aligned} \tag{7d}$$

$$\begin{aligned}\frac{\mathrm{d}S}{\mathrm{d}t} =& 4S^2 + \frac{1}{Y^2}\left(4\beta S - \frac{A^2}{4} - \frac{2\nu A^4}{9} - \frac{1}{Y^2}\right) \\ &- \frac{\gamma_r A^2}{4Y^2}e^{-\frac{2X_m^2}{X^2}} - \frac{2\delta_r A^4}{3Y^2}e^{-\frac{8X_m^2}{3X^2}},\end{aligned} \tag{7e}$$

$$\frac{\mathrm{d}X_m}{\mathrm{d}t} = A^2X_m\left(\gamma_i e^{-\frac{2X_m^2}{X^2}} + \frac{8\delta_i A^2}{9}e^{-\frac{8X_m^2}{3X^2}}\right), \tag{7f}$$

$$\begin{aligned}\frac{\mathrm{d}\phi}{\mathrm{d}t} =& -1 - 2\beta(C+S) + \frac{1}{X^2} + \frac{1}{Y^2} + A^2\left(\frac{3}{4}+\frac{5\nu A^2}{9}\right) \\ &+ \frac{\gamma_r A^2}{2}e^{-\frac{2X_m^2}{X^2}}\left(-\frac{X_m^2}{X^2}+\frac{3}{2}\right) \\ &+ \frac{\delta_r A^4}{3}\left(-\frac{8X_m^2}{3X^4}+5\right)e^{-\frac{8X_m^2}{3X^2}}.\end{aligned} \tag{7g}$$

Eqs. (7a–7g) represent the coupled equations that show how pulse parameters change during propagation. Looking for steady state solutions of the system of Eqs. (7a–7g) after vanishing derivatives of amplitude, width, curvature, and central position, we focus our study on the symmetric steady state solutions, with $X_m = 0$, equal widths ($X = Y$) and spatial chirps ($C = S$). For convenience, all dissipative parameters are considered as small quantities $\theta = \max(\beta, \delta, \varepsilon, \mu)$. The corresponding steady state amplitude has two discrete values A^+ and A^- given by

$$A^{\pm} = \sqrt{\frac{9\beta\left(-4\beta(1+\beta\varepsilon+\gamma_r)\pm\sqrt{\Delta}\right)}{2(\beta\mu+4\nu+4\delta_r)}}, \tag{8}$$

with $\Delta = \frac{(1+\beta\varepsilon+\gamma_r)^2}{16\beta^2} - \frac{4\delta(\beta\mu+4\nu+4\delta_r)}{9\beta}$. We also obtain the width,

$$X = \left(\left(\left(\frac{\mu}{3} + \frac{\delta_i}{2} \right) A^4 + \frac{1}{2}(\varepsilon + \gamma_i) A^2 + \delta \right) / \beta \right)^{-1/2} + 0(\theta^2), \tag{9}$$

and the chirp

$$C = \frac{C_4 A^4 + C_2 A^2 + \delta}{4\beta^2}, \tag{10}$$

with $C_4 = \frac{1}{3}(2\mu + 3\delta_i + 4\beta(\delta_r + \frac{\nu}{3}))$, and $C_2 = \frac{1}{4}(2(\varepsilon + \gamma_i) + \beta(1 + \gamma_r))$.

3 Stability analysis and numerical results

To study the dynamical stability of the vector light bullet solution given above, we first calculate the effective potential. An important criterion for the stability of our stationary solution is to investigate the possibility of bullets to be trapped in the well. We examine the dynamical behaviors of a light bullet using the initial conditions given by Eqs. (8–10), from its symmetric equilibrium. Integration of variational Eqs. (7a–7g) gives [7, 35, 39, 41]

$$\frac{1}{4}\left(\frac{\mathrm{d}X}{\mathrm{d}t}\right)^2 + \frac{1}{4}\left(\frac{\mathrm{d}Y}{\mathrm{d}t}\right)^2 + U(X, Y) = U(X_0, Y_0), \tag{11}$$

where $U(X, Y)$ is the effective potential given in "Appendix". Equation. (11) describes the dynamics of the widths and shows a competition among diffraction and nonlinearity, and can be adopted to study the stability of the optical light bullet through the medium. The existing stationary solution describes the motion of a particle located at the bottom of the potential well. Given the effective potential $U(X, Y)$, we have the equations

$$\frac{\mathrm{d}^2 X}{\mathrm{d}t^2} = -2\frac{\partial U(X, Y)}{\partial X}, \tag{12a}$$

$$\frac{\mathrm{d}^2 Y}{\mathrm{d}t^2} = -2\frac{\partial U(X, Y)}{\partial X}, \tag{12b}$$

which are equivalent to those describing the dynamics of a particle in two-dimensional potential well. When the nonlinearity exactly balances both the diffraction, the curve of the potential shows an extremum, which is an equilibrium solution. In such a direction, the obtained effective potential U, in the plane of nonlinear dissipative parameters, is depicted in Fig. 1, where panel (a) describes the effective potential versus (ε, δ_i), while panels (b) and (c) show U versus (ε, μ), confirming that the effective potential has a global minimum. This reveals the existence of a stable stationary light bullet. This confirms as well the existence of the stationary soliton solution corresponding to the optical dissipative soliton located at the bottom of the effective potential well. From Fig. 1, we observe that the shape of the effective potential depend on both the dissipative and soliton parameters. However, from Fig. 1a–c, the areas corresponding to the bottom of the effective potential well (minima) are the domains of parameters for which the soliton can be trapped, leading to a stable propagation. These confirm the analytical predictions from Eqs. (7a–7g). Figure 1 presents two extrema, minima and maxima. Therefore, depending on the dissipative parameters and the central position, the beam will be either trapped or diffracted. The beam with initial condition corresponding to the point lying on the potential curve below the maximum will always be trapped, therefore, generating a light bullet [7]. Using the variational method, it can be predicted that all beams initially around the minimum of the potential well will form light bullets pulsating around

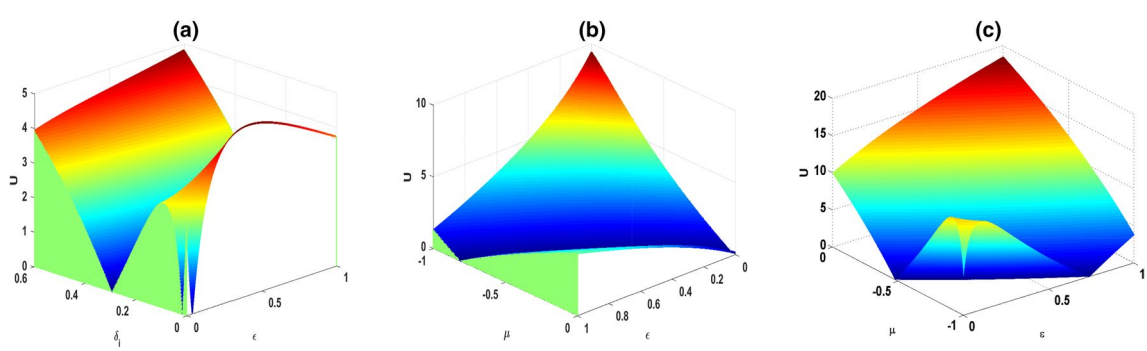

Fig. 1 Effective potential U versus (ε, δ_i) in panel **a**, and versus (ε, μ) in panels **b**, **c** for the parameters $\delta = -0.01059$, $\beta = 0.49$, $\gamma_i = 0.25118$, $\nu = -1$, and: **a** $\gamma_r = 1.1087$, $\delta_r = -0.5074$, $\mu = -.9$, $X_m = 1.3$, **b** $\gamma_r = 0.9$, $\delta_r = -0.5074$, $\delta_i = 0.04289$, $X_m = 1.3$, **c** $\gamma_r = 0.9$, $\delta_r = -0.35074$, $\delta_i = 0.04289$, $X_m = 0.05$

its equilibrium condition, with initial condition focusing until the turning point at the bottom region. The analysis of the potential well reveals the existence of a stable equilibrium which plays the role of an attractor [35, 39].

To confirm the analytical predictions, the coupled (2+1) D cubic–quintic CGL Eqs. (1) have been numerically solved by means of split-step Fourier method (SSFM) with a time-step $\Delta t = 10^{-3}$, on a mesh of size 100×100, with space-steps $\Delta x = \Delta y = 0.01$. The used initial conditions are Gaussian trial function given by Eq.(4), with amplitude $A = A^{-}$ (see Eq. (8)), the unequal spatial widths X given by Eq. (9) and $Y = X/3$, the unequal wavefront curvature C given by Eq. (10) and $S = C$. For SSFM, the propagation of the wave solution from t to $t + \Delta t$ is carried out in two steps. In fact, the main idea behind this method is to obtain an approximate solution by assuming that for the wave solution over a small time Δt, the dispersive and nonlinear effects act independently. In the first step, the nonlinearity acts alone, and in the second step dispersion acts alone [39, 42]. In this context, Eqs. (1) are written as

$$\frac{\partial \psi_+}{\partial t} = (\hat{D} + \hat{\aleph}_+)\psi_+, \tag{13a}$$

$$\frac{\partial \psi_-}{\partial t} = (\hat{D} + \hat{\aleph}_-)\psi_-, \tag{13b}$$

where $\hat{D}$ is the operator for dispersion and absorption in the linear medium,

$$\hat{D} = (\delta + i) + (\beta + i)\left(\frac{\partial^2}{\partial x^2} + \frac{\partial^2}{\partial y^2}\right), \tag{14}$$

while $\hat{\aleph}_+$ and $\hat{\aleph}_-$ are the nonlinear operators for pulse propagation defined by

$$\begin{aligned}\hat{\aleph}_+ =&(\varepsilon + i)\left|\psi_+\right|^2 + \left(\gamma_i + i\gamma_r\right)\left|\psi_-\right|^2 + (\mu + i\nu)\left|\psi_+\right|^4 \\ &+ \left(\delta_i + i\delta_r\right)\left(\left|\psi_-\right|^2 + 2\left|\psi_+\right|^2\right)\left|\psi_-\right|^2,\end{aligned} \tag{15a}$$

$$\begin{aligned}\hat{\aleph}_- =&(\varepsilon + i)\left|\psi_-\right|^2 + \left(\gamma_i + i\gamma_r\right)\left|\psi_+\right|^2 + (\mu + i\nu)\left|\psi_-\right|^4 \\ &+ \left(\delta_i + i\delta_r\right)\left(2\left|\psi_-\right|^2 + \left|\psi_+\right|^2\right)\left|\psi_+\right|^2.\end{aligned} \tag{15b}$$

Then, to improve the accuracy of the standard SSFM over a small interval of time, i.e., $[t, t + \Delta t]$, we adopt the following procedure to propagate the wave:

$$\begin{aligned}\psi_+(x, y, t + \Delta t) \approx \exp&\left(\Delta t \int_t^{t+\Delta t} \hat{D}\left(x, y, t'\right)dt'\right) \\ &\times \exp\left(\Delta t \hat{\aleph}_+\right)\psi_+(x, y, t),\end{aligned} \tag{16}$$

and similarly for $\psi_-(x, y, t + \Delta t)$.

The corresponding results are summarized in Figs. 2, 3, 4, 5. For a good choice of dissipative parameters in the vicinity of the effective potential of Figs. 1, 2a, d show the spatial transverse profiles of the initial asymmetric dissipative light bullets with corresponding values of parameters taken around the bottom of the effective potential of Fig. 1c, with $\delta_r = -0.35074$, $\epsilon = 0.456$, and $\mu = -0.98047$. During the evolution, we note a regular change from an asymmetrical to a symmetrical light bullet for each solution ψ_+ and ψ_- (see Fig. 2c, f). We also observe a small shift of the central position, accompanied by a reduction of the intensity of the solution during a short time of propagation. Thereafter, a stable propagation for longer time is observed. Fig. 2b, e have been recorded at $t = 100$, and Fig. 2c, f correspond to $t = 50000$. The results of Fig. 2 are in very good agreement with analytical results, concerning the soliton trapped at the bottom of effective potential.

To evaluate the influence of dissipative parameters on the stable dynamics of our predicted soliton solutions, the results of Fig. 3a, b have been obtained for $\gamma_r = 0.9$ $\delta_r = -0.3074$, $\varepsilon = 0.456$, $\mu = -0.98047$, $X_m = 1.5$ (values of other parameters are the same as in Fig. 2). Similarly to Fig. 2, we observe a small shift of the central position, a decreasing of the widths and also a small reduction of the intensity during a short-time of propagation, which shows that stable dynamics for longer time of propagation. To better appreciate the influence of the coupled terms on the light bullet stability, Fig. 3c ,d have been obtained for $\gamma_r = 1.109$, (values of other parameters are the same as in Fig. 3a, b). A regime of stable evolution of solutions ψ_+ (see Fig. 3c) and ψ_- (see Fig. 3d) is obtained in comparison to Fig. 3a, b for this value of the coupling coefficient.

Second, we evaluated the influence of the quintic-coupling term, and the results are summarized in Fig. 4. Figure 4a, b display the evolution of the cross-section of the dissipative light bullets obtained from direct numerical simulations of the full coupled (2+1)D cubic–quintic CGL equation for $\delta_r = -0.15074$, $\varepsilon = 0.49$, $\mu = -0.9$, $X_m = 10$, while the other parameters remain the same as in Fig. 3c, d. Figure 4a, b show the generation of the second couple of

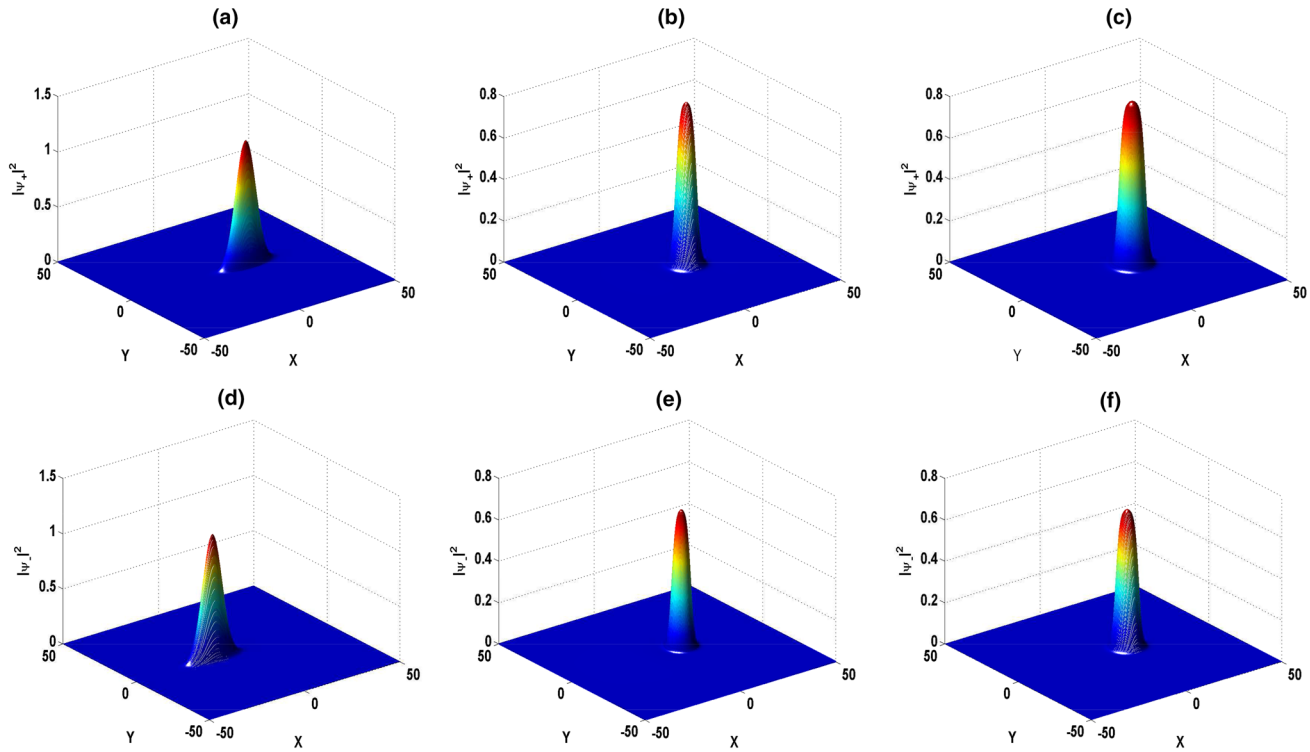

Fig. 2 Spatial profile of $\psi_+(x, y)$ (panels **a** to **c**) and $\psi_-(x, y)$ (panels **d** to **f**). **a**, **d** Correspond to $t = 0$, **b**, **e** correspond to $t = 100$, while **c**, **f** have been recorded at time $t = 50000$, with the parameters: $\delta = -0.01059$, $\beta = 0.45$, $\varepsilon = 0.456$, $\gamma_r = 0.9$, $\gamma_i = 0.25118$, $\delta_i = 0.04289$, $\delta_r = -0.35074$, $\nu = -1$, $\mu = -0.98047$, and $X_m = 10$

light bullets with stable evolution. To have a stable evolution of the coupled dissipative light bullets, we need the balance between gain/loss, diffraction/nonlinearity and, as shown in our analysis, the balance between the coupled effects [35].

In Fig. 5, we have summarized the stable evolution the dissipative light bullets. The obtained (2+1)D stable coupled spatial dissipative light bullets are among new interesting dynamical aspects of laser optics. We have realized through numerical simulations that the intensity of the initially generated asymmetric light bullets (see Fig. 5a, b) decreases in the beginning (see Fig. 5c, d), which is followed thereafter by the reconstitution of the coupled light bullets when the coupling changes (see Fig. 5e, f). This gets more pronounced when time increases and remains very sensitive to the coupling parameters, leading to a stable evolution of the light bullets over longtime propagation (see Fig. 5g ,h).

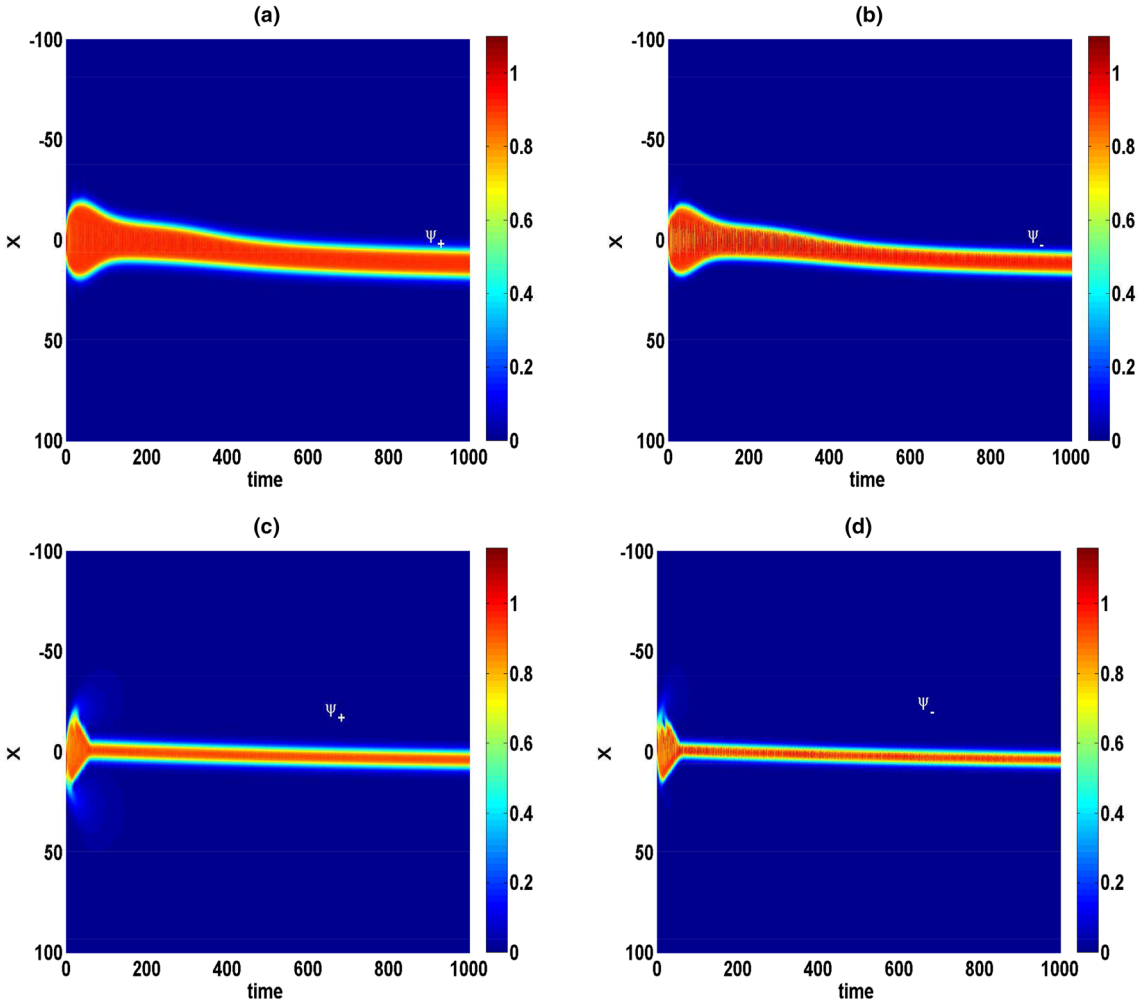

Fig. 3 The density profiles of the cross section of the space-time behavior of ψ_+ (panels **a** and **c**) and ψ_- (panels **b** and **d**). **a**, **b** Correspond to $X_m = 0.5$ and $\gamma_r = 0.9$, while **c**, **d** give the results related to $X_m = 5$ and $\gamma_r = 1.109$. The rest of parameters remains the same as in Fig. 2

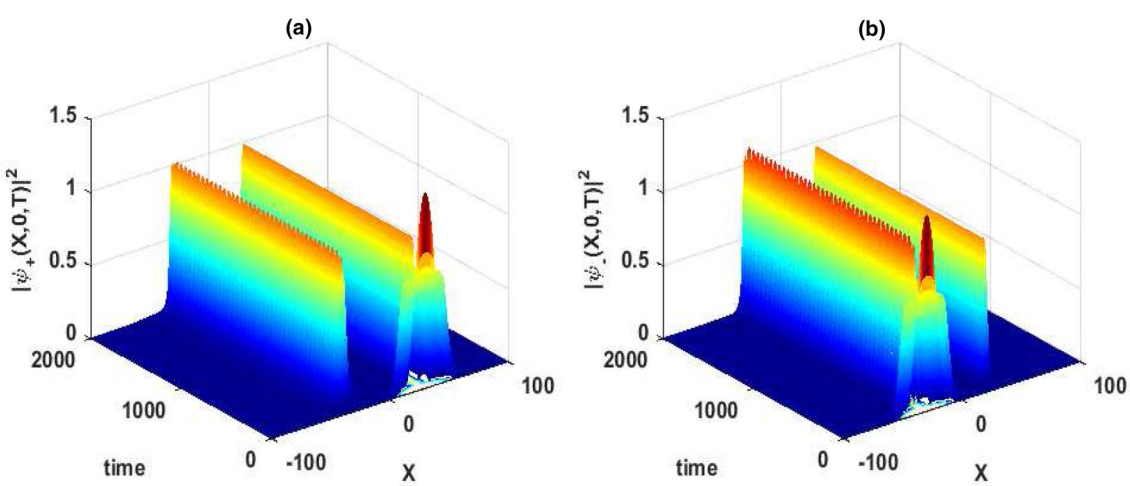

Fig. 4 Cross sections of the wave space-time dynamics, which corroborates the stability of the dissipative light bullets **a** $\psi_+(x, 0, t)$ and **b** $\psi_-(x, 0, t)$ obtained for the $\gamma_r = 1.109$ and $\delta_r = -0.15074$, with the other parameters keeping the similar values as in Fig. 2

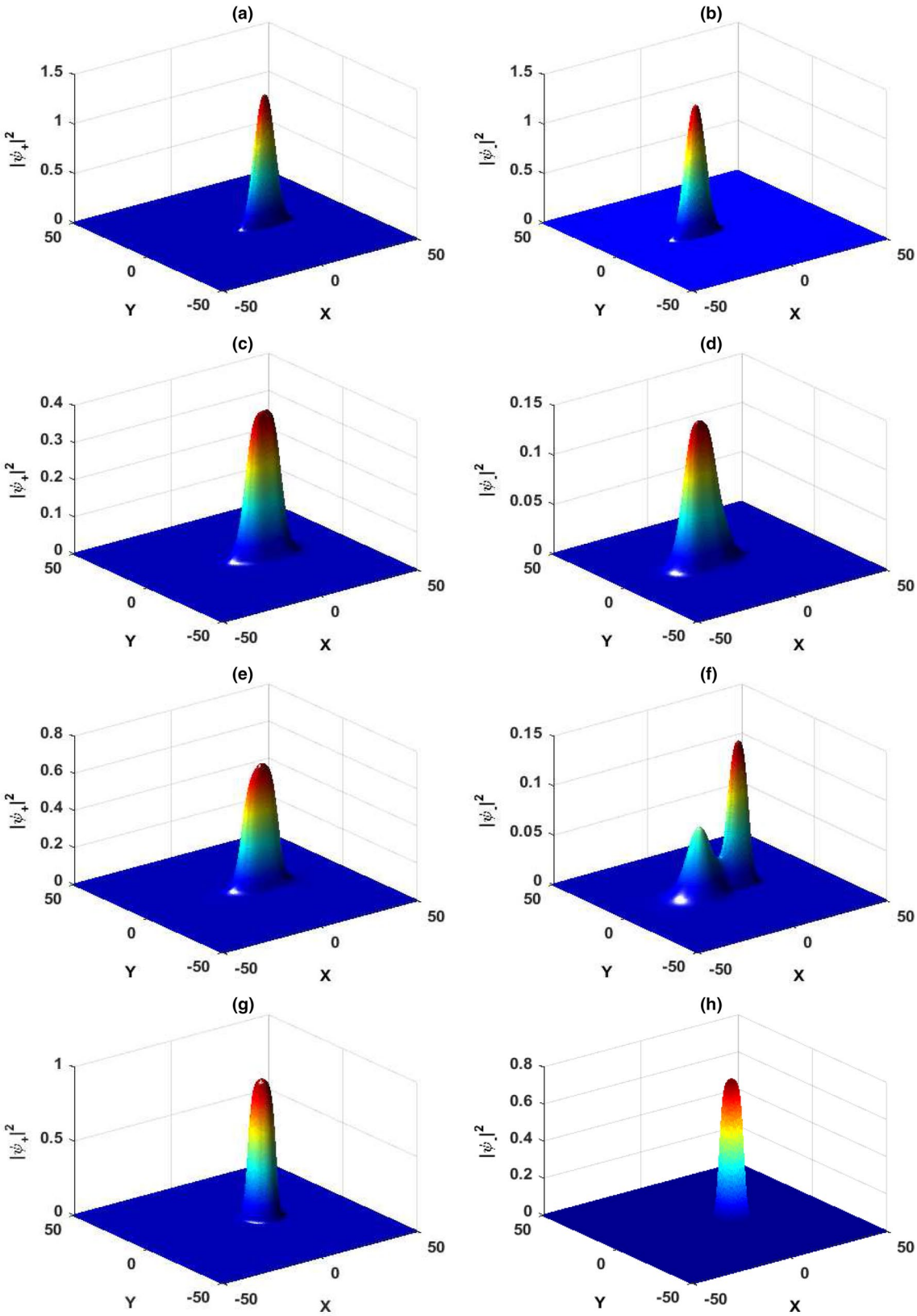

Fig. 5 (2+1)D stable spatial profiles of the light bullet intensities $|\psi_+(x,y)|^2$ (left column) and $|\psi_-(x,y)|^2$ (right column) obtained from direct simulation of Eq. (1) at times $t = 0$ [**a**, **b**], $t = 10$ [**c**, **d**], $t = 25$ [**e**, **f**], and $t = 50000$ [**g**, **h**], with the set of parameters: $\delta = -0.01059$, $\beta = 0.45$, $\varepsilon = 0.49$, $\gamma_r = 0.9$, $\gamma_i = 0.25118$, $\delta_i = 0.04289$, $\delta_r = -0.25074$, $\nu = -1$, $\mu = -0.9$, and $X_m = 10$

4 Conclusion

We have reported a comprehensive analysis on the formation of vector light bullets in an optical nonlinear medium described by a set of (2+1)D cubic–quintic CGL equations. Through the variational method, we have performed the theoretical analysis using a Gaussian trial function as solution, and we have obtained seven coupled first-order differential equations whose solutions have been discussed. Such analytical results have been confronted to direct numerical simulations via the the SSFM, where we have successfully shown that the system is able to interchange energy to keep both light bullets bounded, this under the balance between gain/losses, dispersion/diffraction and nonlinearities. Under such conditions, we have noticed the emergence of asymmetric dissipative light bullets and their disintegration on one hand, and a stable evolution of the coupled dissipative light bullets on the other hand. Moreover, the formation of (2+1)D stable coupled spatial dissipative light bullets has been detected. They have been found to be very sensitive to coupling parameters, whose impact on the long-time dynamics was pronounced. However, this implies new interesting dynamical aspects of laser optics, since the involved coupling mechanism can be adopted as a tool to generate appropriate stabilized vector light bullets which could be otherwise difficult to obtain. Interestingly, no collapse phenomena are observed in simulations when input focussing, chirping, as well as noise both in x and y, are introduced, leading to robust generation of new vector light bullets.

Acknowledgements A. Djazet would like to thank the CETIC (University of Yaoundé I, Cameroon) for their helpful support. The work by CBT is supported by the Botswana International University of Science and Technology under the Grant DVC/RDI/2/1/16I (25). I thank the Kavli Institute for Theoretical Physics (KITP), University of California Santa Barbara (USA), where this work was supported in part by the National Science Foundation Grant no. NSF PHY-1748958

Compliance with ethical standards

Conflict of interest The authors declare that they have no conflict of interest.

Appendix

The effective potential obtained for the stability analysis is given by

$$
\begin{aligned}
U = &\Bigg(\Bigg(\Bigg(\Big(5-\frac{3}{2Y^2}\Big)X^2+\frac{55}{336}+\frac{9}{224X_m^2}+\frac{43}{252}X_m^2 \\
&-\frac{\frac{4X_m^4}{9}+\frac{17X_m^2}{36}+\frac{1}{8}}{X^2}\Bigg)\delta_i\gamma_i A^6-\frac{1}{2}A^2\ln(X)\Bigg)e^{-\frac{14X_m^2}{3X^2}} \\
&+\Bigg(\frac{1}{8}\Bigg(\Big(\frac{7}{2}-\frac{1}{Y^2}\Big)X^2+\frac{3}{16X_m^2}+\frac{7}{9}\Bigg) \\
&+\frac{8X_m^2}{81}-\frac{\frac{1}{16}+\frac{16}{81}X_m^4+\frac{2X_m^2}{9}}{X^2}\Bigg)\delta_i^2A^8e^{-\frac{16X_m^2}{X^2}} \\
&+\Bigg(\Bigg(\Big(4-\frac{1}{2Y^2}\Big)X^2+\frac{8X_m^2}{9}+\frac{1}{2}\Bigg)\frac{\mu\delta_iA^8}{9} \\
&+\Bigg(\Big(7-\frac{1}{2Y^2}\Big)\frac{X^2}{8}+\frac{X_m^2}{9}+\frac{1}{16}\Bigg)\varepsilon\delta_iA^6 \\
&+\Bigg(\Bigg(\frac{\delta}{2}-S+\Bigg(C^2-\frac{1}{2Y^2}+\frac{16C^2X_m^2}{9} \\
&+\frac{4}{3}C\Big)\beta\Bigg)\delta_iX^2+\delta_i\Bigg(\frac{2}{3}-\frac{16CX_m^2}{9}-C\Bigg) \\
&+\beta\delta_i\Bigg(\frac{7}{12}+\frac{3}{16X_m^2}-C^2X^4-\frac{\frac{1}{4}+\frac{4X_m^2}{9}}{X^2}\Bigg)\Bigg)A^4\Bigg)e^{-\frac{8X_m^2}{3X^2}} \\
&+\Bigg(\Bigg(\Bigg(\Big(3-\frac{1}{Y^2}\Big)X^2+1+X_m^2+\frac{1}{4X_m^2}\Bigg) \\
&-\frac{\frac{1}{4}+X_m^2+X_m^4}{2X^2}\Bigg)\gamma_i^2A^4+\frac{\beta\gamma_iA^2}{2}\Bigg)e^{-\frac{4X_m^2}{X^2}} \\
&+\Bigg(\Big(\frac{11}{2}-\frac{1}{Y^2}\Big)\frac{X^2}{18}+\frac{X_m^2}{9}+\frac{1}{18}\Bigg)\mu\gamma_iA^6 \\
&+\Bigg(\Big(1-\frac{1}{32Y^2}\Big)\frac{X^2}{4}+\frac{X_m^2}{8}+\frac{1}{16}\Bigg)\varepsilon\gamma_iA^4 \\
&+\Bigg(\Bigg(-C^2X^4+\frac{1}{8X_m^2}-\frac{1+2X_m^2}{4X^2}\Bigg)\beta\gamma_i \\
&-\gamma_iC(1+2X_m^2) \\
&+\frac{\gamma_r}{2}+\Big(\gamma_i\frac{\delta-2S-2C}{4}+\beta\gamma_i\Big(\frac{C}{2}+2C^2X_m^2 \\
&+C^2+\frac{1}{4Y^2}\Big)\Big)A^2+\frac{1}{X^2}\Big)e^{-\frac{2X_m^2}{X^2}} \\
&+(X^2+Y^2)\Bigg(\frac{\mu^2A^8}{9}+\frac{5\varepsilon\mu A^6}{24}\Bigg) \\
&+\Big(-\frac{4}{9}\big\{(\nu+\beta\mu)(\ln(X)+\ln(Y))+\beta\mu\big(C^2X^4+S^2Y^4\big)\big\} \\
&+\frac{5\varepsilon^2}{64}(X^2+Y^2)+\Bigg(4\beta C\nu+2\mu\delta-4\mu S-\frac{2\beta\mu}{Y^2}\Bigg)\Bigg(\frac{X^2}{9}\Bigg) \\
&+\Bigg(4\beta S\nu+2\mu\delta-4\mu C-\frac{2\beta\mu}{X^2}\Bigg)\Bigg(\frac{Y^2}{9}\Bigg)\Bigg)A^4 \\
&+\Bigg(-\frac{\beta\varepsilon}{2}(C^2X^4+S^2Y^4)-(\ln(X)+\ln(Y))\Bigg(\frac{2+\beta\varepsilon}{4}\Bigg) \\
&+\Bigg(-\frac{\beta\varepsilon}{Y^2}+2\varepsilon C+4\delta\varepsilon-2\varepsilon S\Bigg)\frac{X^2}{8} \\
&+(4\beta S+2\varepsilon S-2\varepsilon C+\delta\varepsilon \\
&-\frac{\beta\varepsilon}{X^2}\Bigg)Y^2\Bigg)A^2 \\
&-4\beta^2(C^4X^6+S^4Y^6)+4\beta(S^3Y^4+C^3Y^4) \\
&-6\beta^2(C^2X^2+S^2Y^2)+12\beta(S\ln(Y) \\
&+C\ln(X))-\frac{\beta^2}{4}\Big(\frac{1}{X^2}+\frac{1}{Y^2}\Big)
\end{aligned}
$$

References

1. Y.S. Kivshar, G.P. Agrawal, *Optical solitons* (2003)
2. N. Efremidis, K. Hizanidis, J. Opt. Soc. Am. B **19**, 1 (2002)
3. S. Shwetanshumala, Prog. Electromag. Res. Lett. **3**, 17 (2008)
4. Z. Chen, M. Segev, D.N. Christodoulides, Rep. Prog. Phys. **75**, 086401 (2012)
5. M. Segev, Opt. Quant. Electron. **30**, 503 (1998)
6. E.A. Ultanir, G.I. Stegeman, C.H. Lange, F. Lederer, Opt. Lett. **29**, 3 (2004)
7. V. Skarka, V.I. Berezhehiani, R. Mmiklaszewski, Phys. Rev. E. **56**, 1080 (1997)
8. D.J. Kaup, B.A. Malomed, R.S. Tasgal, Phys. Rev. E **48**, 3049 (1993)
9. L. Gil, Phys. Rev. Lett. **70**, 162 (1993)
10. J. Lega, J.V. Maloney, A.C. Newell, Phys. Rev. Lett. **73**, 2978 (1994)
11. P. Kockaert, M. Haelterman, J. Opt. Soc. Am. B **16**, 732 (1999)
12. P. Coullet, L. Gil, F. Rocca, Opt. Commun. **73**, 403 (1989)
13. K. Staliunas, C.O. Weiss, Phys. D **81**, 79 (1995)
14. N.N. Akhmediev, V.V. Afanasjev, J.M. Soto-Crespo, Phys. Rev. E **53**, 1190 (1996)
15. J.M. Soto-Crespo, N.N. Akhmediev, V.V. Afanasjev, S. Wabnitz, Phys. Rev. E **55**, 4783 (1997)
16. E. Hernández-García, M. Hoyuelos, P. Colet, M. San Miguel, R. Montagne, Int. J. Bif. Chaos **9**, 2257 (1999)
17. A. Amengual, E. Hernández-García, R. Montagne, M.S. Miguel, Phys. Rev. Lett. **78**, 4379 (1997)
18. R. Montagne, E. Hernández-García, Phys. Lett. A **273**, 239 (2000)
19. L.M. Pismen, Phys. Rev. Lett. **72**, 2557 (1994)
20. L.M. Pismen, Phys. D **73**, 244 (1994)
21. M.S. Miguel, Phys. Rev. Lett. **75**, 425 (1995)
22. M. Hoyuelos, E. Hernández-García, P. Colet, M.S. Miguel, Comput. Phys. Commun. **121**, 414 (1999)
23. E. Hernández-García, M. Hoyuelos, P. Colet, M.S. Miguel, Phys. Rev. Lett. **85**, 744 (2000)
24. M. Hoyuelos, E. Hernández-García, P. Colet, M.S. Miguel, Phys. D **174**, 176 (2003)
25. A. Djazet, S.I. Fewo, C.B. Tabi, T.C. Kofané, On a laser (3+1)-dimensional vectorial cubic-quintic complex Ginzburg-Landau equation and modulational instability, (2019). https://doi.org/10.20944/preprints201910.0171.v1, submitted
26. P.T. Dinda, A.B. Moubissi, K. Nakkeeran, Phys. Rev. E **64**, 016608 (2001)
27. B.G.O. Essama, J. Atangana, F.B. Motto, B. Mokhtari, E.C. Noureddine, T.C. Kofané, Phys. Rev. E **90**, 032911 (2014)
28. J. Fan, S. Jiang, Appl. Math. Lett. **16**, 435 (2003)
29. G.D. Montesinos, M.I. Rodas-Verde, V.M. Pérez-García, H. Michinel, Chaos **15**, 033501 (2005)
30. A. Ankiewicz, N. Akhmediev, N. Devine, Opt. Fiber Technol. **13**, 91 (2007)
31. P.M. Morse, H. Feshbach, *Methods of theoretical physics* (McGraw-Hill, New York, 1953)
32. V. Skarka, N.B. Aleksic, Phys. Rev. Lett. **96**, 013903 (2006)
33. S. Roy, S.K. Bhadra, G.P. Agrawal, Opt. Commun. **281**, 5889 (2008)
34. V. Skarka, D.V. Timotijevic, N.B. Aleksic, J. Opt. A Pure Appl. Opt. **10**, 075102 (2008)
35. M.D. Mboumba, A.B. Moubissi, T.B. Ekogo, G.H. Ben-Bolie, T.C. Kofané, Int. J. Mod. Phys. B **29**, 1550202 (2015)
36. K. Staliunas, Opt. Commun. **90**, 123 (1992)
37. S.I. Fewo, C.M. Ngabireng, T.C. Kofané, J. Phys. Soc. **7**, 074401 (2008)
38. A.I. Maimistov, J. Exp. Theor. Phys. **77**, 727 (1993)
39. M. Djoko, T.C. Kofané, Commun. Nonli. Sci. Numer. Simul. **48**, 179 (2017)
40. M. Djoko, T.C. Kofané, Opt. Commun. **416**, 190 (2018)
41. M. Shen, Q. kong, J. Shi, Q. wang, Phys. Rev. A **77**, 015811 (2008)
42. G. Zakeri, E. Yomba, Phys. Rev. E **91**, 062904 (2015)

Publisher's Note Springer Nature remains neutral with regard to jurisdictional claims in published maps and institutional affiliations.